Biomaterials 178 (2018) 204–280

Contents lists available at ScienceDirect

Biomaterials

journal homepage: www.elsevier.com/locate/biomaterials

Poly(2-oxazoline)s based biomaterials: A comprehensive and critical update

Thomas Lorson [a, 1], Michael M. Lübtow [a, 1], Erik Wegener [b], Malik S. Haider [a], Solomiia Borova [a], Daniel Nahm [a, c], Rainer Jordan [b], Marina Sokolski-Papkov [d], Alexander V. Kabanov [d], Robert Luxenhofer [a, *]

[a] Functional Polymer Materials, Chair for Advanced Materials Synthesis, Department Chemistry and Pharmacy, Julius-Maximilians-University Würzburg, Röntgenring 11, 97070 Würzburg, Germany
[b] Chair of Macromolecular Chemistry, Faculty of Chemistry and Food Chemistry, School of Science, Technische Universität Dresden, Mommsenstr. 4, 01069 Dresden, Germany
[c] Department of Functional Materials in Medicine and Dentistry, University of Würzburg, Würzburg, 97070, Germany
[d] Center for Nanotechnology in Drug Delivery, Division of Pharmacoengineering and Molecular Pharmaceutics, Eshelman School of Pharmacy, University of North Carolina at Chapel Hill, 125 Mason Farm Road, Chapel Hill, NC, 27599, United States

ARTICLE INFO

Article history:
Received 12 February 2018
Received in revised form
11 May 2018
Accepted 14 May 2018
Available online 2 June 2018

Keywords:
Drug delivery
Protein conjugate
Drug formulation
Non-fouling
Nanomedicine
Polyplex

ABSTRACT

Poly(2-oxazoline)s have been investigated for decades as biomaterials. Pioneering early work suggested that hydrophilic poly(2-oxazoline)s are comparable to poly(ethylene glycol) regarding their potential as biomaterials, but the ready commercial availability of the latter has led to its meteoric rise to become the gold standard of hydrophilic synthetic biomaterials. In contrast, poly(2-oxazoline)s almost fell into oblivion. However, in the last decade, this family of polymers has gained much more interest in general and as biomaterials in particular. The rich chemistry and comparably straightforward synthesis of poly(2-oxazoline)s gives many opportunities for tailoring the properties of the resulting biomaterials, allowing the chemist to explore new conjugation chemistry, and to fine-tune the molar mass, hydrophilic-lipophilic balance as well as architecture. Thus, the wide range of demands for various applications of biomaterials can be suitably addressed.

This review aims to give a comprehensive and critical update of the development of poly(2-oxazoline) based biomaterials, focusing on the last 5 years, which have seen an explosive increase of interest. We believe that the research regarding this diverse family of polymers will remain strong and will keep growing, in particular after the promising first-in-human studies of a poly(2-oxazoline) drug conjugate. This review aims at researchers and students new to this polymer family and seasoned poly(2-oxazoline) experts alike and attempts to showcase how the chemical diversity of poly(2-oxazoline)s allows a relatively facile and broad access to biomaterials of all kinds.

1. Introduction

Poly(2-oxazoline)s (POx) have been known for a little over 50 years now [1] and this family of polymers has seen very variable interest by researchers and industry. For decades, only a few members of this diverse polymer family have been investigated in detail, first and foremost poly(2-ethyl-2-oxazoline) (PEtOx) even though the actual and potential chemical space is much larger (see Scheme 1A for a selection of commonly used POx). PEtOx is an amphiphilic polymer that exhibits excellent water- and organo-solubility. The more hydrophilic poly(2-methyl-2-oxazoline) (PMeOx) has also been studied intensively, albeit less than PEtOx. Interestingly, PEtOx may also have interesting applications outside the field of biomaterials, for example in organic electronics, as demonstrated recently by Kim and co-workers [2]. POx with C3 side chains exhibit a lower critical solution temperature, an interesting thermoresponsive behavior, i.e. they are water soluble at cooler temperatures and become water insoluble at higher ones. The exact temperature of this transition can be controlled by composition [3,4], chain length and architecture [5,6], which has

* Corresponding author.
E-mail address: robert.luxenhofer@uni-wuerzburg.de (R. Luxenhofer).
[1] Authors contributed equally.

https://doi.org/10.1016/j.biomaterials.2018.05.022
0142-9612/

Abbreviations

3AT	3-Amino-1H-1,2,4 triazole
83-14 mAb	anti-human insulin receptor antibody 83-14
AB	amphotericin B
AD, Ad	adamantyl, adamatane
AETP	activated endothelium targeting peptide
AFM	atomic force microscopy
AIBN	azobisisobutyronitrile
AP2	angiopep 2
APCN	amphiphilic polymer co-networks
API	active pharmaceutical ingredient
APS	aminopropylsilane
ASA	acetyl salicylic acid
BBB	blood brain barrier
BBB	bottle brush brushes
BCS	biopharmaceutical classification system
BMDC	bone marrow derived DC
Boc	tert-Butyloxycarbonyl
Bpin	boron pinacolato
BSA	bovine serum albumin
BuAc	butyl acrylate
ButBisOx	1,4-butylene-2,2′-bis(2-oxazoline)
CalB	C. antarctica lipase B
CBA	*N*′,*N*′-cystamine bisacrylamide
CBZ	cabazitaxel
CD	cyclodextrin
CFTR	cystic fibrosis transmembrane conductance regulator
CFZ	clofazimine
CHT	chitosan
CIP	ciprofloxazin
CLSM	confocal laser scanning microscopy
CNC	cellulose nanocrystals
CNS	central nervous system
CRE	cremophor EL
CS	chromylium salt
CUR	curcumin
DBCO	Dibenzocyclooctyne
DC	dendritic cells
DDA	dimethyldodecylamine
DDPH	2,2-diphenyl-1-picrylhydrazyl
DDS	drug delivery system
DET	diethylenetriamine
DiI	(2Z)-2-[(E)-3-(3,3-dimethyl-1-octadecylindol-1-ium-2-yl)prop-2-enylidene]-3,3-dimethyl-1-octadecylindole perchlorate
DiO	3,3′-Dioctadecyloxacarbocyanine perchlorate
DiR	10-dioctadecyl tetramethyl indotricarbocyanine iodide
DMF	dimethylformamide
DMEM	Dulbecco's modified eagle medium
DMSO	dimethylsulfoxide
DLS	dynamic light scattering
DOX	doxorubicin
DP	degree of polymerization
DPD	dissipative particle dynamics
DSC	differential scanning calorimetry
DSPE	1,2-distearoyl-*sn*-glycero-3-phosphoethanolamine
DTX	docetaxel
ECE	PEtOx-*b*-PCL-*b*-PEtOx
ECG	electrocardiography
ECH	epichlorohydrin
EDC	1-Ethyl-3-(3-dimethylaminopropyl)carbodiimide
EDS	energy dispersive spectroscopy
EE	encapsulation efficiency
EhAc	2-ethylhexyl acrylate
EI	ethylene imine
ELISA	enzyme linked immunosorbent assay
EpCAM	epithelial cell adhesion molecule
EPR	enhanced permeability and retention effect
ERG	electroretinography
ETO	etoposide
FA	folic acid
FACS	fluorescence activated cell sorting
FBT	fenofibrate
FCS	fetal calf serum
FCS	fluorescence correlation spectroscopy
FDA	food and drug administration
FLIM	fluorescence life-time imaging
FN	fibronectin
FRET	Förster resonance energy transfer
G-CSF	granulocyte colony stimulating factor
GFP	green fluorescent protein
GMA	glycidyl methacrylate
GPC	gel permeation chromatography
HBA	*p*-hydroxybenzaldehyde
HDDA	1,6-hexanediol diacrylate
HDDMA	1,6-hexanediol dimethacrylate
HexBisOx	1,6-hexamethylene-2,2′-bis(2-oxazoline)
HexDiSH	1,6-hexanedithiol
HME	hot melt extrusion
HNK	honokiol
HSA	human serum albumin
HSQC	heteronuclear single quantum coherence (spectroscopy)
HRP	horseradish peroxidase
IBP	ibuprofen
IC_{50}	concentration at half maximum inhibition
ICG	indocyanine green
IDA	imino diacetate
IL-4	interleukin-4
IMC	indomethacin
IND	investigational new drug
IR	infrared
LbL	layer-by-layer
LC	loading capacity: $m_{solubilized\ drug}/[m_{solubilized\ drug} + m_{Polymer}]$
LCROP	living cationic ring-opening polymerization
LCST	lower critical solution temperature
LDH	lactate dehydrogenase
LE	loading efficiency
Maldi-ToF	matrix assisted laser desorption/ionization time of flight
MEW	melt electrospinning writing
MDR	multi-drug resistant
MFI	mean fluorescence intensity
MGP	Microgel particles
MIC	minimal inhibitory concentration
MPT	metoprolol tartrate
MTD	maximum tolerated dose
MTT	3-(4,5-Dimethyl-2-thiazolyl)-2,5-diphenyl-2H-tetrazolium bromide
MTS	3-(4,5-Dimethylthiazol-2-yl)-5-(3-carboxymethoxyphenyl)-2-(4-sulfophenyl)-2H-tetrazolium
NIRF	near infrared fluorescence
NHDF	normal human dermal fibroblasts
NHS	*N*-hydroxysuccinimid

NonDiSH	1,9-nonanedithiol
NP	nanoparticle
NR	nile red
NSCLC	non-small cell lung cancer
NTA	nanoparticle tracking analysis
OctBisOx	1,8-octamethylene-2,2′-bis(2-oxazoline)
OECD	Organisation for economic cooperation and development
OVA	ovalbumin
P4VP	poly(4-vinylpyridine)
PAA	poly(acrylic acid)
PAAm	poly(acrylic amide)
PAAmTMA	poly(3-acrylamidopropyl-trimethylammonium)
PAcM	poly(*N*-acryloyl morpholine)
PAINS	pan assay interfering substances
PAsA	poly(aspartic acid)
PBAD	phenyl boric acid
PBS	phosphate buffered saline
PC	phtalocyanine
PCL	poly(ε-caprolactone)
PCR	polymerase chain reaction
PD	Parkinson's disease
PDC	polymer drug conjugate
PDA	poly(dopamine)
PDL	poly(d-lysine)
PDLLA	poly(DL-lactide)
PDMA	poly(*N*,*N*-dimethyl acrylamide)
PDMS	poly(dimethylsiloxane)
PDMAEMA	poly(2-(dimethylamino)ethylmethacrylate)
PDT	photodynamic therapy
PE	poly(ethylene)
PEG	poly(ethylene glycole)
PEI	poly(ethylene imine)
Pen	penicillin
PEO	poly(ethylene oxide)
PET	positron emission tomography
PET	poly(ethylene terephthalate)
PHEA	poly(2-hydroxylethyl acrylate)
PHPMA	poly(hydroxylpropyl acrylamide)
PHPA	poly(hydroxypropyl acrylate)
PK	pharmacokinetic
PLE	porcine liver esterase
PLA	poly(lactic acid)
P(LA-co-CL))	poly(lactide-co-caprolactone)
PLGA	poly(lactic-*co*-glycolic acid)
PLL	poly(l-lysine)
Plk	propargyl-L-lysine
PMA	poly(methacrylic acid)
PMCL	poly(4-methyl caprolactone)
PMETAC	poly([2-methacryloyloxy)ethyl]trimethylammonium chloride)
PMMA	poly(methyl methacrylate)
PNBA	poly(2-nitrobenzyl acrylate)
PNiPAAm	poly(*N*-isopropylacrylamide)
PNVP	poly(*N*-vinylpyridine)
POI	polypeptoid
PP	poly(propylene)
PP	plasma polymerization
ppOx	plasma polymerized 2-oxazoline
PPCL	poly(4-phenyl caprolactone)
PR	plasma released rotigotine
PropDiSH	1,3-propanedithiol
PSMA	Prostate specific membrane antigen
PSR	poly(sarcosine)
PTHF	poly(tetrahydrofuran)
PTS	pterostilbene
PTX	paclitaxel
PU	polyurea
PVA	poly(vinylalcohol)
PVP	poly(vinylpyrrolidone)
PYMP	prop-2-yn-1-yl-3-mercaptopropionate
QCM	quartz crystal microbalance
QD	quantum dots
ρ	mass concentration
RAFT	reversible addition/fragmentation chain transfer (polymerization)
RB	rose bengal
RBC	red blood cell
RhB	rhodamine B
RLE	rat liver esterase
ROT	rotigotine
ROS	reactive oxygen species
RPMI	Roswell Park Memorial Institute (medium)
SANS	small angle neutron scattering
scFv	single chain variable fragment
SchA	schizandrin A
SCLC	small cell lung cancer
SCN	segmented copolymer network
SD/S.D.	standard deviation
SD	solid dispersion
SDS-PAGE	sodium dodecyl sulfate polyacrylamide gel electrophoresis
SEC	size exclusion chromatography
SEM	scanning electron microscopy
SEM	standard error means
SLS	static light scattering
SOD	superoxide dismutase
SSB	Sjögren syndrome antigen
TA	tannic acid
T_{CP}	cloud point temperature
TEM	transmission electron microscopy
TGase	transglutaminase
TIR	tumor inhibition rate
TNBC	triple negative breast cancer
TNF	tumor necrosis factor
TPGS1000	D-alpha-tocopheryl PEG-1000 succinate
TRR	total releasable rotigotine
uPA	urokinase plasminogen activator
WAXS	wide-angle X-ray scattering
XRD	x-ray diffraction
XPS	x-ray photoelectron spectroscopy
XTT	2,3-bis(2-methoxy-4-nitro-5-sulfophenyl)-5-((phenylamino)carbonyl)-2H-tetrazolium hydroxide

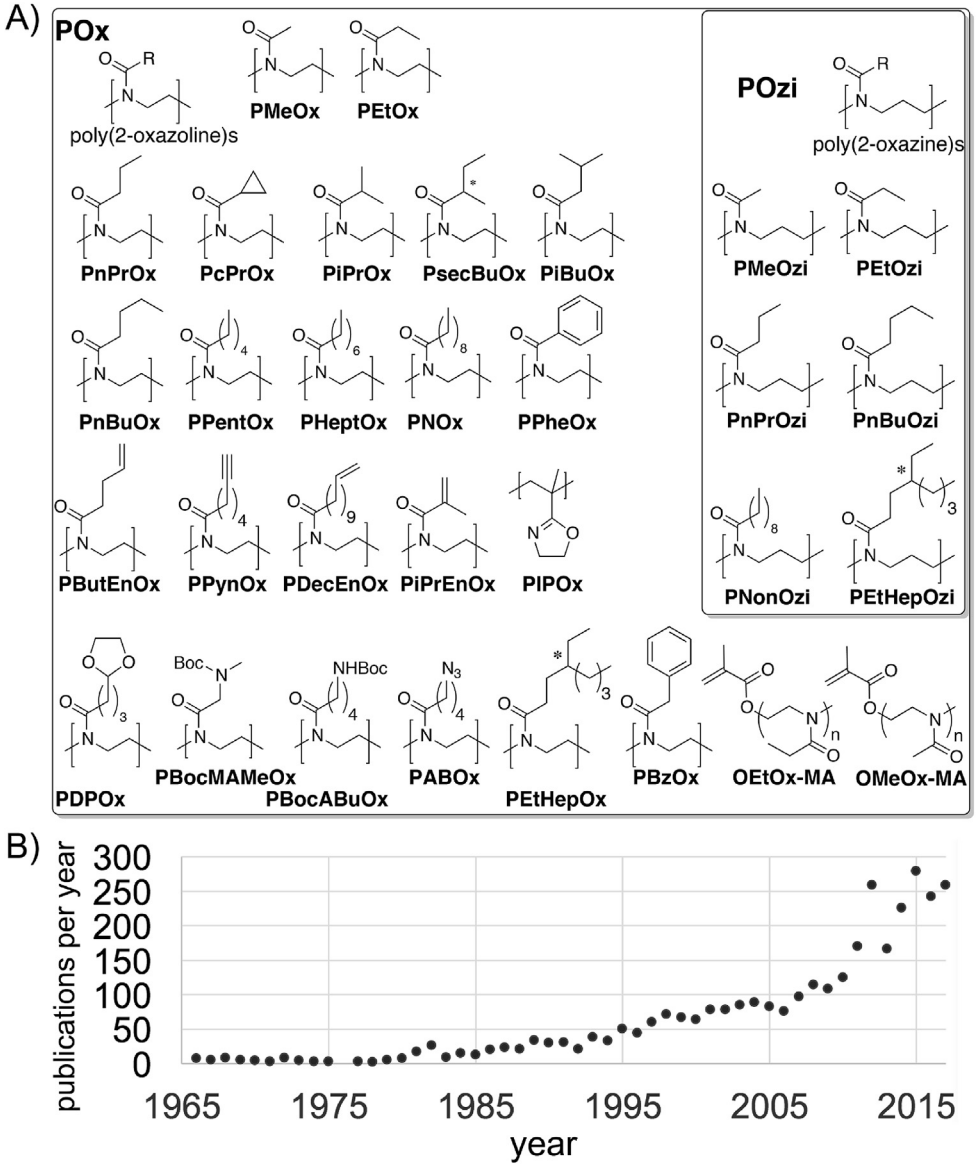

Scheme 1. A) Structures and abbreviations of commonly used poly(2-oxazoline)s (POx) and some poly(2-oxazine)s relevant for this review. B) Development of annual publications on poly(2-oxazoline)s (SciFinder® search term: poly AND oxazoline).

been employed by Jang and co-workers to realize a highly versatile and tunable multicolor emission material [7]. Hoogenboom and Schlaad recently excellently reviewed the state-of-the-art of thermoresponsive POx [8] which is why we will consider herein only select cases with a direct impact in the context of biomaterials. In addition, Dworak also reviewed thermoresponsive polymer-protein conjugates, which included also several examples of POx-protein conjugates [9]. POx with aliphatic side chains longer than C3 are typically non-water soluble and can be employed in amphiphilic systems, which will be reviewed in more detail herein.

In the last few years, several interesting reviews have been published, which give a comprehensive overview on the chemistry of POx and design strategies for functionalized POx [10–12] as well as their physico-chemical properties [13]. Hence, this wide field, which also has seen very interesting developments in recent years will not be covered in detail here. However, as new POx chemistry and novel functionalization strategies may also be directly connected to developments of POx as biomaterials, select examples will also be addressed here. Apart from POx, there are other, closely related polymer families available for the design of biomaterials. For example, the higher homologues of POx, the poly(2-oxazine)s (POzi) have received very little attention so far [14]. Nevertheless, very recent work shows that they can also be used in drug delivery systems and to obtain stimulus-responsive hydrogels. Clearly, the potential of POzi is widely untapped. Also other POx derivatives, such as water-soluble 4-substituted POx [15] have not been investigated in any detail for their potential as biomaterials.

It should be noted that a variety of abbreviations for POx can be found in the literature (POZ, POXA, P(Ox) and others). For the sake of homogeneity, we will only use POx for poly(2-oxazoline)s and POzi for poly(2-oxazine)s even though the original literature might employ another. Similarly, we not always use the abbreviations for specific monomers from the primary literature as this would lead to an insufferable mess within this review.

Also, a few reviews have covered the topic of POx based hydrogels in recent years. Kelly and Wiesbrock reviewed the

various strategies to synthesize POx-based hydrogels and give selected examples for potential application [16]. Dargaville et al. reviewed briefly the up-and-coming field of 3D cell culture. The authors concentrated on POx based hydrogels for cell support and compared them to often used PEG based hydrogels [17]. Similarly, Hartlieb et al. reviewed covalently cross-linked POx hydrogels [18]. Although these excellent reviews give an overview until 2012 and 2014, respectively, we will comprehensively address this topic in the present contribution, especially covering work since 2015. Other reviews have covered the issue of POx at interfaces and on surfaces [19,20]. Nevertheless, we will also cover this topic in the present review, as a review on POx as biomaterials would be incomplete without this important aspect. In general, the research in POx has seen a very significant increase in recent years (Scheme 1B). Even though the simple search performed will certainly not portray the field accurately, the overall trend is likely to be reflective of the actual situation. While before 2010, the number of articles published in this field increased continuously but slowly, the number of articles are now increasing at a much higher rate.

A major breakthrough for the community was indubitably the first-in-human study of a POx-rotigotine conjugate initiated in 2015 [21]. Even though this study is ongoing and final results have not been published, it appears that preliminary results are promising [22].

This review will first look into recent development regarding the toxicity, degradability, immunogenicity, and biodistribution aspects of POx based biomaterials. Subsequently, the extensive work on POx hydrogels are reviewed. In addition, chapters on conjugates, formulations, and complexes are included. Finally, several chapters will summarize the recent research on POx at interfaces and surfaces as well as work on antimicrobial POx.

2. Toxicity, immunogenicity and biodistribution

It has been often written and considered established for some time that POx, in particular hydrophilic POx, are biocompatible. However, relatively little reliable data going beyond simple cytotoxicity has been available in the public domain and more caution should be exerted regarding the term biocompatible. The stealth effect of PEtOx and PMeOx has been probably one of the best established features [23], however new research by Szoka and Frechet questions important aspects of this issue (*vide infra*). Generally, POx have also been established to exhibit excellent cyto- and hemocompatibility and several reports have corroborated and extended our knowledge about this in the past 5 years (*vide infra*). However, it should never be assumed that this can be simply extended to POx with different composition, architectures or end-groups and must always be assessed on a case-by-case basis. Moreover, new studies have investigated the stability of POx with respect to hydrolysis, oxidative and environmental degradation, the latter of which has not been investigated before. For the interaction with biological systems, the solution properties of polymers in general are important. Very recently, Schubert, Nischang and co-workers [24] as well as Hoogenboom, Filippov and co-workers [25] investigated in great detail POx solution properties in aqueous solution (water and phosphate buffered saline (PBS), respectively) in two very interesting, detailed and valuable studies. In water, the hydrodynamic volumes of PMeOx and PEtOx are very similar at the same molar mass and systematically smaller than that of PEG [24]. Viscometric studies suggest that especially at lower molar masses, water is a better solvent for PEG than for PEtOx and, to a lesser extend, PMeOx. At higher molar masses (20 kg/mol and above), this difference becomes smaller or non-existent. Also, and very important to note, the authors caution that molar mass analysis of POx with molar masses of $\leq$10 kg/mol using light scattering based detection should be viewed with some caution, as it may tend to overestimate the molar mass. This is not entirely surprising, as it is clear that sensitivity of light scattering becomes problematic with very small molar masses while the refractive index detectors are sensitive irrespective of the molar mass. While this study investigated PEtOx and PMeOx in water, Hoogenboom and Filippov studied PEtOx in PBS. This study concludes that the conformational rigidity of PEtOx is similar to that of PEG [25].

2.1. Cytocompatibility

Often cyto- and hemocompatibility of a certain polymer class is based on few experiments and generalized too readily, as both strongly depend on the utilized cell type, incubation time, polymer concentration, molar mass and of course, purity. PEG is currently the gold standard for hydrophilic polymers and can be seen as a benchmark for polymers that aim towards usage in medical application, drug delivery or biomaterials in general. Nevertheless, existing or perceived disadvantages or limitations of PEG such as undesired impurities, limited stability, high viscosity and accumulation in some organs have triggered search of new materials [26–29]. In the recent years, POx have been discussed as potential alternatives for PEG. Especially implications on the cell viability for various POx moved into focus. Fischer and co-workers investigated cyto- and hemocompatibility of PEtOx and PEG with different molar masses (0.4–200 kg/mol) at different incubation times (3, 12 and 24 h) [30]. It is important to note that some of the investigated PEtOx samples (5, 50 and 200 kg/mol) were ill-defined commercial polymers ($Đ = 2.4$, 4.1 and 4.7, respectively). However, whether this dispersity would have any considerable impact in this simple assay is not clear. Even at very high polymer concentrations up to 80 g/L, no cytotoxicity was observed for short incubation times (3 h) in L929 mouse fibroblasts. After longer incubation (12 h), low molar mass PEtOx (0.4 and 2 kg/mol) as well as 20 kg/mol PEtOx decreased the cell viability below 70%. However, higher molar mass PEtOx (50 and 200 kg/mol) remained non-cytotoxic also after 24 h of incubation suggesting no influence of the broader molar mass distribution. Although no clear correlation between molar mass and cytotoxicity was found, medium molar masses appeared to exhibit somewhat higher cytotoxicity for unknown reason. A similar pattern was observed for PEG. Up to 40 g/L it was found to be non-toxic after 24 h incubation, the highest cytotoxicity was observed for 10 kg/mol PEG. None of the investigated polymers showed a pronounced influence on the aggregation behavior of erythrocytes or led to significant hemolysis. Specifically, PEtOx up to 40 kg/mol and 80 g/L did not cause erythrocyte aggregation and PEtOx with 200 kg/mol led to only minor erythrocyte aggregation at 40 g/L. Follow-up studies by the same group published in 2013 focused on PMeOx [31]. Similar to the study on PEtOx, *in vitro* cytotoxicity and hemocompatibility of PMeOx with a molecular weight from 2 to 20 kg/mol were assessed. None of the studied polymers caused release of hemoglobin, even at concentrations of 80 g/L. Cytotoxicity studies confirmed the generally high cytocompatibility of PMeOx. Only 2 kg/mol PMeOx (80 g/L) reduced the cell viability of L929 mouse fibroblasts to 60% and 44% after 3 and 12 h incubation, respectively. In general, a similar pattern as for PEtOx was observed [30].

Poly(2-*iso*-propenyl-2-oxazoline) is the product of the polymerization of 2-*iso*-propenyl-2-oxazoline (iPrEnOx), an interesting monomer that can alternatively be polymerized via radical, anionic polymerization or living cationic ring-opening polymerization (LCROP). For the sake of differentiation, we will call/abbreviate the product of the LCROP PiPrEnOx, while the product of radical or anionic polymerization, which leaves the 2-oxazoline ring intact,

PIPOx. Even though this review concentrates on POx obtained by LCROP, we would like to briefly mention a study investigating the cytocompatibility of PIPOx obtained via radical polymerization. Apart from PIPOx, Kronekova et al. studied the cytotoxicity of various 2-oxazoline monomers [32]. Specifically, MeOx, EtOx and iPrEnOx were tested using NIH 3T3 mouse fibroblasts (24 h incubation) and compared against acrylamide. Interestingly, iPrEnOx showed much more pronounced impact on the cell viability with an IC_{50} value of only approx. 0.7 mg/L (6 μM). In contrast, the IC_{50} values of MeOx, EtOx and acrylamide were about 3–4 orders of magnitude higher. Therefore, iPrEnOx exhibits an extraordinarily high cytotoxicity and should be handled with considerable care. Moreover, it is advisable to make sure to remove even traces of this monomer when incorporated into biomaterials. In stark contrast to the monomer, PIPOx shows little if any effect on the cell viability (5 g/L, 24 h) in NIH 3T3 and P388.D1. Surprisingly, PIPOx seems to affect the cells even less than PEtOx tested in this study.

Very recently, Leiske et al. reported their approach to evaluate PMeOx, PEtOx, poly(vinyl alcohol) (PVA) and Pluronic® F127 as surfactants and cryoprotectant in the preparation of poly(lactic-*co*-glycolic acid) (PLGA) nanoparticle via nanoemulsion [33]. Cyto- and hemocompatibility is important in this context as it is almost impossible to completely remove the surfactants after nanoemulsion polymerization. For both POx investigated, no cytotoxic effect or hemolytic activity was found at 5 wt% concentration, corroborating earlier reports (Fig. 1 A). According to the authors, PVA and Pluronic® F127 could not be investigated at the highest concentration due to solubility issues. Regarding hemocompatibility, PVA and Pluronic® F127 did reveal increased hemolytic activity at 1 wt% whereas PMeOx and PEtOx remained inconspicuous (Fig. 1 B). The erythrocyte aggregation tests did not show significant differences between the tested polymers.

Also, the almost forgotten poly(2-oxazine)s (POzi) - the higher homologue of POx - regained interest as potential biomaterials [34–36]. An initial study conducted by Kroneková et al. regarding the cytotoxicity of different 2-oxazine monomers (2-methyl-2-oxazine (MeOzi), 2-ethyl-2-oxazine (EtOzi) and 2-*n*-propyl-2-oxazine (*n*PrOzi)) and homopolymers (PMeOzi (DP = 50), PEtOzi (DP = 50) and PEtOzi (DP = 150)) in 3T3 mouse fibroblasts was reported and is to the best of our knowledge the first on this topic [37]. Cell viability after 24 h incubation decreased to or below IC_{50} at concentration exceeding 20 g/L for MeOzi, 10 g/L for EtOzi and 5 g/L for nPrOzi, compared to untreated control. Therefore, the cytotoxicity of 2-oxazines is about one order of magnitude lower compared to MeOx and EtOx [32]. POzi homopolymers were analyzed at concentrations ranging from 0.001 to 100 g/L. Those with a similar DP but different side chain ($PMeOzi_{50}$ vs. $PEtOzi_{50}$) showed similar cytotoxicity profiles (IC_{50} approx. 70 g/L). The comparison of $PEtOzi_{50}$ and $PEtOzi_{150}$ revealed a somewhat higher cytotoxicity (IC_{50} approx. 20 g/L) with increasing DP. P*n*PrOzi could not be taken into account due to its lower critical solution temperature at around 12 °C [38] and the associated insolubility at physiological temperature. POx- or POzi-based biomaterials may comprise solely these two polymer families with different side chains, or be combined with other polymers like poly(ε-caprolactone) (PCL) [39,40] poly(sarcosine) (PSR) [41], poly(lactide) [42–44] or poly(ethylene imine) (PEI) [45–47]. Most typically, POx have been used as the hydrophilic constituent of amphiphilic block copolymers. Those that contain hydrophobic POx have been also investigated, but considerably less [48]. Recently, Lorson et al. found no dose dependent cytotoxicity up to 10 wt% in NIH 3T3 mouse fibroblast if incubated with $PMeOx_{50}$-*b*-P*n*PrOzi$_{50}$ for 24 h [35]. Even at concentrations of 25 wt%, cells exhibited more than 80% metabolic activity, which is considered non-cytotoxic (Fig. 2 A). Please note that the aqueous solution of this polymer forms thermoresponsive hydrogels above a certain polymer concentration (which will be discussed in detail in the according chapter). Therefore, incubated cells do not sediment and remain 3-dimensionally distributed after incubation for 24 h (Fig. 2 B).

Very recently, Lübtow et al. reported the outstanding drug formulation capabilities of POx/POzi triblock copolymers (which will be discussed in detail in the according chapter) [36]. These polymers were also tested with respect to their cytotoxicity to different cell types (human dermal fibroblasts, Caco-2 and MDMBA-231). Even at 100 g/L, no significant cytotoxicity was observed in Caco-2 and human dermal fibroblasts, while the cancer cell line MD-MBA-231 experienced a marked cytotoxicity with an IC_{50} of 10 g/L. This unexpected observation will require a more detailed investigation as it may have potential implications in cancer therapy, although the required polymer concentration is

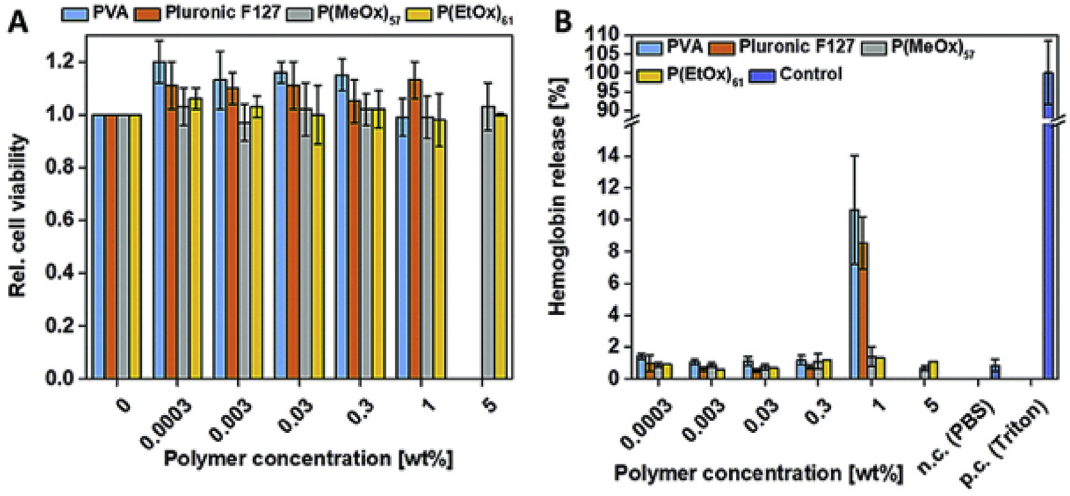

Fig. 1. Concentration dependent cytocompatibility of different non-ionic polymers suitable as surfactants in nanoemulsions. (A) Cell viability after incubation with poly(-vinylalcohol) (PVA), Pluronic® F127 and two POx, PMeOx and PEtOx using AlamarBlue® assay, normalized to negative control. L929 cells were treated for 24 h with the indicated concentrations of the polymers. Values represent means ± S.D. (n = 3). (B) Hemoglobin release of erythrocytes after incubation for 60 min at 37 °C with polymers at indicated concentrations. A value of less than 2% hemoglobin release is classified as non-hemolytic and >5% as hemolytic. Values represent means ± S.D. (n = 3). Reprinted with permission from ref [33]. Copyright 2017 The Royal Society of Chemistry.

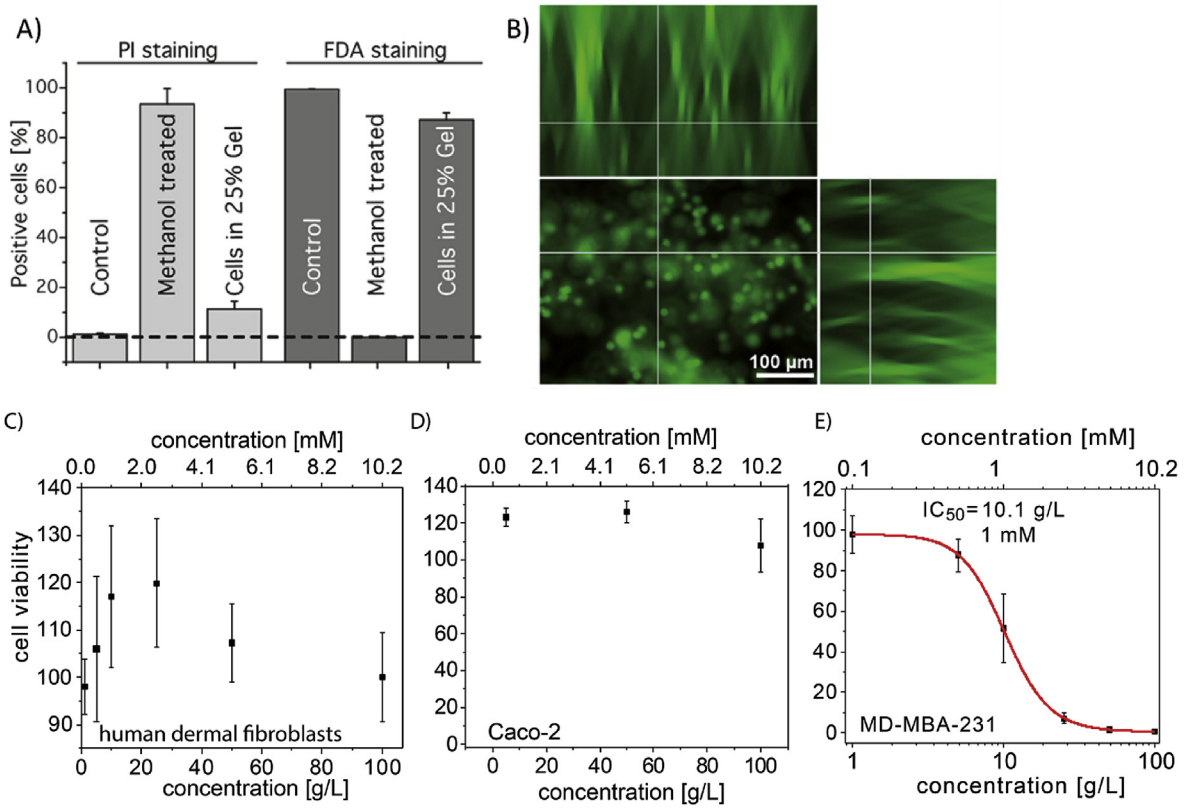

Fig. 2. A) Cell viability of NIH 3T3 fibroblasts and B) z-stack image of FDA stained cells, 24 h at 37 °C after incorporation into the aqueous solutions of $PMeOx_{50}$-b-$PnPrOzi_{50}$ (25 wt %), which forms a hydrogel at physiological temperature. The total volume in (B) comprises 559.54 µm (x) * 419.25 (y) µm * 355 µm (z) with 1 µm z-interval. Reprinted with permission from ref. [35]. Copyright 2017 American Chemical Society. C)-E) Cell viability for indicated cell lines upon incubation with the amphiphilic triblock copolymer PMeOx-b-P*n*PrOx-b-PMeOx as determined by CellTiter-Glo® assay. Cells were incubated for 24 h (Caco-2) and 72 h (human dermal fibroblasts and MD-MBA-231), respectively. Reprinted, with modifications, from Ref. [36].

rather high.

Similar to POx, polypeptoids (POI) also belong to the group of pseudo-polypeptides and are being discussed as an promising alternative to PEG [49]. Guo and co-workers published a first report combining hydrophobic POx and a hydrophilic polypeptoid (POI) very recently [50]. Specifically, the authors reported the synthesis of amphiphilic POx-*b*-POI copolymers poly(2-but(3-enyl)-2-oxazoline)-*b*-polysarcosine (PButEnOx-*b*-PSR) by ring-opening polymerization via one-pot, three-step synthesis ($M_w = 4.7–10.8$ kg/mol; $Đ = 1.15–1.21$) as potential biomaterials for drug delivery and gene therapy. Up to 10 g/L, the block copolymer $PBuOx_{19}$-*b*-$PSar_{92}$ did not show pronounced cytotoxicity in L929 mouse fibroblasts after incubation for 24 h. This low cytotoxicity together with the small micellar size ($D_h \leq 100$ nm) of the spherical polymer particles in aqueous solution (ρ(polymer) = 2 g/L) makes this amphiphilic hybrid a potential candidate for further investigations in e.g. drug-delivery system.

Zwitterionic polymers are being discussed as promising non-fouling materials, drug delivery systems, implants and coating materials for medical devices. Tauhardt et al. investigated zwitterionic POx based on 1,3-propansultone (SB-POx) and β-propiolactone (CB-POx) modified PButEnOx as candidates for anticoagulants (Fig. 3) [51]. *In vitro* cytotoxicity tests of the homopolymer and copolymers show no cytotoxicity after incubation (24 h) at various concentrations (0.1–10 g/L) (Fig. 3).

Blood compatibility tests also showed no hemolytic effect as the hemoglobin release was below 2% (Fig. 4 A). Blood viscosity was not strongly affected by any of the investigated polymers up to concentrations of 5 g/L. Only a very small increase was noticed at the highest concentration of 10 g/L. (Fig. 4 B) There was no effect on the P-selectin (CD62p) membrane glycoprotein expression in CD42 (surface antigen) positive cells according to platelet activation test. Furthermore, no activation of the complement system was observed (C3a levels were observed) following the incubation with the zwitterionic polymers and the PEtOx control (ρ(polymer) = 1, 5, and 10 g/L) after incubation for 10, 30 and 60 min, most likely due to the pronounced hydrophilic character of the polymers. Prothrombin time was not affected in a clinically relevant manner (coagulation time >7 and < 10 s). In contrast, the activated partial thromboplastin time was significantly affected, for CB-POx even at the lowest tested concentrations of 1 g/L, while PEtOx did not show any influence on the coagulation characteristics.

Yildirim et al. also synthesized amphiphilic, heterografted comb polymers based on oligomeric polylactide (PLA) and oligo-EtOx-methacrylate (OEtOx-MA) ($M_n = 21–41$ kg/mol; $Đ = 1.17–1.37$) as potential drug carriers (Fig. 5 A) [52]. In this contribution, different hydrophilic (OEtOx)/hydrophobic (PLA) ratios were investigated, ranging from 70/30 (P1), 65/35 (P2), 80/20 (P3), 85/15 (P4), to 90/10 (P5). Neither polymer did show any cytotoxicity after 24 h, albeit only extremely low concentrations of up to 0.2 g/L were investigated (Fig. 5 B). One should be careful to consider the polymer as cytocompatible unless higher concentrations are tested.

Wang and co-workers synthesized PEtOx-*b*-poly(D,L-lactide) (PEtOx-*b*-PDLLA) diblock copolymers that were also suggested for use as drug carrier for intravenous (i.v.) administration [53]. The hemolytic activity, platelet activation, blood coagulation and protein adsorption of PEtOx-*b*-PDLLA micelles was investigated and did not reveal problematic results. At all tested polymer

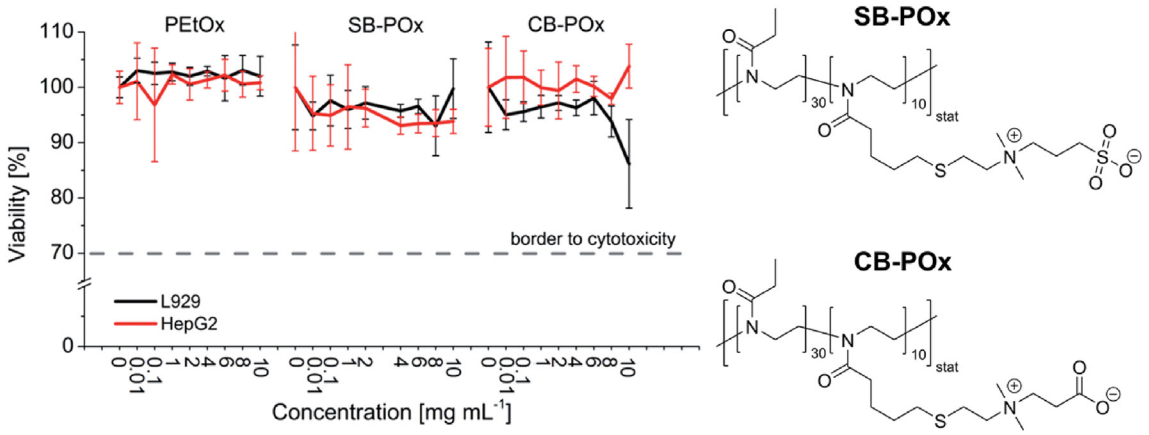

Fig. 3. Cell viability of L929 mouse fibroblasts and human hepatocytes HepG2 after incubation with zwitterionic polymers SB-POx and CB-POx (right side) up to 10 g/L after 24 h. Cells incubated with polymer free culture medium served as control. The cell viability was determined by XTT assay according to ISO 10993-5. Data are expressed as means ± SD (n = 6). Reprinted with permission from ref. [51]. Copyright 2014 The Royal Society of Chemistry.

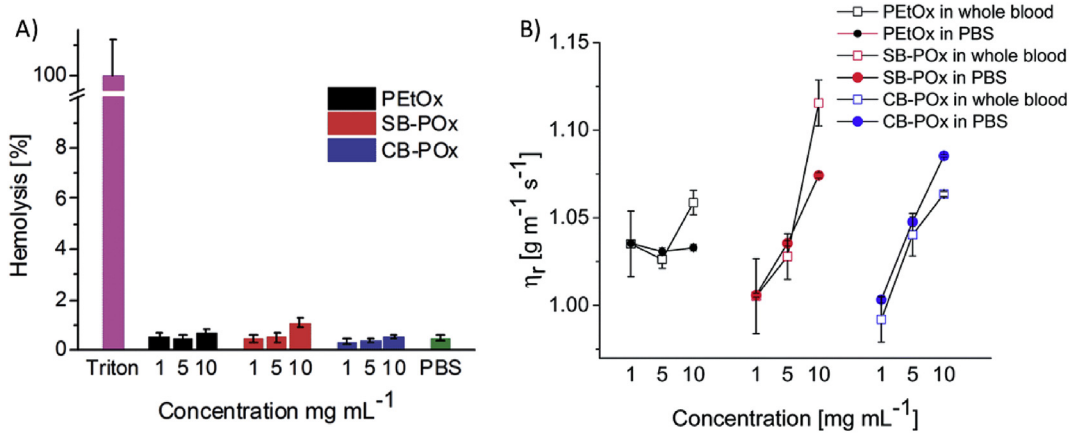

Fig. 4. (A) Photometric determination of hemolytic activity after incubation with different polymer concentrations for 1 h at 37 °C. Triton X-100 (1%) served as positive and PBS as negative control. Experiments were run in triplicate and were repeated once; data are presented as means ± SD compared to the positive control set as 100%. (B) Blood compatibility of PEtOx and zwitterionic POx-based polymers concerning their influence on the whole blood viscosity: relative viscosity of the polymer solutions in PBS and in whole blood. Experiments were run in quadruplicate at three inclination angles, data are presented as the means ± SD. Reprinted with permission from ref. [51]. Copyright 2014 The Royal Society of Chemistry.

concentration hemolysis percentage was below 0.3% and only 0.25 ± 0.18% hemolysis was detected at the highest (albeit still rather low) tested concentration of 0.82 g/L. *In vitro* blood coagulation study also did not reveal any significant effect of PEtOx-*b*-PDLLA on the blood/erythrocytes aggregation. Moreover, protein interaction, platelets activity and cytocompatibility did not show any significant effects at block copolymer concentration up to 12 g/L and 24 h incubation. Accordingly, this preliminary analysis suggests that PEtOx-*b*-PDLLA are potential candidates for further evaluation just as their well-established PEG analogs are.

The possibility to incorporate a positive charge into polymers opens up manifold opportunities in various biomedical applications such as drug delivery, gene engineering, tissue engineering, and cell encapsulations. PEI is one of the most intensively investigated polycations for biomedical applications. Due to its high condensation capability towards DNA, strong buffering capacity in a pH range of 5.1–7.4, and relatively high transfection efficiency, PEI is used for non-viral vectors design. However, the high charge density also contributes to its pronounced cytotoxicity. This problem has been addressed by partial hydrolysis of the POx, yielding P(Ox-*co*-EI). Early studies investigated P(Ox-*co*-EI) with at least 56 mol% EI [45,54]. Hoogenboom and co-workers studied biocompatibility of partially hydrolyzed POx with a EI content ranging from 0.025 wt% (5 mol% EI) to 0.515 wt% (75 mol% EI) [55]. They used commercially available PEtOx with a molecular weight of 200 kDa, performed acidic hydrolysis and utilized human dermal fibroblast cells for toxicity test at concentrations up to 5 g/L. Compared to untreated PEtOx, up to 43 mol% EI, the cytotoxicity of P(EtOx-*co*-EI) was similar to PEtOx which did show some reduced cell viability compared to control, despite the relatively low concentrations. Increasing the degree of the hydrolysis up to 71% entails high cytotoxicity comparable to linear PEI. Important to note, the relatively high cytotoxicity of PEtOx reported in this study is in some contradiction to other reports, where comparable levels of cytotoxicity were typically found at higher concentrations of hydrophilic POx or PEtOx [30,48]. However, since the cell viability can be quite cell type specific, this nicely demonstrates that one has to be careful in generalizing "biocompatibility" of biomaterials from simply cytotoxicity tests with a few selected cell lines/types. Furthermore, the slug mucosal irritation test was applied to perform a simple but informative *in vivo* experiment. PEtOx and the P(EtOx-*co*-EI) with up to 25 mol% PEI show minimal mucus production that was on average lower compared with the negative control (PBS) indicating that they are non-irritating. Additionally,

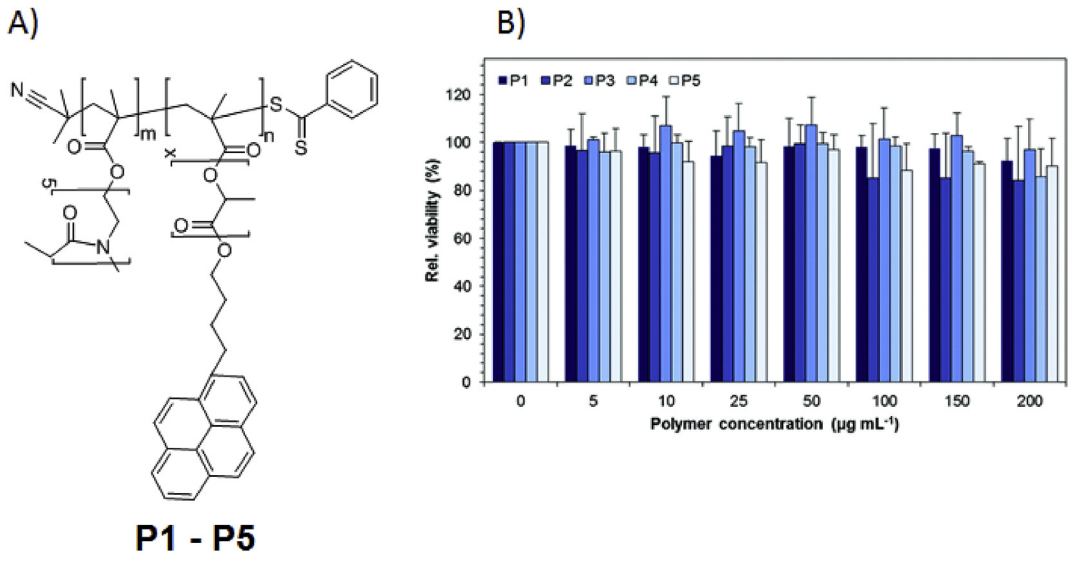

Fig. 5. (A) Schematic representation of the heterografted comb polymers obtained via RAFT polymerization. The molar ratios m/n defining the hydrophilic/hydrophobic balance were 70/30 (P1), 65/35 (P2), 80/20 (P3), 85/15 (P4), to 90/10 (P5). (B) Relative cell viability of L929 cells after 24 h of incubation with heterografted comb polymers (P1 to P5) at the indicated concentrations. Values represent the means ± S.D. (n = 3). At these low concentrations, no cytotoxicity was found. Reprinted with permission from ref. [52]. Copyright 2016 The Royal Society of Chemistry.

no lactate dehydrogenase (LDH) release was induced implying that no tissue damage was caused. Polymers with a higher L-PEI content resulted in a mucus production that was statistically comparable with the negative controls and let to LDH release in one of five tested slugs. It is important to note that the described hydrolysis of POx only occurs at a reasonable rate under biologically irrelevant conditions (5.8 M HCl; > 80 °C). This is important to keep in mind regarding their use as biomaterials.

In 2015, Kronek et al. revisited this issue and reported *in vitro* studies of partially hydrolyzed PEtOx [56]. Cytotoxic studies were performed using copolymers with different molar mass (8–36 kg/mol), degree of hydrolysis (3–60 mol% PEI) using fibroblasts as the most common cells in connective tissue, βTC3 cells as secretory and regulatory cells and macrophages P388.D1 as the cells of immune system. Obtained results corroborated earlier work in that increasing degree of hydrolysis decreased the cell viability in all cases. The highest cytotoxic effect was seen for 19.6 kg/mol and a PEI content of 50 mol%. More detailed analysis of the dependence of the cytotoxicity on PEI content was done with PEtOx - 9.6 kg/mol (Fig. 6 A) and PEtOx - 19.6 kg/mol (Fig. 6 B) at concentrations of up to 20 g/L. After 48 h of incubation (0 mol% of EI), a partial decrease of cell viability was observed in the βTC3 and macrophages, while fibroblasts were unaffected. Not surprisingly, the cytotoxicity increased with increasing degree of hydrolysis, concentration and incubation time. Regarding partially hydrolyzed copolymers, it is evident that cytocompatibility is cell-type dependent with fibroblasts having the highest viability in this study and macrophages, as representatives of the immune system, being the most sensitive cells. PEtOx-19.6 kg/mol with a degree of hydrolysis of 59% (P388.D1; 48 h) showed a cytotoxicity comparable to PEI. The reason why the medium size copolymers exhibit the highest cytotoxicity remains unclear but again, corroborates findings by Bauer et al. [30,31].

Hsiue and co-workers also attempted to revisit block copolymers of PEtOx and a mixed P(EtOx-*co*-EI) block obtained by partial hy drolysis. Unfortunately, the presented synthetic route does not allow for any controlled synthesis and no adequate characterization of the resulting polymers is provided. Insufficient materials characterization notwithstanding, the commonly observed trend that low hydrolysis degreed results in relatively cytocompatible materials while high degree of hydrolysis leads to pronounced cytotoxicity is also found in this contribution [57].

England et al. investigated the cytocompatibility of poly(L-lysine) (PLL) dendrimers grafted with POx or PEG intended for use as drug carriers [58]. The molar mass of the studied polymer grafts was 2 kg/mol. Cytotoxicity studies confirmed that POx and PEG modified dendrimers were leading to less apoptosis than the unmodified dendrimer (2–3% compare to 36% for unmodified dendrimer) at a concentration of 0.5 g/L. Blood compatibility studies also showed that POx and PEG modified dendrimers did not result in hemolysis or red blood cell aggregation at 2 g/L.

Wang et al. recently reported a comparative study on the stealth properties of nano-graphene oxide grafted with PEG and PEtOx [59]. The protein corona cytotoxicity and haemolysis of the materials was investigated. While similar levels of complement proteins were found associated with the grafted nano-graphene oxide, some distinct differences in the protein corona were found.

2.2. POx for immunomodulation and immunocamouflage

Kronek and co-workers investigated possible immunomodulatory effects of POx prior to the period in focus of the present review [60,61]. These studies were later backed up by further work by the same group. Specifically, the activation of mouse lymphoid macrophages P388.D1 using PEtOx and a copolymer of EtOx and 2-(4-aminophenyl)-2-oxazoline (P(EtOx-*co*-AmPheOx)) [62]. The release of reactive oxygen species (ROS) and pro-inflammatory cytokines was investigated. Interestingly, PEtOx at 5 g/L was found to lead to a moderate increase in IL-1alpha, IL-6 and TNF-alpha, as well as ROS levels compared to control. In contrast, P(EtOx-*co*-AmPheOx) only lead to a minor increase in ROS. The authors try to put the results in context with the polarity of the two polymers. However, it should also be mentioned that the AmPheOx monomer leads to side reactions during polymerization, which is clearly apparent by the very large dispersity for this polymer. This can be easily understood as a free amine will lead to termination reactions and the resulting polymer will have invariably an unknown but likely very complex structure. Therefore, structure-

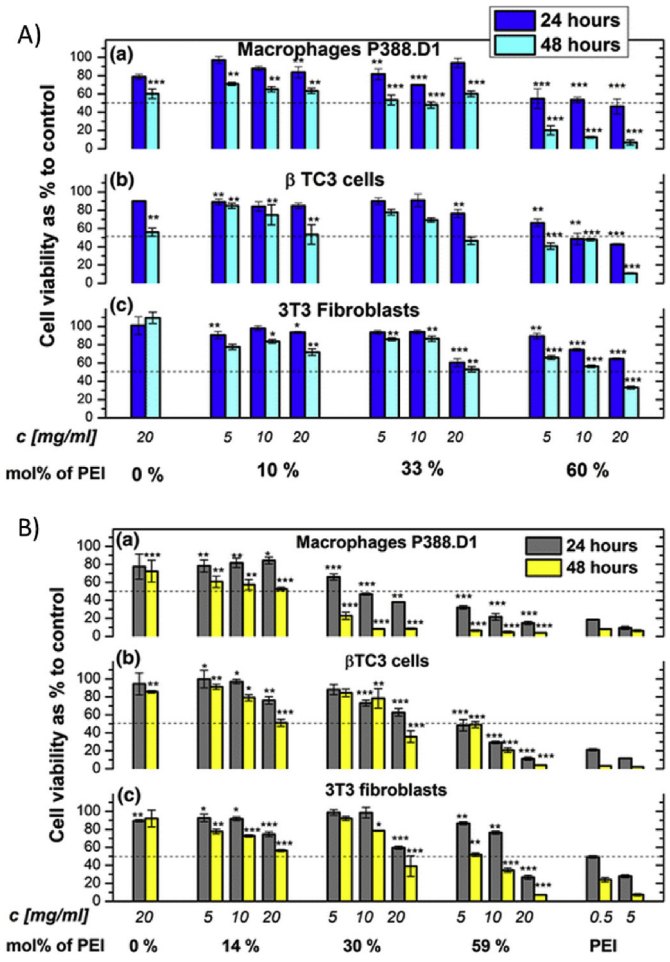

Fig. 6. (A) The cell viability of partially hydrolyzed PEtOx (9.6 kg/mol) with 10, 33 and 60 mol% degree of hydrolysis and (B) PEtOx (19.6 kg/mol) with 14, 30 and 59 mol% degree of hydrolysis after 24 and 48 h incubation in DMEM at 5, 10, and 20 g/L of copolymer. The MTT assays were performed using macrophages P388.D1 (a), pancreatic βTC3 cells (b), and 3T3 fibroblasts (c). The dashed line indicates the IC_{50} value. Mean viability and a standard deviation (SD) were computed for each group from triplicates (n = 3). Statistical significant difference in viability between the samples treated cells and untreated control is shown as * for (P=0.05), ** for (P=0.01), and *** for (P=0.001), using Dwass-Steel-Critchlow-Fligner post hoc test. Reprinted with permission from ref. [56]. Copyright 2015 Springer Science + Business Media.

property relationships should be viewed with great care. In our opinion, a careful study using a larger library of well defined POx with varying hydrophilic/lipophilic balance seems to be warranted to address this interesting and important point. As part of their research on PIPOx, Kronekova et al. observed a slight increase in apparent cell viability in P388 cells, which, according to the authors suggest the potential for immunomodulatory properties. This was backed up by a stimulatory effect of PIPOx on spleen cells [32].

Kyluik-Price and co-workers compared the ability of PEtOx and mPEG to protect blood cells from immune surveillance [63]. For this, both polymers were covalently grafted onto human red blood cells (RBC). The authors studied RBC morphology after grafting and report a slightly better result in the case of 30 kg/mol PEtOx compared to 30 kg/mol PEG. Apart from this, in the majority of experiments in this study, PEtOx and PEG were quite comparable. However, overall it was found that at similar surface grafting, mPEG exhibited superior immunocamouflage properties. This was demonstrated by antibody binding and phagocytosis of opsonized RBC. Testing the opsonization of PEtOx and PEG conjugated RBC, the PEG modified RBC outperformed the PEtOx modified RBC. Regarding the comparison of PEG and POx of various molar masses, we would like to note an important difference between PEG and POx. Often the argument is made that POx have a lower viscosity than PEG at the same molar mass. This is of course true, and obviously attributable to the fact that the PEG chain length is much greater than the POx chain length at the same molar mass. Whereas one repeat unit for both polymers has similar dimensions regarding extended chain length, the molar mass of POx repeat unit is much higher than that of PEG. For example, the molar mass of PEtOx repeat unit is 99 g/mol, while in PEG, each repeat unit accounts only for 44 g/mol. In other words, at the same molar mass, the extended polymer chain of PEG is about 2.5 times longer than that of POx. Not surprisingly, this should lead to a higher viscosity of PEG at the same molar mass. Apart from this, it would be interesting to test PMeOx in such assay, as PMeOx is more hydrophilic and slightly more comparable to PEG with respect to the molar mass of the repeat unit.

2.3. Systemic compatibility or stealth properties

In this chapter, we review the knowledge on systemic compatibility and stealth properties of POx based polymers. The biodistribution of hydrophilic PMeOx and PEtOx has been investigated before by Goddard et al. [64] as well as Jordan, Essler and co-workers [65]. Also, Woodle et al. reported very early on excellent biodistribution of POxylated liposomes [23]. More recently, Hoogenboom and co-workers revisited this issue. In one report, Wyffels et al. investigated the pharmacokinetic behavior of medium and high molar mass PEtOx and compared it to PEG [66]. The molar masses ranged from 5 kg/mol to 111 kg/mol for PEtOx and 20 kg/mol and 40 kg/mol for PEG. The polymers were labeled with ^{89}Zr and injected i.v. into mice. Not surprisingly and corroborating other studies, up to 20 kg/mol, the polymers were rapidly excreted via the kidneys. The overall biodistribution found was similar to previous work by Goddard, including uptake in the skin, with the exception that Wyffels found significant uptake in the spleen for 70 and 111 kg/mol PEtOx. In a follow-up study, Glasner and co-workers investigated the effect of labels on the apparent biodistribution [67]. Of course, the radiochemical purity and stability of the label is of great importance when assessing the biodistribution of labeled compounds. This was corroborated in this contribution, comparing ^{18}F and ^{89}Zr labeled 5 kg/mol PEtOx. The ^{89}Zr was complexed using desferioxamine, while ^{18}F was covalently attached. It was shown, that the apparent kidney uptake was much higher for the ^{89}Zr labeled polymers, compared to the ^{18}F labeled polymer, with most of the radioactivity being retained in the renal cortex, most likely being attributable to retention in the proximal tubules. Also in this respect, results from an earlier study using ^{111}In labeled PEtOx (5 kg/mol) [65] were corroborated.

Apart from the biodistribution of POx polymers themselves, polymer modified liposomes can be seen as a litmus-test for the respective polymer. As mentioned, Woodle reported long circulating liposomes employing POx lipopolymers early on [23]. Szoka, Frechet and co-workers revisited this issue and compared PEGylated and POxylated liposomes with liposomes bearing poly(-vinylpyrrolidone) (PVP), poly(hydroxypropylacrylate), poly(*N*,*N*-dimethyl acrylamide) (PDMA) and poly(*N*-acryloyl morpholine) (PAcM) [68]. Important to note, the size of the liposomes was very similar, but the dispersity differed notably, from PDI = 0.03–0.14, which is quite a significant difference. Most importantly, the biodistribution of liposomes was evaluated after single injection and after two consecutive injections spaced 6–8 days apart. After single injection, PMeOx (approx. 3 kg/mol as determined by mass spectrometry while the molar mass determined by GPC was much

higher) modified liposomes performed similar to PEGylated liposomes. Both outperformed all other liposomes in terms of circulation time ($t_{1/2} \approx 30$ h) and liver uptake (Fig. 7 A). An entirely different, essentially inverted picture presented when the labeled and polymer modified liposomes were injected a week after the first injection (Fig. 7 B). Here, both PEGylated and POxylated liposomes exhibited very short blood pool residence ($t_{1/2} < 2$ h), while the blood circulation of all other liposomes was essentially unaltered. Importantly, POxylated liposomes were unaffected by previous administration of PEGylated liposomes. The authors could connect the accelerated blood clearance with a pronounced increase in immunoglobulin M (IgM). Notably, these findings are somewhat contrasting data by Moreadith and co-workers, who could not elicit any antibody response for a copolymer of EtOx and 2-(pent-4-ynyl)-2-oxazoline (PynOx) [22]. Obviously, both materials were significantly different being a polymer modified liposome and a presumably unaggregated polymer chain, respectively. Moreover, in one case, essentially PMeOx was employed while a PEtOx copolymer was used in the other case. It should also be mentioned that some aspects of the polymer characterization are somewhat ambiguous. While the dispersities of the lipopolymers are quite low as determined by Maldi-ToF mass spectrometry, much higher values ($Đ = 1.2$ and 1.5, as determined by GPC) are found in the supporting information.

Apart from liposomes, nanoparticles have been coated with hydrophilic polymers to provide stealth properties and to improve their blood circulation. Bludau and co-workers investigated the POxylation (i.e. the covalent modification of another entity such as proteins, drugs or particles with POx) of tobacco mosaic virus particles with PMeOx and its effect on the circulation of the particles *in vivo* [69]. It was reported that POxylation afforded a higher degree of polymer coating of the virus particles, compared to PEGylation. This was tentatively attributed to a different degree of hydration of the two polymers. In accordance with the higher coating density, the POxylated virus particles were better shielded from antibody recognition, as assessed by ELISA assay. Similarly, uptake by RAW 264.7 macrophages was reduced for the POxylated virus particles compared to PEGylated ones. Subsequently, the clearance of the polymer modified virus particles was investigated *in vivo*. The data suggest a somewhat slower initial clearing for the POxylated particles compared to the PEGylated ones. However, the difference was not pronounced and the initial clearing half-lives were very short in both cases. Moreover, considering a potential reduction of the immunogenicity of the virus particles by the polymer, a repeated injection experimental setup would have been interesting.

Berke, Kampmann et al. reported on a novel strategy to radiolabel nanoparticles to investigate their biodistribution [70]. An amphiphilic and telechelic block copolymer (P[$MeOx_{31}$-*b*-(2-heptyl-2-oxazoline$_4$-co-$PynOx_5$)] = P[$MeOx_{31}$-*b*-($HeptOx_4$-co-$PynOx_5$) bearing a di-*tert*-butylfluorosilane moiety introduced via the initiator route was used as a reactive emulsifier. The micelles formed by the polymer were swollen with different amounts of 1,6-hexanediol dimethacrylate and subsequently crosslinked via free radical polymerization. The resulting nanoparticles ranged in size from 20 to 70 nm (hydrodynamic diameter) and were radiolabeled with simple isotope exchange using ^{19}F and investigated with respect to their biodistribution in tumor bearing (EMT6 shoulder grafts) mice using PET. Most of the injected nanoparticles ended up in the liver. While tumor-to-muscle ratio was reasonably high, the tumor-to-organ ratios in the organs of the mononuclear-phagocyte system were not quite promising. Tumor uptake was highest for 33 and 42 nm nanoparticles.

The biodistribution of an amphiphilic POx ABA triblock copolymer (10 kg/mol) with a modestly hydrophobic central B block (PMeOx-*b*-PBuOx-*b*-PMeOx) used as a drug carrier (*vide infra*) was investigated recently by He et al. [71]. The polymer was labeled using ^{64}Cu and biodistribution was evaluated by positron emission tomography (PET) and post-mortem necropsy. Interestingly, the biodistribution of the amphiphilic polymer mirrored that of a purely hydrophilic POx of the same molar mass. First-pass renal clearance with very little non-specific organ uptake was observed.

Kronek and co-workers also tested the toxicity of PEtOx and an amphiphilic copolymer P(EtOx-co-ButEnOx) to terrestrial plants, specifically seeds of *sinapis alba* [72]. No clear trends were found. In particular, at higher concentrations, no toxicity was found. At lower concentration, PEtOx with a DP of 100 exhibited some growth stimulation while P(EtOx-co-ButEnOx) (DP 100) exhibited growth inhibition, which were deemed significant. However, as $PEtOx_{200}$ exhibited growth inhibition in the same assay and any differences vanished at higher concentration, any deduction of actual structure-property relationships should be considered with utmost caution at this point.

2.4. Systemic toxicity

He et al. investigated the toxicity of PMeOx-*b*-PBuOx-*b*-PMeOx. In mice, the maximum tolerated dose was determined to be 500 mg/kg (i.v., q4dx4), corroborating the excellent biocompatibility profile of POx reported in other studies. For single

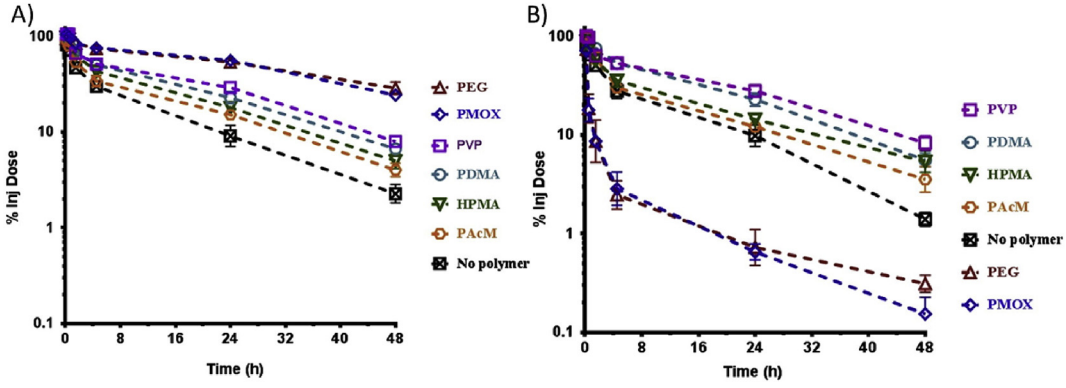

Fig. 7. Comparison of biodistribution (here: blood circulation) of polymer modified liposomes after a single injection (A) and a second injection one week after a first injection (B). Polymers investigated were poly(ethylene glycol) (PEG), PMeOx (here PMOX), poly(vinylpyrrolidone) (PVP), poly(hydroxypropyl acrylamide) (HPMA), poly(*N*-acryloyl morpholine) (PAcM) and poly(dimethyl acrylamide) (PDMA). As control, liposomes without lipopolymer modification were also studied. Reprinted with permission from ref. [68]. Copyright 2015 Elsevier.

administration, even higher doses were tolerated. Clinical chemistry and histology of major organs showed no major effects of the polymer after injection in Balb/c mice at MTD [71]. Also, neither platelet aggregation, hemolysis nor complement activation was observed at concentrations up to 1.52 g/L. On the one hand, this concentration is not particularly high, but since the polymer enables very high drug loading (*vide infra*) of approx. 50 wt%, this corresponds to a very high drug dose that can be safely administered. The blood coagulation parameters prothrombin time and thrombin time were not affected while the activated partial thromboplastin time was significantly prolonged. We would like to remind the reader, that Tauhardt et al. observed a similar effect for zwitterionic POx [51] but not for PEtOx (*vide supra*).

Akbulut and co-workers investigated the effects of PEtOx exposure on the development of ovarian follicle of zebrafish (*Danio rerio*) [73]. Unfortunately, the authors did not give any information regarding the used PEtOx, neither source, purity, molar mass nor dispersity are provided. Nevertheless, these studies appear to be the first studies of POx in zebrafish. Two concentrations of PEtOx in the aquaria were tested (10 mg/L and 50 mg/L) with exposure of 5 days. Such concentrations are well below the concentrations, for which any cytotoxicity would be expected in cell culture. The authors report that PEtOx induces apoptosis and inhibits oogenesis in female zebrafish. Even though the work by Akbulut lacks fundamental aspects of scientific work such as proper identification of materials studied, it would be interesting if these results could be reproduced using defined POx and different POx with variable molar mass.

One obvious application for hydrophilic polymers in a biomedical context are hydrogels. In turn, hydrogels are very interesting materials for an intraocular usage. For this purpose, it is necessary to investigate the respective long term *in vivo* biocompatibility. In 2013, Hwang et al. published a comparative study investigating the intraocular biocompatibility of PEtOx-*b*-poly(ε-caprolactone)-*b*-PEtOx (ECE), Matrigel® and Pluronic® F127 in albino rabbits [74]. After 2 weeks, Matrigel as well as Pluronic® F127 dispersed in the vitreous (Fig. 8 left side, Row B). In contrast, ECE hydrogel was still detectable. Furthermore, severe cataract with iris atrophic change was found in eyes containing Matrigel® or F127 two month after injection. (Fig. 8 Insert, Row C). The authors attribute the ocular toxicity of Matrigel® to its biological origin (mouse-derived) while the cause of toxicity of F127 is unknown. Optical coherence tomography (OCT) revealed that the retina of the F127 and Matrigel® treated eyes were atrophic, whereas the retinal thickness of the ECE containing eye was still comparable to the control. Furthermore, electroretinography (ERG) was examined to evaluate the physiological retinal functions. Again significant decrease of the photoreceptor signals were observed for the Matrigel® and the Pluronic® treated eyes, while ECE injection revealed no significant changes compared to pre-injection. Furthermore, retinal histology demonstrated neither necrosis nor morphological changes in the ECE eyes. In contrast, the Matrigel® and the Pluronic® eyes showed signs of neuroretinal toxicity. The drastic loss of photoreceptors after injection of Matrigel® or Pluronic® was visualized via TEM micrographs (Fig. 8 right side) supporting the ERG results. The ECE eyes showed similar morphology as the control group. These results highlight the potential of POx-based hydrogels for biomedical applications while at the same time illustrates major issues for Pluronic® based gels or even Matrigel® which are both used widely in tissue engineering and biology *in vitro*.

2.5. Degradability

Every time exogenous materials are brought into the body, the question of their removal and degradability needs to be asked. As already mentioned above, POx are amendable to acidic and basic hydrolysis. However, at physiological conditions no significant hydrolysis was observed in simulated stomach and intestine fluid [55]. Of course, this is not the only possibility for the degradation of polymers. Another mechanism, relevant in a biological context is oxidative degradation by reactive oxygen species (ROS). Despite the fact that ROS are of major importance in physiological and pathophysiological processes, generally little information can be found in the literature on the oxidative degradation of hydrophilic polymers/biomaterials in water. Although PEG and POx are in most cases regarded as non-biodegradable, PEG is long known to be sensitive to oxidative degradation [27,75]. Without giving any experimental data, Viegas et al. suggest that POx do not form

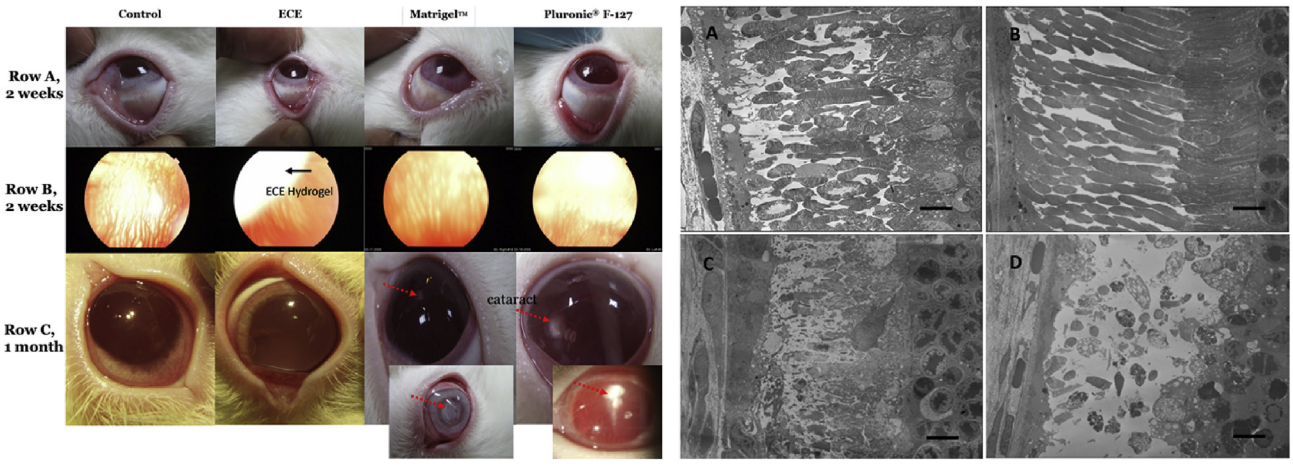

Fig. 8. Left Side: (**Row A**) External photos of control, 20 wt% PEtOx-*b*-poly(ε-caprolactone)-*b*-PEtOx (ECE) hydrogel, Matrigel®, and Pluronic F127® at two weeks after injection (from L to R). (**Row B**): The fundus oculi of control, 20 wt% ECE hydrogel, Matrigel, and Pluronic F127® at two weeks after injection (from L to R). (**Row C**) The external color photos of control, 20 wt% ECE hydrogel, Matrigel, and Pluronic F127 for ocular media at one month after injection (from L to R). The red arrows indicate the cataract formation. The black arrow indicates the ECE *in situ* hydrogel formation. The inset photo of Matrigel is at two months after injection, which had a denser cataract formation and perilimbal ciliary injection. The inset photo of Pluronic F127® is the high magnification of the cataract.
Right Side: TEM micrographs of the outer retina, which demonstrates the morphology of outer nuclear layer (cell body of rod and cone cells). The control eyes (A), the 20 wt% ECE hydrogel (B), Matrigel® (C), Pluronic F127® (D) after two months of injection. (C) and (D) demonstrate more cell loss than ECE and control eyes. (scale bar is 6.1 μm). Reprinted with permission from ref. [74]. Copyright 2013 Public Library of Science (PLOS).

peroxides as PEG does [76]. In contrast, Luxenhofer and co-workers reported that PEG, POx and POI are degradable by oxidative degradation under conditions that have been claimed biologically relevant by others [77]. For their study, PEG, PEtOx and the watersoluble polypeptoid poly(*N*-ethylglycine)s with molar mass ranging from 2 to 11 kg/mol were used. The development of the apparent molar mass after incubation with different concentration of reactive oxygen species (ROS), generated from H_2O_2 and Cu(II) as catalyst, was determined as degradation. Surprisingly, the results show that PEG is the most stable of the three at peroxide concentrations below 50 mM, while there was no difference in the absence of catalyst. It was also found that the apparent degradation rate was dependent on the DP and molar mass, respectively. More recently, this study was expanded to higher molar masses and also to include poly(*N*-vinylpyrrolidone) (PVP) [78]. The trend that higher molar masses are degraded faster was corroborated, as was the result that PEG is more stable in this assay than PEtOx. These observations stand in contrast to the notion by Viegas and also to a report by Pidhatika et al., that showed that POx-modified surfaces retained their non-fouling character longer than PEG-modified ones when challenged with oxidative stress [79]. Taken together, these studies only begin to let us understand the stability of POx against oxidative degradation, and it is important to note that the actual concentration of ROS *in vivo* is difficult to assess and may be highly variable.

Recently, Luef et al. investigated the degradation of a poly(-$EtOx_{100}$-*co*-$NonOx_{50}$-*co*-$ButEnOx_{30}$) based hydrogel (UV-cross-linked with glycol dimercaptoacetate) at various pH values in the presence and in the absence of esterases [80]. Degradation was quantified through the release of encapsulated Eosin B (8 mg Eosin B per 2 g copolymer) by UV/Vis absorption. At the lowest investigated pH of 4, no degradation could be observed even after 2 weeks in the absence of enzymes. At pH 6 slight degradation started approx. after 8 days storage and after 14 days, 10% Eosin B were released. In general, the rate of dye release increased with increasing pH. However, still only modest release of 20% Eosin B occurred after 14 days at pH 10. Interestingly, degradation in the presence of rabbit liver esterase (RLE) at pH 8 was found to be very close to enzyme-free degradation at pH 10. The by far highest degradation was realized with porcine liver esterase (PLE) at pH 8 (Fig. 9). Unfortunately, the authors did not suggest any explanation, as to why PLE is more effective than RLE.

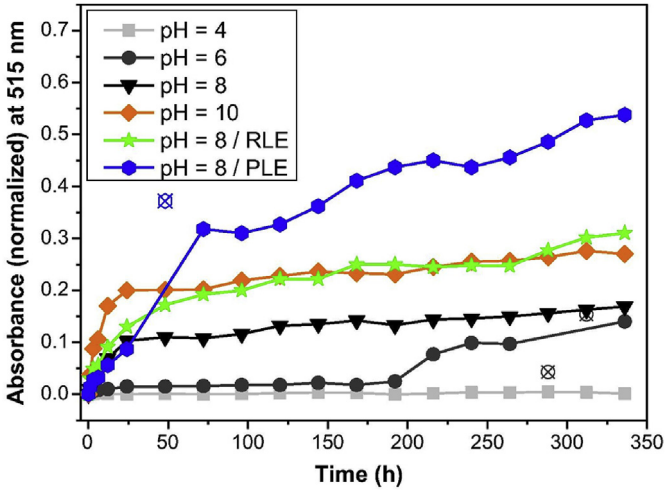

Fig. 9. (Normalized) Absorbance at 515 nm for the quantification of the released dye Eosin B during degradation studies of cross-linked poly($EtOx_{100}$-*co*-$NonOx_{50}$-*co*-$ButEnOx_{30}$) at different conditions. Reprinted with permission from ref. [80]. Copyright 2017 Elsevier.

Very recently, Kronek and co-workers also investigated the issue of degradability of POx using activated sludge (OECD guideline 209) [72]. Four different polymers were investigated, PEtOx and an amphiphilic copolymer P(EtOx-co-ButEnOx) with targeted DPs of 100 and 200 each. It should be noted that the synthesis of the higher degrees of polymerization apparently proved challenging, as the determined molar masses were much lower than expected, in case of $PEtOx_{200}$, the M_n (determined by GPC) was actually lower than that of $PEtOx_{100}$. The authors tested to oxygen consumption of activated sludge in the presence and absence of POx and found no difference, suggesting that these POx and perhaps POx in general cannot be degraded by activated sludge.

Summarizing the knowledge on safety of POx and interaction with biological systems, one can state that in general the picture has become much more detailed in the last few years. It has become evident beyond reasonable doubt that POx can be designed such that further development POx-based biomaterials into actual products seems feasible. However, some studies are raising important questions and indicate that, at least in certain circumstances, POx may not be able to overcome limitatios seen also in other systems. Of course, any new material must always be thoroughly studied and scrupulously tested with respect to its safety. This process often starts with simple cytocompatibility studies. In this context, we'd like to posit a few comments and suggestions. First, it is always advisable to test new materials up to maximal concentrations possible in a given assay. In many reports, authors test their polymers only to a few hundred mg/L and deduce general biocompatibility from such miniscule concentrations. It is obvious that different cell lines may give a very different read-out, some may be robust, others may be more sensitive. Regarding endocytosis studies, also too often one finds very basic experimental protocols, where only one or a few concentrations and/or few time points are studied. A full concentration range is a prerequisite to properly assess concentration-dependent effects. The question of medium and long-time fate of POx in a biological and environmental context is insufficiently understood and should be studied with carefully designed experimental protocols. No doubt, the community will be following the further development of SER-214 very closely. To the best of our knowledge, at least four more companies (apart from Serina Therapeutics Inc.) have recently started evaluating commercial development of POx. In combination with the recently boosted academic interest, one can expect much more detailed information on the safety of POx in the near future.

3. POx-based hydrogels in biomaterials

In recent years, many excellent reviews have described the importance of hydrogels as soft biomaterials in tissue engineering, medicine as well as for the new and upcoming field of biofabrication [17,81–83]. In general, any watersoluble polymer can serve as a basis for hydrogels after cross-linking. Accordingly, POx-based hydrogels have been established for decades. Chujo and co-workers reported in a series of papers on POx based hydrogels [84–91]. In this series, thermo- and redox-responsive POx-based hydrogels were pioneered. Due to their good cytocompatibility, combined with tunable physicochemical properties, hydrophilic POx are ideally suitable as hydrogel based biomaterials. This was already summarized in a comprehensive review by Hartlieb et al. in 2015 [18] in which the authors focused on chemically cross-linked gels. These are polymeric networks based on covalently cross-linked macromolecules. According to the authors, POx-based hydrogels can be subdivided into three main classes: (1) polymeric networks that are formed *in situ* by the copolymerization of mono- and bis-functional monomers, (2) hydrogels prepared via

the macro-monomer method using α,ω-functionalized POx bearing polymerizable groups such as methacrylates, and (3) hydrogels which are synthesized from POx comprising different reactive side- and end-group moieties in combination with multifunctional crosslinkers. Alternatively, gels can be formed based on physical interactions including hydrogen bonding, ionic interactions or hydrophobic interactions between the individual polymer chains. In 2012, Wiesbrock and co-workers published an excellent overview including these topics [16]. Very recently, Dargaville et al. published another excellent review specifically on POx based hydrogels [92]. In the present review, we want to highlight recent developments of POx-based hydrogels in the context of biomaterials. Thus, we outline the potential of these soft materials for possible biomedical applications.

Depending on the desired application, a biomaterial has to fulfill various requirements. From a biological point of view the requirements typically include not being cytotoxic or even being bioinstructive. Furthermore, the mechanical properties are a critical parameter that needs to be adjustable, ideally from very soft to stiff gels as this can influence cell differentiation as was already shown for PEG-based and other hydrogels [93]. As already mentioned in the previous chapter, POx homopolymers as well as POx- and POzi copolymers are typically highly cytocompatible in solution. However, cytocompatibility needs to be verified for *in situ* cross-linked gels in detail. Zahoranová et al. synthesized a series of hydrogels from EtOx and three different bis(2-oxazoline) crosslinkers with increasing hydrophobicity - 1,4-butylene-2,2′-bis(2-oxazoline) (ButBisOx), 1,6-hexamethylene-2,2′-bis(2-oxazoline) (HexBisOx) and 1,8-octamethylene-2,2′-bis(2-oxazoline) (OctBisOx). The resulting hydrogels were investigated with respect to their cytotoxicity toward murine fibroblasts and pancreatic βTC3 cells [94]. By elucidating contact as well as extract toxicity studies, the authors found that hydrogels with low crosslinking density were most suitable. At crosslinker content of 3% and higher, the nature of the crosslinker seemed to have little effect (Fig. 10 A). Very recently, Šrámková et al. published a comparable study in which they investigated cytotoxicity and mechanical characteristics of hydrogels prepared by photo induced thiol-ene “click” reactions [95]. However, we want to emphasize that Dargaville and co-workers first introduced thiol-ene cross-linked hydrogel formation in 2012 [96]. Šrámková et al. used four different dithiol crosslinkers with varying chain length. The necessary double bond bearing monomer ButEnOx, was randomly copolymerized in different ratios with MeOx or EtOx to create a reliable data base. They found mean cell viability around the threshold of 75%, with no significant differences for all prepared hydrogels (Fig. 10 B).

It is important to note, that the above discussed studies investigated the interaction of cells covered by a hydrogel disk. In order to promote cell adhesion to hydrophilic polymers in general and also to hydrogel matrices, a functionalization of the material with adhesion-mediating peptide sequences is often required. In this context, the tripeptide arginine-glycine-aspartic acid (RGD) sequence is frequently utilized. In 2013, Farrugia et al. presented the first study dealing with the cell-adhesion of RGD-functionalized POx hydrogels [97]. Copolymers of MeOx and 2-(dec-9-enyl)-2-oxazoline (DecEnOx) were prepared and RGD functionalized via UV-mediated thiol-ene reaction, utilizing dithiothreitol (DTT) as cross-linking agent and Irgacure 2959 (I2959) as photoinitiator. Subsequently, the polymer-chains were cross-linked using again UV-mediated thiol-ene reaction utilizing the remaining alkene-functions. Cell-attachment to the fabricated hydrogels was evaluated after 3 days of incubation with fibroblasts. The RGD-functionalized gels showed significantly higher cell-attachment compared to the control-groups (no-; 2-mercaptoethanol-; RDG-functionalization) confirming the superiority of the RGD functionalized material. Changing the RGD-loading did not significantly influence the number of adherent cells but higher amounts resulted in a better alignment of the cells (Fig. 11).

The curing time, light-power and initiator concentration were optimized to decrease cytotoxicity, which allows the hydrogel curing in presence of cells. The cell viability after curing was high with values of 80–90% but only if a bis-cysteine RGD peptide was utilized as cross-linking agent, supporting the cytocompatibility of the process and allowing direct incorporation of cells. Although these results are promising, the authors also pointed out that the relatively high stiffness of the gels (3.4–4.5 kPa) and the lack of degradation sites might hinder the applicability of the material as, e.g. 3D-cell supports. Shortly thereafter, Schenk et al. presented a report on RGD-functionalized POx gels showing enhanced adhesion of $\alpha_v\beta_5$-expressing cancer cells *in vitro* [98]. In this study EtOx, NonOx, and DecEnOx were *in situ* cross-linked, utilizing the bis-functional monomer ButBisOx. Again, the incorporated DecEnOx was used for further functionalization of the prepared material via thiol-ene reaction. A library of 25 gel compositions with varying monomer ratio and crosslinking degree was prepared. The swelling degree was determined in water, ethanol and DCM. Pure PEtOx

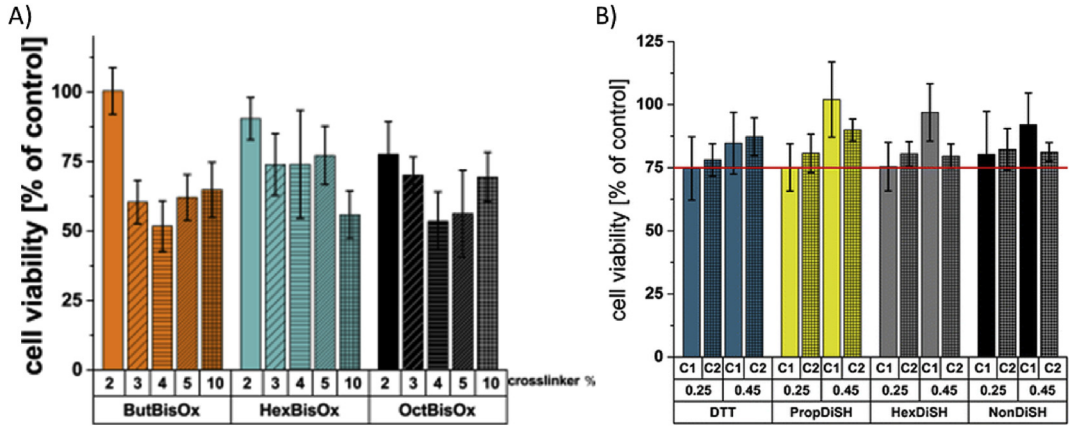

Fig. 10. Direct contact toxicity of hydrogels prepared A) *in situ* using EtOx and 1,4-butylene-2,2′-bis(2-oxazoline) (ButBisOx), 1,6-hexamethylene-2,2′-bis(2-oxazoline) (HexBisOx) or 1,8-octamethylene-2,2′-bis(2-oxazoline) (OctBisOx) as crosslinker or B) by using thiol-ene “click” reactions. MeOx (C1) and EtOx (C2) were randomly copolymerized with 2-(3-butenyl)-2-oxazoline and cross-linked with dithiothreitol (DTT), 1,3-propanedithiol (PropDiSH), 1,6-hexanedithiol (HexDiSH) or 1,9-nonanedithiol (NonDiSH). A) Reprinted with permission from ref. [94]. Copyright 2015 John Wiley & Sons. B) Reprinted with permission from Ref. [95]. Copyright 2017 Springer Science + Business Media.

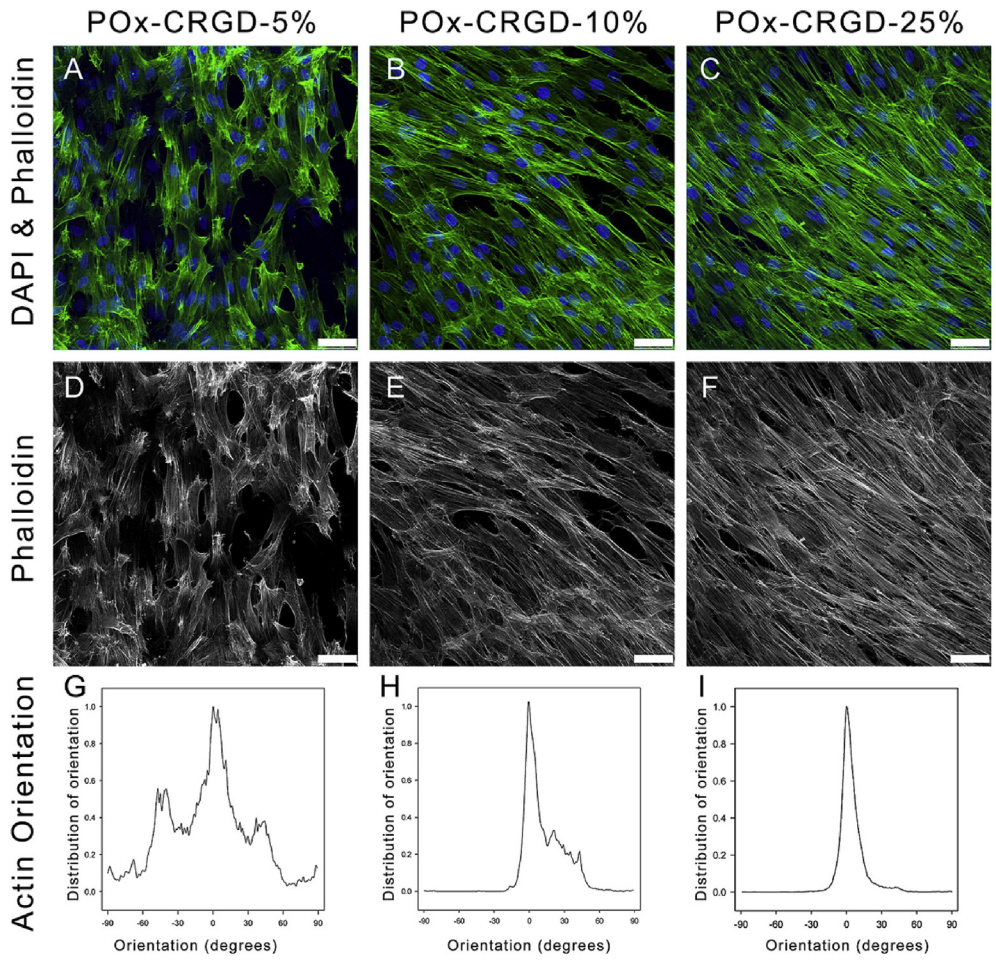

Fig. 11. Comparison of fibroblast adhesion and morphology to POx hydrogel surfaces with increasing amount of cell adhesion peptide: (A, D) 5% CRGDSG, (B, E) 10% CRGDSG, (C, F) 25% CRGDSG. For immunofluorescent analysis (A, B, and C), samples were stained with phalloidin and DAPI for visualization of actin and nuclei, respectively. Actin-only channel from immunofluorescent analysis is shown in panels D, E, and F. Scale bar = 50 μm. Actin alignment (G, H, and I) of fibroblasts adhered to the surface of POx hydrogels with increasing amount of RGD incorporated. Reprinted with permission from ref. [97]. Copyright 2013 American Chemical Society.

hydrogels exhibited comparable swelling degrees (SWD) in all three solvents (max. SWD in water: 8.0) and are therefore identified as amphigels, which was already noted by Chujo [85]. Due to the increased hydrophobicity of the longer 2-oxazoline side-chains, all other gels showed much lower swelling in water. These amphi-to lipogels could be successfully loaded with fluorescein isothiocyanate (FITC), serving as a model compound, either during or post synthesis. In water, the lipogels showed no release of the incorporated molecules. Selected gels were ground in a ball mill (in aqueous suspension) to yield particles with broad size distributions ranging from <1 to 100 μm. Unfortunately, these particles tended to aggregate irreversibly and could only be handled in aqueous dispersion for a limited amount of time. Subsequently, the particles dispersions were functionalized with RGD motives and it was shown via scanning electron microscopy with energy dispersive spectroscopy (SEM-EDS) that the functionalization occurred preferentially on the bead surface. Cell adhesion tests with the prepared materials were performed using endothelial EA.hy926 cells and human pancreatic cancer BON cells. The RGD functionalized gels showed significantly higher adhesion to the cancer BON cells compared to the endothelial EA.hy926 cells. It is important to note that adhesion of the two cell types was investigated in two independent experiments. Target specific drug delivery is envisioned as a potential application for this material. However, as mentioned by the authors poor colloidal stability and the lack of degradation sites are challenges that have yet to be addressed. Also, the reported size range seems very problematic for intravenous application, even considering the relative softness of the hydrogel particles. In addition, it must be considered that for a majority of tumor targeting applications the particles would have to leave circulation, which will be almost impossible for such large particles.

Due to the manifold synthetic possibilities using POx, specific side chains can be incorporated into the polymer to bind and release particular biological molecules like DNA. By using a 3D matrix like a POx-based hydrogel, the loading capacity can be increased multiple times compared to two-dimensional DNA chips [99,100].

Hartlieb et al. published two papers, in which the use of a statistical copolymer of EtOx and a 2-oxazoline monomer with a tert-Butyloxycarbonyl (Boc) protected amino group in the side chain - 2-(4-((*tert*-butoxycarbonyl)amino)butyl)-2-oxazoline (BocABuOx) - was reported to implement the positive charge required to immobilize negatively charged gene material [101,102]. After deprotection, the hydrogel was formed by crosslinking the copolymer with epichlorohydrin (ECH) in aqueous sodium hydroxide solution. Although a certain amount of amino functionalities is consumed during cross-linking, the remaining primary amines as well as the formed secondary and tertiary amines are sufficient for the envisioned application, making this approach very interesting. In a first approach, the authors used the ethidium bromide assay to

investigate the interaction of DNA and cationic polymer by measuring the fluorescence intensity [101]. No clear correlation between the percentual amount of amino groups in the gel and DNA complexation was found. DNA-release studies were carried out using the polyanion heparin, which is often used for this purpose, followed by the assay. A rapid but incomplete release was detected for all samples.

In the follow-up paper, the same synthetic approach was employed. Additionally, a matrix supported composite gel was synthesized [102]. For preparation of the host network, a porous polyethylene or polypropylene filter substrate (Fig. 12 A) was incubated in a basic aqueous polymer solution containing ECH (ratio ECH/amine: 33, 66 and 100%). After crosslinking, a second component consisting of POx hydrogel beads could be detected within the host matrix. (Fig. 12 B–D). DNA binding was investigated using Cy5 labeled DNA allowing the direct measurement of location and concentration of the labeled DNA by microscopy and spectroscopic techniques. The authors were able to convincingly show the DNA binding to the POx hydrogel while any influence of the PP or PE matrix could be excluded. Regarding the release, they tried to avoid using heparin that is usually used to regain DNA as it acts as an inhibitor in PCR. Alternatively, changes in temperature and pH-value were investigated as potential release triggers. However, no sufficient release could be detected using either stimuli.

Another approach to incorporate positively charged segments into a cross-linkable copolymer was demonstrated by Englert et al. [103]. Initially, PEtOx with a molar mass of 50 kg/mol was fully hydrolyzed yielding L-PEI and subsequently 3-butenyl side chains were introduced. A small library of nine polymers with a L-PEI content between 5% and 100% was characterized by GPC and NMR before six hydrogels were synthesized. The hydrogels were formed by a thiol-ene photoaddition reaction using 3,6-dioxaoctane-1,8-dithiol as crosslinker and 2,2-dimethoxy-2-phenylacetophenone as initiator. DNA binding and release was investigated utilizing the above described assay. In contrast to gels bearing the positive charge in the side chain [101], a trend dependent on the PEI content could be observed. The gel with the highest amount of PEI (62 mol %) showed the highest DNA binding capacity. Interestingly the polymer with PEI content of 36% showed no DNA binding.

Overall, these studies showcase the potential of POx-based hydrogels for biomedical applications, not least due to the rich possibilities their chemistry offers. However, as the DNA release is rather restricted at the moment, there is still need for a design that could be useful in practice.

In biomaterials, the protection of bio(macro)molecules against aggregation and degradation often plays a critical role. Hartlieb et al. demonstrated that *in situ* formed PEtOx networks can stabilize Factor VIII, an essential coagulation factor in humans [104]. A small library of four different polymers with a monomer to initiator ratio of 200 and a BisOx content of 4% (sample 4), 5% (sample 5), 7.5% (sample 6) and 10% (sample 7) was synthesized (Fig. 13). Factor VIII was incorporated into the gels and its activity tested over time. After 2 days, less than 10% of the protein was active in the reference (stock solution in falcon tube) and without gel. In contrast, at least 50% activity could be determined when using PEtOx hydrogels. Particularly, the sample with 7.5% crosslinker showed a well

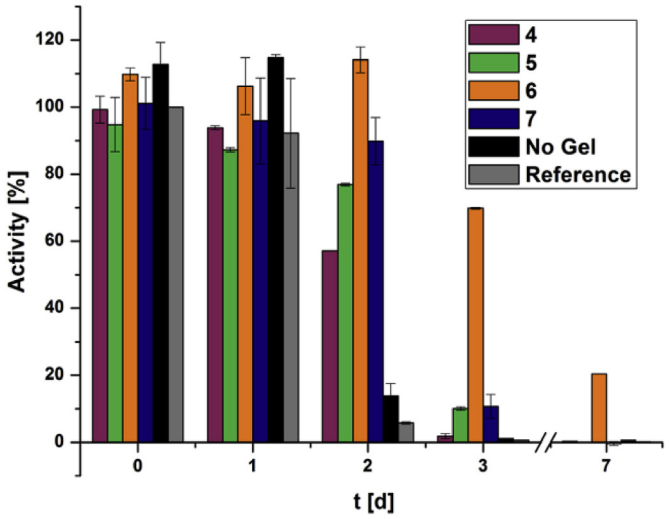

Fig. 13. Activity of Factor VIII depending on the storage time (0–7 days) in different PEtOx hydrogels. Reprinted with permission from ref. [104]. Copyright 2015 John Wiley & Sons.

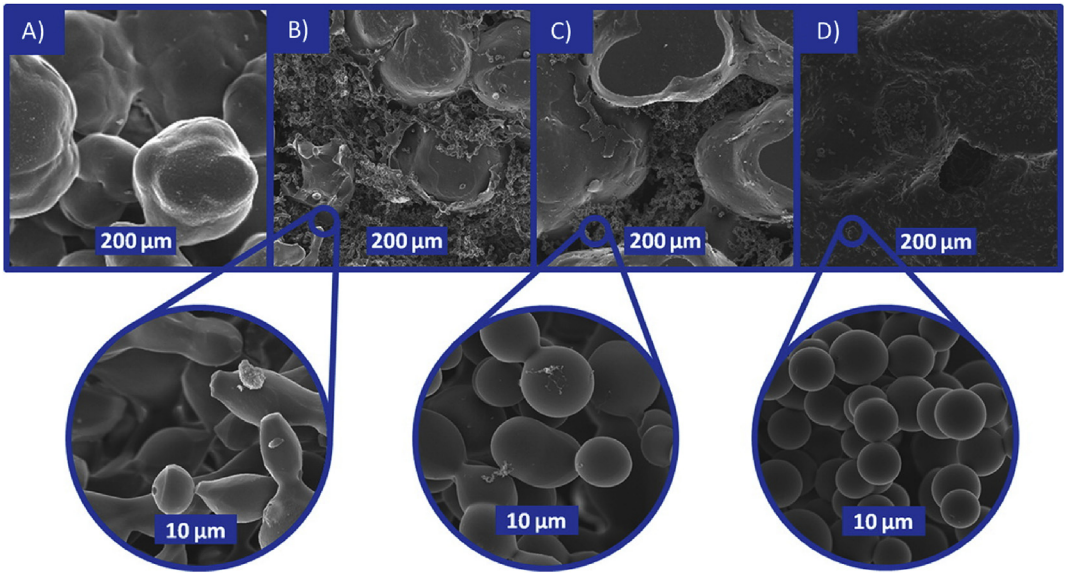

Fig. 12. SEM pictures of A) PP host structure with large pores and B) - D) PP-based POx-hydrogel composites with increasing (33%, 66% and 100%) epichlorohydrin to amine ratio. The magnified images show the appearance of hydrogel beads with a diameter of 5–10 µm. Adapted with permission from ref. [102]. Copyright 2014 American Chemical Society.

pronounced stabilization with a value of almost 20% after 7 days. The authors suggest that the different degree of crosslinking and the associated change of swelling degree and pore size might influence the interplay of factor VIII and the POx based hydrogel. It would be interesting to study how the side chain influences the stabilization properties and if a comparable effect can be observed for other biomacromolecules too.

Tiller and co-workers published a series of papers investigating the increasing specific enzyme activity of different enzymes dispersed in organic media [105–107], which revisits the issue of enzyme interaction with amphiphilic POx, investigated by Naka et al. two decades ago [108]. Their first approach was to use amphiphilic polymer co-networks (APCN) comprising PEtOx and poly(2-hydroxyethyl acrylate) (PHEA). Lipase was entrapped during photopolymerization and swelling degree of the resulting free-standing membranes as well as enzyme activity were examined [105]. In comparison to a literature known PHEA-*l*-PDMS co-network, a significant increase in specific activity up to 6-fold was found. However, the described APCN are not nanostructured, strongly limiting diffusion mechanisms. To address this problem, Schoenfeld et al. prepared enzyme containing PHEA-PEtOx films which were subsequently milled and sieved to obtain microparticles with narrow size distribution [106]. Furthermore, another particle system consisting of PHEA and PDMS (50/50, w/w) was prepared via suspension or aerosol polymerization. Utilizing these particles, the activity of α-Chymotrypsin increased with decreasing particle diameter in *n*-heptane. Additionally, PHEA-PEtOx microparticles showed an almost tenfold higher carrier activity with a lower enzyme content compared to commercially available products. However, even for the smallest particles a diffusion limitation of the reaction was observed. In a follow-up paper, the origin of the enzyme activation was investigated in more detail [107]. Therefore, two different APCN comprising PMeOx and butyl acrylate (BuAc) or 2-ethylhexyl acrylate (EhAc), respectively, were synthesized (Fig. 14). According to the authors, the former swells in toluene but not in *n*-heptane whereas the latter swells in both solvents. The lipase from *C.antarctica* lipase (CalB) was incorporated during the polymerization step and the activity was tested in both solvents. It was found, that the activity increases between 0 and 50 wt% acrylate, which is, according to the authors, in accordance to the required interconnectivity of the hydrophobic phase for optimal substrate accessibility to the enzyme in the hydrophilic phase. In PBuAc-*l*-PMeOx the maximal activity changes from 1900 U/g (*n*-heptane; swelling degree ~ 1.1) to 3500 U/g (toluene; swelling degree ~ 2.5) which is 6 and 24 times higher than the suspended enzyme powder in *n*-heptane or toluene, respectively. By using two systems with different swelling behavior, it was possible to demonstrate that the swelling degree as well as the nanostructure are highly relevant for enzyme activation. It would be interesting to repeat the approach employing these co-networks as microparticles. More recently, enzymes were also incorporated into electrospun PEtOx fibers [109]. Also, PEtOx coatings were used by Ross et al. for stabilization of ink-jet printed insulin on steel microneedles [110]. Compared to other formulations (gelatin, trehalose dehydrate, poly(caprolactame)-*co*-poly(vinyl acetate)-*co*-PEG) used, PEtOx showed strong interactions (as observed by circular dichroism) with insulin along with poor release profiles. The observed destabilization is in contrast to the well pronounced stabilization of Factor VIII discussed earlier.

Very recently, POx based hydrogels were applied as bioink for the first time [35]. Lorson et al. developed an adjustable and thermoresponsive polymer platform based on an amphiphilic diblock copolymer comprising a hydrophilic PMeOx and a thermoresponsive P*n*PrOzi block. Synthetically, the transition between POx and POzi was possible without problems as verified by GPC and NMR-spectroscopy. The gelation temperatures (T_{gel} 15 °C - 35 °C) of the optically clear gels increased with increasing polymer chain length (at the same PMeOx/P*n*PrOzi ratio). The properties and the nanostructure of the resulting gels were investigated utilizing rheology, viscometry and small angle neutron scattering (SANS). Additionally, a simple two layered mesh was printed with (Fig. 15 A) and without embedded cells (NIH 3T3) (Fig. 15 B & C) showing an excellent cell survival rate of over 90% after 24 h (incubation at 37 °C and 5% CO_2) post printing (Fig. 15 D). No significant difference could be observed between the printed cells and the control (cells redispersed in the bioink but not printed).

However, using the selected experimental parameters, it was not possible to increase the height of the printed construct, which would be necessary if more complex structures should be printed. Although, this might be possible by increasing the polymer concentration. The limited shape fidelity notwithstanding, the (preliminary) high cytocompatibility, easy and reproducible preparation, reversible gelation with sufficient high gel-stiffness makes this material a promising candidate for potential

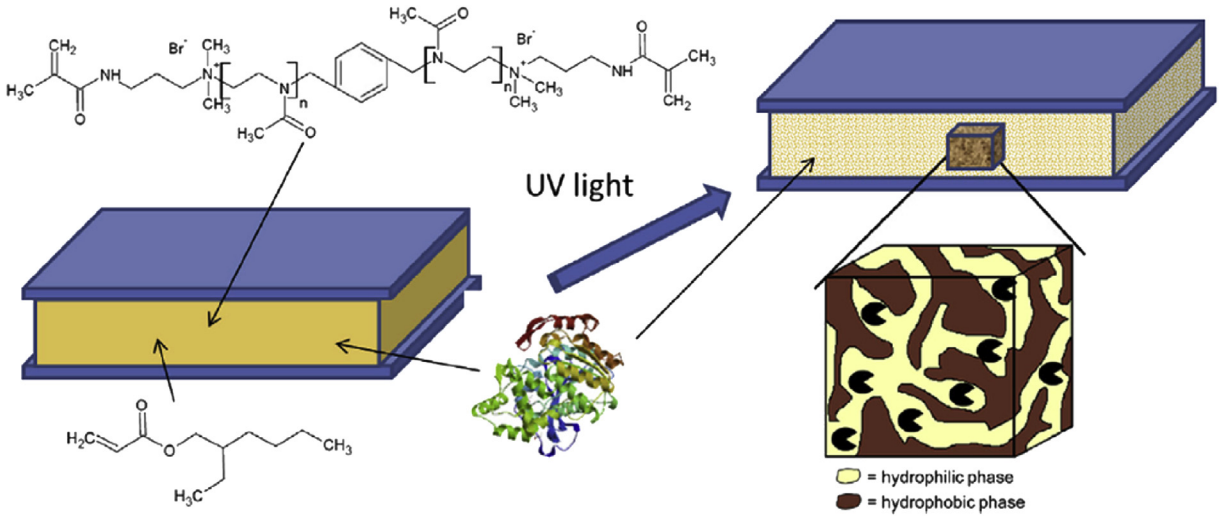

Fig. 14. Schematic illustration of lipase entrapment into an amphiphilic polymer co-networks (APCN) during polymerization on the example of a poly(2-ethylhexyl acrylate)-*l*-PMeOx APCN. Reprinted with permission from Ref. [107]. Copyright 2015 Elsevier.

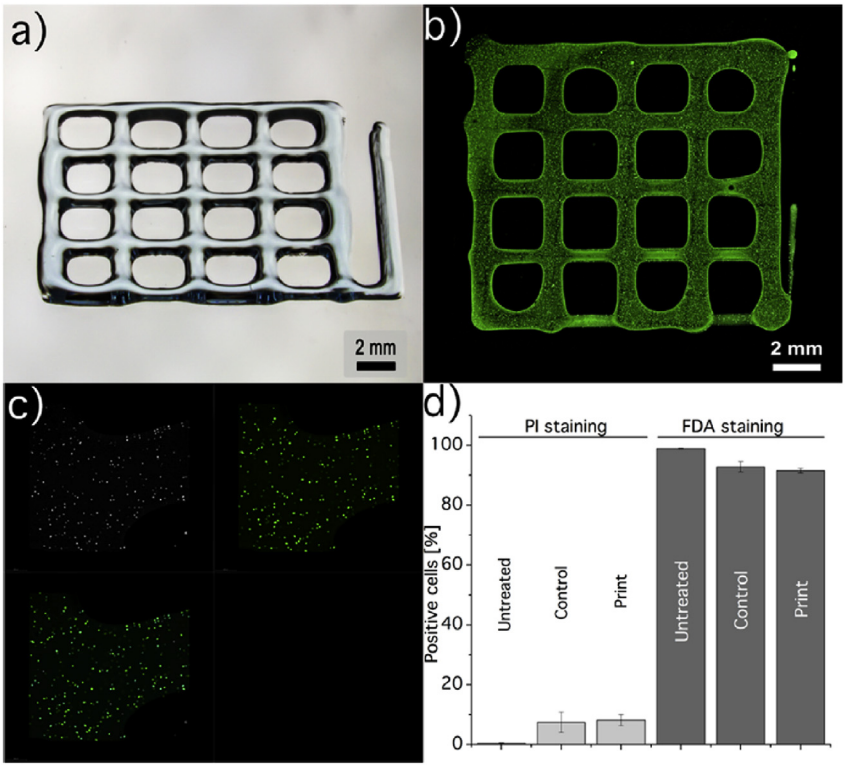

Fig. 15. (a) Light microscope image of a printed constructs composed of orthogonal stacks of hydrogel strands with a base area of 12 × 12 mm^2 and a strand-center to strand-center distance of 3 mm. (b) Cell-ladden constructs and (c) detailed view showing cell nucleus stained with Hoechst dye (top left), FDA stained cells (top right), and an overlay image (bottom left). (d) Results of flow cytometric analysis on the influence of the printing process on the viability of NIH 3T3 fibroblasts. While the untreated control represents cells in medium, the control represents cells that were redispersed in the bioink but not printed. Reprinted with permission from ref. [35]. Copyright 2017 American Chemical Society.

applications not only in the field of biofabrication and tissue engineering, but also for drug delivery.

Another thermogelling POx-based hydrogel was developed by Grossel and co-workers [111]. The thermoresponsive part was realized by grafting amine-capped PiPrOx or P(*i*PrOx-*co*-*n*BuOx) onto the hydrophilic backbone carboxymethylcellulose. Unfortunately, in contrast to the PMeOx-*b*-P*n*PrOzi based hydrogels, these gels became opaque in the solid state. This might be a drawback regarding the analysis of cells using microscopy. The gelation temperature for polymers bearing P*i*PrOx side chains was found to be above 49 °C, which is obviously too high for biological applications. However, using P(*i*PrOx-*co*-*n*BuOx), the gel temperature could be decreased to 29 °C at 4 wt%, demonstrating the advantage of simple LCST tuning of POx using copolymers comprising different monomers [3]. However, the storage (G′) and loss (G″) moduli of these gels were rather low (10 Pa - 20 Pa), limiting the applicability of these gels for e.g. biofabrication. On the other hand, this low stiffness could be beneficial for e.g. neuronal cell culture. Increasing the polymer content to 10 wt% led to a decrease of the gelation temperature to 20 °C (increase in G′ was mentioned, but no data was provided). A decrease of the storage modulus from 10 Pa to 2 Pa was observed after two week storage at both pH 3 and pH 7. The authors claim the gels to be mechanically stable but the reported moduli do not support such claim.

One of the most critical points in artificial tissue construction is the issue of vascularization. Especially for larger constructs, this issue has paramount importance. A very interesting approach to address this problem was presented recently by Dargaville and coworkers. A copolymer comprising PEtOx and PButEnOx was employed for the fabrication of hydrogels containing microchannels [112]. Woodpile-like PCL scaffolds with a fiber diameter of 28 ± 5 μm, a fiber spacing of 200 μm and a stacking height of 220 μm were produced via melt electrowriting (MEW) [113] (Fig. 16 A). These scaffolds served as sacrificial template and were embedded into an aqueous hydrogel precursor solution followed by UV-cross-linking of the polymers via thiol-ene coupling (Fig. 16 B). Subsequently, the material was immersed into an acetone-water mixture to remove the PCL scaffolds (Fig. 16C). This resulted in stable interconnected channel-pores with a mean diameter of 18 μm that could be flushed with fluorescent-molecules for proof of principle and imaging purpose (Fig. 16 D). Although these results are promising and applications as biomaterials are envisioned, no cell-studies were presented in the scope of this work. Due to the removal of PCL using acetone-water, a direct incorporation of cells most likely has to be ruled out at this point. However, MEW printed scaffolds that simply dissolve in water, such as reported by Hochleitner et al. [114], might not be stable for prolonged periods of time before curing of the hydrogel. Sanyal et al. reported on solution electrospun POx which were crosslinked via thiol-ene [115]. Although not studied in a specific application, such fibers may be also interesting matrices for biomedical applications.

In addition to the described macroscopic gels, micro- and nanogels based on POx have been investigated by different groups. On the one hand, self-assembly in organic solvents followed by a cross-linking step was used to generate such particles [116]. On the other hand, microfluidic devices or emulsion polymerization was utilized [117,118]. Hartlieb et al. reported on the synthesis of a doubly hydrophilic block copolymer comprising a hydrophilic, non-ionic block (PEtOx) and a hydrophilic, polycationic block (PABuOx) [116]. Analogue to the previously discussed DNA-binding studies [101,102], the cationic charge was introduced through the polymerization and subsequent deprotection of BocABuOx. As both

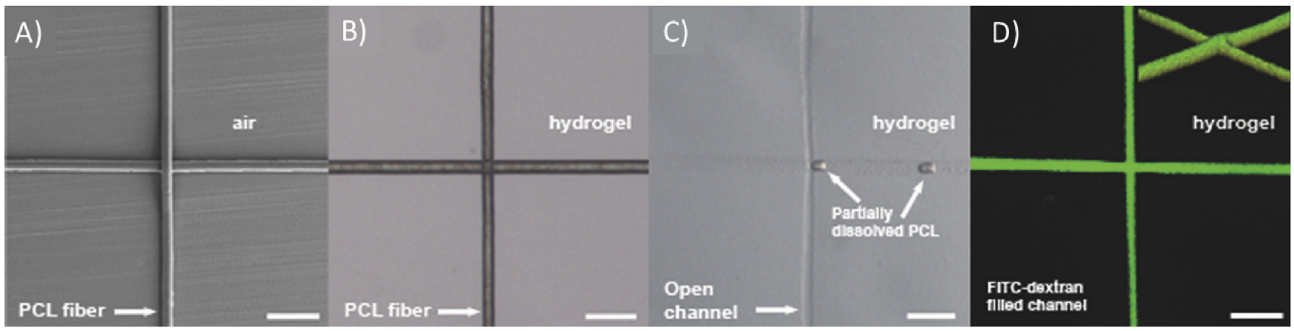

Fig. 16. (A) Scanning electron microscope image of printed PCL fibers obtained by melt electrowriting, (B) optical microscopy of fibers embedded in hydrogel, (C) optical microscopy of partially leached fibers showing channels within the hydrogel, and (D) CLSM of channels backfilled with FITC-dextran. Scale bar = 100 μm. Reprinted with permission from ref. [112]. Copyright 2015 John Wiley & Sons.

blocks are readily soluble in water, the self-assembling behavior was investigated in methanol, 2-propanol and $CHCl_3$. The size of the formed aggregates was barely influenced by the composition of the block copolymers (e.g. 4–17 nm in $CHCl_3$). However, the polarity of the solvents effected to radii (e.g. 17 nm ($CHCl_3$) vs. 77 nm (MeOH)). Glutaraldehyde was used for cross-linking and its excess was quenched with diethylamine and 6-amino fluorescein (Fig. 17 top panel).

Dependent on the solvent used for self-assembly, either micellar or vesicular structures were formed. *In vitro* cytotoxicity was investigated via XTT assay with micelle/vesicle concentrations ranging from 0.005 to 5 g/L. At 5 g/L, a significant reduction of cell viability after incubation for 24 h (L929 fibroblasts) was observed (Fig. 17 lower panel 13A). In contrast, vesicular structures did not show cytotoxicity at this concentration even though the data trend suggest that cytotoxicity might appear at slightly higher concentrations. In a follow-up paper it was recently reported that a higher amount of cross-linking consequently leads to reduced zeta potential as the amount of free amine groups is reduced [119]. Cellular uptake was found to decrease with an increasing cross-linking degree for concentration between 1 g/L and 0.1 g/L corroborating other reports that showed a more efficient uptake of positively charged objects compared to neutral or anionic structures. To further investigate the biocompatibility the hemolytic activity as well as erythrocyte aggregation was analyzed. The former was found to be below 2% for all nanogels up to 0.1 g/L. At this, albeit quite low, concentration erythrocyte aggregation was comparable to the negative control (PBS) and therefore negligible.

Legros et al. prepared POx-based nanogels by emulsion polymerization using partially hydrolyzed PEtOx cross-linked with 1,6-hexanediol diglycidyl ether [117]. They were able to monitor the formation precisely by utilizing DLS and HSQC NMR spectroscopy.

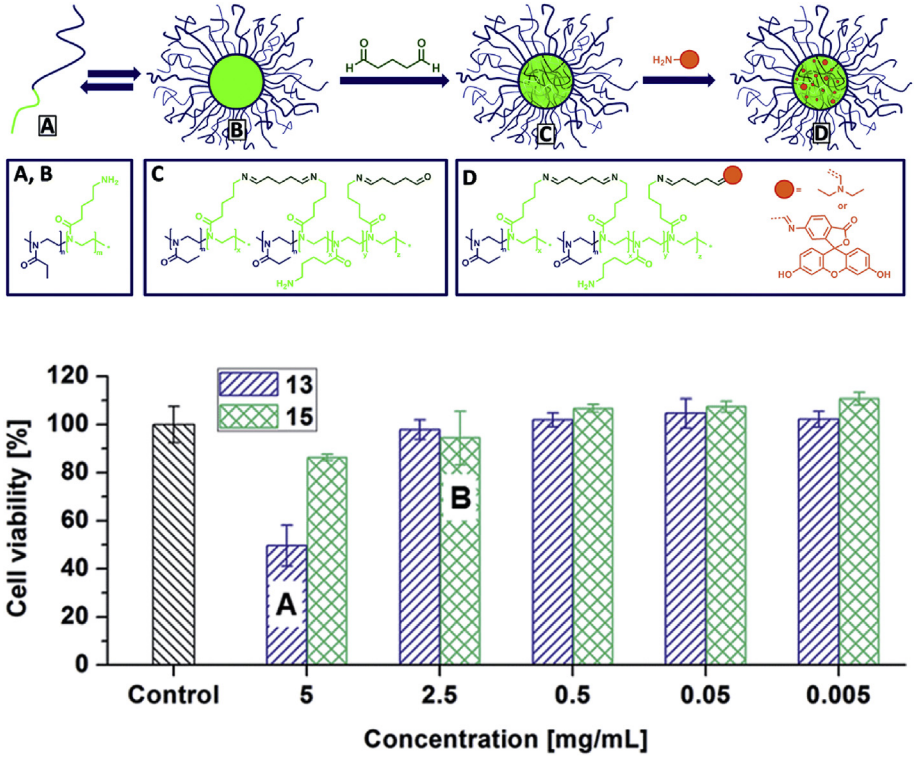

Fig. 17. Top panel) Self-assembly of P(EtOx-b-ABuOx) followed by cross-linking and quenching/loading. Lower panel) Cell viability of L929 mouse fibroblasts after incubation with micelles (**13**)/vesicles (**15**) up to 5 g/L for 24 h. Reprinted with permission from ref. [116]. Copyright 2015 The Royal Society of Chemistry.

Cell proliferation and viability of L929 cells after 72 h was assessed using the MTS test. Due to the remaining ethylene imine functionalities after cross-linking cellular toxicity could be suspected. No cytotoxicity was found at low polymer concentrations of 0.4 g/L or below. Furthermore, the authors report that non-specific interactions with BSA were observed.

POx based microgel particles that can possibly substitute commercial glass particles as neuronal cell carriers were investigated by Platen et al. [118]. In a first approach, they used telechelic PMeOx (DP = 30) as cross-linker and 2-hydroxyethyl methacrylate to produce microparticles in the size range of 30–250 μm. The microparticles exhibited nonfouling properties preventing sufficient cell adhesion. In the next step, a layer-by-layer (LbL) approach was utilized to introduce a charged PLL to the particle surface which promoted cell growth of HEK cells. However only marginal signs of interactions could be detected for primary rat E18 hippocampal cells. Additionally, the cross-linking density was increased by increasing the amount of telechelic PMeOx (50:50 and 70:30) to improve particle surface properties. Subsequently, the particles were coated utilizing 5 cycles of LbL process. HEK cell adhesion on the particles could be improved markedly (Fig. 18 A & B), while attachment of E18 hippocampal cells to the particle surface was still quite low (barely any attachment) after 7 days (Fig. 18C & D).

In order to increase neuronal cell adhesion, PHEMA was replaced with poly([2-methacryloyloxy)ethyl]trimethylammonium chloride) (PMETAC) having an intrinsic positive charge. Again, only the adhesion of HEK cells could be improved. Finally, the PMeOx-PMETAC particles underwent five deposition cycles followed by PLL coating resulting in much improved neuronal cell adhesion compared to the coated PMeOx-PHEMA particles. It should be noted, that the adhesion properties of PMeOx-PMETAC particles are similar to PLL-coated glass particles. Based on these first promising results, the authors suggest to investigate further properties such as thermosensitivity for neuro-engineering applications which could be easily introduced due to the versatility of POx based systems.

Hydrogels are also often investigated as potential drug depots. Very recently, Wiesbrock and co-workers presented an extensive library of 80 oxazoline-based hydro-, lipo-, and amphigels [80]. The monomer basis consisted of monofunctional EtOx, ButEnOx, NonOx, DecEnOx and one of 4 bisoxazolines containing either ether or ester bonds. The gels were prepared *in situ* via copolymerization of the mono- and bisfunctional monomers. Alternatively, thiol-ene reaction using ButEnOx or DecEnOx containing polymers was employed, allowing -in principle- the incorporation of active pharmaceutical ingredients (API). The as-prepared gels were assessed regarding their thermal transition, swelling properties and, for one exemplary ester-cross-linked gel, the degradation upon treatment with different pH and esterases as already discussed in the previous chapter dealing with degradability. Regarding the glass transition temperature, the materials followed the general trend of a decreasing T_g for increasing hydrophobic content. The swelling behaviors were assessed in water, ethanol and DCM. Due to the high content of hydrophobic moieties most of the produced gels are classified as either amphigels or lipogels.

Additionally, hydrogels can be used as a depot for drugs or other small molecules like dyes. Here too, versatile and fine-tunable physico-chemical properties that can be adjusted during synthesis demonstrate the great potential of POx-based hydrogels. Kostova et al. synthesized APCN comprising PEtOx and PHEMA or poly(hydroxypropyl acrylate) (PHPA) [120]. To this end, they used a

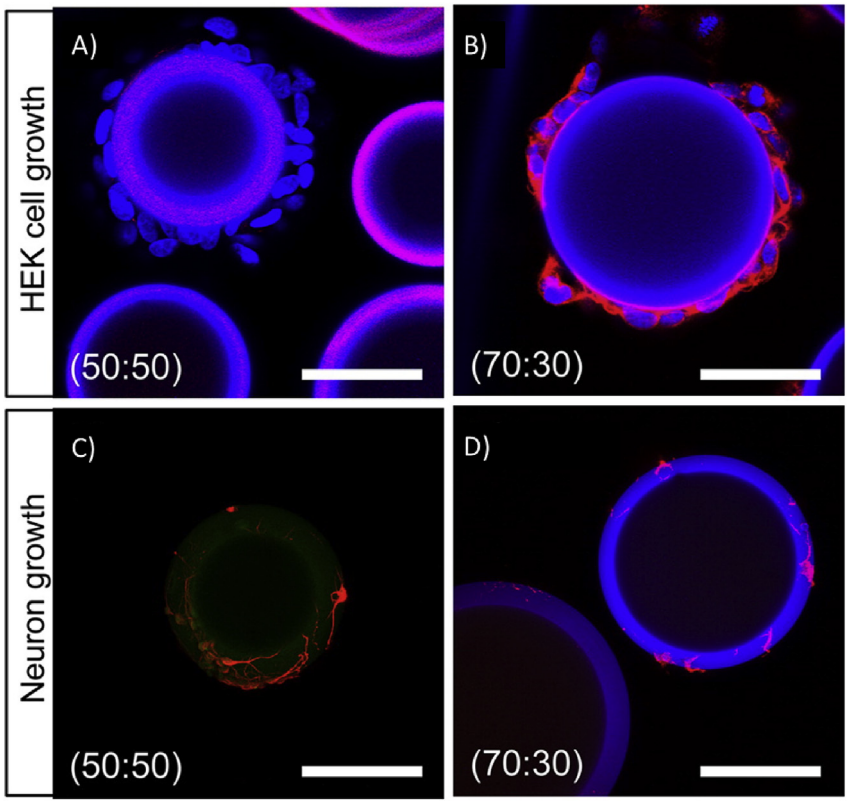

Fig. 18. Laser scanning confocal microscopy (LCSM) images of one Z-section taken at the equatorial plane of microgel particles (MGP). (A, B) HEK cell adhesion on 50:50 and 70:30 $PMeOx_{30}$:HEMA MGPs. HEK cells stained for DAPI (blue) and phalloidin (red) after 7 days in culture. (C, D) Adhesion and differentiation of E18 neuronal cells on 50:50 and 70:30 $PMeOx_{30}$:HEMA MGPs. Neuronal cells stained for DAPI (blue) and Tuj-1 (red) after 7 days in culture. Scale bars = 100 μm. Reprinted with permission from ref. [118]. Copyright 2015 American Chemical Society.

bis-macromonomer, PEtOx-bisacrylate and 2,2′-azobis(2-methylpropionitrile) as initiator. Swelling degrees in buffer (pH 7.2) at 37 °C were found to be largest for conetworks containing 70% PEtOx and 30% PHEMA (swelling degree = 800%). The corresponding APCN comprising PHPA swells less. This can be attributed to the LCST of PHPA at around 16 °C. Ibuprofen loading as well as the release studies will be discussed below in the corresponding chapter of this review.

Recently, Sedlacek et al. investigated the radiation stability of PEG, PHPMA, PNIPAAm, PVP as well as PEtOx as bulk material or 1 wt% aqueous solution and the resulting consequences [121]. PEtOx and PEG were cross-linked rapidly whereas PHPMA and PVP proved to be more resistant towards β-irradiation (Fig. 19). Furthermore, irradiation in aqueous solution has a much higher impact than irradiation in bulk. When irradiated with γ-rays, a comparable trend was observable although higher doses of irradiation are necessary to cause gelation (Fig. 19). GPC analysis revealed that even comparatively small doses of γ-rays below 10 kGy lead to considerable increase of the dispersity. Especially with regard to radiation sterilization, the reported alterations need to be taken into account. Even though the basic polymers are considered biocompatible, the authors did not investigate the biocompatibility of the prepared hydrogels. Notwithstanding, this approach enables a fast and straightforward route for the preparation of hydrogels originating from PEtOx and PEG homopolymers.

Van Hest and co-workers report on the use of NHS-ester bearing POx as reactive material in hemostatic sponges [122]. This very interesting approach utilized the comparatively simple side chain modification of POx to create reactive POx which are coated on a gelatin sponge. Excess NHS ester will then react with blood and tissue proteins and help to seal a wound.

In summary, POx based hydrogels have been among the most dynamic subfield of POx based biomaterials in the last five years. The timing seems perfect considering the significantly increased interested in 3D cell culture, tissue engineering and biofabrication in recent years. The synthetic variability of POx combined with a generally good cytocompatibility seem to be ideal starting points for the design of hydrogels with versatile biological, chemical and viscoelastic properties. Also, stimuli-responsive characteristics are readily incorporated. However, from an application point of view, the large majority of studies in this context are very basic at this point. This is probably due to the fact that many studies at this point seem to be driven from synthetic groups to provide basic proof-of-principle. It will be interesting to see if the community will be able to convert, at least in part, to more application driven study designs.

4. Conjugates with POx

The covalent conjugation of polymers with other (macro)molecules or particles of interest requires the presence of appropriate functional groups for coupling. The LCROP of 2-oxazolines is sensitive to the presence of nucleophiles and electrophiles. Therefore, most functional groups require protection groups during LCROP. Arguably, one of the most straightforward ways to incorporate functional groups in POx is through the termination reaction, which is done by addition of nucleophiles. Probably the most common termination found in the literature is with water, yielding an OH terminus, which is of limited use. More facile and versatile follow-up functionalization is possible using piperazine as a terminating reagent, but one has to take care to use a sufficient excess of piperazine, lest risking chain-chain coupling. In addition, piperidine derivatives are very well suited. More recently, termination using carboxylates has become more common. The POx termination reaction, however, is not always quantitative nor does it always follow the desired path. Termination with water may lead to unwanted attack at the C2 atom and subsequent ring-opening yielding a secondary amine and an ester [123]. Termination with piperidine or piperazine may in fact lead to termination with water, if the reagents are not strictly dry [124]. In any case, it is advisable to check and verify the extend of the success of termination reaction. Introduction of functional groups through the initiation is possible, but requires more stringent design, as the functional groups must not interfere with the LCROP, if defined polymers are to be obtained. An advantage of the initiation route is that it is typically easier to ensure quantitative functionalization, if clean reagents are used and rapid initiation over propagation is provided. Finally, functional groups can be introduced via functional monomers or, alternatively via appropriate coupling to ethylene imine units in partially hydrolyzed POx [84]. While a little over 10 years ago, very few functional 2-oxazolines have been described, the molecular toolbox for POx has been enlarged very significantly in the last decade. Most prominently is the alkyne bearing 2-oxazoline 2-(Penty-4-nyl)-2-oxazoline (PynOx), first introduced by Luxenhofer and Jordan [125], which is the only commercially available functional 2-oxazoline at this point. This monomer is also employed in the POx-drug conjugate currently in clinical evaluation (*vide infra*). Other notable monomers, which are more often employed by the community, are ButEnOx (introduced by Greß and Schlaad [126]) and DecEnOx, which are typically functionalized by UV-initiated thiol-ene coupling. For more details, the interested reader is referred to more specialized reviews on the subject matter of functional POx and their modification [10].

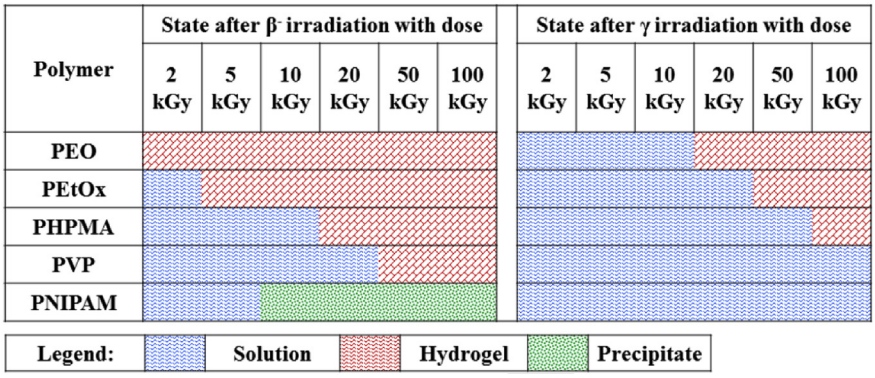

Fig. 19. Macroscopic state of the investigated polymers after exposure to different doses of radioactivity. All polymers were irradiated in their 1 wt% aqueous solution. PEO: Poly(ethylene oxide); PEtOx: poly(2-ethyl-2-oxazoline); PHPMA: poly(hydroxypropyl acrylate), PVP: poly(vinylpyrrolidone), PNIPAM: poly(*N*-isopropylacrylamide). Reprinted with permission from ref. [121]. Copyright 2017 Elsevier.

4.1. Nanoparticle-POx conjugates

A major challenge for the application of nanoparticles as biomaterials is the interaction of the particle surface with complex proteins, lipids and sugars present in a biological environment *in vitro* and *in vivo* [127,128]. Understanding and controlling the composition of the so-called "protein corona", which represents the surface-adsorbed layer of proteins, is a key element for promoting nanoparticle based applications in biology [129,130]. One prominent option for controlling the particle-protein interaction and, directly related to that, the colloidal stability of nanoparticles in biological media is the introduction of a polymeric surface coating [131]. Considering the properties of POx, these polymers might prove as promising candidates for these applications. Up to now, these systems are still only sporadically investigated. Very recently, Kempe and co-workers have already reviewed POx based micro- and nanoparticles comprehensively, however not with a special focus for the application as biomaterials [131]. Here, we want to highlight the recent biomaterial related publications.

A key property of POx is the tunable thermoresponsive behavior [3,4,13], which results in a temperature dependent hydration of the polymer shell and related to that to modified particle-protein interactions, particle-cell interactions and colloidal stabilities in aqueous media [132]. Koshinka et al. studied such a thermoresponsive system by *grafting* P*i*PrOx (DP = 67, M_n = 7.7 kg/mol) to poly(organosiloxane)-nanoparticles (d = 0.06 chain/nm^2) [128]. Below the LCST of 31 °C the functionalized particles were colloidally stable under physiological conditions (RPMI 1640 media, w/and w/o 5% fetal calf serum, FCS). Upon heating to 37 °C, large particle agglomerates formed rapidly. The transition from a hydrophilic (T < 31 °C) to a hydrophobic (T > 31 °C) surface is accompanied with a two-fold increase in total protein adsorption on the hard corona quantified by BioRad protein assay. The agglomeration as well as the increased protein adsorption could be reverted by simply lowering the temperature below the phase-separation temperature. However, as stated by the authors the presented system needs further improvement regarding the application in a biological system as the phase-separation temperature is well-below the body temperature. However, since the POx thermosensitivity is readily fine-tunable, this should not pose a major obstacle.

More recently, Kurzhals et al. [133] reported superparamagnetic iron-oxide (Fe_3O_4) nanoparticles (core size = 11 nm) which were functionalized via *grafting-to* with P*i*PrOx$_{100}$, PEtOx$_{100}$ and P(*i*PrOx$_{87}$-*co*-EtOx$_{13}$). A high grafting density of approx. 1 chain/nm was reported for all three particle systems. The thermoresponsive behavior was studied in medium (RPMI-1640) w/or w/o 10% BSA. Below the LCST of each polymer-particle system, the particles were colloidally stable in both dispersing media. Again, upon heating above the LCST, agglomerates formed. Only for the P*i*PrOx and the copolymer functionalized particles, the agglomeration was reversible by simply lowering the temperature without any external agitation necessary. An important result for future work on thermoresponsive particle coatings is that the LCST of the free polymer is only a poor guidance for the LCST of the final particle system. The presented results show a drastic decrease in the LCST of a particle surface bound polymer compared to a free polymer coil in solution. It could be assumed that the higher local concentration and lower hydration forced by the polymer-polymer interactions of a densely grafted brush facilitate the switching form hydrogen bonding to the dehydrated state with stronger intra- and inter-polymer interactions. Furthermore, the dispersing medium was also a critical parameter, as the LCST decreased from MilliQ-water (38 °C) to cell-medium (32.5 °C) but was not further influenced by the presence of FCS. Notably, it was not possible to trigger the agglomeration by magneto-thermal actuation of the iron-oxide particle core. This could be attributed to rapid heat dissipation as the particles remained stable until the global temperature raised above the LCST. Overall, a low cellular uptake of the particles (particle concentration: 1 g/L) by HeLa cells after incubation for 24 h at 37 °C was found. Here the copolymer functionalized particles showed the lowest cellular uptake followed by the PEtOxylated and the P*i*PrOxylated particles. This result is unexpected as the incubation temperature was only below the LCST of the PEtOxylated particles and a more hydrated shell should decrease cellular uptake. Therefore, cellular uptake of the particle-polymer systems did not result in a clear trend regarding the hydrophilicity of the particle coating. In comparison, the cellular uptake of the POxylated particles was lower than that of corresponding poly(*N*-isopropylacrylamide) PNiPAAm functionalized particles, but higher than that of PEGylated particles [134]. The POxylated particles showed no cytotoxicity in HeLa cells after 24 h of incubation at 37 °C.

The cellular uptake of POxylated and PEGylated particles was also investigated by Koshkina et al. [135]. Rhodamine B labeled poly(organosiloxane) nanoparticles with a diameter of 9 nm were assessed regarding the protein adsorption and non-specific cellular uptake. Interestingly, sterically stabilized *grafting-to* functionalized PEtOxylated and PEGylated as well as non-coated electrostatically stabilized, positively and negatively charged particles were directly compared. The amount of proteins adsorbed in the hard corona for all particles after incubation in serum was determined by photometric assay. The protein concentration decreased from the negatively charged particles (1.3 μg/cm^{-2}) to the PEGylated (0.7 μg/cm^{-2}) and the PEtOxylated (0.5 μg/cm^{-2}) particles. The cellular uptake by microvascular ISO-HAS1 cells and macrophage-like THP-1M cells was monitored in the presence and the absence of serum up to 72 h of incubation. In both cell lines the highest uptake was observed for the non-coated poly(organosiloxane) nanoparticles and much less for both polymer functionalized particle species. Interestingly, the cellular uptake of the PEGylated particles by the ISO-HAS1 cells in the absence of medium was greater than the uptake of the corresponding PEtOxylated particles, whereas in the presence of serum, this effect was much less pronounced. Generally, in the presence of serum, the difference in cellular uptake between electrostatically and sterically stabilized particles was considerably smaller. This shows that the uptake of the polymer functionalized particle species may still be, to a certain extent, determined by the adsorbed protein corona and not (only) by the surface coating. In both assays, the performance of the PEtOx coating was, at least, equal to that of the PEG coating, once more corroborating the early study on lipopolymer modified liposomes by Woodle et al. [23]. However, the PEG chains, used for functionalization, were considerably smaller (~2 kg/mol; DP = 44; σ: 0.11 chain/nm^2) and carboxyl end-group functionalized while the PEtOx has a much higher molar mass (~6 kg/mol, DP = 63; σ: 0.09 chain/nm^2) and a tertiary amide as end group (Scheme 2). This situation is also reflected in the zeta-potential of both particle species (PEGylated: 14; PEtOxylated: 5) and could explain the slight differences in both assays. With this altered surface chemistry, a direct comparison of both particle species might not be straightforward and not only related to the polymer.

In two publications, Mansfield et al. investigated the influence of a POx surface coating on the nanoparticles diffusion through mucus [136,137]. Thiolated, fluorescent (either maleimide terminated Alexa 546 or fluorescein-O-methacrylate) silica nanoparticles with a diameter of 50 nm were functionalized with either PEtOx (M_w = 5 kg/mol, DP = 50,) or PEG (M_w = 5 kg/mol, DP = 113,). A gastric mucus dispersion (1% w/v in deionized water) was used (MilliQ water served as reference medium) to determine the diffusion coefficients of polymer-coated and non-coated particles

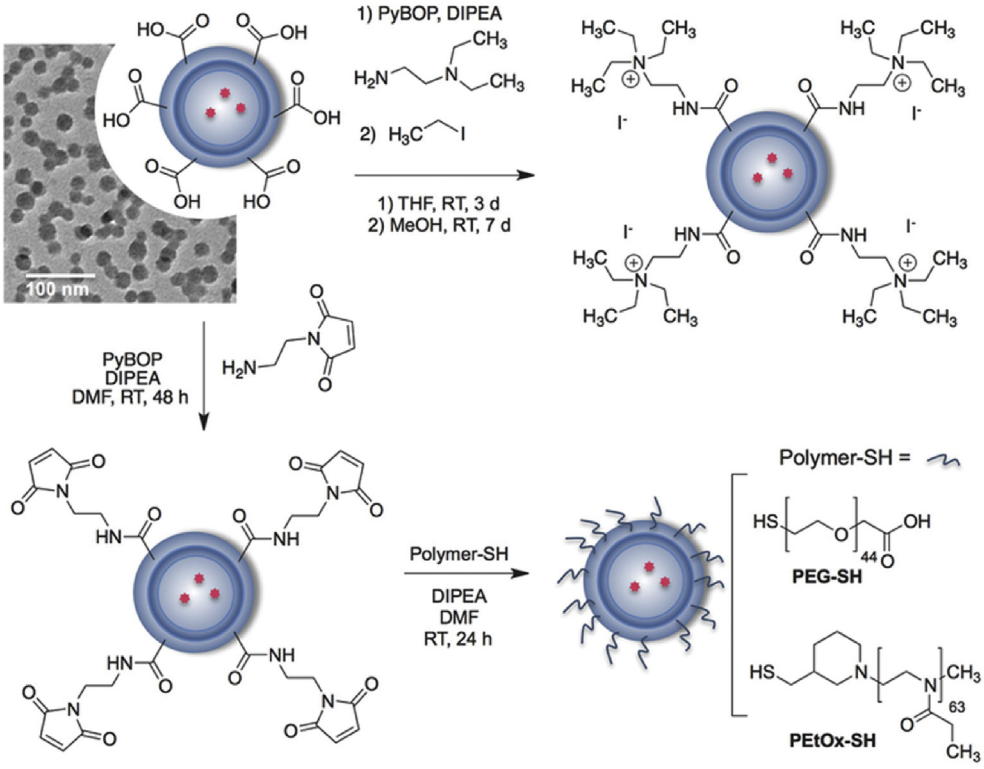

Scheme 2. Post-synthesis surface modification of carboxy-modified rhodamine B labeled nanoparticles (top left: TEM image, scale bar 100 nm) to positively charged, quaternized or polymer-coated particles (PEtOx vs. PEG), respectively. Reprinted with permission from ref. [135]. Copyright 2016 John Wiley & Sons.

via Nanoparticle Tracking Analysis (NTA). While the non-functionalized particles diffuse faster in MilliQ, both polymer-functionalized particles diffuse faster in the gastric mucus dispersion compared to the control. This is attributed to the stealth character of PEG and PEtOx, which suppresses interactions with the components of the mucus gel. Furthermore, penetration of the particle-systems through freshly excised porcine stomach mucosa was examined. After 45 min of incubation, both polymer-coated particle species showed significant penetration of the tissue while the unfunctionalized particles showed only minimal penetration (Fig. 20). Of course, it must also be noted that thiolated systems have been discussed specifically as mucoadhesive systems [138]. It might have been more appropriate to compare nanoparticles bearing similar functional termini as the polymers. In this study, the POxylated particles showed comparable values in the diffusion coefficient and the degree of penetration compared to the PEGylated ones. The tendency for slightly higher values of the POxylated system may be attributed to the much shorter POx chains, making a direct comparison troublesome. However, considering the experimental error, no difference between the polymer modified particles was observed.

In a follow-up study, the influence of the 2-oxazoline side chain on the diffusion capabilities of the POxylated silica nanoparticles was investigated in a similar experimental setup [136]. The polymers PMeOx, PEtOx and P*n*PrOx with a molar mass ranging from 4.5 to 5.1 kg/mol (DP_{theo} ranging from 58 to 45) were used as polymeric coating. A grafting density of about 0.1 μg/nm^2 was reported. This seems quite high. Considering a molar mass of 5 kg/mol, this would translate into 1.2×10^{13} chains per nm^2, which seems quite improbable. This unclear surface coverage notwithstanding, the diffusion coefficient of the particles in the mucus dispersion decreased with increasing hydrophobicity from PMeOx over PEtOx to P*n*PrOx coating. In fact, the P*n*PrOx functionalized particles showed no significant difference to the non-coated control. Striking, but not further discussed by the authors, the diffusion coefficient of PEtOx functionalized particles, reported in the earlier study [137], was much higher than the values reported here. The values reported earlier are comparable to the PMeOx-coated particles of this study, which would result in a different trend for the diffusion coefficient. This discrepancy in absolute values nicely demonstrates the issue of reproducibility in polymer science and nanomedicine which remains a major challenge in the field [139,140]. The penetration distance into gastric mucosa tissue was also monitored. It followed the same trend as the diffusion coefficient and decreased with increasing hydrophobicity of the POx side-chain. Interestingly, although the diffusion coefficients of the non-coated and the P*n*PrOx coated particles were similar, the polymer functionalized particles showed a significantly deeper penetration into the mucosa tissue. Noteworthy, by reviewing the literature [4,131], one might expect agglomeration of the P*n*PrOxylated particles in all experiments as the temperature of 25 °C is above the LCST of P*n*PrOx as free coil (24 °C) and consequently, as already discussed, above the LCST of a particle surface bound. Yet, apparently the authors did not face this issue.

Bissadi and Weberskirch reported the functionalization of silica-nanoparticles with PMeOx via *grafting-to* and *grafting-from* [141,142]. The *grafting-from* approach yielded up to 3 times higher grafting density (0.5 chains/nm^2 vs. 1.5 chains/nm^2). While the *grafting-to* functionalized particles were not further investigated as biomaterials, the *grafting-from* coated particles were functionalized with fluorescein or the cancer targeting ligand, folic acid. Moreover, as an alternative to the fluorescent surface functionalization, tris(-bipyridine)ruthenium(II) was successfully incorporated into the silica-core during particle synthesis. Analogue to the fluorescein labeled particles, the dye-doped particles were also coated with PMeOx. These systems could find application as biomaterial for e.g.

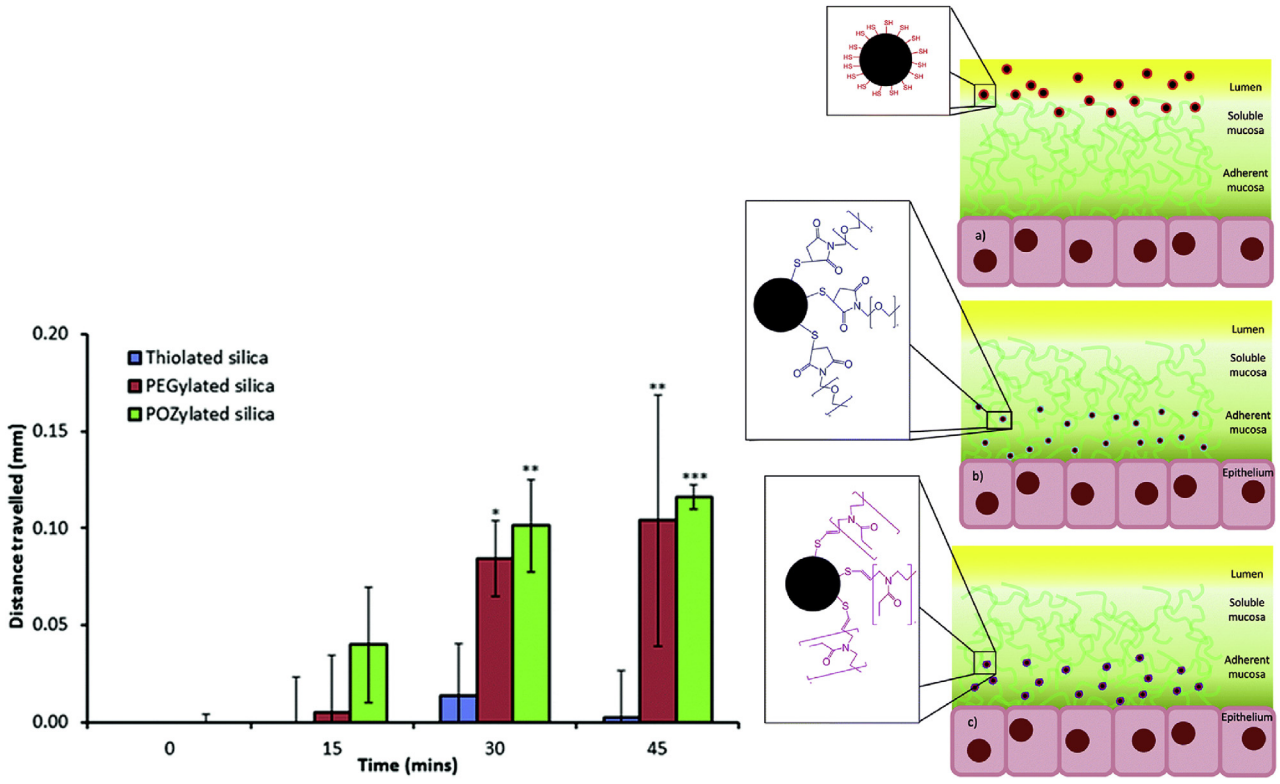

Fig. 20. a) Penetration depth of thiolated, PEGylated and POxylated silica-nanoparticles into porcine gastric mucosa. Since thiolated compounds are well-known muco-adhesives, an alternative control would be advisable. b) Schematic illustration of the penetration depending on the type of functionalization. Reprinted with permission from ref. [137]. Copyright 2015 The Royal Society of Chemistry.

diagnostic purposes, however no further stability or cytocompatibility tests were performed.

In all of the above discussed publications coating with linear POx was utilized. A very interesting alternative was recently presented by Morgese et al. [143]. Here, iron-oxide nanoparticles with a diameter of 9 nm were functionalized via *grafting-to* with either linear or cyclic PEtOx (DP = 50 and 100) yielding very high grafting densities between 1.2 and 3.3 chains/nm^2. The use of cyclic polymers resulted in approximately 70–80% higher grafting densities compared to their linear equivalents, which may reflect the lower hydrodynamic volume of cyclic polymers at the same molar mass. Nanoparticles were initially colloidally stable in water and in PBS-buffer. However, upon 1 month storage, the particles coated with linear polymer showed increasing signs of aggregation as observed by DLS. In contrast, particles coated with the cyclic PEtOx remained stable for up to 60 days. Regarding the thermoresponsive behavior of the PEtOx coating, the cyclic-brush functionalized particles showed an increase of 10 °C in aggregation temperature compared to the linear brushes. This is rather surprising, as in another report cyclic polymers were reported to exhibit a lower cloud point compared to their linear counterparts [144,145] and polymer chain ends are considered important for solvation. Similar to the report of Kurzhals et al. [133], the aggregation of the linear PEtOx brush coated iron-oxide particles was irreversible after heating above the cloud point. Interestingly, the cyclic brush coated species redispersed spontaneously upon lowering the temperature. After incubation of both particle species in 1 g/L BSA solution in PBS, the cyclic brush coated particles did not show changes in size (by DLS and AFM). In contrast, the size of the linear counterpart increased by approximately 15 nm. Based on these results, the authors hypothesize that the cyclic-brush shell more effectively/completely prevents interaction of proteins like BSA with the particles core, whereas even high-density linear brushes still allow such interactions. Therefore, it is suggested that utilizing cyclic brush shells could yield nanoparticle systems with unique performance.

Silva et al. investigated fluorescently labeled gold nanoparticles (d = 30 nm) for active targeting of lung cancer cells [146]. The particles were functionalized by *grafting-to* with oligo(2-ethyl-2-oxazoline) (OEtOx) bearing a carbamic acid end-group, followed by labelling of the particles with the laminin derived peptide YIGSR for specific cell targeting. Fluorescence properties, direct targeting of A549 lung cancer cells and general cell viability are reported. Tethering the oligomers to the gold surface was realized by either standard thiol coupling or via rather unorthodox electrostatic interaction with a chromylium salt. The synthesis of the chromylium salt from OEtOx and 2,4-dihydroxybenzaldehyd via the aromatization of the oxazoline side-chain was suggested. (OEI-CS) Unfortunately, only very limited characterization of the functionalized polymer was given. Therefore, the reaction mechanism and the chemical structure remain unclear. The fluorescent properties of both particle species were confirmed via absorbance and fluorescence spectroscopy. Increased cellular uptake of the particles after conjugation with the YIGSR sequence was suggested by confocal fluorescence scanning microscopy images (Fig. 21) and the viability of A549 cells after 72 h of incubation with the different particle species quantified via MTS assay. The viability was at least 80% and higher for all particle species after 72 h of incubation but only very low concentrations were investigated (particle conc. 0.2 g/L).

In a follow-up study, the same group utilized the aforementioned OEtOx coated gold nanoparticles for the fabrication of respirable microparticles for deep lung delivery [147]. The

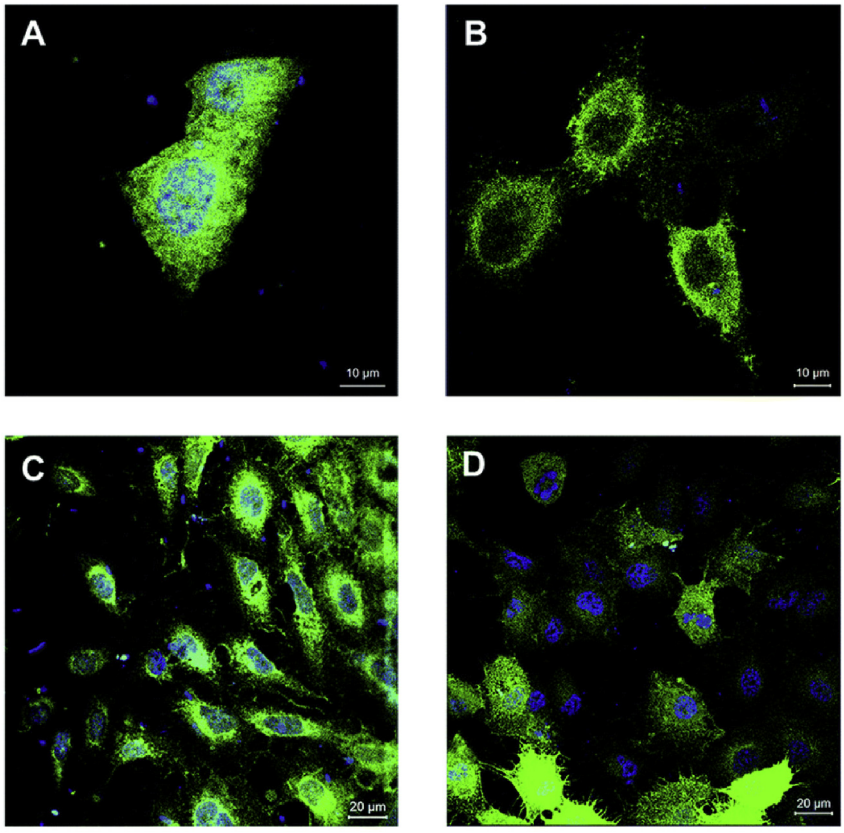

Fig. 21. Cellular uptake of nanogold POxylated probes. CLSM images show A549 cells containing Au–OEtOx–SH (A), Au–OEI–CS (B), Au–OEtOx–SH–YIGSR (C), Au–OEI–CS–YIGSR (D). Green color – CellLight® Actin-GFP, BacMam 2.0; blue color – POxylated gold nanoprobes. Original magnification × 40. Reprinted with permission from ref. [146]. Copyright 2016 The Royal Society of Chemistry.

nanoparticles were incorporated into a chitosan matrix by supercritical CO_2-assisted spray drying to yield nano-in-micro powder formulation. This process resulted in spherical chitosan microparticles with a mean size between 3.2 and 3.8 µm, loaded with the OEtOx-coated nanoparticles. The delivery performance via respiration was evaluated with an Andersen Cascade Impactor and was found to be comparable to already marketed dry powder inhalers. The release of the nanoparticles from the chitosan beads was monitored at pH = 7.4 and 6.8 by UV–Vis spectroscopy. A higher release rate was found at pH = 6.8. After 100 h, 90% of the thiol-coupled and 44% of the chromylium salt-coupled particles were released. Due to the fluorescent properties of the OEtOx particle coating, the particles could be visualized inside the chitosan microbeads. No comments on the long-term stability of the fluorescence were made. However, this would have been of particular interest, as the carbamic-acid end group of OEtOx (considered responsible for the fluorescence) is usually considered to be unstable. Cytotoxicity tests for the fabricated nano-in-micro-beads with the A549 cell-line proved the cytocompatibility, as cell viability was above 80% for all samples (1 g/L).

In recent years, several other reports were published on POx coated nanoparticle systems, which did not include data of immediate biological relevance. However, since they may be interesting for further studies in this context, some of them are very briefly outlined below. For instance, Eckardt et al. report about the *grafting-to* functionalization ($\sigma = 0.3$ to 0.9 chains/nm^2) of silica nanoparticles (r = 7 nm, 31 nm and 152 nm) with PEtOx (DP = 20 or 28) [148]. The grafted PEtOx chains were successfully (partially) hydrolyzed by concentrated HCl resulting in a cationic P(EtOx-*co*-EI) coating. Further assessment of the system for non-viral gene delivery was proposed. Similarly, Soma and Jin reported on polystyrene microparticles modified with PMeOx which was subsequently hydrolyzed to PEI [149]. An original *grafting-to* functionalization for silica nanoparticles (r = 15 nm) with PMeOx (~5.5 kg/mol) by host-guest interaction was proposed by Volet and Amiel [150]. A layer of β-cyclodextrin adsorbed on the particle surface served as host and the C_{12} or C_{18} end-groups of the PMeOx served as guest. Morgese et al. report about ZnO nanocrystals functionalized with PMeOx (DP = 25 or 50; 2 or 4 kg/mol) by ligand exchange, yielding polymer coated particles with excellent colloidal stability in water [151]. Combined with a potential lanthanide doping application as novel inorganic labels for bioimaging are proposed. In two separate publications, Safari et al. report about the aqueous stabilization of iron-oxide nanoparticles either by a linear-dendritic copolymer, composed of a PEG core and PEtOx-*b*-PCL arms, or by a PEtOx-*b*-PCL block copolymer [152,153].

4.2. POx-glyco conjugates

It is well understood that carbohydrates are important moieties in signaling and recognition in the biological realm. Furthermore, it has been argued that carbohydrates can encode a much higher density of information compared to nucleic acids and proteins. However, the “sugar code” is often somewhat neglected compared to the genetic code and proteins [154]. Therefore, glycopolymers have seen significantly growing interest in recent years and also a few glycoconjugates with POx have been investigated.

Weber et al. combined the simple access to tosylates and triflates of carbohydrates with their excellent initiator-qualities for the LCROP of POx [155]. Linear α-glyco-OEtOx-MA were

synthesized and subsequently oligomerized to yield small polymer brushes. No biological studies were reported using these materials. Instead, a different synthetic approach for POx glycopolymers was reported [156]. Here, copolymers of EtOx and ButEnOx were prepared and modified with both, terpyridine moieties for Pt complexation and thioglucose/thiogalactose for potentially enhanced endocytosis in tumor cells. The polymers exhibited a somewhat lower cytotoxicity compared to free platinum at the same Pt equivalent dose. The lower cytotoxicity is ascribed to a slower uptake of the polymer compared to free cisplatin, however, no quantitative endocytosis studies were performed. It could also be hypothesized that the polymer complexed Pt is not as available to reach the DNA, as is free cisplatin. The authors hypothesize that the glycopolymers might show a better performance *in vivo*, but to date no follow-up study using the materials was published. Moreover, as the authors reported, the polymers did not form aggregates but exhibit hydrodynamic radii of about 3–4 nm. As such, one must expect first-pass renal clearance and cannot expect any pronounced EPR effect, which requires long circulation. In addition, significant hemolysis was observed already at sub-mM concentrations. The polymer complexed Pt showed a minor but significant attenuation in hemolysis at the same equivalent Pt dose. The polymer concentration at which hemolysis started to show ranged between 1 and 2 g/L. Considering the very low hemolysis reported from POx otherwise, it stands to reason that this hemolysis was caused by the Pt-terpyridine moieties. In contrast, no erythrocyte aggregation was observed at concentrations up to 1.25 mM (approx. 10 g/L).

Hoogenboom and co-workers investigated the reductive amination of partially hydrolyzed POx with glucose and maltose [157]. Dynamic light scattering revealed different solution behavior of the glycopolymers, depending on the attached carbohydrate. The glucose binding protein concanavalin A was utilized to assess the binding properties of the glycopolymers. Because of the way the carbohydrates were attached, the conjugate with glucose did not give the specific interaction, while the maltose conjugate did.

Takasu and co-workers reported on glycol-conjugates, which were functionalized with Arg-Arg sequences to enhance cell-penetration. These polymers were used as efficient inducers of protein expression in E.*coli* [158]. Since the level of protein expression correlated with the amount of the galactosides, it is suggested that a clustering effect of the sugar moieties is responsible for how well the lac-suppressor is inhibited.

4.3. POx-peptide conjugates

Peptide-polymer conjugates are typically employed to ensure more or less specific interactions of the respective polymers with cells via peptide/protein interactions. The rich chemistry of POx allows multiple synthetic strategies to obtain POx-peptide conjugates. Previously, several chemoselective reactions such as Cu(I) catalyzed azide/alkyne click chemistry, aldehyde/aminooxy coupling and native chemical ligations have been employed to prepare RGD-, MTII- and CREKA-POx conjugates [159,160]. More recently, Groll and co-workers presented an alternative approach to use native chemical ligation for the conjugation of peptides to POx [161]. In a first step, a N,S-protected cysteine reagent was conjugated to POx side chains via thiol-ene coupling, which afforded *N*-terminal cysteines after deprotection. Native chemical ligation was then achieved by using a peptide sequence bearing a C-terminal thioester. As such, this approach is orthogonal to the approach by Luxenhofer, who introduced thioester side chains and coupled a peptide bearing a *N*-terminal cysteine [159].

4.4. POx-protein conjugates

Already very early on, POx homopolymers have been used to covalently modify proteins. This was typically done closely resembling the much more common and wide-spread PEGylation of proteins. Therefore, mainly PMeOx and PEtOx homopolymers have been used, which are, in many aspects, similar to PEG. Prior to 2012, about a dozen proteins have reportedly been POxylated [162]. Also in recent years, POx homopolymers and block copolymers have been used to modify proteins, in particular, enzymes to improve their catalytic activity, stability, and solubility as well as cellular uptake and biodistribution.

Specifically, POxylation of enzymes was evaluated as a way to increase solubility of enzymes in organic solvents to carry enzymatic reactions in organic solvents that could not be catalyzed by native enzymes due to their inactivation and/or insolubility in these solvents [163]. The enzymes used in this study were hen-egg white lysozyme, RNase A and α-chymotrypsin, which were conjugated with PMeOx or PEtOx. A new coupling method was employed, in which ethylenediamine terminated POx polymers were activated using pyromellitic acid dianhydride and subsequently reacted with the amino groups of the corresponding enzymes. Upon conjugation with the polymers, RNase A and lysozyme became fully soluble in DMF. The authors claim that this represents the first examples of fully POxylated organo-soluble proteins. However, already the first report of Saegusa on POxylated catalase states that the protein becomes soluble in organic solvents [164] and probably most previously reported POxylated proteins were organosoluble, even if that was not explicitly stated. The approach was less successful in the case of α-chymotrypsin, having nearly double the molecular mass of lysozyme and RNase A, which suggests that the molecular mass of the modified protein may affect the modification outcome and/or solubility of this protein in the organic media.

Another study by the Tiller group evaluated the effects of the POx molar mass and chemical composition on the ability to produce polymer-enzyme conjugates soluble in organic solvent that retain high catalytic activity [165]. The POxylation of several enzymes with different POx, ranging from the hydrophilic PMeOx to the hydrophobic PHeptOx as well as P*n*BuOx-*b*-PMeOx diblock copolymer resulted in the enzyme-POx conjugates soluble in various organic solvents from DMF to toluene. In some cases these conjugates showed significantly (up to 153,000 fold) higher activities than the respective native enzymes in organic solvents. Needless to say, the “catalytic activity” in this study was measured not under condition of the saturation of the enzyme by the substrate but at standard conditions at fixed concentration of the substrate. Therefore, the observations do not reflect the true catalytic potency of the enzyme in the media ($V_{max} = k_{max}\,[E]_o$, where $[E]_o$ is the concentration of the active enzyme and k_{max} is the catalytic constant), but rather the changes of the effective reaction rate ($V_{max} = k_{max}\,[E]_o/(K_m + [S]_o)$, where K_m is the effective Michaelis constant, and $[S]_o$ is the substrate concentration) that are likely to be affected by differential solubility of the substrate in water and organic solvent as well as partitioning of the enzyme between bulk solvent and the enzyme's immediate environment. Interestingly, the conjugation “inverted” the performance of the enzymes in water and organic solvents resulting in the loss of “residual activity” of the majority of the 14 tested enzymes (with exception of CalB, Laccase, horseradish peroxidase (HRP) and α-chymotrypsin) in aqueous media. This may be due to both, changes of the enzyme conformation resulting in “true inactivation” (decrease in V_{max}), or aggregation, which may impose diffusional limitations to the enzyme transformation. A thorough analysis of the enzyme kinetics typical for such studies would be needed to understand the mechanistic underpinning of the observed effects. That said, having

the enzyme-conjugate dissolved and being able to efficiently catalyze hydrophobic substrate transformation in organic solvent is very important from the practical standpoint. On the other hand, from a biomaterials standpoint, the low activity in aqueous media is not particularly encouraging.

Taken together, POxylation was shown to be a versatile method to render the proteins soluble in organic solvents, which can preserve enzyme activity and would be of importance for developing novel biocatalysts for transformation of organo soluble substrates. The case in point was the study by the same group [166] that used organo soluble conjugates of α-chymotrypsin and other enzymes with PMeOx not as biocatalysts but rather solubility enhancers for an inorganic catalyst, potassium osmate for Sharpless dihydroxylation of alkenes. In this case potassium osmate, insoluble in water saturated chloroform was able to disperse in the solutions of the conjugates, probably due to amphiphilic character of the latter. By adjusting the structure of the protein and the temperature of the reaction medium a highly enantioselective dihydroxylation of alkenes has been achieved.

As previously mentioned, similar to PEGylation, POxylation has been used to increase stability, solubility and circulation time of proteins that can be used in development of new therapeutic agents. A distinct type of POxylation of proteins with amphiphilic block copolymers PMeOx-*b*-P*n*BuOx was reported by Tong et al. [167] with the goal to increase delivery of the modified protein across biological barriers. It is noteworthy that PEGylation typically impedes crossing of biological barriers. The general approach to modify proteins with amphiphilic block copolymers instead of hydrophilic polymers has been pioneered by Kabanov and coworkers using Pluronics® [168]. In a follow-up study, the same group reported on the synthesis and characterization of the conjugates of superoxide dismutase 1 (SOD1) with amphiphilic diblock copolymers PMeOx-*b*-P*n*BuOx and PEtOx-*b*-P*n*BuOx, which displayed enhanced uptake into brain cells and increased delivery to the brain in mice [169]. The POx block copolymers were terminated with piperazine at the P*n*BuOx blocks, and the free terminal secondary amines were linked to the amino groups of SOD1 through non-degradable disuccinimidyl propionate or degradable dithiobis(succinimidyl propionate) linkers, respectively. The degree of modification (number of polymer chains per SOD1 dimer) varied from about 2.2 to 3.5. Based on circular dichroism spectra, the secondary structure of SOD1 in the conjugates remained unaffected when compared to native SOD1, but the activities of the conjugates were reduced to values in the range of 31–47% of initial SOD1 activity (which is similar to the previously reported for PEGylated SOD1). POxylated SOD1 formed nanoscale-sized aggregates in phosphate buffered saline (PBS) with the particles effective diameters of 5 nm for PMeOx-*b*-P*n*BuOx-SOD1 and 20 nm for PEtOx-*b*-P*n*BuOx-SOD1. Both conjugates exhibited little if any toxicity in CATH.a neuronal cells. Interestingly, the modification the POx block copolymers improved the uptake of SOD1 in CATH.a neurons when compared to native SOD1 and PEGylated SOD1. The uptake enhancement was nearly 10-fold and was more pronounced for PEtOx-*b*-P*n*BuOx-SOD1 than for PMeOx-*b*-P*n*BuOx-SOD1. Since both conjugates had approximately same degree of modification and same hydrophobic P*n*BuOx block length, the improved cellular uptake of PEtOx-*b*-P*n*BuOx-SOD1 was probably due to more pronounced amphiphilic character of PEtOx vs. PMeOx. Moreover, this different uptake is mirrored by the structure-property relationships regarding endocytosis of the respective polymers [48]. PEtOx-*b*-P*n*BuOx-SOD1 utilized the lipid rafts/caveolae cell entry pathway, previously reported for the block copolymer alone, and localized mainly in endoplasmic reticulum and mitochondria. Consistent with the improved cellular uptake and demonstrated ability to escape lysosomal entrapment *in vitro*, the PEtOx-*b*-P*n*BuOx-SOD1 conjugate was significantly more effective in scavenging the intracellular superoxide in CATH.a neurons when compared to native and PEGylated SOD1. PEtOx-*b*-P*n*BuOx-SOD1 conjugated also displayed improved pharmacokinetics parameters *in vivo*, including nearly 2-fold increased plasma circulation half-life after *i.v.* administration. Moreover, this conjugate was capable crossing the intact blood brain barrier (BBB) and accumulating in both brain capillary and parenchyma (67% in parenchyma vs. 33% in brain capillary), whereas neither native nor PEGylated SOD1 reach the brain. This result indicates some therapeutic potential of POxylated SOD1 for various CNS diseases with an intact BBB. However, unspecific coupling of therapeutic proteins to polymers may cause product heterogeneity introducing challenges to pharmaceutical development and potential immunogenicity therefore developing methods of site specific modifications is of high importance.

For example, Mero et al. [170] reported on the synthesis and characterization of a conjugate of granulocyte colony stimulating factor (G-CSF) with PEtOx. To produce conjugates, 5–20 kg/mol PEtOx were used that had either aldehyde or amine functional terminal groups. The aldehyde-functionalized PEtOx chains were linked to the G-CSF *N*-terminal methionine amino group via reductive alkylation, resulting in approximately 50% modified G-CSF. Alternatively, the amine-terminated PEtOx chains were linked to the glutamine of G-CSF via transglutaminase (TGase) mediated conjugation. In this case, presumably due to steric hindrance between the TGase and conjugated macromolecules, the reaction yield was depending on the length of the spacer separating PEtOx and G-CSF and varied from about 30% to about 75% of modified G-CSF. The secondary structure of the protein, measured by circular dichroism, was preserved using both conjugation methods. However, the modification sites at the protein surface were obviously different. The reductive amination reaction resulted in the attachment of PEtOx to *N*-terminal methionine, while, by analogy with the previous study of PEG conjugation to G-CSF [171], the TGase-catalyzed reaction resulted in selective modification of Gln 135 residue. Although the stability of both types of conjugates toward aggregation at 37 °C was improved compared to the native G-CSF, the Gln 135 modified conjugates displayed slower aggregation rates compared to *N*-terminal modified conjugates. In general, POxylation of G-CSF decreased the aggregation propensity of G-CSF and resulted in different types of aggregates that were soluble, when compared to aggregates of the native GM-CSF that precipitated. At the same time single chain POxylated G-CSF remained active *in vitro* as determined by cell proliferation assays and *in vivo* as assessed by their effects on white blood cell and neutrophil counts in normal rats.

Nawroth et al. [172] as well as Alvaradejo et al. [173] presented to different approaches to modify proteins with maleimide-functionalized POx. While Nawroth used a protected maleimide to directly terminate POx, Alvaradejo used a protected maleimide initiator. Both approaches have advantages and disadvantages but ultimately allow, after maleimide deprotection, preparation of POx-protein conjugates. Nawroth et al. showed this using an elastin-like polymer, while Alvaradejo et al. provide proof-of-concept using serum albumin.

Finally, Lühmann et al. [174] tackled the challenge of site specific POxylation by introducing non-natural amino acids into the protein backbone at one predefined site, providing a distinctive functional group for site specific modification. To achieve this goal, genetic code expansion integrating pyrrolysine derivatives, e.g., *N*-propargyl-L-lysine (Plk), through recombinant protein expression was utilized to obtain a modified interleukin 4 (IL-4) i.e. Plk-IL-4. Following introduction of propargyl group into the protein structure, bio-orthogonal copper catalyzed azide alkyne cycloaddition (CuAAC) was used for POx conjugation (Fig. 22). Azide

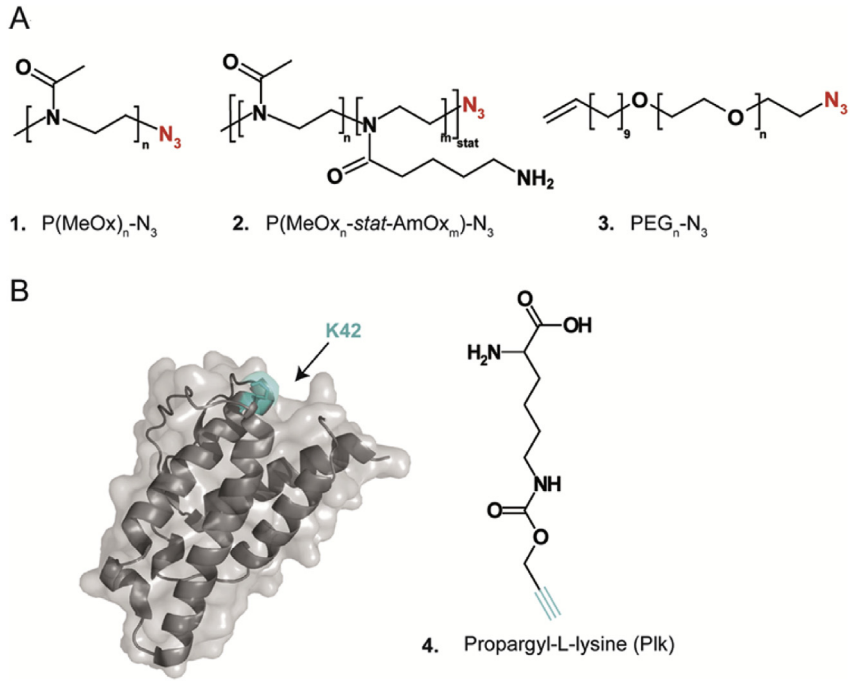

Fig. 22. (A) Structure of polymers and copolymers employed for Plk-IL4 conjugation. (B) Crystal structure of IL-4 (Pdb = 2B8U). The introduction site of the non-natural amino acids highlighted (cyan). Structure of the non-natural amino acid propargyl-L-lysine (Plk), (4), which was incorporated at the K42 position of IL-4. Reprinted with permission from ref. [174]. Copyright 2017, American Chemical Society.

functionalized hydrophilic PMeOx and azide functionalized random copolymers composed of MeOx and BocABuOx were synthesized. The conjugates of Plk-IL-4 with PMeOx (IL-4/PMeOx) and P(MeOx-*co*-ABuOx) (IL-4/P(MeOx-*co*-ABuOx)) were synthesized and compared with PEGylated IL-4. The molar mass and composition of the polymers markedly affected the conjugation yield. The highest yield of modifications was obtained with the low molecular weight PMeOx (DP = 30, 2.5 kg/mol) followed by a slightly higher molar mass PMeOx (DP = 50, 4 kg/mol) and DP = 108 (10 kg/mol) with no dependence on copper(II) sulfate concentration. Conjugation of IL-4 with P(MeOx-*co*-ABuOx) was similarly effective. However, the PEGylation of IL-4 was not effective with majority of IL-4 remaining unmodified, likely due to nonspecific side reactions between polyether groups and copper catalyst. This appears unusual as click-chemistry also using PEG certainly is well established in the literature. Modification of Plk-IL-4 with PMeOx and P(MeOx-*co*-ABuOx) resulted in 100% protein modification, with no traces of non-modified IL as was confirmed by SDS-PAGE, HPLC, SEC and analytical ultracentrifuge. The conjugates remained chemically stable as was confirmed by urea challenge. Under thermal stress (100 °C), the similar changes in secondary structure of the proteins were observed in all tested groups, however, the modification with PMeOx or P(MeOx-*co*-ABuOx) improved IL-4 thermal stability as was confirmed by the ability to re-fold and restore the proper secondary structure upon cooling. The conjugates were active *in vitro* as was confirmed by proliferation of TF-1 suspension cells (hematopoietic cells expressing both the type I and the type II IL-4 receptor). The activity of IL-4/PMeOx and IL-4/P(MeOx-*co*-ABuOx) was comparable to wild type IL-4.

An unusual kind of conjugate was very recently described. A new and exciting concept in the context of polymer-enzyme interactions was introduced by Tiller employing PMeOx with a particular end-group, iminodiacetate (IDA) [175]. The enzyme employed in this study was HRP. While OH-terminated PMeOx did not show any significant interaction with HRP (as determined by isothermal titration calorimetry), the IDA-terminated led to pronounced, entropy-driven binding. Thus, the IDA seems to direct or initiate that contact with HRP which triggers a secondary binding, driven by release of water molecules from the hydration sphere of protein and/or polymer. Investigation of enzymatic activity showed that the binding has a non-competitive inhibition effect. Apart from the novel concept for enzyme inhibition, the presented results should be of great importance in the context of POx/protein interactions. It shows that while a particular polymer, here PMeOx, may not show any significant binding to proteins, smallest changes such as a small chain end, may lead to dramatically altered binding. This result highlights once more, that one should be very careful with the assumption that some particular polymer is biocompatible, as smallest changes may strongly affect the interaction with biological systems.

4.5. POx-lipid conjugates: lipoPOx

Conjugation of hydrophilic POx with long alkyl moieties is another feasible path to amphiphilic compounds with tunable hydrophilic/hydrophobic balance. If lipid or lipid-like moieties are used, so-called lipopolymers are obtained. Predominantly, POx have been linked to lipids via the chain termini by either the LCROP termination reaction using nucleophilic lipids (i.e. amino functionalized lipids or long alkyl chains) [176] or via the LCROP initiation using a lipid triflate or tosylate initiator [177,178]. Although both approaches are feasible and yield well-defined lipoPOx, the latter might be more advantageous as the degree of lipid conjugation is somewhat higher and significantly lower amount of costly lipids are needed for the synthesis. Alternatively, the lipid can also be conjugated later to functionalized POx by various polymer analogue reactions [23].

Very early, lipoPOx were studied as biomaterials. In fact, one of the first accounts of POx in a biomedical context by Zalipsky et al. [23] reported on the long blood-circulation times of liposomes

comprising PMeOx-, PEtOx- (lipoPMeOx and lipoPEtOx, respectively) in comparison with PEG-lipopolymers (lipoPEG) (Fig. 23). For all three lipopolymer-decorated liposomal systems, a very similar stealth effect and favorable tissue distribution was found. It is also noteworthy that already this study suggested that lipoPMeOx slightly outperforms lipoPEtOx and lipoPEG liposomes in terms of liver and spleen accumulation and lipoPEG and lipoPEtOx showed a very similar biodistribution. This is probably related to the higher hydrophilicity of PMeOx than the slightly amphiphilic PEG or PEtOx found in a later study by Naumann et al. [178]. Again, the reader is referred to the recent work showing accelerated blood clearance in lipoPOx decorated liposomes.

Although, in very early studies the stealth effect of lipoPOx were reported, lipoPEG and in the following PEGylated compounds became the gold standard for hydrophilic biomaterials while POx-based compounds were rarely studied. Certainly, this was not because of either polymer's properties but the broad commercial availability of a broad range of well-defined PEGs already in the 1990s. Despite the first report by Zalipsky et al., in the rare reports on the use of lipoPOx in liposomal systems [162,179–181] the specific advantageous properties for lipoPOx systems were not fully exploited. Only recently, the potential of lipoPOx for liposomal drug formulations regained attention. Xu et al. [182,183] used lipoPEtOx for pH-sensitive liposomes for doxorubicin (DOX) delivery as an alternative to lipoPEG systems. Besides the long blood-circulation time an enhanced endosomal escape property for these systems are reported.

In several papers, Pippa, Demetzos et al. [184–187] reported on the physicochemical, morphological and thermotropic behavior of mixed and chimeric liposomes with lipoPMeOx or lipoP(MeOx-*grad*-PheOx) incorporated in the lipid bilayer. They used indomethacin as a model drug and investigated the influence of the lipoPOx on the bilayer membrane stability and thus permeability for the drug. Liposomal formulations with targeting (folate) and a pH-triggered drug-release (doxorubicin) was reported by Ma and co-workers [188]. The authors used lipid-PEtOx, which was functionalized by a folate at the distal chain terminus to target the folate receptor (FR) of FR overexpressing cancer cells.

Although not a liposomal system but nevertheless of relevance along this line is a very recent report by Hespel et al. [189] on a dual-sensitive micellar drug delivery system (DDS). They synthesized core-cross linked micelles from a mixture of lipoPAA (poly(-acrylic acid)) and lipoP*i*POx with unsaturated lipids via thiol-ene click chemistry. The polymers provided the pH (PAA) as well as temperature sensitivity (P*i*POx) of the micelles. Phyllochinon (vitamin K_1) was incorporated in the cross-linked hydrophobic micellar core and effectively released only by passing both the critical temperature and pH threshold.

Liposomes strongly benefit from the incorporation of lipopolymers. First, the steric stabilization by the formation of brush-like layers at the outer and inner lipid bilayer interfaces renders them mechanically more stable and secondly, the dense corona of a hydrophilic linear polymer is the prerequisite for the so-called “stealth effect” that reduces protein-bilayer interaction and provides protection against lipases and the immune system. As the self-assembled lipid bilayer of liposomes and other bilayer constructs such as free standing or blank lipid membranes are simple models for the highly complex cell and cell organelle membranes, addition of synthetic lipopolymers results in the more complex biomimetic constructs that mimic biomembranes with extra- and intracellular matrices. Such constructs are used for fundamental studies of biomembrane associated interaction and transport phenomena. For a long time, such studies were impaired by the very low mechanical stability of lipid bilayers but addition of lipopolymers and especially the development of polymer-tethered lipid bilayers on solid supports [190,191] enabled meaningful and detailed studies of biomembrane associated phenomena. Again, initially lipoPEG has been used for the construction of polymer-

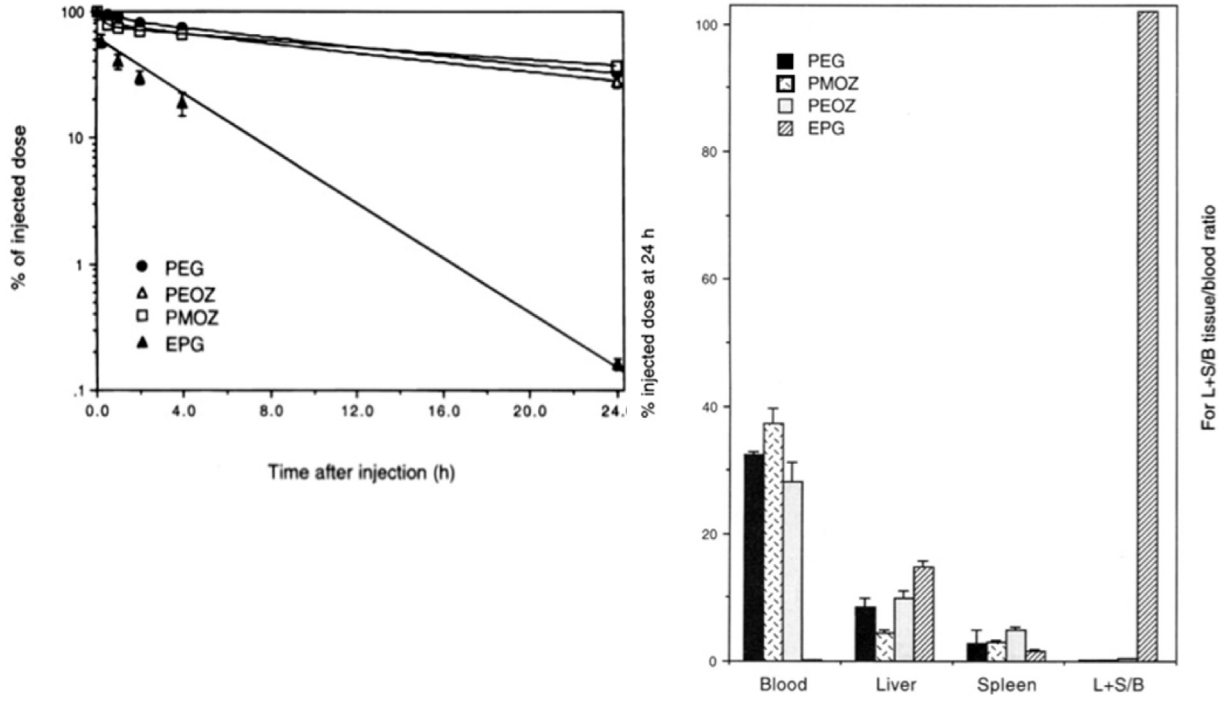

Fig. 23. One of the first studies of POx in a biomedical context show the stealth effect for liposomes with incorporated PEG, PMeOx (PMOZ) and PEtOx (PEOZ) lipopolymers. Left: Blood circulation times of ^{67}Ga-labeled liposomes with PMeOx, PEtOx and PEG lipopolymers and egg phosphatidylglycerol (EPG) as the control. Right: Tissue distribution of the liposomes at 24 h p.i. (mice). Reproduced, with permission from Ref. [23]. Copyright 1994 American Chemical Society.

tethered biomimetic membranes. However, the interaction of the PEG tether with the lipid bilayer itself as well as with incorporated transmembrane proteins was noted and in consequence lipoPOx-based systems were reported. In a series of papers, Tanaka and Jordan described the construction, properties and use of biomimetic membranes on solid supports with PMeOx and PEtOx as the hydrophilic tethers and ether lipids because of their better long-term stability as compared to the commonly used ester lipids [192–197]. Such lipoPOx biomimetic membranes were found to be structural stable for a very long time, showed a very high lipid mobility within the bilayer and can even be used as quantitative models for the study of integrin-mediated cell adhesion [197] and description of the frictional coupling of transmembrane proteins in complex biomembranes [196]. Naumann et al. [178,195,198–205] used lipoPOx-based bilayer systems for the detailed study of the influence of the lipopolymer on the lipid-raft formation and membrane protein sequestering. Also, the findings indicate a favorable (lower) interaction of lipoPOx as compared to lipoPEG with the biomembrane itself.

4.6. POx-drug conjugates

Polymer-drug conjugates (PDCs) are DDS containing one or more drug(s) covalently attached to functional groups of the polymer directly or through a linker molecule. This strategy not only increases the drug solubility but rather offers a potential for a drug to be delivered in a controlled manner. This can also pave the way to targeted DDS by fine tuning of the carriers. PDCs have been pioneered more than 60 years ago by Jatzkewitz [206,207]. In this truly groundbreaking work, Jatzkewitz demonstrated that drugs can be covalently attached to a polymer backbone and that this can lead to a dramatic prolongation of bioactivity. After subcutaneous administration of a conjugate of mescaline to PVP, the drug could be detected in the animal's urine after 17 days. In contrast, if the drug was administered alone or as a mere mixture with PVP, no drug was detectable after 16 h. During the past decade, many state of the art reviews have been published on PDCs for cancer and non-cancer applications. However, the concept of PDCs are not only limited to small molecules but also encompass high molecular weight drugs and various biologics like protein and nucleic acids [208–213]. Although research on anti-cancer drugs is quite predominant, public organizations, companies and private foundations also combat other diseases. For example, the Michael J. Fox foundation, pursues an aggressively funded research agenda to find a cure for Parkinson's disease (PD).

Currently available dopaminergic drugs have shown remarkable improvement in PD, but at the same time, they often lead to significant motor complications. Such complications are generally attributed to the pulsatile nature of dopaminergic agents. To effectively address this important issue, Serina Therapeutics Inc. developed POx based rotigotine (ROT) conjugates (Fig. 24) [214].

ROT is FDA approved dopamine receptor agonist. The ROT-POx conjugates were prepared using three different linkers. Depending on the linker, *in vitro* release of ROT in the rat plasma revealed the half-life of 2.4 h (fast; SER-212), 7.1 h (medium; SER-213) and 11.9 h (slow; SER-214). Plasma concentrations over a 7 days period were also evaluated by subcutaneous injection of pure ROT, and fast and slow release ROT-POx conjugates. Male sprague-dawley rats treated with ROT (0.5 mg/kg) had a plasma concentration below the detection limit after 24 h, while the slow release ROT-POx conjugate (1.6 mg/kg ROT equivalent) had a plasma drug concentration above 0.5 ng/ml for 7 days with half-life of 40 h. The pharmacokinetic (PK) profile of the slow release conjugate remained stable by repeated weekly administration for up to 12 weeks in normal rats. The ROT level remained at or above the therapeutic range (0.5 ng/ml) up to 4 days (Fig. 24).

This laid the foundation for more extensive research to treat PD. Non-human primate studies on *cynomolgus macaques* (n = 3) were performed subsequently. The test subjects received weekly doses of slow release ROT-POx (1 mg/kg) by subcutaneous injection. During the four weeks period the plasma level of released ROT (Plasma ROT, PR) was similar to the total releasable ROT (TRR). Plasma level of both released and total drug rose continuously the first three to four days and reached steady state by day 7. By repeated dosing, a stable plasma ROT level of 1–2 ng/ml could be achieved. This study led the way to a first in human study of ROT-POx. The progression of ROT-POx conjugate into clinical trials is the major breakthrough, highlighting the potential of POx as biomaterial. The first ROT-

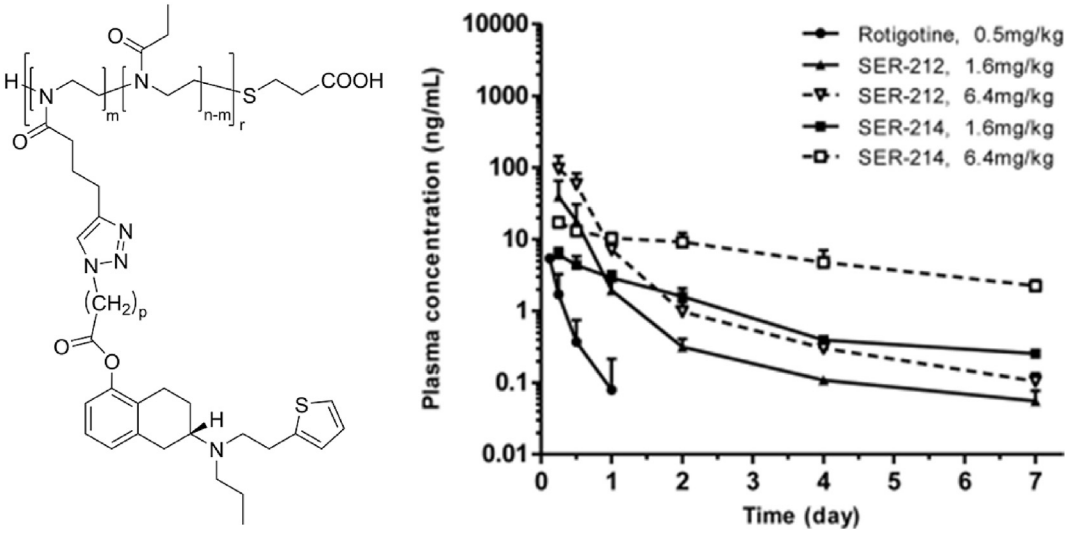

Fig. 24. Left: Structure of POx-conjugated rotigotine hydrochloride (SER-214), which is currently in clinical trials for the treatment of Parkinson's disease (m = 10, n = 200, p is a value from 1 to 4, and r for random copolymer). The ester moiety is hydrolyzed *in vivo* and the hydrolysis rate can be controlled by adjusting p. The overall molar mass if the polymer is small enough to ensure rapid renal clearance. Right: Pharmacokinetic profiles of SER-212 and SER-214 following a single subcutaneous injection in male Sprague-Dawley rats. Plasma was collected at various time points from 6 to 168 h post injection with either rotigotine HCl (0.5 mg/kg), SER-212 (1.6 or 6.4 mg/kg), or SER-214 (1.6 or 6.4 mg/kg). Reprinted with permission from Ref. [214]. Copyright 2013 John Wiley and Sons.

PEtOx (SER-214) conjugate for the treatment of PD has entered phase I of the clinical trials. Serina Therapeutics filed the Investigational New Drug (IND) application with the FDA in July 2015, and the first subjects were enrolled in the study in the first quarter of 2016 [21]. The first cohort of subjects (single dose cohort having four subjects designated as cohort 0) has completed dosing, a single 20 mg dose of SER-214 (equivalent to, 2.4 mg of ROT) was administered subcutaneously. Dosing was completed without any adverse effects. No changes were recorded in blood pressure, blood chemistries, liver panels, hematology and ECG etc. The assessment of the plasma concentrations over time after administration are of greatest interest regarding the side effects of dopaminergic drugs. Most importantly, a slow and steady rise in plasma levels for both PR and TRR, that reaches an approximate C_{max} on about day 3–4. Importantly, there is no "burst" release of ROT in the first 8 h, which could have been a safety concern. After day 7 there is a drop in both PR and TRR levels to below the levels of detection. These observations were similar with monkey plasma levels of ROT at low dose (1 mg/kg). The calculation of PR/TRR ratio by extrapolation of results obtained from this cohort revealed that in human, 3–4% of attached ROT is released, while in macaques, a release of only 1–2% was found. This difference is not surprising because *in vitro* ROT release was faster in human plasma than in monkey plasma [22]. After the successful completion of single dose cohort, multi-dose phase of the study is in-progress and progression to phase 2 is expected soon.

Following the approach of the Jaunarajs, i.e. 3 linker chemistries capable of giving 3 different release profiles, England and coworkers [215] reported a conjugate of SN-38 (hydrophobic, active metabolite of irinotecan) with partially POx modified 5th generation PLL dendrimer. Irinotecan and SN-38 both suffer the problem of narrow therapeutic index. All dendrimer conjugates had approximately 8 wt% of SN-38, which equates to 25 drug molecules per dendrimer on average. Significantly different release profiles were obtained upon *in vitro* drug release evaluation in PBS (overall release was low) and plasma (overall release high) possibly because of enzymatic processes in plasma. The release half lives were 2.5 h (fast), 21 h (medium) and 72 h (slow). *In vivo* studies in mouse SW620 xenograft model revealed that only medium release conjugate achieved the desired sustained exposure of SN-38 and showed maximum tumor regression i.e 69% while no regression was observed with irinotecan treatment. The fast and slow release conjugates showed no antitumor effect due to the low plasma concentration which was observed during *in vivo* pharmacokinetic evaluation. Besides significantly improved efficacy of the medium release conjugate, it was accompanied by reduced gastrointestinal effects relative to both irinotecan groups and the fast release conjugate.

A few other studies have also dealt with conjugation of POx to various drugs and dyes. Because of the immense use of antibiotics, resistant strains to almost all antibiotics are known. Therefore, new methods of antibiotic design and delivery are urgently needed. Schmidt et al. synthesized POx and PEG based ciprofloxacin (CIP) conjugates [216]. More specifically, CIP possessing a COOH functionality and a piperazine ring for conjugation, was covalently attached to the chain termini of PMeOx, PEtOx and PEG. The direct coupling of PMeOx and CIP resulted in the reduction of overall antimicrobial activity (MIC value of PMeOx conjugate at piperazine end group was 1.25 g/L and 0.625 g/L for COOH conjugated CIP, while for plain CIP it is 0.5 mg/L against *S. aureus* strain). The author argue that the reduced activity could be attributed towards reduction in biological activity upon conjugation or inability of the conjugate to enter the bacteria. The antimicrobial activity of different conjugates containing spacers was tested against 5 different microbial strains (Fig. 25). The comparison of PMeOx with 10 and 30 repeat units revealed that antimicrobial activity of the former is 3 times higher (0.3 μmol/L) than that of pristine CIP against *S. mutans* and *S. aureus* (Fig. 25 B). In comparison, $PMeOx_{30}$ conjugates showed reduced activity against both strains (Fig. 25 A). Increasing the side chain by one methylene group ($PEtOx_{30}$) showed a lower activity for *S. aureus*, *S. mutans* (Fig. 25C). In case of gram negative bacteria all investigated conjugates were less effective compared to the pure drug. Overall, the antimicrobial activity of these conjugates increased in the order of PMeOx < PEtOx < PEG. This raises the question, whether the spacer molecule has increased the biological activity of the whole conjugate or it merely helped the conjugate for intracellular transport showing enhanced pharmacological activity. Besides this, incorporation of the biocidal satellite group dimethyldodecylamine (DDA) via the initiator yielding a quaternary ammonium terminus did not strongly improve activity for most bacterial strains (Fig. 25 E&D).

For further investigations regarding the antimicrobial activity of POx based antibiotic conjugates, *Schmidt* et al. synthesized POx based penicillins (Pen) G and Pen.V conjugates via direct termination of the LCROP of POx with the appropriate antibiotic [217]. Specifically, PMeOx (DP = 5–45) was conjugated to Pen.G. The activities of all antimicrobial polymers were in same range (MIC against *S.aureus* 0.5 ± 0.2 to 1.4 ± 0.05 mg/L) independent of the polymer chain length. Additionally, the impact of hydrophobicity was investigated by utilizing PMeOx, PEtOx and P*i*PrOx based conjugates. Overall, the activity of POx conjugates against *S.aureus* was about 2 orders of magnitude lower compared to free Pen.G and Pen.V. Again, the incorporation of a secondary biocidal group (DDA) was investigated which increased the activity of each conjugate in this case. Thus, the difference reduced to one order of magnitude between free antibiotic and conjugate.

These findings (incorporation of DDA group increased the activity and highest activity with PMeOx based conjugates) are in contrast to the previous study on CIP conjugates by the same authors. This contrast indicates the presence of structure activity relationships regarding antibiotic, polymer structure, number of repeat units and also the bacterial strain that remain to be understood. DDA based conjugates were 4 (Pen.G) to 9 times (Pen.V) more active against *E.coli* than free antibiotic (Fig. 26). The hydrolytic activity of penicillinase was also tested on the Pen.V conjugates. The PMeOx and PEtOx based Pen.V conjugates were hydrolyzed 50 times slower than the free drug. This might have significant implications for the treatment of resistant bacterial strains. Methyl initiated antibiotics polymer conjugates did not show hemolytic activity up to 10 g/L. DDA-X-PMeOx (Pen.G) conjugates showed 3% lysis at 10 mg/L while Pen.G based similar conjugate showed lysis of 50%. While the hemolytic activity of PEtOx based similar conjugates were much higher. DDA-X-PEtOx-Pen.G and Pen.V showed 50% cell lysis at 2 g/L and 5 g/L respectively. These results show that conjugation of antibiotics with POx is a promising method not only to increase the biological activity but also renders them more stable against various microbial enzymes. At the same time, there is strong need to further optimize these systems with respect to biodegradability, different antibiotics and blood plasma half-life.

Very recently, in a very interesting contribution Sedlacek et al. directly compared POx-drug conjugates as a DDS to much more intensively investigated PHPMA based DDS [218]. Keeping in mind the slightly acidic pH environment of tumors, DOX was conjugated to the polymer backbone via an acid sensitive hydrazone linker. Three different DOX conjugates with molar masses of the polymers ranging from 20 to 40 kg/mol (PEtOx-D-40, PEtOx-D-20 and PHPMA-D-40) were prepared. The DOX content was 5.3, 6.1 and 6.2 wt% for PEtOx-D-40, PEtOx-D-20 and PHPMA-D-40,

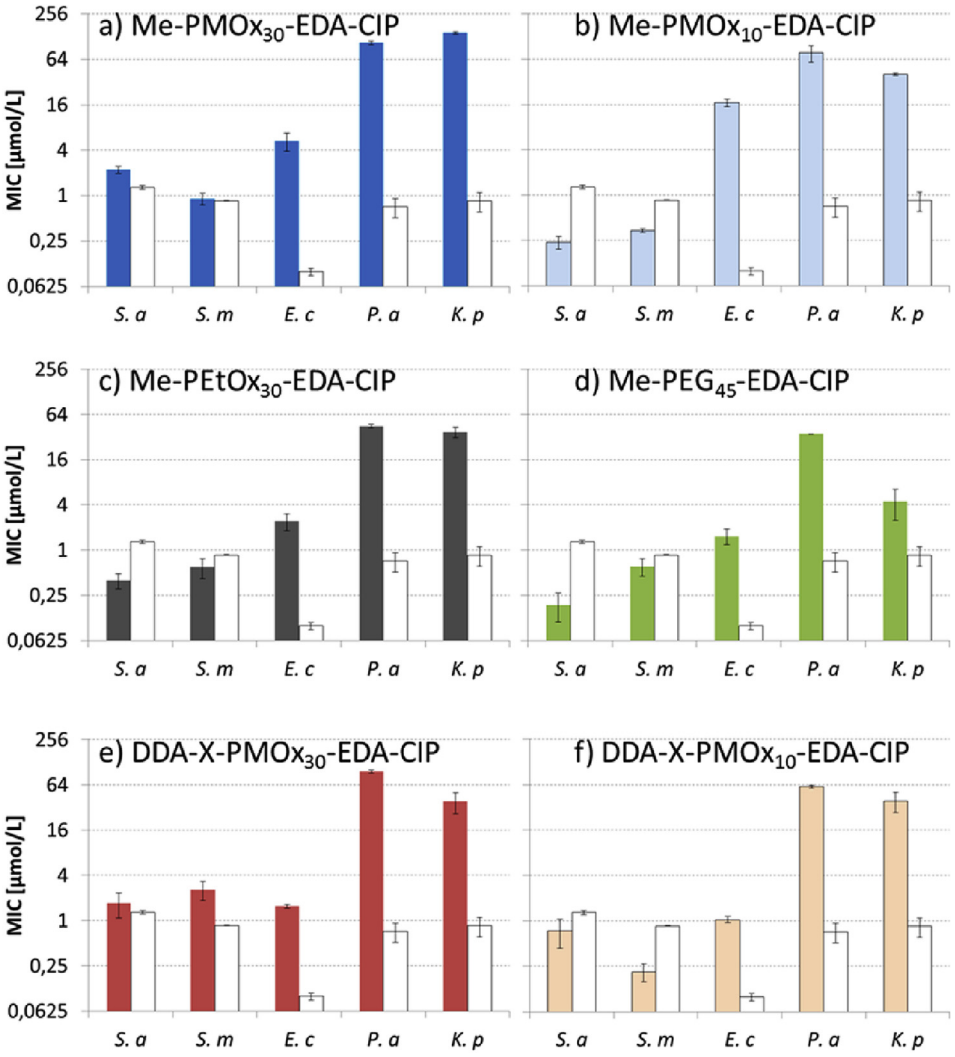

Fig. 25. Molar MIC values for the different conjugates against *S. aureus* (S.a.), *S. mutans* (S.m.), *E. coli* (E.c.), *P. aeruginosa* (P.a.), and *K. pneumoniae* (K.p.) in comparison to the molar MIC value of CIP against each strain (white columns). Data are presented as means ± SD (n = 3). Reprinted with permission from Ref. [216]. Copyright 2015 American Chemical Society.

respectively. Interesting to note, the hydrodynamic size of PEtOx-D-20 and PHPMA-D-40 was very similar while PEtOx-D-40 was slightly larger. Fluorescence lifetime imaging microscopy (FLIM) confirmed the cellular uptake of all the conjugates including DOX free polymer carrier. The quantitative analysis of ATTO-655 labeled conjugates by flow cytometry analysis revealed that PHPMA-D-40 exhibits higher cellular uptake than PEtOx-D-40 and PEtOx-D-20. The results of *in vitro* cytotoxicity studies (MCF-7,HeLa, EL4 and Jurkat) revealed cell line dependent cytotoxic behavior. All conjugates were much less cytotoxic than pristine DOX, presumably due to delayed release of the drug from the conjugate. It should also be noted that the cell viability data presented do not fit the calculated IC_{50} values. Iodine-125 labeled conjugates showed the longest blood circulation time for PEtOx-D-40 (3.09 ± 0.46% ID/g), followed by PHPMA-D-40 (1.50 ± 0.38% ID/g) and PEtOx-D-20 (0.04 ± 0.05% ID/g) after 24 h post injection. The tumor accumulation of PEtOx-D-40 (2.11 ± 0.48% ID/g 24 h p.i.) and PHPMA-D-40 (1.92 ± 0.58% ID/g 24 h p.i.) was significantly higher compared to that of PEtOx-D-20 (0.13 ± 0.22% ID/g 24 h p.i.). Accordingly, the *in vivo* studies in 57BL/6 mice revealed that PEtOx-D-40 is more effective than PEtOx-D-20 in terms of tumor inhibition and survival. Interestingly, PHPMA-D-40 showed superior tumor growth inhibition at early time points, but this difference became non-significant at day 21 of therapy and overall survival was the same as that of the PEtOx-D-40 group. A possible reason for this could be enhanced cellular uptake of PHPMA-D-40 in the beginning of therapy and a slow but sustained release from PEtOx-D-40 during the course of treatment.

Kanazaki et al. conjugated indocyanine green (ICG) to partially hydrolyzed PEtOx for the photoacoustic imaging of tumors [219]. The impact of 3 factors, namely molar mass of the polymer, hydrolysis ratio and number of ICG molecules attached to PEtOx were investigated. An unusually high tumor uptake (11–13% ID/g) and increased half-life in blood was observed for molecular weights above 12 kg/mol (Fig. 27). It would be very interesting if such high tumor uptake could be also obtained using e.g. radiolabeled cargo, which is arguably better to quantify.

The tumor to blood ratio was larger than 3 when the molecular weight of POx was less than 50 kg/mol, which is significantly higher than PEG-ICG conjugate (T/B ratios; 1.2 and 0.7 at 24 h post-injection for PEG-ICG (20 kg/mol) and PEG-ICG (40 kg/mol), respectively). Increasing the degree of hydrolysis from 2.5 to 20% reduced the plasma half-life from 4.9 h to 1.1 h. *In vivo* biodistribution studies using tumor bearing mice demonstrated that 5% hydrolyzed PEtOx (50 kg/mol) conjugated with ICG (ICG/

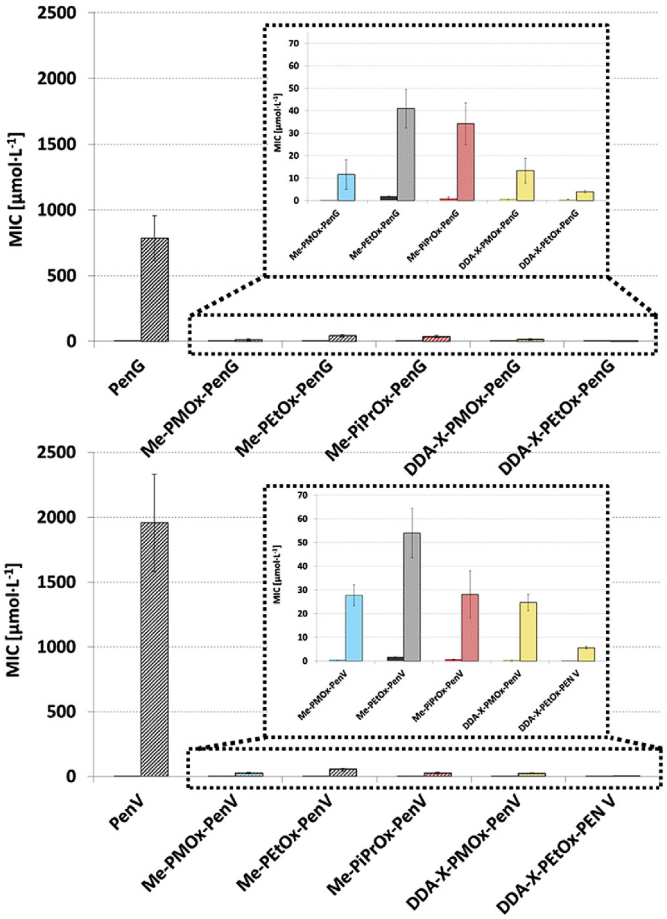

Fig. 26. MIC values against S. *aureus* of Pen.G (top), Pen.V (bottom), and the different conjugates with (right columns) and without (left column) penicillinase. All measurements were performed at least in triplicate, data are presented as means ± SD. Reprinted with permission from Ref. [217]. Copyright 2017 American Chemical Society.

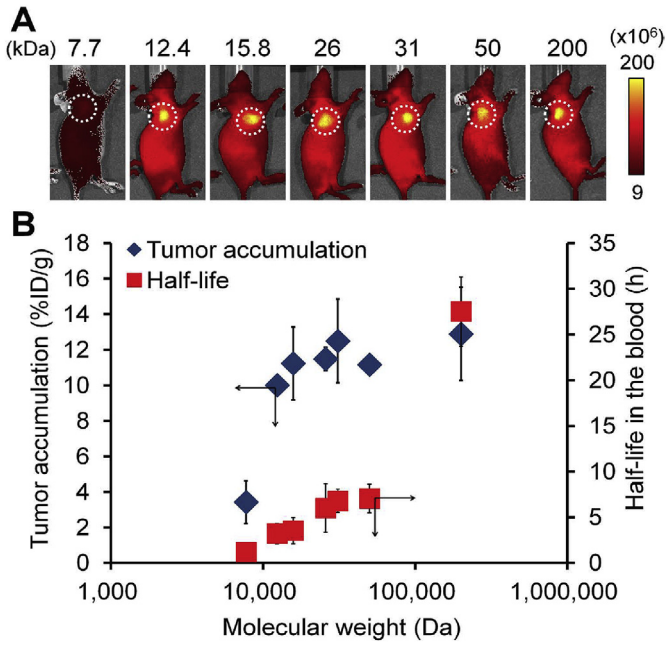

Fig. 27. *In vivo* fluorescent measurement of PEtOx-ICG derivatives with different molar mass. (A) *In vivo* fluorescence imaging of tumor-bearing mice administered with PEtOx-ICG (left to right; P1-ICG1.1, P2-ICG1.1, P3-ICG0.9, P4-ICG0.7, P5-ICG0.8, P6-ICG1.0, and P7-ICG1.1) (P1 to P7 increasing molecular weight, number of ICG conjugated to PEtOx are in range of 0.7–1.1). Dotted circles indicated the tumor regions. (B) Tumor accumulation (%ID/g) (blue) and half-life in the blood (h) (red) of POx-ICG. Reprinted with permission from Ref. [219]. Copyright 2016 Creative Commons Attribution 4.0 International License.

POx = 7.8), showed relatively high tumor accumulation, resulting in delivery of the highest dose of ICG among the conjugates tested. This combination showed the clear visualization of the tumor region 24 h after administration. The other samples with 10% degree of hydrolysis showed lower tumor accumulation as the number of ICG increases.

Overall, the number of studies on POx based PDCs in the last years is limited. However, one might expect this might change significantly as SER-214 progresses through clinical trials. Clearly, this is a hallmark for POx based PDCs and could be the most exciting area of development for the POx-community in the near future.

Apart from therapeutic molecules, therapeutic radionuclides are also valuable therapeutic entities, which can be coupled to polymer to better control the therapeutic effect. Very recently, two contributions were published in this context. In both cases, the well-known LCST, which can be nicely adjusted using POx, was employed. Sano et al. investigated the brachytherapy of Y-90 labeled POx using intratumoral injections [220]. The idea is that the polymers, below their cloud point at room temperature, agglomerate at body temperature. Thus, localization of the radionuclide within the tumor is ensured to some extent. For such an application, the narrow interval of thermoresponse of POx is particularly important. The authors investigated the influence on the polymer structure and molar mass. PEtOx, having a cloud point well above physiological temperature, was not retained in the tumor, similar P*i*PrOx while the polymers with lower cloud points and higher molar mass (20 kg/mol) were retained much better. Thus, prolonged survival of about 50% of animals could be achieved at an injected dose of 3.7 MBq. Hruby and co-workers used a similar approach, however, instead of applying single linear POx chains, polymer brushes comprising a β-glucan-backbone and POx side chains were investigated [221]. The thermoresponsive POx were copolymers of *i*PrOx and *n*BuOx. Through the β-glucan component, the authors could integrate an immunostimulatory aspect, in addition to the brachytherapy. Again, about 50% of the animals were cured.

4.7. Soluble antimicrobial POx

Soluble antimicrobial POx were pioneered by the Tiller group, who used quaternized amine groups to achieve an antibacterial effect of bioinert PMeOx [222]. Subsequently, the Tiller group enhanced the effect of the antimicrobial action, often expressed by the minimal inhibitory concentration (MIC), by altering the so-called satellite groups of the telechelic POx. Such, MIC of around 100 µM–6 µM against *S. aureus* could be achieved [223,224]. Recently, this work has been expanded by use of functional satellite groups, again mainly by the Tiller group. Fik et al. were able to introduce various functions via the terminating agent during LCROP of PMeOx [225]. Basis was the use of the unprotected, antibacterial end-group as initiating agent for LCROP. The authors were able to realize primary and quaternized amines or methacrylamides as functional groups with high end-group fidelities. MIC values as low as 3 µM against *S. aureus* or 8 µM against *E. coli*, respectively, were found. The system of telechelic POx with one antibacterial and one functional end-group was enlarged even further by usage of esters of n-alkyl alcohols as satellite groups [226]. The esters can be

hydrolyzed by diluted NaOH or lipases, which deactivates the polymer. Specifically, an increase in MIC (Fig. 28) of the polymer with non-hydrolyzed octyl ester by 2-orders of magnitude from 26 μM to ≥2.5 mM for the hydrolyzed ester against *S. aureus* was found. This switching effect may be helpful to prevent development of resistance by the bacteria.

Moreover, the influence of polymer architecture as well as different hydrophilicities has been explored [227]. A series of homo-, random and block-copolymers (of two monomers from) of MeOx, EtOx, and *i*PrOx were synthesized. Octyl ester and DDA were chosen as end-groups, since this combination led to best results in MIC values. It could be shown that the MIC was dependent on architecture, hydrophilicity, and location of DDA group and satellite group in relationship to the location of more or less hydrophilic monomers. Best performance was found for a statistical copolymer of PMeOx and PEtOx with PEtOx content around 60%, which had an MIC value against *S. aureus* of only 1 μg/L. Also, a synergistic effect of was observed for the combinations of MeOx/EtOx (for statistical and block copolymers) and MeOx/*i*PrOx (for statistical copolymers). It should be noted, that compared MIC values are given in mass concentrations, i.e. they are not taking into account that the molar mass of the polymers differ.

Martins et al. screened the performance of PMeOx-DDA compared to PEI against 69 different strains of 13 different bacteria, isolated from clinical samples [228]. Until now, this seems to be the biggest collection of determined MIC values for the given polymers for a variety of species and strains. Within the data, large variations are observed concerning MIC values between strains and species as well as efficacy between POx and PEI. Again, comparison between POx and PEI is somehow challenging since different molar concentrations were used as MIC values are given in mass concentrations and both polymers possess different amounts of antibacterial groups. However, the authors show that both antibacterial polymers kill bacteria within the first minutes of contact if used well above MIC.

Another recent contribution by the Tiller group further expanded the use of end-group quaternized POx as soluble antimicrobials [229]. Here, the POx was equipped with two quaternized long alkyl termini and subsequently hydrolyzed. The effect of the polymer chain lengths as well as alkyl chain length was investigated. Interestingly, the longer alkyl termini prevented deactivation in the presence of Ca^{2+} ions, which is a known limitation for antimicrobial activity of PEI. Balancing the effect of terminal side chains and polymer backbone is readily accomplished through the polymer synthesis.

5. POx-based formulations

Drug formulations, in which drugs are physically incorporated into POx based micelles or nanoparticles have been well known for some time. Most commonly, POx is present in form of hydrophilic PMeOx or PEtOx. In these cases again, POx are used as an essentially equifunctional analogue of PEG. Often, well established hydrophobic polymers such als PCL or PLA/PGA are employed for drug formulation. Of course, as such, DDS essentially equifunctional to more established PEG-containing DDS are obtained. However, arguably the real potential of POx lies were PEG itself has limitations, i.e. multifunctionality or fine-tuning of the hydrophilic/lipophilic balance. This potential of POx has been elucidated significantly in recent years. Some aspects of this topic have been reviewed recently by Pispas and co-workers [230] and Kempe et al. [131]. Here, we will first briefly revise literature on solid drug dispersions before we review the development of formulations of paclitaxel, curcumin and DOX, which represent some of the most commonly studied APIs. Subsequently, we will look into developments with other cargo, address targeted DDS and finally systems that contain some diagnostic functionality.

5.1. Solid dispersions

Due to their high versatility and broad choice of excipients, solid dispersions (SDs) are widely used for the formulation of both, water soluble and insoluble drugs. Policianova et al. [231] investigated the influence of four different polymer matrices, PVP, PHPMA, PEtOx and PEG on the drug release of the BCS Class I API acetylsalicylic acid (ASA). Compared to the reference physical mixture of ASA with lactose (30/70 wt%), only the PEG-based solid dispersion exhibited an increased dissolution rate (PEG (M_w = 10 kg/mol): 5.4 [%/min]). All other SDs significantly reduced drug dissolution kinetics (PVP (M_w = 360 kg/mol): 1.42 [%/min]; PHMPA (M_w = 81 kg/mol): 2.24 [%/min]). In particular, PEtOx with a M_w of 500 kg/mol exhibited the lowest dissolution rate (0.75 [%/min]; linearity of drug release indicated concentration-independent zero-order dissolution kinetics) correlating to a 7-fold decrease in drug release compared to PEG with a M_w of 10 kg/mol (highest M_w PEG investigated in this study). However, as the dissolution rates were strongly reduced with increasing M_w of the polymer (4-fold faster dissolution rate of PEtOx with a M_w of 50 kg/mol compared to 500 kg/mol), it would have been interesting to investigate higher M_w PEG or lower M_w POx. Clearly, due to the broad parameter space, fine-tuning of the drug release over a wide range of dissolution rates could be facilitated by the type and molar mass of the polymer.

Without going into detail about the characterization techniques (solid-state NMR, wide-angle X-ray scattering (WAXS), differential scanning calorimetry (DSC)), four distinct types of ASA solid dispersions (polymer/ASA = 70/30 w/w) were found: (i) crystalline solid dispersions containing ASA nanocrystallites (ca. 300 nm) dispersed in a crystalline PEG matrix (Fig. 29 A); (ii) amorphous

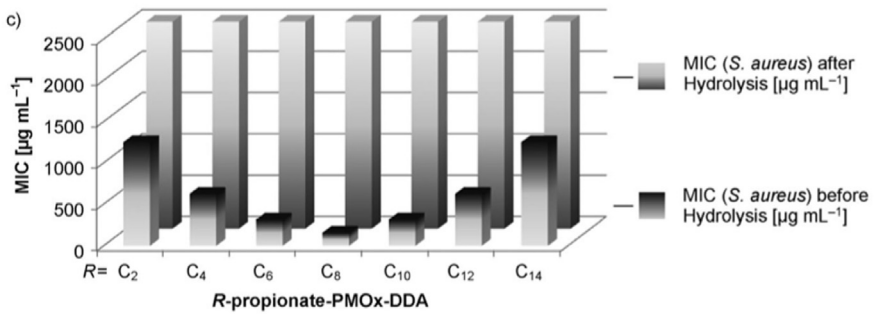

Fig. 28. Observed change in minimal inhibitory concentration (MIC) against S. aureus of telechelic POx with hydrolyzable ester satellite groups. Reprinted with permission from Ref. [226]. Copyright (2014) John Wiley & Sons, Inc.

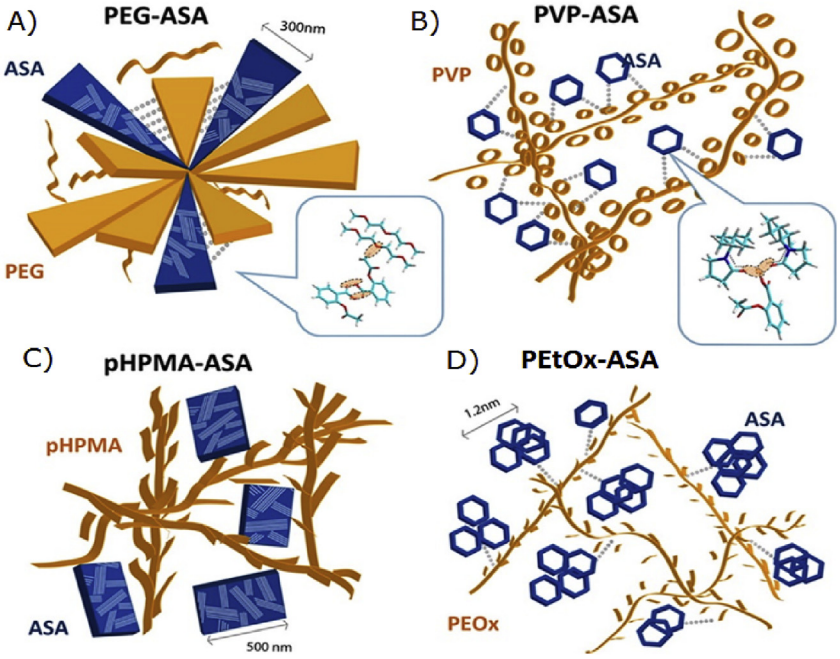

Fig. 29. Schematic representation of 4 distinct types of polymer-ASA (acetyl salicylic acid) solid dispersions: (A) PEG-ASA crystalline solid dispersions; (B) PHPMA-ASA amorphous solid dispersions; (C) PVP-ASA solid solutions; and (D) PEtOx-ASA nano-heterogeneous solid solutions/suspensions. Reprinted with permission from ref. [232]. Copyright 2014 American Chemical Society.

solid dispersions of ASA crystallites (>450 nm) embedded in an amorphous PHPMA matrix (Fig. 29 B); (iii) solid solutions with molecularly dispersed ASA in an amorphous PVP matrix (Fig. 29C) and (iv) nano-heterogeneous solid solutions containing nanosized ASA clusters (ca. 1–2 nm) dispersed in a semiflexible PEtOx matrix (Fig. 29 D) [232]. Important to note, the structure of the ASA solid dispersions was controlled by the chemical structure of the applied polymer, while varying the M_w of the respective polymers had no effect. In more detail, the structural properties of the systems seemed to be determined by (i) the accessibility and affinity of suitable molecular binding sites to form hydrogen-bonds (e.g. amide groups in PEtOx or PVP and acid-moiety of ASA) and (ii) the segmental dynamics of the polymer excipients (higher segmental mobility of PEtOx compared to PVP interferes with hydrogen bonding between PEtOx and ASA). Due to the low T_g of ASA ($T_g = -30\,^{\circ}C$), the amorphization of ASA requires stabilization via hydrogen-bonding and steric interactions with excipients at room temperature. Without this stabilization, ASA can migrate through the polymer matrix resulting in nano-heterogenous PEtOx-ASA systems with a flexible, drug-rich phase ($T_g = 6\,^{\circ}C$) and a rigid, polymer-rich phase ($T_g = 70\,^{\circ}C$). Due to this cluster formation in PEtOx-ASA systems, ASA recrystallized and multiple polymorphs of ASA could be detected. Considering the large structural versatility of the POx family, it would be interesting to evaluated such solid dispersions with other POx then PEtOx.

Claeys et al. also used PEtOx as matrix excipient for both, a water-soluble (metoprolol tartrate (MPT)) and a water-insoluble (fenofibrate (FBT)) model drug by hot melt extrusion (HME) followed by injection molding [233]. Again, release kinetics for the hydrophilic drug MPT could be slowed down by increasing the M_w of PEtOx (approx. release of MPT from PEtOx/MPT = 50/50 w/w after 50 min: 95, 80 and 60 [%] for 50, 200 and 500 kg/mol PEtOx, respectively). Even at the highest investigated drug loadings of 50 wt% MPT or 20 wt% FBT (authors did not mention if higher FBT-loadings would have been feasible, however, due to the hydrophilic/lipophilic discrepancy of polymer and drug, drug loadings comparable to MPT are unlikely to achieve) the absence of the melting peak of the drug as well as a single glass transition temperature T_g of the mixture in between the T_g of both components (investigated for first cycle by DSC) indicated good miscibility without pronounced phase separation. However, after 4 weeks storage, recrystallization occurred in the case of 50 wt% MPT (investigated by XRD), whereas in tablets containing 25 wt% MPT recrystallization was suppressed more efficiently. Tablets containing 50 wt% MPT showed faster dissolution rates compared to 25 wt % (40% and 60% release for 25 and 50 wt%, respectively (after 50 min; PEtOx: 500 kg/mol)), however no sustained release could be achieved and all MPT was released after 3 h. The authors suggest that this might have been slowed down by increasing the length of the POx alkyl side chain. Compared to pure FBT, formulated FBT (20 wt%) exhibited a greatly enhanced dissolution rate (approx. 20 and 60% release of neat FBT and formulated FBT, respectively (after 2 h; PEtOx: 500 kg/mol)) as well as total availability (100% drug release after 2 h, PEtOx: 50 kg/mol).

5.2. Paclitaxel

Paclitaxel (PTX) is a natural compound, one of the most important cancer chemotherapeutics and exhibits extremely low water solubility of approx. 0.4–4 mg/L. Accordingly, it is often used to investigate the formulation capacity of amphiphilic DDS. Previously, amphiphilic POx triblock copolymers of the general composition PMeOx-*b*-PBuOx-*b*-PMeOx, where the DP of the flanking PMeOx blocks is typically approx. 35 and the DP of the central BuOx is 20 (values between 10 and 30 have been investigated as well) have been described as excellent solubilizers for hydrophobic drugs. In particular, this polymer exhibits extraordinary high loading capacities ($LCs = m_{solubilized\ drug}/[m_{solubilized\ drug} + m_{Polymer}]$) of up to 50 wt% for PTX (Fig. 30A) [234]. Detailed physicochemical characterization of the drug-loaded micelles revealed that with the introduction of small quantities of PTX ($LC < 20$ wt%), the micelles became smaller, more defined and also

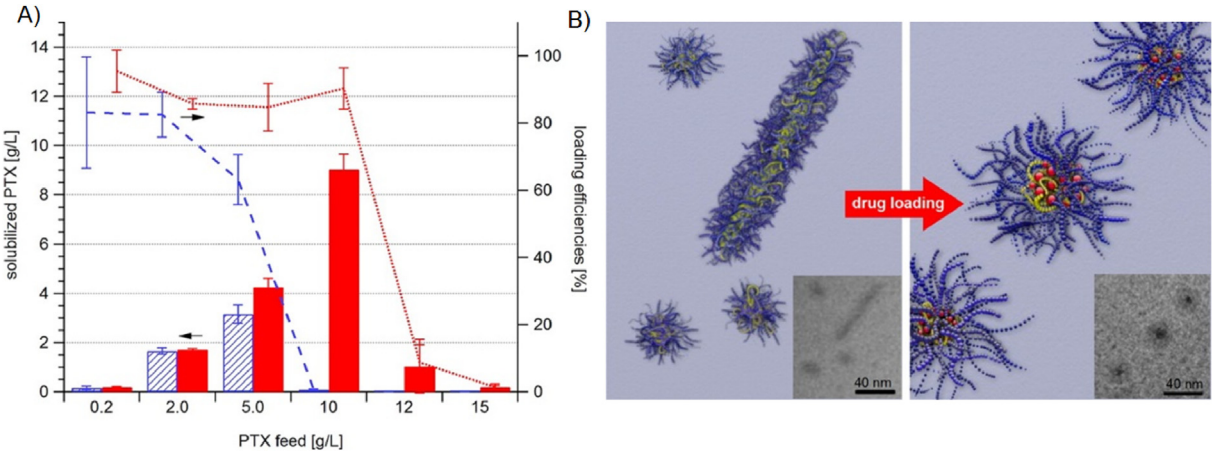

Fig. 30. A) Solubilized PTX (bars, left axis) and loading efficiencies (lines, right axis) of PMeOx-*b*-P*n*BuOx-*b*-PMeOx (red) and PMeOx-*b*-PNOx-*b*-PMeOx (blue) at ρ(polymer) = 10 g/L and different PTX feeds. Data is presented as mean ± SEM (n = 3–5); B) Artistic representation inspired from cryo-TEM images showing coexistence of wormlike structures and spherical micelles of unloaded PMeOx-*b*-P*n*BuOx-*b*-PMeOx, while upon incorporation of 5 g/L PTX, exclusively spherical micelles were observed with a clearly discernible core-shell structure. Reprinted with permission from ref. [235]. Copyright 2014 American Chemical Society.

the formation of worm-like micelles was suppressed (Fig. 30B). However, at higher PTX content, micellar size increased but remained very small (R_h = 23.8 nm @ *LC* = 49 wt%) [235] associated with a transformation into raspberry-like particles [236] as investigated by small angle neutron scattering (SANS). Seo et al. [209] investigated the influence of the chemical structure of the hydrophobic core of ABA-triblock copolymers (all comprising the same hydrophilic PMeOx shell) on the loading capacity for paclitaxel and the structurally related taxane docetaxel. Interestingly, most drug-loaded triblock copolymers comprising from highly polar and weakly hydrophobic 2-*iso*-butyl-2-oxazoline (*i*BuOx) cores to those having hydrophobic HepOx cores exhibited high PTX loadings between 7.8 and 9.6 g/L PTX at ρ(polymer) = 10 g/L. Only the copolymers with the least hydrophobic 2-sec-butyl-2-oxazoline and the most hydrophobic NOx core seemed to be either too polar or too hydrophobic for extraordinary high PTX loadings (Fig. 31, squares).Furthermore, the PTX formulation based on the triblock copolymer comprising the very hydrophobic PNOx central block (PMeOx-*b*-PNOx-*b*-PMeOx, LC_{max} = 24 wt%) exhibited precipitation and formation of larger aggregates after 3 months storage (@ *LC* = 14.5 wt%), whereas the PMeOx-*b*-P*n*BuOx-*b*-PMeOx based formulation was stable for at least 7 months storage at ambient conditions (@ *LC* = 49 wt%; Fig. 31).

Important to note, all these formulations were prepared on a rather small scale of 0.1 mL volume. Scaling up the formulations to 1.5 mL had no major influence on the loading capacity for copolymers comprising weakly hydrophobic cores, whereas drug-loading significantly decreased utilizing polymers with more hydrophobic pentyl, heptyl and nonyl side-chains (Fig. 31, empty circles). Since POx with longer side chains are semicrystalline materials as homopolymers, it was assumed that this might be due to polymer crystallization resulting in phase separation and drug precipitation. Overall, PMeOx-*b*-P*n*BuOx-*b*-PMeOx remained the polymer with the highest PTX loading, exhibiting the highest long-term stability in PBS of at least 7 months at the same time (Fig. 31 filled circles). Notably, several formulations of ρ(PMeOx-*b*-P*n*BuOx-*b*-PMeOx/PTX) = 50/40 g/L formed aggregates with diameters > 300 nm in DI water after 10-day storage, whereas the same formulations in PBS or 5% dextrose solution remained stable in the same timeframe of at least 7 months. However, the formation of larger aggregates can be circumvented by simply lyophilizing (freeze-drying) the respective formulations after preparation and

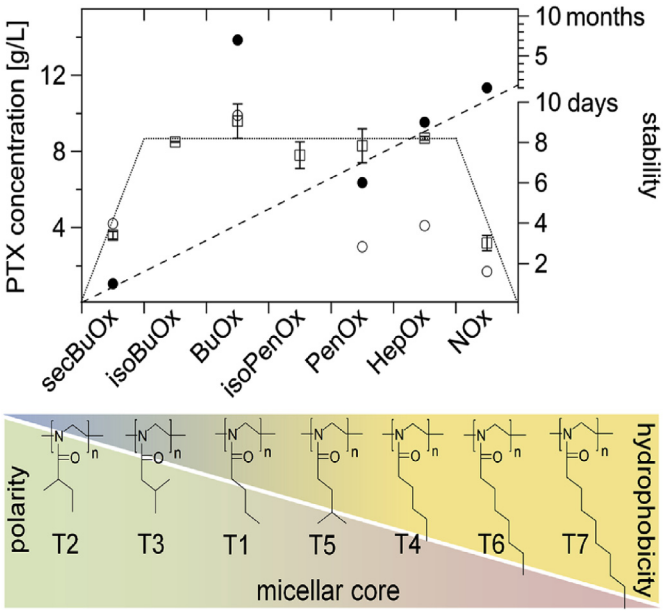

Fig. 31. Influence of the chemical structure of the hydrophobic block of POx based PTX formulations on the maximum drug loading (squares: 0.1 mL volume; empty circles: 1.5 mL volume) and long-term stability (filled circles) in PBS. Stability studies were carried out using multi-angle DLS with a goniometer and formation of large aggregates and/or precipitation was considered as end point. Reprinted with permission from ref. [235]. Copyright 2014 American Chemical Society.

subsequent re-dispersion right before usage without suffering drug-loading.

Hennink et al. have reported increased PTX loading and formulation stability by introduction of aromatic side chains enabling π-π stacking between polymer and drug [237]. However, introduction of aromatic 2-benzyl-2-oxazoline (BzOx) moieties along with *n*BuOx hampered PTX loading (ρ(PTX, max = 5.6 g/L). Also, the corresponding PMeOx-*b*-P*n*BuOx diblock-copolymer enabled only rather low PTX loadings of 2.0 g/L. Interestingly, maximum drug-content of the diblock copolymer for docetaxel was twice as high with 4.0 g/L, suggesting pronounced polymer-drug specificities.

Besides Paclitaxel, also so-called 3rd generation taxoids being

able to overcome drug resistance could be solubilized with PMeOx-*b*-P*n*BuOx-*b*-PMeOx with essentially quantitative drug loading efficiency and final drug/polymer ratios around unity (e.g. ρ(POx/SB-T-1214) = 50/41.8 g/L (= 9500 fold increase in water solubility); *LC* = 46 wt%) [238]. It is interesting that such high loading capacities for the different taxoids were feasible, since, as discussed above, various formulation parameters including (i) the drug and polymer structure; (ii) the drug and polymer concentration; and (iii) the composition of the aqueous medium can have significant influence on the solubilization behavior and physicochemical properties of POx based formulations [239]. Similar to PTX loaded micelles, the micelles loaded with 3rd generation taxoids exhibited small hydrodynamic diameter below 100 nm with spherical morphology excellent for parenteral administration [238]. After 24 h, > 80% of the drug (ρ(POx/SB-T-1214) = 50/40 g/L) was released *in vitro* at pH = 7.4. However, this burst release could be slowed down by increasing the polymer/drug ratio from 50/40 to 50/10 g/L at constant drug content. However, it is questionable if such a simple *in vitro* experiment has relevance for a much more complex *in vivo* situation. More importantly, the formulation with the taxoid SB-T-1214 was 1-2 orders of magnitude more active *in vitro* ($IC_{50,24h}$ = 34.6 mg/L) than paclitaxel against the multidrug resistant breast cancer cell line LCC6-MDR, whereas no difference was observed in wild-type LCC6.

In a q4dx4 dose regimen, POx/SB-T-1214 (maximum tolerated dose (MTD) = 20 mg/kg) significantly inhibited growth of LCC6-MDR orthotopic tumors (700 mm^3 after 28 d), outperforming the commercially available PTX formulation Taxol® and Cremophor EL formulated SB-T-1214 (2000 mm^3 after 28 d) using MTD doses for all groups (Fig. 32). Abraxane treated groups showed tumor inhibition comparable to POx/SB-T-1214, however no statistically significant difference in survival compared to saline control group was observed, whereas POx/SB-T-1214 significantly extended survival time with a median survival of 67 days.

Furthermore, POx/SB-T-1214 (50/40 g/L; SB-T-1214 = 20 mg/kg) formulation was able to suppress the tumor growth of very difficult to treat T11 orthotopic syngeneic transplant model and treatment outcomes differed significantly to Chremophor/SB-T-1214 and Taxol® treated groups (Fig. 33). This is particular noteworthy, as this challenging model has not shown any response in chemotherapy prior to this study. However, it also has to be noted that the MTD was not found to be higher compared to Cremophor (CRE) formulated taxoid, in contrast to what was observed for PTX.

In contrast to 3rd generation taxoids, the POx based PTX formulations resulted in a much higher MTD (150 mg/kg) in NCI-Nu/Nu mice in a q4dx4 dose regimen compared to the clinically approved formulations Taxol® (20 mg/kg) and Abraxane (90 mg/kg) leading to a higher exposure of PTX at tumor site (Fig. 34) [71]. However, at early time points, also moderate uptake of PTX in spleen, liver, kidney and heart were observed (utilizing ^{3}H-labeled PTX). In this study, the high concentration at tumor site can probably not be explained by the widely discussed “enhanced permeability and retention” (EPR) effect, as 80% of PTX (@ POx/PTX = 50/40 g/L) were transferred to serum albumin *in vitro* after 1 h incubation in transfer studies. This transfer is in fact probably much faster (unpublished results). Important to note, mice administered four times with 175 mg/kg PTX-loaded micelles lost over 15% body weight, whereas a single injection of 200 mg/kg POx/PTX micelles was well tolerated without obvious sign of toxicity. This can be partially explained by the fast renal clearance and minimal liver uptake as investigated with ^{64}Cu labeled POx (Fig. 34 A–D). In all cases, whether the polymer was administered alone or with drug, a very rapid, essentially first pass clearance was observed. Similarly, the drug clearance was fast (Fig. 34 A–D). Nevertheless, drug concentration peaked 1 h *p.i.* (Fig. 34 E). After 24 h *p.i.* and in

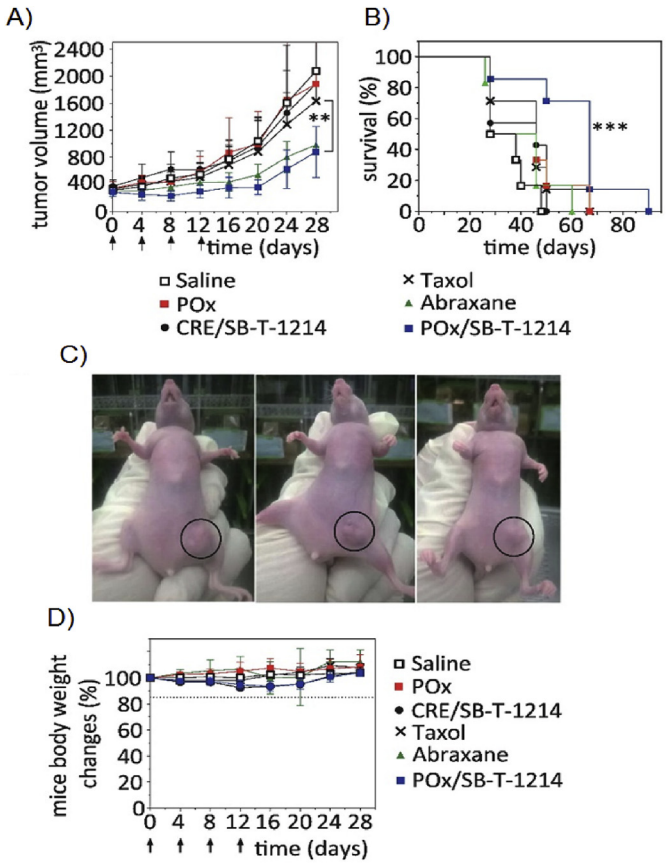

Fig. 32. Efficacy of various paclitaxel and 3rd generation taxoid drug formulations at maximum tolerated doses in LCC6-MDR tumors. (A) Tumor growth inhibition of POx/SB-T-1214 = 50/40 formulation (20 mg/kg) compared to Taxol® (20 mg/kg), Abraxane (80 mg/kg) and CRE/SB-T-1214 (20 mg/kg), saline as well as POx polymer alone (equivalent polymer amount as in POx/SB-T-1214 micelle formulation). Each formulation was injected on days 0, 4, 8, and 12 (indicated by arrows). Data is expressed as means ± SEM, n = 7. ***p < 0.001 (vs. saline group). (B) Kaplan–Meier survival plot for all groups. (C) A representative image of treated mice at day 26. Left, saline group; middle, CRE/SB-T-1214 group; right, POx/SB-T-1214 group. (D) Body weight loss for each treatment group. Reprinted with permission from ref. [238]. Copyright 2015 Elsevier.

contrast to 1 h *p.i.*, the tumor/organ ratio exceeded unity for all investigated organs in case of POx/PTX, while in the Taxol® group the %ID/g in the liver was still higher than %ID/g in the tumor (Fig. 34 G, H). Single injection of the MTD of Taxol® slowed down tumor growth and prolonged survival only for approx. 5 days in A2780 human ovarian tumor bearing mice. In contrast, a single injection of MTD of POx/PTX formulations apparently eradicated the tumor in 4 out of 7 animals, with no observed re-growth for at least 35 days post injection (Fig. 34 I, J).

To address the issue of limited micellar stability, Weberskirch and co-workers reported an approach to create core-cross-linked micelles [240]. The authors terminated amphiphilic diblock copolymers comprising a hydrophobic P(HeptOx-*co*-PynOx) core and a hydrophilic PMeOx shell with either primary or secondary amines to enable further functionalization with for example cell specific ligands. After micellization in aqueous solution (cmc = 0.7 and 1.8 μM; R_h = 6.2 and 6.7 nm), the hydrophobic core was photo-crosslinked by radical polymerization of the alkynyl moieties to potentially enhance the stability of the aggregates ($R_{h,MeOH}$ = 6–7 nm) *in vivo* as well as to reduce release kinetics of encapsulated compounds. Surface functionalization with three different model compounds revealed a higher degree of

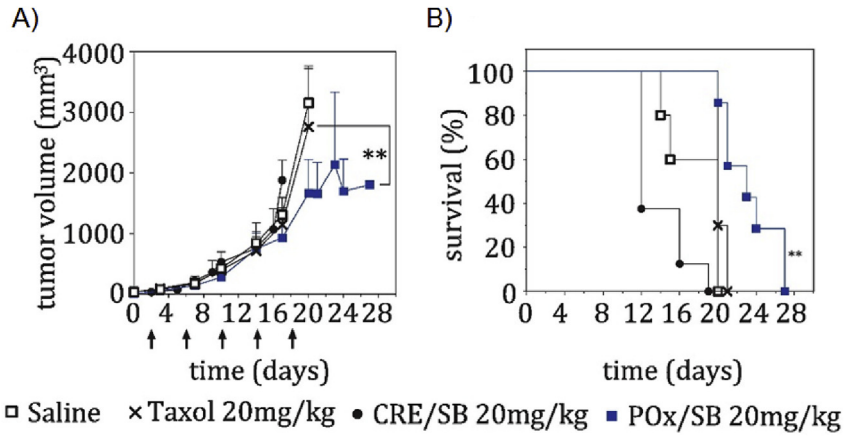

Fig. 33. Efficacy of various drug formulations in T11 OST tumors. (A) Tumor growth inhibition of POx/SB-T-1214 = 50/40 formulation compared to Taxol®, CRE/SB-T-1214 as well as saline. Each formulation was injected on days 2, 6, 10, 14 and 18 (indicated by arrows). Data is expressed as mean ± SEM, n = 10, **p < 0.01. (B) Kaplan–Meier survival plot for all groups. Reprinted with permission from ref. [238]. Copyright 2015 Elsevier.

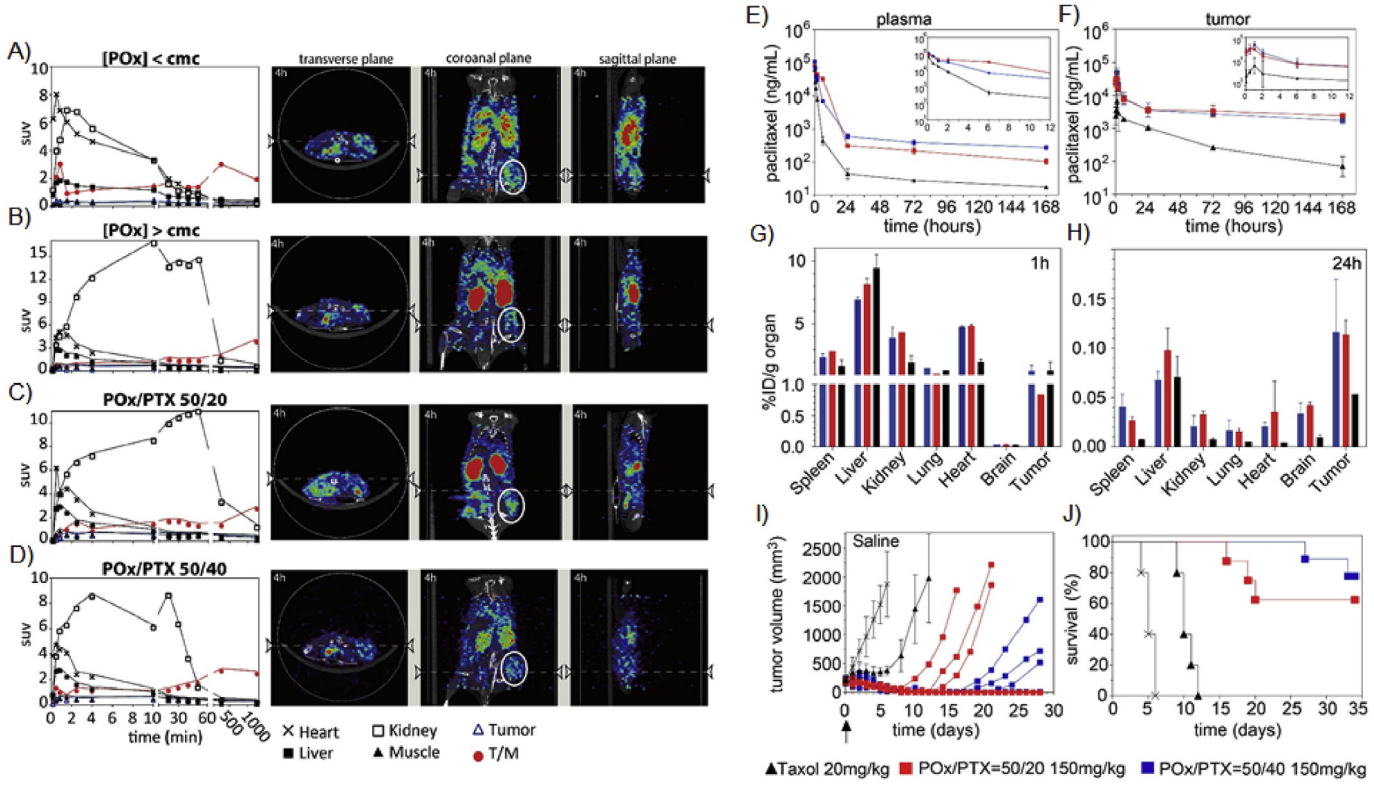

Fig. 34. Biodistribution of polymer (A–D) and drug (E–J) in POx/PTX formulations. Tissue biodistribution and PET/CT images of ^{64}Cu-labeled triblock copolymers (A–D) after *i.v.* injection of polymers and various formulations, respectively. Mice were injected with (A) 0.2 mCi ^{64}Cu-POx polymer alone below cmc concentration, (B) ^{64}Cu-POx micelles without drug (at equivalent dose as 50/20), (C) ^{64}Cu-POx/PTX 50/20 and (D) ^{64}Cu-POx/PTX 50/40 micelle formulation at dose of 150 mg/kg. PET/CT images were taken dynamically for the first hour and then at 4 h and 24 h post *i.v.* injection. Biodistribution data were obtained from quantification of PET images. Strong ^{64}Cu signals were mainly observed in the kidney. Representative PET/CT images were taken 4 h post injection (*p.i.*) (n = 1 for each group). Abbreviations: suv-standardized uptake value; T/M-tumor/muscle ratio. Tumor region is circled white. Pharmacokinetics (E,F), biodistribution (G,H) of PTX and resulting tumor inhibition (I–J) in tumor bearing (A2780 xenograft) nude mice. Plots of PTX concentration in plasma (E) and tumor (F) over 168 h following single *i.v.* injection of POx/PTX 50/40 or 50/20 and Taxol® formulations at MTD dose. (G,H) Organ distribution after single *i.v.* injection of PTX administered as POx/PTX 50/40, POx/PTX 50/20 and Taxol® formulation at 1 h *p.i.* (G) and 24 h *p.i.* (H). Tumor growth inhibition (I) and Kaplan-Meier survival plots (J) of A2780 human ovarian tumor bearing mice after single *i.v.* injection of POx/PTX 50/40, POx/PTX 50/20 and Taxol® formulation at MTD. (E–H) Data expressed as means ± SD, n = 3 for all groups. For I, data for Taxol® and saline control are expressed as means ± SEM, n = 7, while for POx/PTX 50/40, POx/PTX 50/20 nanoformulations, the data of individual animals are presented. Reprinted with permission from ref. [71]. Copyright 2016 Elsevier.

functionalization of the nanoparticles comprising primary amines compared to the ones comprising secondary amines. Instead by photo-crosslinking, such core cross-linked micelles could also be obtained by thermal treatment via microemulsion approach utilizing AIBN as azo-initiator in the presence of 1,6-hexanediol diacrylate (HDDA) to influence particle size [240]. However, no drugs were incorporated into these systems. A similar crosslinking strategy for POx-based micelles was carried out by Schulz [241], but

the core-crosslinked micelles exhibited much diminished drug loading (unpublished data).

Using a q4dx4 regimen, POx/PTX 50/40 at MTD exhibited significant tumor inhibition and after the third dose, all tumors showed complete response [85] for small (volume at start of therapy 100–200 mm^3) tumors in A2780 human ovarian cancer xenografts (Fig. 35 A–D). In late stage, larger tumors (volume at start of therapy 400 mm^3), POx/PTX formulations resulted also in complete remission of tumors (Fig. 35 F,G) in all animals at MTD and ½ MTD even after 120 days post treatment. In orthotopic model of LCC6 multi drug resistant (MDR) human triple negative breast cancer (TNBC), POx/PTX 50/40 g/L (120 mg/kg) reduced tumor growth similar to that of Abraxane, however in contrast to POx/PTX, Abraxane did not lead to increased survival (Fig. 35H,I). Furthermore, a clear trend of tumor inhibition in the very aggressive and resistant T11 OST breast cancer model using POx/PTX = 50/40 g/L at 1/2 MTD was observed, even though this did not result in prolonged survival compared to control groups (Fig. 35 J, K). In contrast to the 3rd generation taxoid SB-T-1214, paclitaxel was not able to affect this tumor model, even at such very high doses.

Concurrent delivery of multiple drugs can improve outcomes of cancer treatments, but typically face challenges because of differential solubility and fairly low threshold for incorporation of many drugs. Incorporation of multiple drug in high capacity POx-based micelles has been an area of active research [242–244]. Very recently Wan et al. [245] evaluated drug combination synergy in POx-based polymeric micelles co-loaded with etoposide (ETO) and an alkylated platinum prodrug (EP/PE). ETO and an alkylated cisplatin prodrug therapy (EP/PE) is the backbone for treatment of prevalent and deadly small cell lung cancer (SCLC). The previously described amphiphilic triblock copolymer PMeOx-*b*-PBuOx-*b*-PMeOx was used to co-formulate EP/PE and ETO in a single high-capacity vehicle. A broad range of drug mixing ratios and exceptionally high two-drug loading of over 50 wt% drug in dispersed phase was demonstrated. These POx micelles have elongated morphology, unprecedented for highly loaded polymeric micelles, which usually form spheres upon drug loading (*vide supra*). The co-loading of EP/PE in the micelles resulted in a slowed-down drug

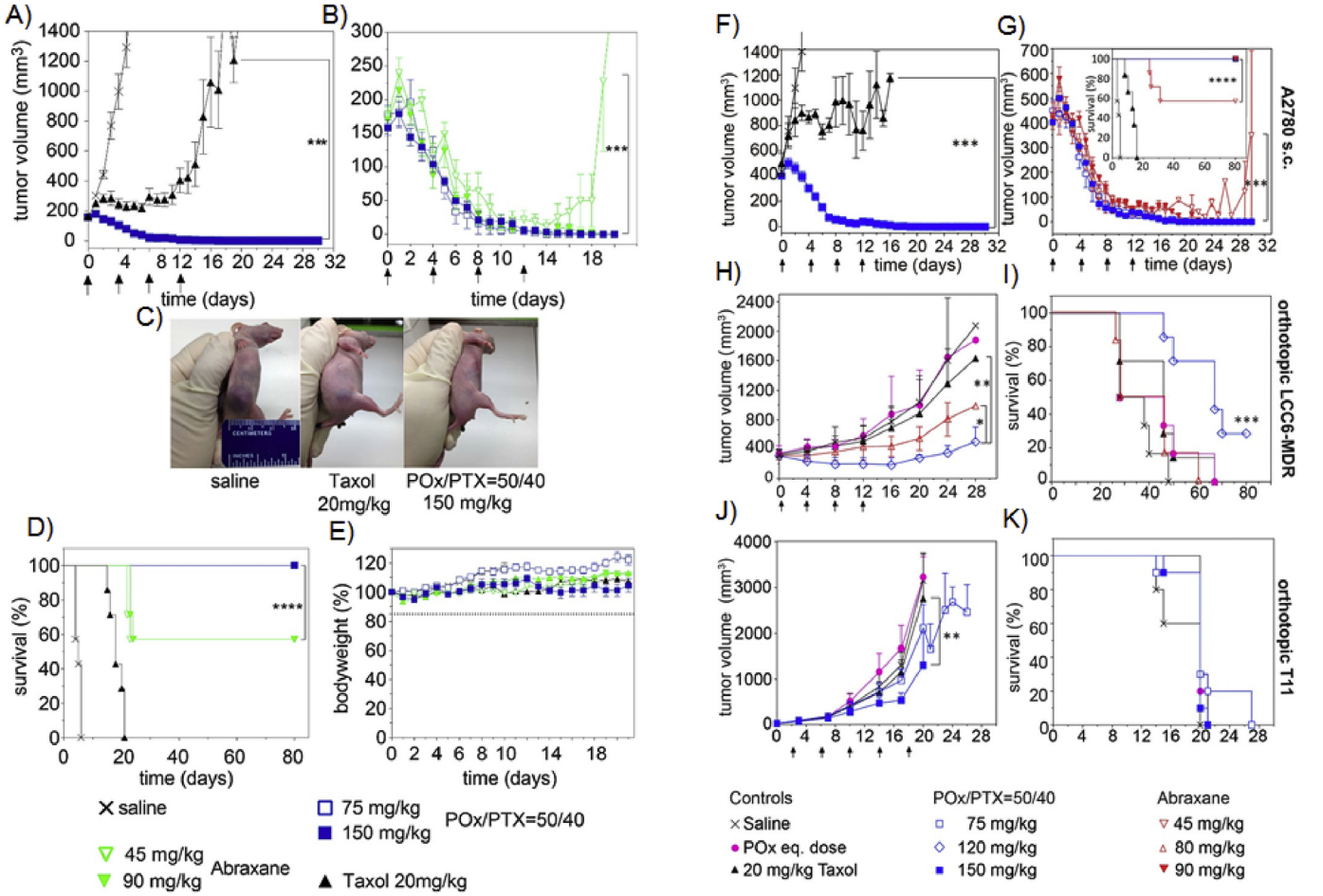

Fig. 35. Antitumor efficacy of various PTX formulations in different tumors. (A–E) Antitumor efficacy of PTX formulations in A2780 tumors of small size. Comparison of tumor growth inhibition of (A) POx/PTX 50/40 formulation (@MTD = 150 mg/kg) and Taxol® (@MTD = 20 mg/kg), and (B) POx/PTX 50/40 formulation (@MTD and ½MTD dose = 150 and 75 mg/kg, respectively) and Abraxane (@MTD and ½MTD = 90 and 45 mg/kg, respectively). Each formulation was injected on days 0, 4, 8, 12 (indicated by arrows). Data is expressed as means ± SEM, n = 7. ***p < 0.001. (C) Representative image of mice (day 6) treated with saline (left), Taxol® (middle) and POx/PTX 50/40 (right), respectively. (D) Kaplan-Meier survival plot for all groups in (A) and (B) ****p < 0.0001. (E) Changes of body weight of animals in each group (means ± SEM, n = 7). (F,G) Antitumor efficacy of various PTX formulations in A2780 tumors of large size. Comparison of tumor growth inhibition of (F) POx/PTX 50/40 formulation (@MTD dose = 150 mg/kg) and Taxol® (@MTD dose = 20 mg/kg), and (G) POx/PTX 50/40 formulation (@MTD and ½MTD dose = 150 and 75 mg/kg, respectively) compared to Abraxane (@MTD and ½MTD dose = 90 and 45 mg/kg). (H) Tumor growth inhibition and (I) survival of mice bearing LCC6-MDR multidrug resistant tumors. Treatment was performed at respective MTDs or dose of polymer corresponding to MTD (POx control). (J,K) Tumor growth inhibition (J) and survival (K) of mice bearing orthotopic, syngeneic T11 tumors. Treatment was performed at respective MTD and ½MTD dose or dose of polymer corresponding to MTD (POx control). The formulations were injected on days (F–I) 0, 4, 8, and 12, or (J,K) 2, 6, 10, 14, and 18, respectively. Data is expressed as mean ± SEM, n = 7. *p < 0.05, **p < 0.01, ***p < 0.001. Reprinted with permission from ref. [71]. Copyright 2016 Elsevier.

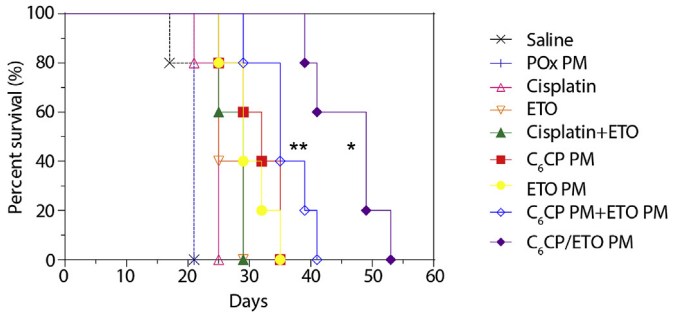

Fig. 36. Kaplan-Meier survival plot showing anti-tumor effects of the single and co-loaded drug PM in 344SQ/Luc. NCSLC animal model. The treatments regimen was q4d x 4. Drug injection doses were: 30 mg ETO/kg and 15 mg C_6CP/kg for C_6CP/ETO PM (4/8/10) and mixture of C_6CP PM (4/10) and ETO PM (8/10); 30 mg ETO/kg for ETO PM (8/10), 15C_6CPs mg/kg for C_6CP PM (4/10); 2 mg/kg cisplatin or 4 mg/kg ETO for free drugs; 2 mg/kg cisplatin and 4 mg/kg ETO for free drugs mixture. Empty PM were injected at the polymer dose equivalent to that in the co-loaded micelle formulation. *$p < 0.05$ (vs. C_6CP PM and ETO PM mixture group), **$p < 0.01$ (vs. C_6CP PM group). Reprinted with permission from ref. [245]. Copyright 2018 American Chemical Society.

release, as well as improved pharmacokinetics and increased tumor distribution of both drugs. The major manifestation of the drug co-loading effect was a considerably increased anti-tumor activity of co-loaded EP/PE drug micelles compared not only with the individual single drug micelles but also with the mixture of the two single drug micelles administered at the same dose (Fig. 36). This has been demonstrated using several animal models of SCLC non-small cell lung cancer (NSCLC) along with the observed great improvement of the co-loaded drug micelle therapy compared with the maximal tolerated dose (MTD) of the free drug combinations. Overall, the highly loaded, worm-like micelles carrying ETO and cisplatin prodrug have shown promise in treatment of lung cancer. The ability of controlling the nanoparticle morphology, drug retention, pharmacokinetics, and therapeutic efficacy by blending multiple drugs in a single particle is of both basic and practical significance.

Another strategy for the encapsulation of the hydrophobic drug PTX was recently investigated by Qu et al., utilizing polymeric micelles based on PEtOx-vitamine E succinate (PEtOx-VES) (cmc = 5.8 mg/L; $pK_a = 6.02$) [246]. While loading efficiency was excellent, the achieved paclitaxel concentration and *LC* was low (ρ(PTX) = 0.08 g/L; *LC* = 2.6 wt%; *LE* = 84%; D_h = 30 nm; zeta potential = 4.86 mV). *In vitro* drug release at 37 °C gradually accelerated with decreasing pH (49% (pH = 7.4), 61% (pH = 6.5) and 72% (pH = 5.0) release after 12 h). Therefore, the acidic pH at tumor site could support PTX release, especially in endo- and lysosomes, even though the difference in release may be too small to make a therapeutic difference *in vivo*. According to the authors, ionization of the tertiary amide of PEtOx at $pH < pK_a$ might result in electrostatic repulsion between the PEtOx chains loosening the micellar structure. It is noteworthy that several researchers have discussed this protonation of the tertiary amide in POx. However, no convincing experimental proof that this could happen has ever been provided and considering the very weak basicity of tertiary amides (in contrast to amines) it seems exceedingly unlikely that this would happen at pH 5 to any considerable degree. In fact, we have recently revisited the possible protonation of POx and found no evidence for protonation of PEtOx above pH 2 by acid-base titration [247]. However, hydration of the polymer could be altered at lower pH resulting in a modified release profile.

Zhang et al. [248] prepared cabazitaxel (CBZ, a second generation taxoid) loaded micelles based on an adamantane (Ad) capped, linear poly(DL-lactide) (PDLLA) hydrophobic core and a β-cyclodextrin (CD) centered seven armed star PMeOx as hydrophilic shell (7PMeOx-AdPDLLA). *LC* for CBZ was 17.5 wt% and size of drug loaded micelles (R_h = 89 nm (major distribution)) was reduced as compared to blank micelles (R_h = 119 nm (major distribution)). The authors suggest that this could be attributed to the compact arrangement of CBZ inside the hydrophobic core. As mentioned before, similar effects have been reported for PTX [235] or CUR [36] encapsulated in POx-based amphiphiles. After 24 h, 40% of the drug was released followed by a cumulative drug release of 74% up to 11 days. Dose dependent cytotoxicity was analyzed on A549 cells for 48 h. The IC_{50} value of formulated CBZ (23.2 μg/L) was higher than for free CBZ (5.2 and 8.1 μg/L) possible due to delayed drug release from the micelles. Since CBZ is a 2nd generation taxoid, the CBZ formulation showed significant activity in a PTX resistant A2780/T cancer cell line. Cellular uptake studies revealed a higher PTX uptake in PTX resistant cells when PTX was formulated with the POx based system. Furthermore, a time dependent distribution of the micelles in multicellular tumor spheroids could be detected. The *in vivo* antitumor efficiency in H22 hepatocellular carcinoma-bearing mice of the CBZ-loaded polymer micelles was much higher compared to unformulated CBZ or PTX and the survival of the mice could be prolonged as well (Fig. 37).

5.3. Curcumin

Another biologically active natural compound of extremely low water solubility is curcumin (CUR). Its use in medicine is well established for thousands of years in traditional asian medicine and as a food supplement in the west, but is not established in modern western medicine as a drug. Similar to PTX, the main issue of CUR is its extremely low solubility in water (0.6 mg/L). In addition, the molecule is quite reactive and reportedly not very stable in solution. Thousands of papers investigating CUR can be found in the scientific literature, but its usefulness is not universally accepted. Rather, CUR can be considered as a prime example of so-called pan assay interfering substances (PAINS), which are considered invalid pharmaceutical substances [249,250]. This ongoing debate notwithstanding, CUR may be considered as excellent candidate to test new DDS, specifically because it's instability and low solubility.

Accordingly, several triblock copolymers comprising PMeOx and PEtOx were investigated for encapsulation of CUR. A series of triblock copolymers comprising PMeOx-*b*-poly(tetrahydrofuran)-*b*-PMeOx (PMeOx-PTHF-PMeOx) were used to encapsulate CUR up to maximum concentrations of ρ(CUR) = 0.3 g/L (PMeOx-*b*-PTHF-*b*-PMeOx = 4 g/L; *LC* = 7 wt%; *LE* = 75%) [251]. Interestingly, enhanced CUR solubilization was mainly obtained with copolymers having a high PTHF/PMeOx ratio corresponding to a high aggregation number (N_{agg} increased with decreasing PMeOx block length at constant PTHF block length; determined by static light scattering, SLS). MeOx density of the unloaded micelles decreased with increasing PMeOx length at constant PTHF length, which is important to consider, as in the case of Pluronics, interactions with bovine serum albumin (BSA) were reduced when the density of the hydrophilic corona was high. In various epithelial cells, 100% of the cells of a given culture exhibited fluorescence after addition of the CUR-loaded nanoparticles indicating a rapid penetration of CUR into the cytoplasm (Fig. 38; however not or significantly less into the nucleus). Interestingly, even low PMeOx-PTHF-PMeOx concentrations (45–225 mg/L) induced a significant dose dependent increase in chloride current after 16 h incubation, suggesting the creation of transient pores across the cellular membrane. Furthermore, the PMeOx-PTHF-PMeOx/CUR formulation promoted restoration of the expression of the cystic fibrosis transmembrane conductance regulator (CFTR) protein in the plasma membrane of human airway epithelial cells carrying the F508del CFTR mutation

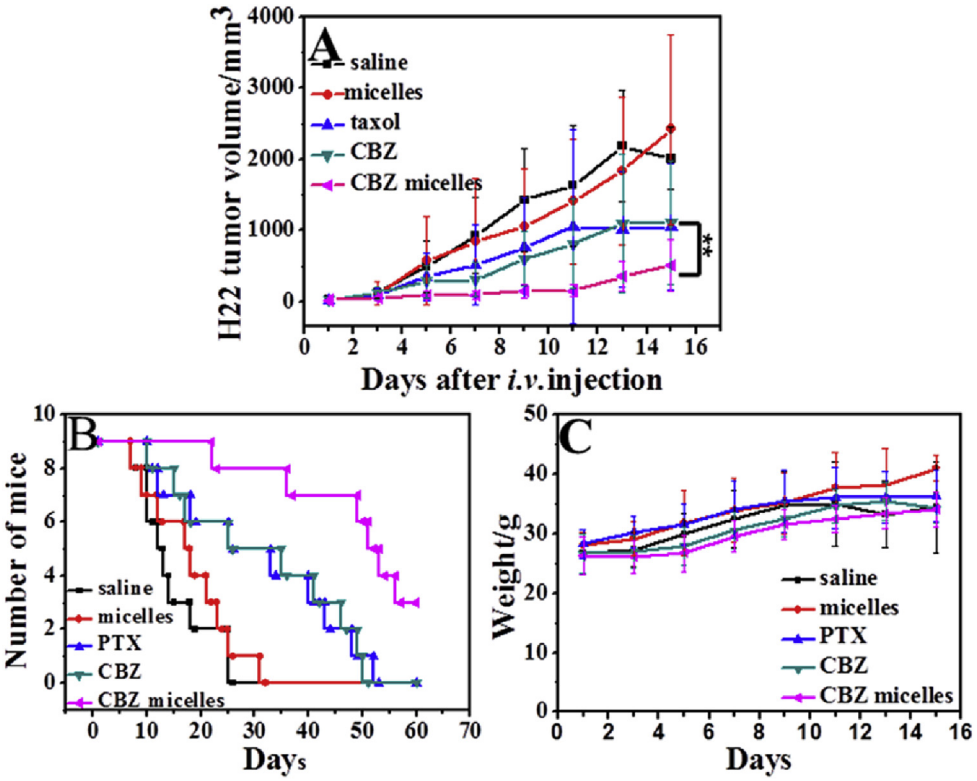

Fig. 37. (A) *In vivo* tumor inhibition of subcutaneous H22 tumor bearing mice treated with saline, empty 7PMeOx-AdPDLLA micelles, Taxol® (10 mg/kg), free CBZ (10 mg/kg), or CBZ-loaded 7PMeOx-AdPDLLA micelles (10 mg/kg based on cabazitaxel). Data are shown as means ± SD (n = 9). ** represents $p < 0.01$ since the ninth day. (B) Kaplan–Meier curves presenting survival of H22 tumor-bearing mice in different groups. (C) Body weight changes with different treatments. The treatment doses of both PTX and CBZ are 10 mg/kg per mice. Empty micelles (the same amount of polymers as CBZ-loaded micelles). Reprinted with permission from Ref. [248]. Copyright 2017 American Chemical Society.

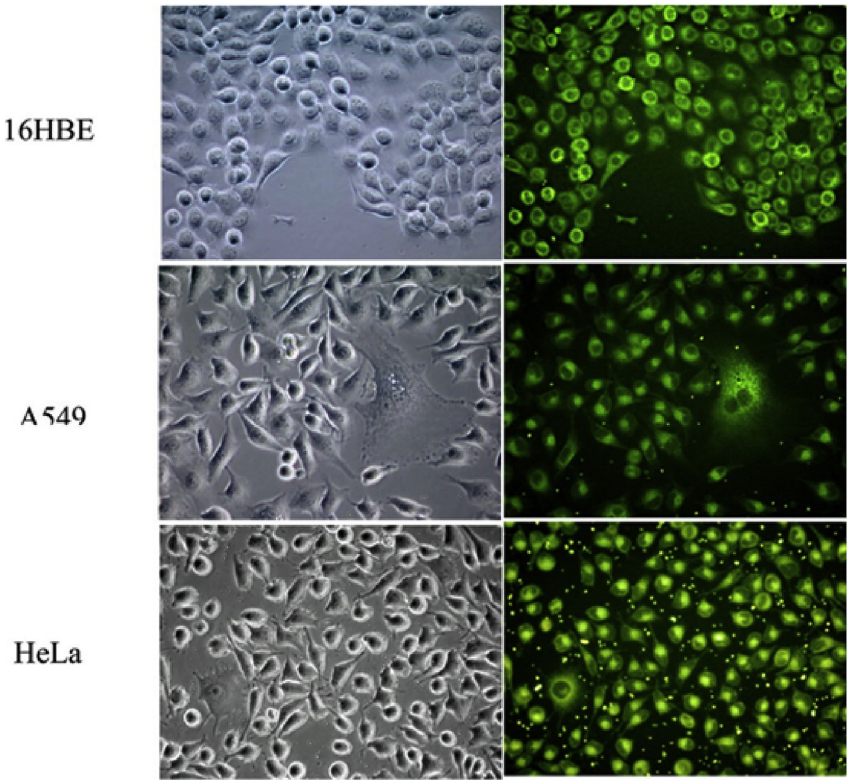

Fig. 38. Fluorescence microscopy of different cell lines incubated for 1 h with CUR-loaded PMeOx-PTHF-PMeOx micelles ([CUR] = 1 mM) after washing several times with PBS. Reprinted with permission from ref. [251]. Copyright 2014 American Chemical Society.

[252].

In 2017, Raveendran et al. reported on the use of amphiphilic diblock copolymers comprising a modestly hydrophobic PButEnOx core and a hydrophilic PEtOx shell for the encapsulation of curcumin (maximum $LC = 12$ wt%; $LE = 83\%$; $\rho(\text{CUR}) = 0.04$ g/L (0.11 mM); $D_h = 80–108$ nm; stable over a period of 30 days in water at 25 °C) [253]. However, the authors suggested that PPheOx as hydrophobic core may have resulted in higher CUR solubilities, as the Hildebrand Scatchard equation predicts a better compatibility between CUR and PPheOx (Flory-Huggins interaction parameter (χ) = 0.0045) than between CUR and ButEnOx ($\chi = 0.05$). Nevertheless, PButEnOx was chosen as it can be potentially functionalized or cross-linked due to the double bond in the side-chain. It should be noted, that even the poorest performing POx (NOx: $\chi = 2.03$) was superior (in theory) to PCL ($\chi = 2.91$) with regard to CUR miscibility. In contrast to the discussed CUR-loaded PMeOx-PTHF-PMeOx micelles [251], where the length of the hydrophobic block did not have major effects on the drug loading, *LC* increased almost by 60%, by increasing the ButEnOx content more than threefold at similar M_n of the block copolymer. Dependent on the polymer used, 13–34% of CUR was released over 168 h in PBS (pH = 7.4), while at pH = 4.5, the release was much faster (approx. 80% release after 168 h). Empty POx nanoparticles showed no cytotoxicity on C6 glioma cells at concentrations up to 5 g/L, whereas CUR-loaded micelles exhibited a dose dependent cytotoxicity ($IC_{50,24h} \approx 8–16$ μM). In contrast to the study of Gonçalves et al. using human airway epithelial cells [252], CUR incorporated into polymeric micelles exhibited enhanced cellular uptake in C6 glioma cells compared to DMSO formulated CUR as visualized by fluorescence imaging. Although the mentioned CUR nanoformulations exhibited moderate loading capacities of 7 [251] - 12 wt% [253], they suffered rather low overall aqueous CUR concentrations (0.3 g/L [251]; 0.04 g/L [253]. This low drug concentration might cause problems especially for relatively unstable compounds like curcumin, being unable to fully unfold their therapeutic potential *in vivo*.

Often one simply distinguishes between hydrophilic and hydrophobic, but fine-tuning the microenvironment of the hydrophobic core of the polymer amphiphile could help to tailor and maximize drug loading. With this in mind, Lübtow et al. [34] investigated a small library of structurally similar amphiphiles based on POx and the much less investigated POzi with respect to their solubilization capacity for CUR and PTX. The hydrophilic PMeOx shell (A blocks) of the ABA-triblock copolymers remained the same, whereas the chemical structure of the hydrophobic core was slightly changed. Utilizing the discussed ABA triblock copolymer A-P*n*BuOx-A (exhibiting *LC*s of almost 50 wt% for PTX), maximum CUR-concentrations of 3.2 g/L with 10 g/L polymer ($LC = 25$ wt%) were achieved (Fig. 39A). Even though this was exceeding any reported nano-formulated CUR concentration, it was dwarfed by its smaller side-chain homologue comprising a P*n*PrOx core ($\rho(\text{CUR}) = 7.8$ g/L; $LC = 44$ wt%). Most interesting, by formally shifting a methylene group from the polymer side-chain (B = P*n*BuOx) to the polymer main-chain (B = P*n*PrOzi), unrivalled high CUR-concentrations of 11.9 g/L (polymer = 10 g/L; $D_h = 46.5$ nm) could be obtained corresponding to an extraordinarily *LC* of 52.2 wt

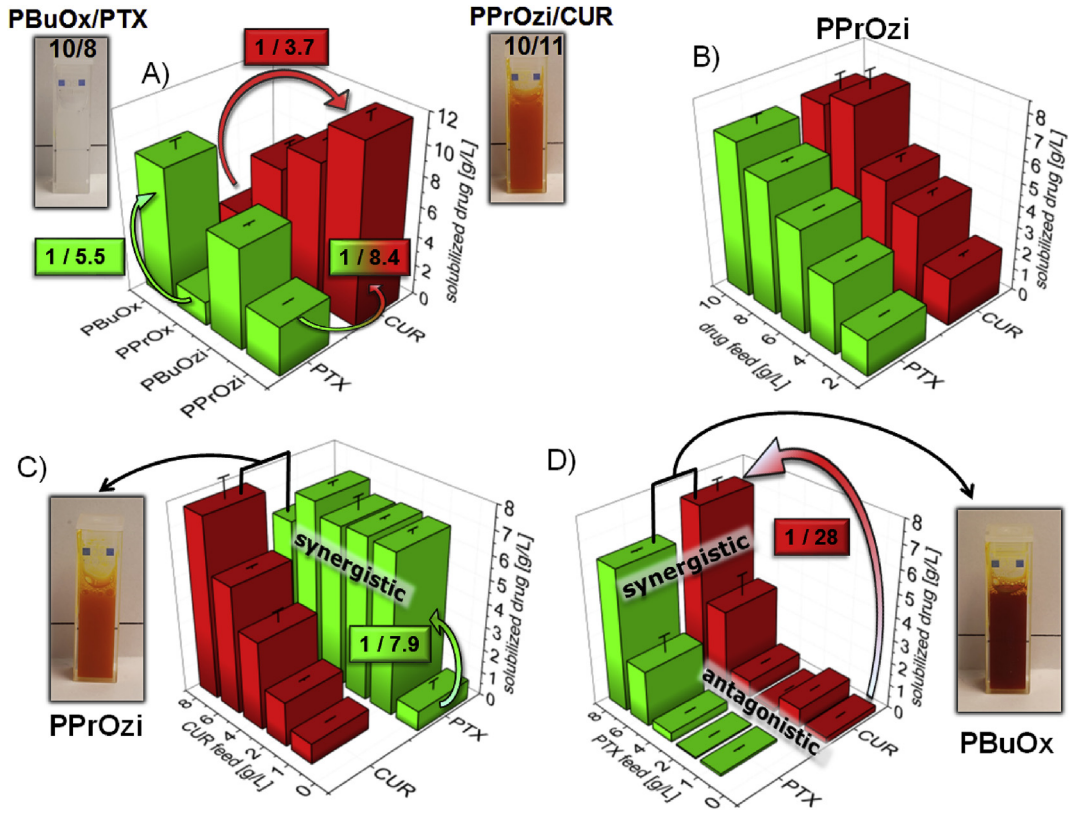

Fig. 39. A) Maximum solubilized aqueous drug concentrations (PTX = green bars; CUR = red bars; ρ(polymer) = 10 g/L). Selected ratios are given as [mol/mol]. Polymer abbreviations (P*n*BuOx, P*n*PrOx, P*n*PrOzi and P*n*BuOzi) correspond to hydrophobic block B within ABA-triblock copolymers of the general structure PMeOx-B-PMeOx; B) co-formulated aqueous drug concentrations in dependence of the drug feed concentrations. PTX & CUR were added at same feed concentrations and solubilized with A-P*n*PrOzi-A (ρ = 10 g/L); C) addition of increasing CUR feed concentrations at constant PTX feed concentration of 8 g/L (ρ(A-P*n*PrOzi-A) = 10 g/L); D) addition of increasing PTX feed concentrations at constant CUR feed concentration of 8 g/L (ρ(A-P*n*BuOx-A) = 10 g/L). Data is given as means ± SD (n = 3). Reprinted with permission from ref. [34]. Copyright 2017 American Chemical Society.

% (ρ(CUR) = 54.5 g/L @ 50 g/L polymer) [36]. To put this into stoichiometric perspective, per polymer molecule, approximately 27 drug molecules were incorporated, or in other words, every repeating unit of the hydrophobic core apparently carried more than one CUR molecule. Furthermore, the addition of CUR triggered micellization, as A-P*n*PrOzi-A itself does not form micelles at the investigated polymer concentration and temperature [36]. Importantly, the pronounced differences in the *LC* were not due to batch-to-batch variation of the polymer amphiphiles themselves, as three different polymer batches of A-P*n*BuOx-A and A-P*n*PrOzi-A exhibited excellent reproducibility with respect to CUR-loading [36]. The polymer A-P*n*PrOzi-A was able to solubilize 3.7 times more CUR than its structural isomer A-P*n*BuOx-A [34]. In contrast, in the case of PTX, the P*n*BuOx based amphiphile clearly outperformed the P*n*PrOzi based one which enabled PTX concentrations of "only" 3.27 g/L (*LC* = 25 wt%). Comparing the amount of PTX and CUR solubilized, A-P*n*PrOzi-A exhibited a specificity of 8.4 [mol_{CUR}/mol_{PTX}]. Notably, the polymer amphiphile with a poly(2-n-butyl-2-oxazine) (P*n*BuOzi) core did not exhibit any particular specificity for the tested compounds and was an excellent solubilizer for both drugs, albeit less efficient than either best-in-class polymer. Incorporating the solvatochromic Reichardt's dye into the four triblock copolymers resulted in different absorption patterns dependent on the polymer structure indicating a different micellar microenvironment. However, by co-incorporating PTX, the spectra aligned, indicating that the added drug remodeled the micellar microenvironment. Although PTX is highly hydrophobic, its incorporation seemed to establish a more polar microenvironment for Reichardt's dye, which was surprising but may be attributed to the large number of polar moieties present in PTX.

Good water solubility of a drug is only one aspect which needs to be considered for administration. Among others, long-term stability of the aqueous formulations plays a major role for the translation of a formulation into the clinics. Although CUR is highly susceptible to degradation in aqueous solution, the P*n*PrOzi based CUR-nanoformulations exhibited excellent 30 day stability with no major loss in CUR content up to CUR concentrations of 9 g/L at 10 g/L polymer (*LC* = 47 wt%) [36]. Interestingly, after 1 year storage, the CUR content of all investigated nanoformulations converged at ≈ 3 g/L (*LC* = 23 wt%; under the assumption that only CUR and no polymer degraded/precipitated) irrespective of the utilized polymer and CUR feed concentrations indicating that the POx/POzi based amphiphiles not only slowed down the kinetics of CUR crystallization, but also drastically shifted the thermodynamic equilibrium with regard to the CUR solubility. Analogue to the PTX formulations of A-P*n*BuOx-A, the A-P*n*PrOzi-A based CUR formulations could easily be lyophilized (freeze-dried without the need of cryoprotectants) and re-dissolved in H_2O, PBS or PBS containing 10 g/L BSA without compromising drug-content, potentially strongly increasing their shelf life. Strong interactions between the P*n*PrOzi based amphiphile and the encapsulated CUR were not only present in solution (drug-induced micellization; initial size reduction of the drug-loaded micelles with increasing CUR content up to 5 g/L investigated by DLS) but also in the solid state, as lyophilized powders of even drug-dominant formulations (*LC* > 50 wt%) showed no sign of drug-crystallinity by differential scanning calorimetry (DSC) and x-ray diffraction (XRD) measurements. Thus, the freeze-dried formulations represent solid amorphous dispersions.

The IC_{50} values of CUR dissolved in DMSO or A-P*n*PrOzi-A in conventional 2D cell cultures using human dermal fibroblasts ($IC_{50,72h}$ (nano-CUR) = 45 μM), colorectal adenocarcinoma Caco-2 cells ($IC_{50,24h}$ (nano-CUR) = 60 μM) and triple negative breast cancer cells MDA-MB-231 ($IC_{50,72h}$ (nano-CUR) = 19 μM) were similar (Fig. 40 A–F), showing that CUR was fully bioactive when incorporated into the polymer micelles. As already mentioned, the polymer alone showed a dose-dependent cytotoxicity only against MDA-MB-231, suggesting a cytotoxic effect of the polymer at rather high doses ($IC_{50,72h}$ (polymer) = 1 mM (10.1 g/L)). Compared to conventional 2D cell cultures, an increased resistance of the cancer cells was observed in 3D tissue models derived from a decellularized porcine intestine (SISmuc, **S**mall **I**ntestinal **S**ubmucosa with preserved mucosa) that allows tumor cell growth in multilayers within the former crypt structures and the invasion into deeper parts of the tissue matrix across the basement membrane (Fig. 40 G). As DMSO/CUR precipitated at [CUR] ≥ 500 μM, the nanoformulation might allow high-dose *in vivo* therapy using parenteral CUR administration necessary for effective therapeutic high-dose intervention. This might result in significant benefits for the pharmacotherapy using CUR *in vivo* as was previously shown in the case of high-dose therapy using POx/paclitaxel nanoformulations [71].

As discussed, even small structural changes of the alkyl-based side chains within POx or POzi based hydrophobic cores can have major impact on the solubilization properties for highly insoluble drugs. Another reported strategy to optimize polymer-drug interactions is to maximize π-π interactions between small molecules and the polymer amphiphile [237]. Most recently, Hahn et al. [254] investigated four different polymer amphiphiles, again all comprising the same hydrophilic PMeOx shell and a hydrophobic core with varying aromatic content based on either P*n*BuOx, P(*n*BuOx-*co*-2-benzyl-2-oxazoline) (P*n*BuOx-co-PBzOx), PBzOx or PPheOx for the encapsulation of the natural products PTX, CUR and Schizandrin A (SchA) containing different relative content of aromatic moieties (Fig. 41). While for PTX, having the lowest relative content of aromatic moieties, the maximum drug loading decreased with increasing relative aromatic amount within the polymer, the loading of CUR, having a much higher relative aromatic content, increased (Fig. 41). Interestingly, the loading of SchA having an intermediate aromatic content was not influenced significantly by the aromatic content of the polymer employed. With increasing aromatic character of the polymer amphiphile, more CUR (LC_{PnBuOx}: 24.4 wt% [34]; $LC_{P(nBuOx\text{-}co\text{-}BzOx)}$: 33.2 wt%, LC_{PBzOx}: 41.0 wt%) and less PTX (LC_{PBuOx}: 47.5 wt% [34]; $LC_{P(BuOx\text{-}co\text{-}BzOx)}$: 36.8 wt%, LC_{PBzOx}: 35.6 wt%) could be solubilized. This trend was not observed for the PPheOx based amphiphile which did not show pronounced specificity. While *LC* for PTX decreased further (*LC* = 28.6 wt%), also the solubilization of CUR (*LC* = 33.4 wt%) and SchA (LC_{SchA}: 28.6 wt%) was less efficient. Important for a potential application as solid dispersion, a freeze-dried PBzOx/SchA formulation (*LC* = 30 wt%; R_h = 20 & 150 nm in PBS) showed no sign of drug-crystallinity as investigated by DSC. Furthermore, only a single T_g was observed, ruling out significant microphase separation. In general, all formulations of PTX, CUR and SchA showed excellent stability within 30-day storage.

In conclusion, the presented results underline the complex and to a certain extent unpredictable interactions between the polymer amphiphiles and the incorporated small molecules. It appears that π-π interactions can improve drug-loading and formulation stability in selected cases, however this needs to be assessed on a case-by-case basis.

5.4. Doxorubicin

Doxorubicin (DOX) is another common chemotherapeutic used to treat various cancers and a popular model drug in preclinical evaluation of novel DDS. It has a moderate aqueous solubility in the protonated form (10 g/L) as well as low bioavailability up to 5%, wherefore it is administered intravenously and intravesical (liposomal formulations e.g Caelyx® or Doxoves®). However, due to rapid development of drug-resistance and poor prognosis of existing therapies, efforts have been made to design and develop

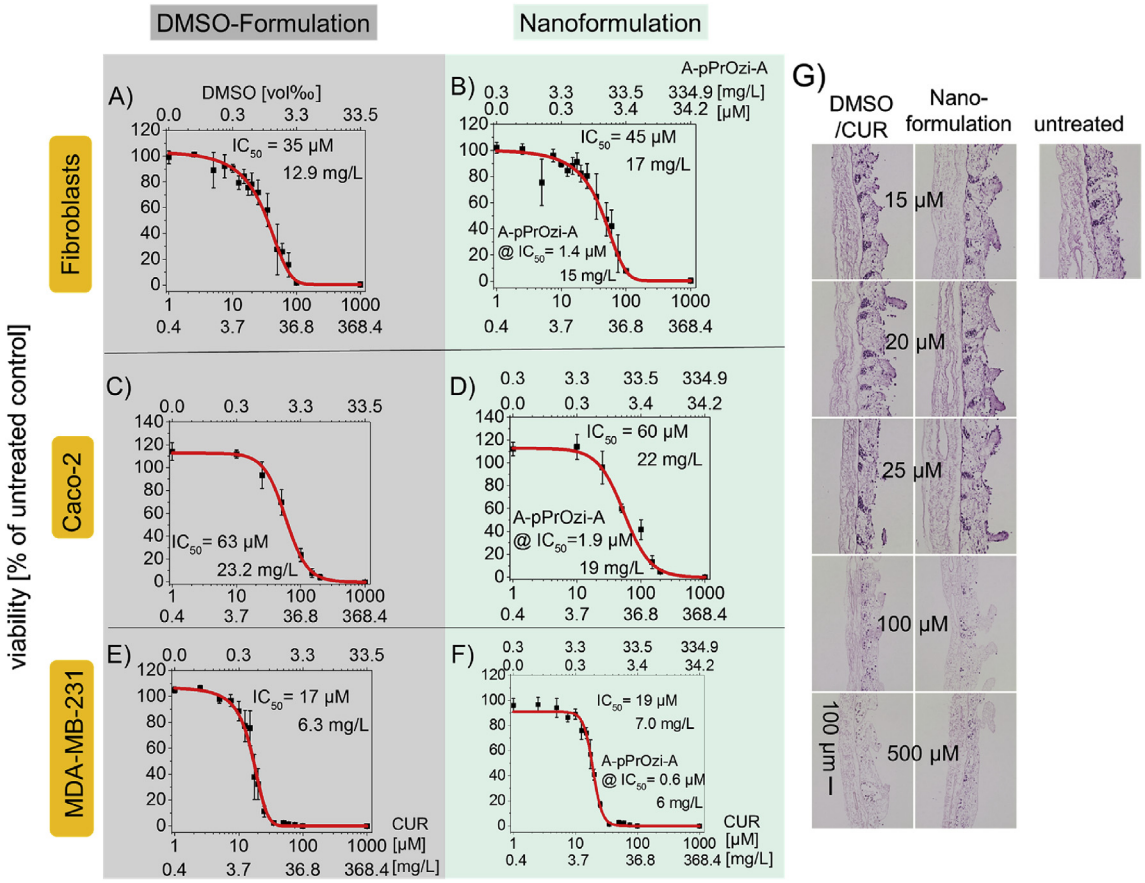

Fig. 40. Dose-dependent cytotoxicity of DMSO-formulated curcumin and CUR loaded PMeOx-*b*-P*n*PrOzi-*b*-PMeOx micelles in (A,B) human dermal fibroblasts; (C,D) Caco-2 and (E,F) MDA-MB-231 breast cancer cells. Data is presented as means ± SD (n = 3 × 3) for every drug and polymer concentration. Cell viability was determined by CellTiter-Glo® assay; G) H&E staining of 3D tissue model of MDA-MB-231 cell line. The scaffold SISmuc is composed of the small intestinal submucosa (SIS) and the mucosa (Muc). Villi and crypt structures of the mucosal part are preserved and tumor cells (purple spots) grow on the mucosal surface and migrate into the former crypts as well as into the mucosal layer of the scaffold. Scale bar represents 100 µm. Reprinted, with modifications, from Ref. [36].

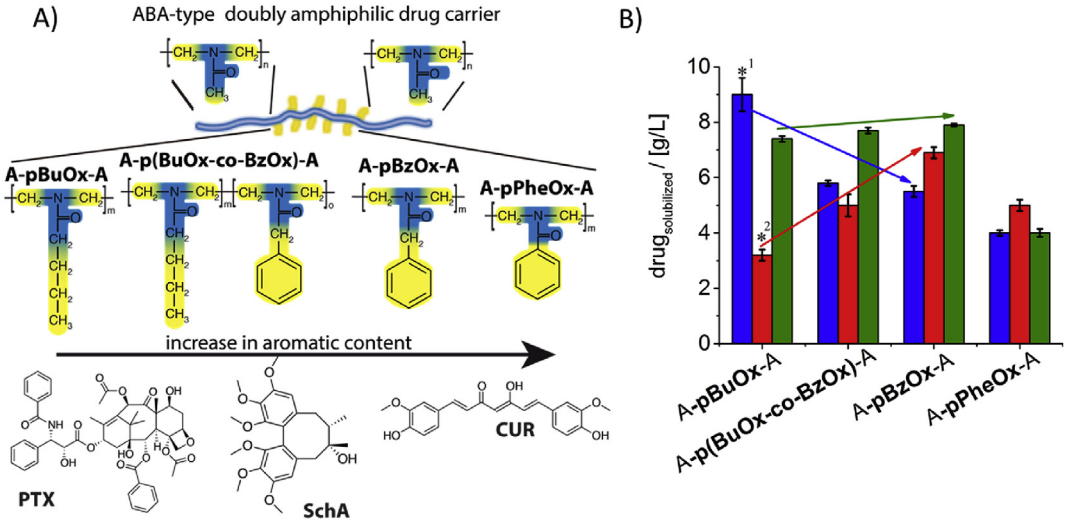

Fig. 41. A) Schematic representation of the polymers and insoluble small molecules according to increase in aromatic content. B) Maximum solubilized aqueous drug concentrations of drugs PTX (blue), CUR (red) and SchA (green) using four different ABA triblock copolymers (ρ(polymer) = 10 g/L). Data is given as means ± SD (n = 3). Reprinted from Ref. [254].

more efficient and at the same time less toxic delivery strategies.

Knop and co-workers [255] investigated the impact of side chain length and molar mass on the solution properties of POx based polymers for drug delivery. DOX was used as model drug and

various star-shaped PCL-*b*-POEGMA and PCL-*b*-POEtOxMA based amphiphilic polymers were synthesized as drug carriers. Size of PCL-*b*-POEGMA in acetone ($R_h = 9–17$ nm) was mainly greater than that of PCL-*b*-POEtOxMA ($R_h = 6–13$ nm), whereas in water PCL-*b*-POEtOxMA was somehow greater ($R_h = 17–31$ nm) than that of PCL-*b*-POEGMA ($R_h \leq 20$ nm). Hemoglobin release was below 2% for all polymers investigated even at very high concentrations (ρ(polymer) = 5, 25 and 50 g/L). Furthermore, the polymer amphiphiles were non-cytotoxic against L929 mouse fibroblasts up to 10 g/L upon 24 h incubation (Fig. 42). However, drug loadings were critically low, as per star-shaped block copolymer only 2 molecules of DOX could be encapsulated. The IC_{50} values of neat DOX, its commercially available liposomal formulation (Caelyx®) and star-shaped polymer based formulations on different cell lines were evaluated (Table 1). No major differences were found in the biological activity of polymers with different shells and repeat units. The authors assume that much higher IC_{50} values of the formulated DOX could be attributed towards delayed DOX release. This assumption was supported by significantly improved IC_{50} values after longer incubation. However, the IC_{50} values of free DOX also were reduced significantly and remained about 3 orders of magnitude lower than those of formulated DOX.

Peng et al. [256] individually loaded DOX and indomethacin (IMC) into poly(4-phenyl caprolactone)-*block*-PEtOx (PPCL-PEtOx) and poly(4-methyl caprolactone)-*block*-PEtOx (PMCL-PEtOx) based micelles (CMC = 0.6–11.1 mg/L). At constant drug feed, drug loading decreased as the length of hydrophilic segment increased from $PMCL_{33}$-$PEtOx_{50}$ ($LC = 7.8$ wt%) to $PMCL_{31}$-$PEtOx_{18}$ ($LC = 50.3$ wt%). Overall, IMC loading was much higher in PPCL-PEtOx than in PMCL-PEtOx. Unfortunately, the given drug loading and entrapment efficiencies are not in accordance with the formulas written for the calculations and the values given are misleading. $PMCL_{33}$-$PEtOx_{50}$ showed a sustained drug release *in vitro* (approx. 20% IMC was released after 24 h) as compared to $PMCL_{31}$-$PEtOx_{18}$ (40% IMC was released after 8 h). Cytotoxicity analysis for 24 h on HeLa cell line revealed that upon administering 0.01–1 g/L of $PMCL_{27}$-$PEtOx_{50}$, at least 70% of the cells remained viable. Cellular uptake of DOX was determined by utilizing its intrinsic fluorescence (Fig. 43). Unfortunately, drug loading data for DOX was not reported. Cellular uptake by endocytosis was further confirmed by the use of endocytosis inhibitors on HeLa cell line. The major route from the endocytosis for such formulations was found to be macropinocytosis which was confirmed by addition of the macropinocytosis inhibitor amiloride. However, what is very peculiar regarding the published data is that virtually no difference was observed in the uptake of the PMCL-PEtOx between 5 min and 2 h incubation, which has to be regarded as quite unusual.

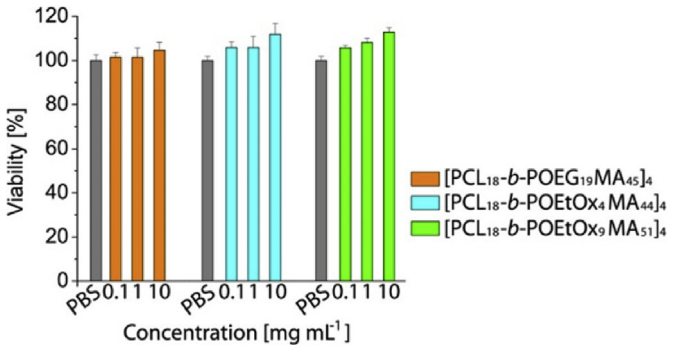

Fig. 42. Cell viability of L929 mouse fibroblasts after incubation with star-shaped polymers bearing POEGMA and PEtOxMA star-shaped polymers at concentrations up to 10 g/L for 24 h. Cells incubated with polymer free culture medium served as control. Cell viability was determined by XTT assay according to ISO 10993-5. Data are expressed as means ± SD (n = 6). Reprinted with permission from ref. [255]. Copyright 2013 American Chemical Society.

Haktaniyan et al. [257] synthesized hydrogen-bonded films of P*i*PrOx and tannic acid (TA) which released DOX in acidic conditions while releasing minimal DOX at physiological pH. DOX was conjugated to the hydroxyl groups of TA at molar ratios of OH/DOX = 7/1 up to 27/1. The remaining free hydroxyl groups on TA were used for layer-by-layer (LBL) deposition of DOX-TA conjugate and P*i*PrOx on silicon wafers. AFM images showed that DOX-TA/P*i*PrOx multilayers had a higher thickness and roughness than blank TA/P*i*PrOx layers. Furthermore, surface roughness increased by increasing the number of layers. Due to P*i*PrOx (LCST = 36 °C), the films exhibited temperature responsive behavior *in vitro* and presumably are capable to release DOX at body temperature. AFM images revealed a higher swelling of the films at 37.5 °C than at RT irrespective of the pH (pH = 5.5 or 7.5) which was correlated to the LCST behavior of P*i*PrOx (Fig. 44). According to the authors, it is expected that at higher temperature, the polymers transform from extended coil to globular conformation retaining a greater amount of salt ions and water molecules. This explanation of the authors seems counterintuitive, as e.g. hydrogels deswell when reaching the LCST and soluble polymers precipitate by shedding their solvation sphere.

Films were stable from pH 3 to pH 8.5 upon short term exposure of 30 min. At pH 9, films were completely disrupted due to

Table 1
IC_{50} (μg/mL) values obtained for DOX, Caelyx and micellar formulated DOX in $[PCL_{18}$-b-$P(OEG_{19})MA_{45}]_4$, $[PCL_{18}$-b-$P(OEtOx)_4MA_{44}]_4$, and $[PCL_{18}$-b-$P(OEtOx_9MA)_{51}]_4$ star-shaped block copolymers for the L929 mouse fibroblasts, HEK 293 human embryonic kidney cells, as well as MCF-7 and MDA-MB 231 human breast cancer cells. Reprinted with permission from ref. [255]. Copyright 2013 American Chemical Society.

cell line	doxorubicin	Caelyx	$[PCL_{18}$-b-$POEG_{19}MA_{45}]_4$	$[PCL_{18}$-b-$POEG_4MA_{44}]_4$	$[PCL_{18}$-b-$POEG_9MA_{51}]_4$
24 h					
L929	42	20	–	80	–
HEK 293	–	–	–	–	–
MCF-7	40	19	–	110	–
MDA-MB 231	48	20	–	180	–
72 h					
L929	0.1	0.6	50	29	29
HEK 293		0.2	10.8	47	47
MCF-7	0.0042	0.8	100	48	–
MDA-MB 231	0.12	0.8	100	40	100
72 h + 72 h					
L929	0.05	4	30	30	45
HEK 293		0.038	25	21	8.9
MCF-7	0.003	0.18	39	32	7
MDA-MB 231	0.0032	0.0028	40	32	7

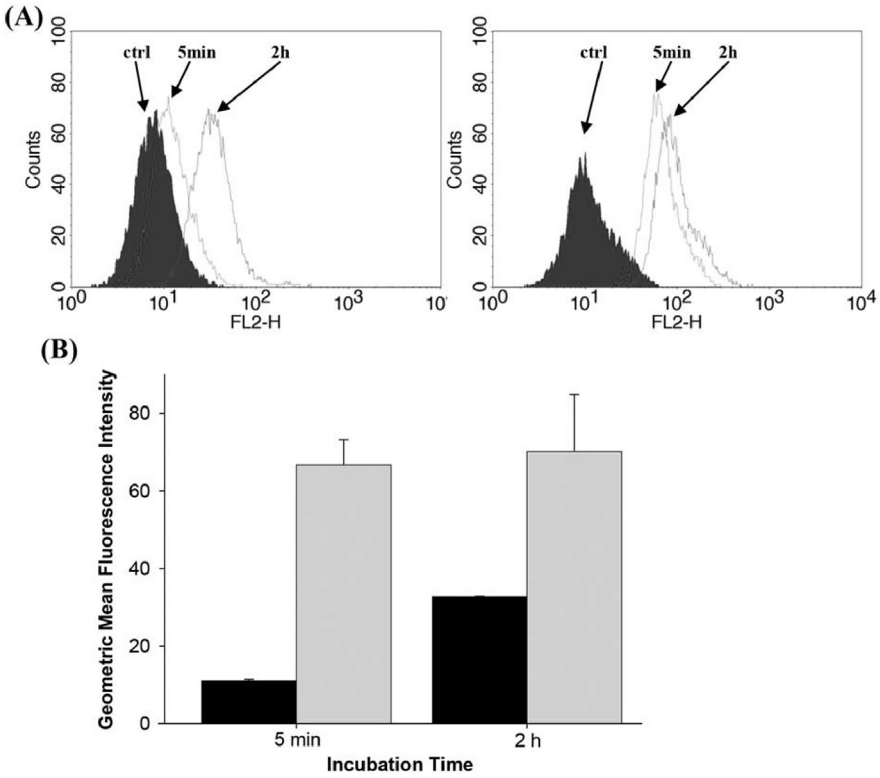

Fig. 43. Histograms of HeLa cells treated with free DOX (A, left), and DOX-loaded $PEtOz_{50}$-b-$PMCL_{27}$ micelles (A, right) for 5 min and 2 h. Control groups were cells without any treatment, representing basal fluorescent levels. (B) Geometric mean fluorescence intensities of free DOX (black) and DOX-loaded $PMCL_{27}$-b-$PEtOx_{50}$ (gray). Data are shown as means (n = 3). Reprinted with permission from Ref. [256]. Copyright 2013 Wiley Periodicals, Inc.

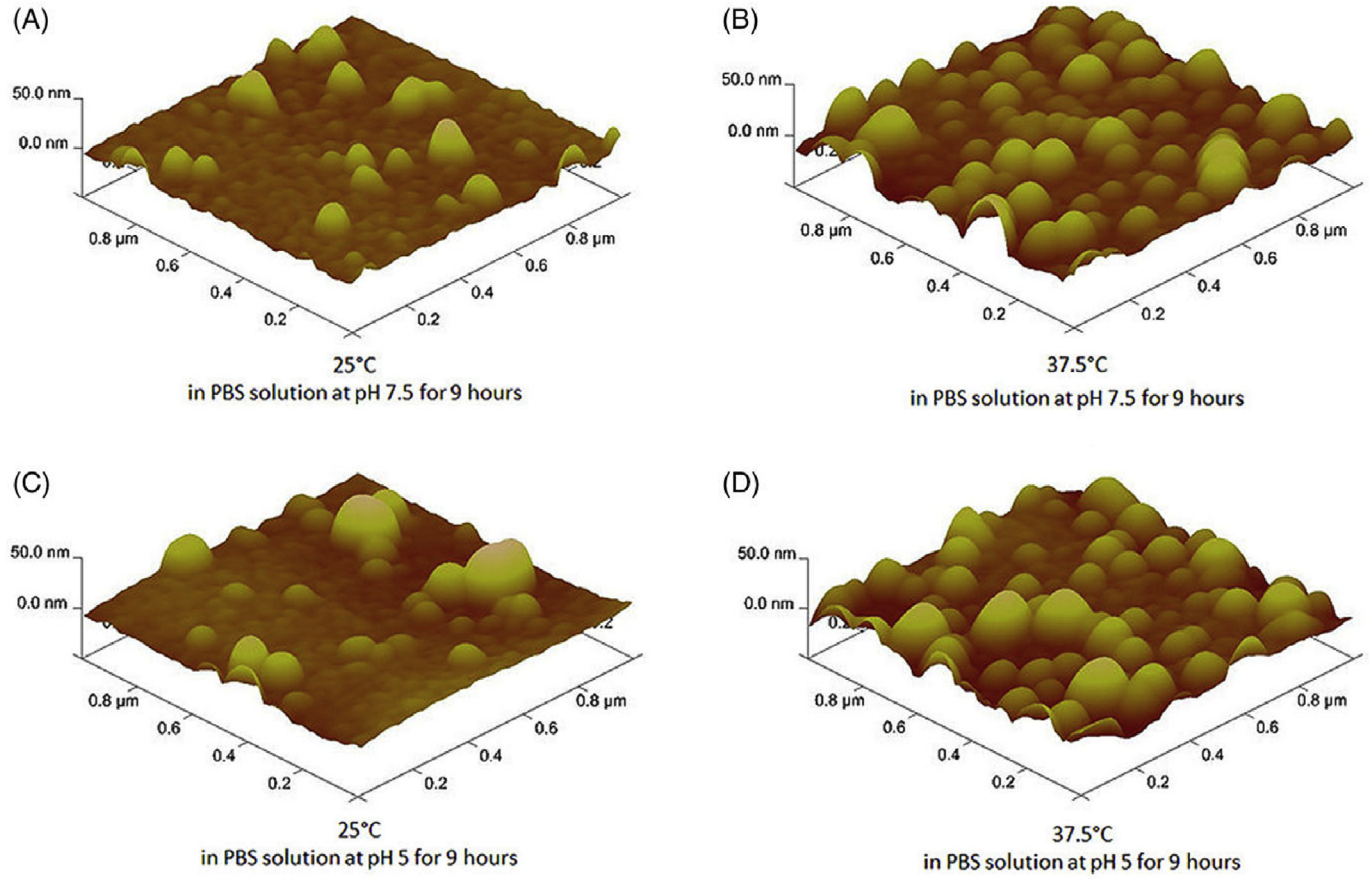

Fig. 44. AFM images of seven-bilayer films of PiPOx/TA–DOX after exposure to PBS solution for 9 h at (A) pH 7.5; 25 °C, (B) pH 7.5; 37.5 °C; (C) pH 5; 25 °C and (D) pH 5 at 37.5 °C. Reprinted with permission from Ref. [257]. Copyright 2017 Society of Chemical Industry.

ionization of TA. Temperature change did not have any significant impact on the film behavior at short term exposure in PBS. Multilayers were stable up to 3 days at pH = 6.5 and 7.5. The amount of DOX released at 37 °C from 40-bilayer PiPOx/TA–DOX films increased with decreasing pH (0.044 μg (pH = 7.5); 0.088 μg (pH = 6.5); and 0.224 μg (pH = 5.5). Again, as with many studies using POx, the increased solubility of DOX at lower pH must be considered.

In summary, we can conclude that also POx based drug carriers can face the problem of poor drug loading. However, the work by Kabanov, Jordan and Luxenhofer has shown repeatedly unparalleled high drug loading for PTX, CUR and several other, highly water insoluble drugs using POx and POzi based triblock copolymers. The series of studies by these groups clearly show that fine-tuning the structure of amphiphilic polymers can be essential and can lead to higher solubilizing capacity of polymer micelles. In particular, triblock copolymers appear to be favorable vs. diblocks and low amphiphilic contrast seems to be favorable over high amphiphilic contrast. The particular molecular structure-property relationships remain to be elucidated.

Besides the most common drugs PTX, CUR and DOX, POx based DDS have also been investigated in combination with various dyes as model drugs, anticancer, non-steroidal inflammatory, antileprotic drugs etc. Moreover, efforts have been made to explore the potential of POx for non-conventional therapies including photodynamic and boron neutron capture therapy. These versatile applications of POx will be discussed in the following.

Most recently, Romio et al. [258] coupled PMeOx to a short, functionalizable poly(2-methylsuccinate-2-oxazoline) (PMestOx) segment at different molar ratios ($PMeOx_n$-*b*-$PMestOx_m$; n/m = 40/4, 50/7, 80/2 and 160/6). Subsequently, the lipophilic model drug pterostilbene (PTS) was conjugated by ester linkage to PMestOx forming the core of the micelles for the encapsulation of the second drug clofazimine (CFZ; *LC* = 0.5 wt%). A minor CMC increase from 5.6 mM to 11 mM was observed as the PMeOx repeat unit increased from 40 to 160. Average size of the blank NPs ranged between 40 and 150 nm and size increased (approx. 40% increase in size on average) upon encapsulation of CFZ. Independent of the chemical composition of the block copolymers, all formulations showed less than 20% drug release at pH 7.4 after 10 days except $PMeOx_{40}$-$PMestOx_4$/PTS, which exhibited more than 60% drug release after 2 days. However, *in vitro* release studies for extremely insoluble compounds should be viewed with great care as it is difficult to determine proper sink conditions and it is unclear how the release in the absence of serum proteins is relevant to any *in vivo* situation. *In vitro* studies with RAW 264.7 macrophage cells indicated that PMeOx-*b*-PMestOx-COOH is non-cytotoxic at 0.5 g/L and at polymer concentrations of 5 g/L, cell viability was still above 70% after incubation for 24 h. PMeOx-*b*-PMestOx-PTS exhibited a concentration dependent cytotoxicity after 6 h incubation with IC_{50} values between 19 and 71 mg/L, dependent on the polymer composition. The cellular uptake was investigated using confocal laser scanning microscopy (Fig. 45 A–F) and FACS (Fig. 45H).

Von der Ehe et al. [259] synthesized 4-arm star shaped sPCL with alkyne end groups which was coupled with azide end group functionalized PEtOx (sPCL-*b*-PEtOx) or PEG (sPCL-*b*-PEtOx) by copper catalyzed azide alkyne cycloaddition. Pyrene fluorescence assay revealed a slightly higher cmc for sPCL-*b*-PEtOx (5.56 mg/L; D_h = 96 nm) than for sPCL-*b*-PEG (4.56 mg/L; D_h = 150 nm) which the authors attributed to the slight difference in the molar masses (7.1 and 11 kg/mol for sPCL-*b*-PEtOx and sPCL-*b*-PEG, respectively, as determined by GPC). However, such minute difference is probably within the experimental error of the method. At polymer concentrations of up to 5 g/L no erythrocyte aggregation could be observed giving a first hint for its compatibility in biological context. Subsequently, the hydrophobic dye fat brown as model compound could be incorporated in rather high amounts into sPCL-*b*-PEtOx (*LC* = 25.4 wt%) and sPCL-*b*-PEG (*LC* = 25.9 wt%).

Hartlieb et al. investigated prop-2-yn-1-yl-3-mercaptopropionate (PYMP) and PEtOx based hyperstar copolymers [260]. Although dispersities of hyperstar copolymers are commonly beyond 3, the dispersity of the polymers could be tuned to 1.3 by using thiol-yne chemistry and monomer feeding approach. The PYMP core was synthesized with a degree of branching of 0.9. Subsequently, thiol end-group functionalized PEtOx was coupled to the surface of the hyperbranched structure by the terminal alkyne moieties. Two different types of hyperstar polymers with different lengths of the hydrophilic shell were synthesized (DP (PEtOx) = 25 and 50), whereas the degree of functionalization of the PYMP core was kept constant. Nile red as hydrophobic model compound could be incorporated at very low *LC*s of 0.3 and 0.9 wt%. IC_{50} of the blank hyperstar polymers using the A2780 cell line was quite low with 0.7 g/L regardless of the length of PEtOx. Such low IC_{50} values are rather surprising for PEtOx based polymers and it would be interesting to understand what is the reason for this pronounced cytotoxicity.

In another study, Jana et al. [261] synthesized four different photocleavable PEtOx-*b*-poly(2-nitrobenzyl acrylate) (PEtOx-b-PNBA) block copolymers with varying block lengths of PNBA. Hydrodynamic diameter of the micelles increased from 52 to 230 nm with increasing PNBA block length. Furthermore, the formation of primary micelles was followed by a time dependent aggregation into compound micelles. Interestingly, the same polymers could be used to form reverse micelles in the organic phase (dichloromethane) capable of encapsulating the hydrophilic dye Eosin B as confirmed by photoluminescence spectroscopy. Nile red (NR) as model compound was incorporated into the micelles (no data for *LC* and *LE* is provided) and exposed to UV light for different time intervals. A time dependent NR release pattern was observed, as irradiation with UV light (Fig. 46) led to cleavage of PNBA within the micellar core which transforms the polymer amphiphile to doubly hydrophilic PEtOx-b-poly(acrylic acid) (PAA), resulting in the rupture of micelles and release of cargo.

Restani et al. [262] coated polyurea (PU), PU-PEtOx, PU-PMeOx nanoparticles with chitosan (CHT) for the local delivery of ibuprofen (IBP) to the lungs by inhalation route (Fig. 47). Pure PU based formulations yielded the highest *LE*s of 41%, while PU-PEtOx and PU-PMeOx gave 21 and 16%, respectively. Using 100 mg of PU-EtOx and PU-MeOx, only 3.2 and 2.6 mg of IBP could be encapsulated, corresponding to very low *LC*s of 3.2 wt% and 2.5 wt%, respectively. *In vitro* drug release experiment showed that 90% of drug was released from CHT uncoated formulations at pH 6.6 and 7.4, while the CHT coating gave the system sustained release (70% drug release up to 60 h). MTS assay revealed that non-formulated IBP at a concentration of 1 mM does not affect the metabolic activity of epithelial A549 cells. However, metabolic activity was dramatically reduced to 30% at [IBP] = 5–7 mM after 24 h of incubation. Similar behavior was shown by IBP-PU, whereas the IBP loaded PU-POx micelles did not effect the metabolic activity up to 120 h. In case of normal human dermal fibroblasts (NHDF), the free drug did not effect the metabolic activity up to 24 h but after 120 h, 40% reduction in viability was observed. IBP/PU-POx formulations reduced the cytotoxic effect of IBP on NHDF advantageous for sustained drug delivery. Biodegradability studies (ρ(lysozyme) = 0.2 g/L; incubation for 40 days) revealed a 85%, 93% and 98% weight loss for pure CHT, CHT-PU-PEtOx and CHT-PU-PMeOx, respectively. However, if this relates to dissolution or degradation is unclear. It would be interesting to consider the mucus, being a highly efficient barrier for drug delivery to the lungs, in a follow-up study.

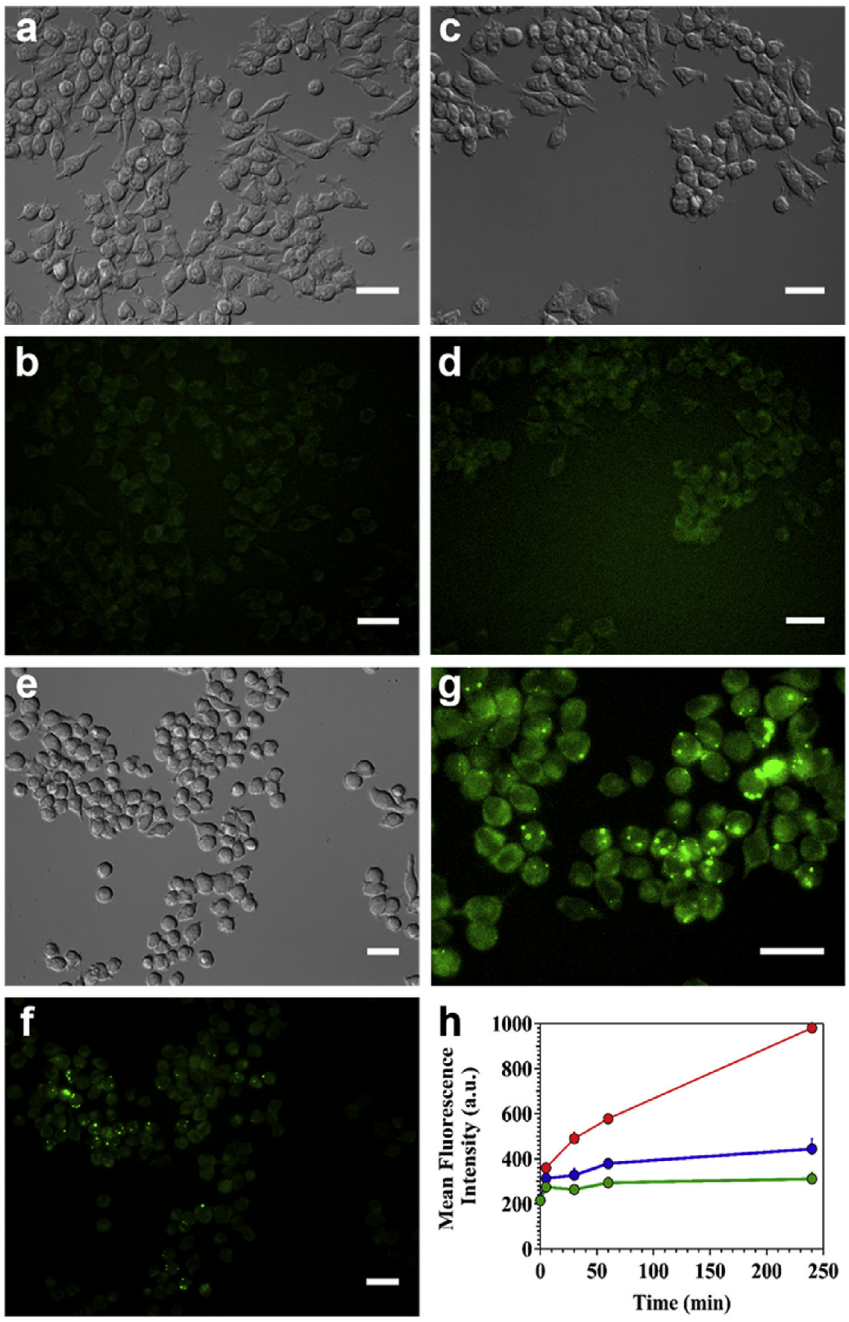

Fig. 45. (a, b) Untreated cells visualized by (a) DIC and (b) fluorescence microscopy. (c, d) Internalization of fluorescein labeled F-PMeOx$_{160}$–PMestOx$_6$/PTS (0.5 g/L) polymeric micelles on RAW 264.7 cells after 4 h of incubation. (e, f) Internalization of fluorescein labeled CFZ–F-PMeOx$_{160}$–PMestOx$_6$/PTS (0.5 g/L) loaded polymeric micelles on RAW 264.7 cells after 4 h of incubation. (g) Region magnifications of the panel f image. Scale bars = 50 μm. (h) FACS analysis of RAW 264.7 cells treated with 0.6 g/L (●), 0.3 g/L (●), and 0.1 g/L (●) suspension of CFZ–F-PMeOx$_{160}$–PMestOx$_6$/PTS NPs in DMEM without phenol red. Reprinted with permission from Ref. [258]. Copyright 2017 American Chemical Society.

Zhang et al. [263] synthesized an adamantyl (AD) terminated poly(aspartic acid) (AD-PAsA) and a β-cyclodextrin (CD) capped seven armed star PMeOx (7PMeOx-CD) which can form pseudo block copolymer by interaction between CD and AD. AD-PAsA replaced with its carboxylic groups the chloride (Cl^-) ligands of cisplatin resulting in very high *LC* of 53 wt% (D_h = 95 nm). The drug-loaded NPs (7PMeOx-PAsA) were stable up to several hours in PBS. After that, significant decrease in size (D_h = 20 nm after 24 h) was observed, which was attributed to release of the drug. About 25% cisplatin release was observed in PBS after 120 h. In contrast, in deionized water, only 10% release was observed. Drug loaded NPs showed higher release in the presence of Cl^- suggesting that the complexation interaction of cisplatin with AD-PAsA gradually disappeared due to exchange of chloride ions in the medium and the carboxylate group of AD-PAsA. Cytotoxicity analysis with H22 cancer cells was performed for up to 48 h. The IC_{50} value of the cisplatin loaded NPs (IC_{50} = 11.3 mg/L) was higher than that of free cisplatin (IC_{50} = 2.6 mg/L). According to the authors, this was attributed to a retained drug release from the NPs. The blank PMeOx-PAsA copolymer was non-cytotoxic against NIH-3T3 cells up to the very low concentration of 0.075 g/L after 48 h of incubation. CLSM studies revealed the endocytosis of Rhodamine-B

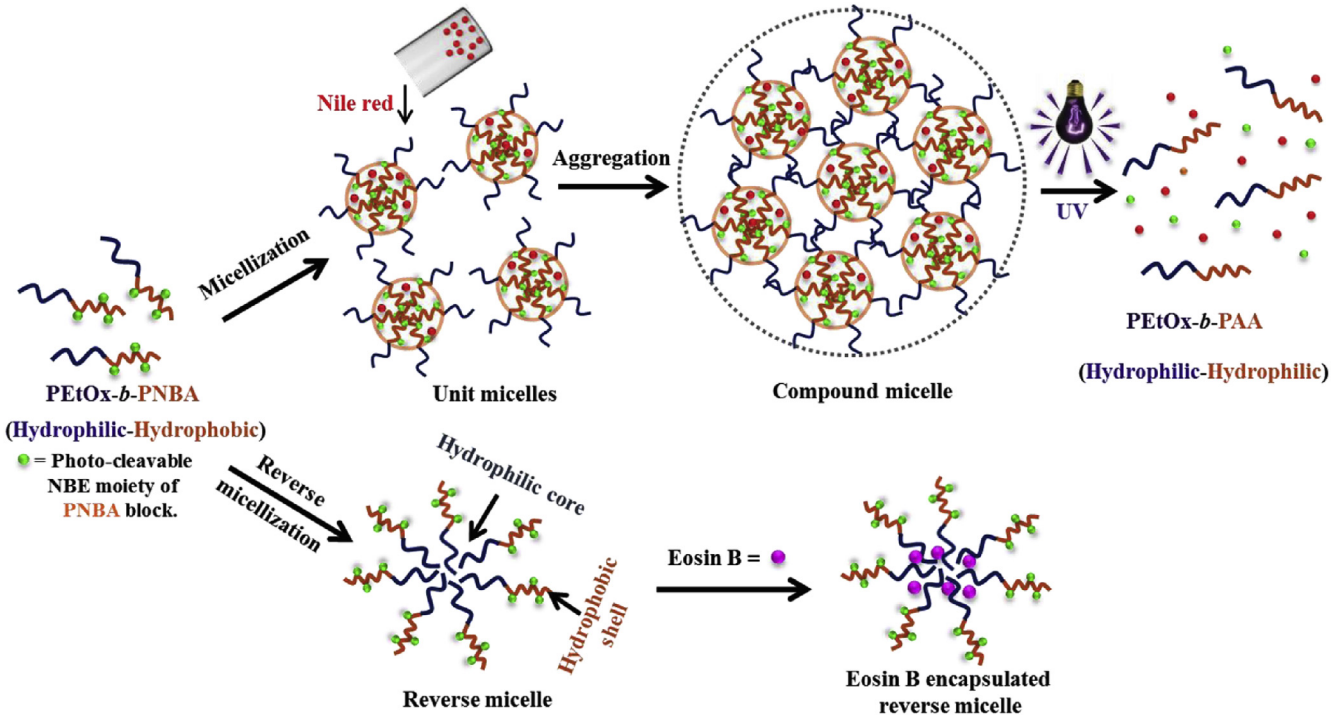

Fig. 46. Schematic representation for self-aggregation of block copolymer into single and compound micelles in THF/water mixture and representation of formation of reverse micelle of PEtOx-b-PNBA as well as its eosin B Dye encapsulation in dichloromethane. Reprinted with permission from Ref. [261]. Copyright 2016 American Chemical Society.

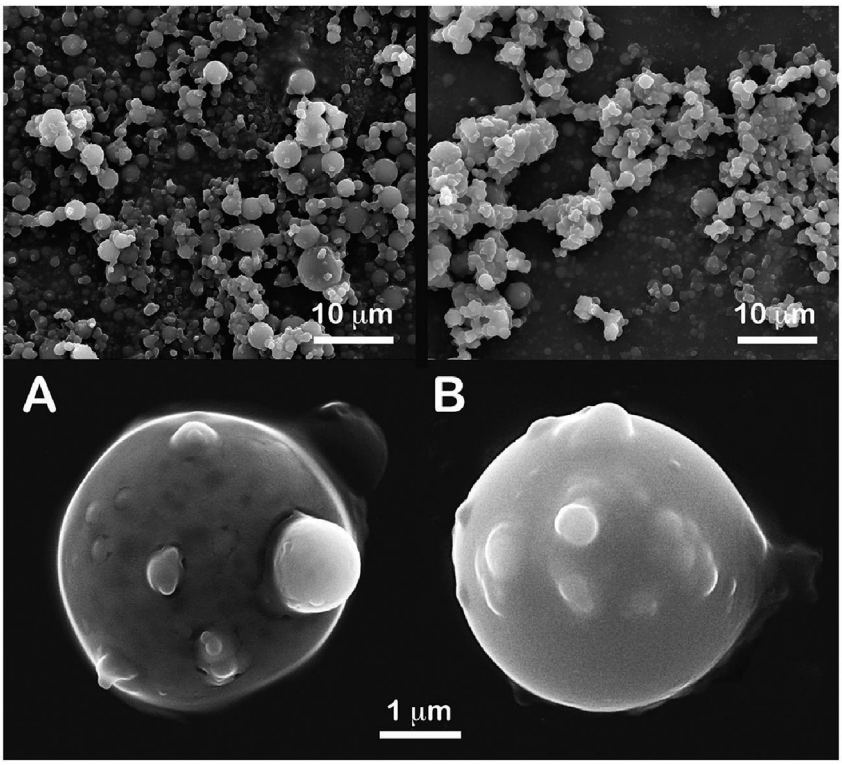

Fig. 47. Scanning electron micrographs of nano-in-micro particles processed by supercritical-fluid-assisted spray drying (top) and single microparticles (bottom) of [PU-EtOx]-chitosan A) and [PU-MeOx]-chitosan B). Amplification 2000 × (top) and 20000 × (bottom). Reprinted with permission from Ref. [262]. Copyright 2016 WILEY-VCH Verlag GmbH & Co. KGaA, Weinheim.

labeled cisplatin loaded NPS. Furthermore, NIRF imaging revealed a maximum accumulation of NPs in H22 tumors after approx. 15 h post injection. Subsequently, signal intensity kept on decreasing up to 168 h. However, besides a strong accumulation in the liver, also

significant high signal intensity was detected in most normal tissues even after 36 h p.i. (Fig. 48).

Kostova et al. [264] prepared a segmented copolymer network (SCN) based on PEtOx containing PHEMA, PHPA, and/or poly(-methyl methacrylate) (PMMA) segments by UV induced radical copolymerization for the sustained drug delivery of the highly hydrophilic drug metoprolol. SCN discs (thickness = 1 mm, diameter = 0.6 cm) with a high PEtOx content showed higher swelling degree in PBS and water. The drug was loaded by immersing the films into the drug solution and the films with a higher PEtOx content (70 repeat units) showed a higher degree of swelling and higher drug loading. $PHEMA_{30}$-$PEtOx_{70}$ disc encapsulated the maximum weight of drug i.e 135.8 mg (84.2 wt%), while the $PHEMA_{30}$-*co*-MMA_{50}-$PEtOx_{20}$ had least weight of drug i.e. 69.6 mg (46.6 wt%). Discs containing PMMA showed minimum swelling because of its highest hydrophobic character. *In vitro* drug release study showed a burst release with 60% drug released after 30 min from all type of films except $PHEMA_{30}$-$PEtOx_{30}$ which showed 30% drug release. $PHEMA_{30}$-$PEtOx_{70}$ and $PHPA_{30}$-$PEtOx_{70}$ showed cumulative release of 80% up to 8 h. A similar system was used for the sustained drug release of IBP [120]. Drug loading was done by swelling the disks (0.6 cm in diameter) in ethanolic solution of IBP (250 mg/mL) for 24 h. All 4 co-networks i.e $PHEMA_{30}$-$PEtOx_{70}$ (PL-1), $PHEMA_{50}$-$PEtOx_{50}$ (PL-2), $PHPA_{30}$-$PEtOx_{70}$ (PL-3) and $PHPA_{70}$-$PEtOx_{30}$ (PL-4) showed a IBP loading of 79, 70, 76 and 58 wt%, respectively. Unlike significant impact of PEtOx content on swelling behavior of four different APCN, no major differences were found in overall drug content. *In vitro* drug release analysis showed PHEMA (PL-1 & PL-2) based conetworks showed rapid release of IBP (98%) within 14 h at pH 7.2. PL-1 and PL-2 showed similar release pattern (30%) up to 4 h followed by abrupt drug release (60%) by PL-1 in hour 5. In contrast, PL-3 and PL-4 showed a somewhat more sustained release of 60% and 40% IBP at similar conditions (Fig. 49). However, it should be noted that these release studies were apparently only performed once, wherefore the results should not be overinterpreted. DSC analysis revealed the significant decrease in IBP melting temperature from 74 °C for pure IBP to 35 °C and 53 °C in case of PL-1 and PL-3 respectively which the authors attribute to H-bonding between the carboxylate of IBP and carbonyl moieties in the APCNs.

Huang et al. [265] synthesized a boron containing POx-based polymer micelles intended for use in boron neutron capture therapy. The utilized system consisted of boron pinacolato terminated PLA-PEtOx (Bpin-PLA-PEtOx). In addition, a derivative of phenyl boric acid (PBAD) having a low aqueous solubility was encapsulated into the hydrophobic core. The synthesized Bpin and PBAD had a boron content of 5 wt% and 2.5 wt%, and the aqueous suspension of Bpin-PLA-PEtOx and PBAD loaded Bpin-PLA-PEtOx had a boron concentration of 6 and 16 mg/L, respectively. The PBAD was loaded into the micelles, which increased the boron content about two-fold. The preliminary cytocompatibility evaluation on HeLa cells showed that the boron containing Bpin-PLA-PEtOx micelles had a low cytotoxicity compared to PBAD, indicating Bpin-PLA-PEtOx could be a potential DDS for boron drugs. However, the boron content would likely have to be increased very significantly to enable any therapeutic potential.

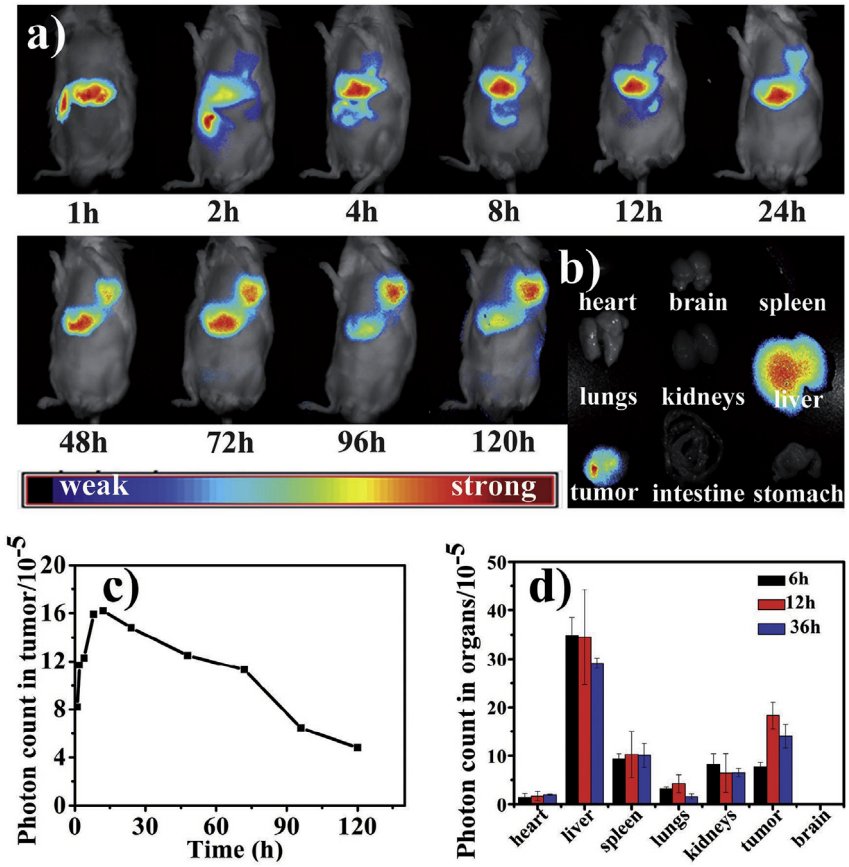

Fig. 48. a) In vivo NIRF images of H22 tumor-bearing mice after i.v. injection of NIR-797-labeled cisplatin-loaded 7PMeOx-PAsA nanoparticles. b) Ex vivo NIRF images of different organs at 168 h post administration. c) Time-dependent fluorescent intensities of a tumor ($n = 1$). d) Fluorescent intensity of different organs from H22 tumor-bearing mice ($n = 3$) at different time points after i.v. injection. Reprinted with permission from Ref. [263]. Copyright 2017 WILEY-VCH Verlag GmbH & Co. KGaA, Weinheim.

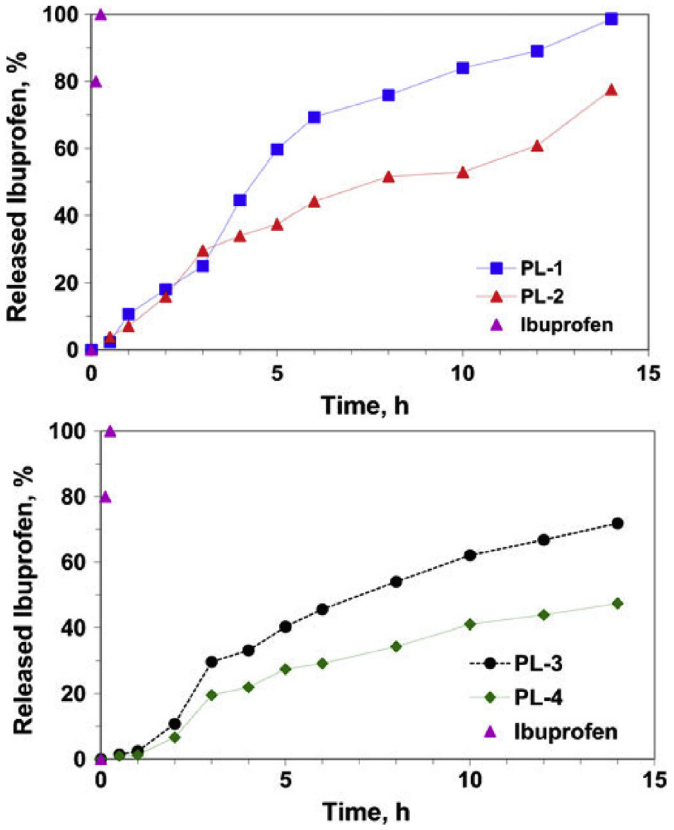

Fig. 49. Release kinetics of ibuprofen from loaded PEtOx containing polymer conetworks (PL-1, PL-2, PL-3 and PL-4, please refer to main text for further details) and dissolution profile of pure ibuprofen at pH 7.2 (37 °C). Reprinted with permission from Ref. [120]. Copyright American Association of Pharmaceutical Scientists 2013.

Baumann et al. [266] investigated PMeOx-*b*-PDMS-*b*-PMeOx and PVP-*b*-PDMS-*b*-PVP based polymersomes for photodynamic therapy. The dye rose bengal (RB) was conjugated to bovine serum albumin (RB-BSA) and encapsulated into both types of vesicles. BSA conjugation improved the encapsulation efficiency (*EE*) by increasing the overall solubility of RB and also avoided the interaction with the membrane of the polymer (not further confirmed by analytical data). The *EE* and cellular uptake (HeLa cells) was higher in PMeOx–*b*-PDMS–*b*-PMeOx ($EE = 13\%$) vesicles as compared to PNVP-*b*-PDMS-*b*-PNVP based systems ($EE = 8.6\%$). Besides that, vesicles within a size range of 50–120 nm had higher uptake than bigger vesicles. *In vitro* stability of the vesicles was tested by encapsulating DOX and applying the vesicles to the HeLa cell line (Fig. 50). DOX was not detected in nuclei after 24 h, which confirmed the stability of the vesicles. RB-BSA treated HeLa cells were exposed to artificial daylight for 30 min and the viability decreased to 50% as compared to non-exposed control. Important to note, the dose of RB–BSA encapsulated in the vesicles was around 1.3 μM, which is about 100 times lower than the commonly administered doses (200–300 μM). Therefore, lower doses of photosensitizer could be utilized to achieve same outcomes as compared to conventional photodynamic systems. The level of ROS increased 40-fold after illuminating the cells for 25 min.

Mahata et al. [267] synthesized lignin grafted PMeOx (lig-*g*-PMeOx) based nanogel which were analyzed for wound healing and anti-inflammatory properties. These nanogels were either loaded with antibiotics or antifungals. 3-Amino-1*H*-1,2,4 triazole (3AT) conjugated nanogels were also synthesized. The *LC* of amphotericin B (AB) was found to be 17 wt%. AB loaded nanogels showed sustained release of 33, 21, 40 and 50% after 7 days at pH 8.5, 7.5, 6.5 and 5.5, respectively. Using a 2,2-diphenyl-1-picrylhydrazyl (DDPH) based radical scavenging protocol, free lignin, lig-*g*-PMeOx and 3AT-lig-*g*-PMeOx showed antioxidant activity of 10.5, 7.6, 7.0%, respectively (lignin radical scavenging ability strongly depends on its amount of free phenolic hydroxyl groups). MTT assay revealed that low concentrations of up to 50 mg/L free lignin, lig-*g*-PMeOx and 3AT-lig-*g*-PMeOx did not affect the cell viability (HEK293 cell line). The inhibitory effect of these 3 derivatives on activation of NF-kB in lipopolysaccharide stimulated raw macrophages was also tested and a dose dependent inhibitory effect was found. Maximum inhibition was found at 60–100 mg/L

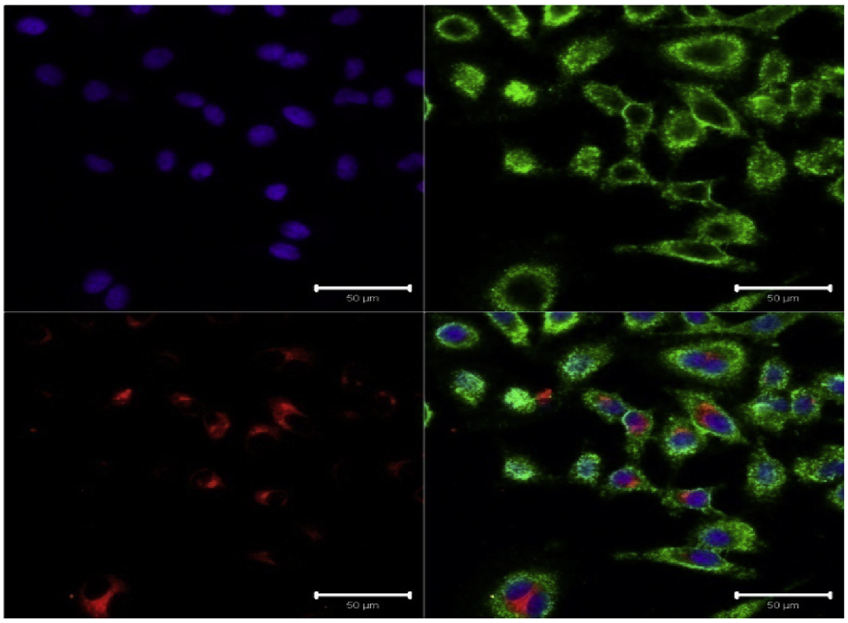

Fig. 50. HeLa cells incubated for 24 h with doxorubicin-containing vesicles. Violet channel: Hoechst DNA staining; green channel: cell mask deep red staining; red channel: doxorubicin-loaded vesicles (scale bar 50 μm). Reprinted with permission from Ref. [266]. Copyright 2014 American Chemical Society.

concentration of lignin derivatives, which is unfortunately above the concentration tested for cell viability. Antimicrobial activity was also tested against various bacteria and fungi. No significant growth reductions were observed at concentrations of 0.97 mg/L to 1 g/L for free lignin and lig-*g*-PMeOx. AFM analysis of untreated and 3-AT-lig-*g*-PMeOx treated *P.aeruginosa* biofilm had revealed significant difference in thickness of the biofilm structure from 30 nm (untreated) to 8 nm (treated) after 12 h of incubation. *In vivo* wound healing was also accessed on the flame burn wounds on rats. Lignin based nanocomposites mixed with piperacillin and tazobactam progressively decreased the wound to 1% of its original size while in untreated animals the wound size only decreased to 72%.

5.5. Drug combination formulations

We have previously discussed the drug specificity between CUR and PTX loading of some POx based ABA triblock copolymer amphiphiles. However, by co-incorporating PTX and CUR at same drug feed concentrations, the above mentioned P*n*PrOzi based triblock copolymer amphiphile seemed to lose any specificity, as both drugs were incorporated neatly with even higher overall drug loadings possible (ρ(CUR & PTX) = 7.1 & 7.0 g/L @ 10 g/L polymer; *LC* = 58.6 wt%) while the D_h remained below 100 nm (Fig. 39B). Even the smallest addition of CUR (1 g/L) led to an immediate maximization and 8-fold increase of PTX loading which could be interpreted as a pronounced synergy between CUR and PTX (Fig. 39B). In contrast, the co-incorporation of small amounts of the unfavoured CUR prevented efficient loading with PTX (antagonistic effect) in the case of PMeOx-*b*-P*n*BuOx-*b*-PMeOx. Only when the PTX/CUR feed ratio approached unity, the loading efficiency of the otherwise preferred PTX exceeded 10% (Fig. 39B).

A similar synergism with respect to the loading capacity for PTX and CUR by co-incorporating both drugs simultaneously has also been observed with the structurally related POx and POzi triblock copolymers exhibiting the same hydrophilic PMeOx shell but a strongly hydrophobic core based on either PNOx, poly(2-(3-ethylheptyl)-2-oxazoline) PEtHepOx, poly(2-*n*-nonyl-2-oxazine) (PNOzi) or poly(2-(3-ethylheptyl)-2-oxazine) (PEtHepOzi) [268]. Especially PTX could be incorporated more efficiently by co-encapsulating CUR at same drug-feed concentrations. However, with these polymers it was much more difficult to find conclusive structure-property relationships, as the standard deviation between the samples prepared in triplicates was quite high (especially at the single drug-formulations). Even more complicating, maximum drug-concentration was not always reached right after preparation of the drug-loaded micelles, but after 5 or even 10-day storage. Physicochemical characterization of the precipitate revealed that not only the water-insoluble drug, but also the water-soluble polymer precipitated right after preparation of the drug-loaded micelles. These aggregates re-dissolved over time explaining the increase in drug-content over time (formulations were stored in Eppendorf tubes containing the precipitate). A similar increase in solubility over time (*LC* = 21 wt% (day 0); 46 wt% (day 10); 45 wt% (day 30)) has been observed for CUR encapsulated in a PBzOx based copolymer [254].

Nevertheless, the maximum *LC* for PTX or CUR of the block copolymers comprising very hydrophobic C9-alkyl side chains within the hydrophobic core could not rival that of the discussed best-in-class polymers comprising short C4-side chains.

Very recently, Wang et al. [269] co-encapsulated PTX and honokiol (HNK) in PEtOx-*b*-PLA based micelles (PEtOx-PLA) (D_h = 41–44 nm (spherical); PDI < 0.3; *LC* (PTX) = 5.0 wt% (ρ(PTX) = 0.1 g/L); *LC* (HNK) = 4.1 wt% (ρ(HNK) = 0.08 g/L); *LC* (PTX&HNK) = 4.2 & 3.6 wt% (ρ(PTX&HNK) = 0.09 & 0.08 g/L)) to suppress multidrug resistance (MDR) and metastasis of MDA-MB-231 breast cancer cells. *In vitro* release of co-encapsulated PTX & HNK exhibited biphasic pattern with a slightly faster initial release followed by a sustained drug release at both, pH = 7.4 (approx. 60% (PTX) & 40% (HNK) release after 50 h) and pH = 5 (approx. 80% (PTX) & 60% (HNK) release after 50 h). Therefore, the authors suggested that the drug loaded particles could distinguish between endo/lysosomal pH from physiological pH. However, the difference of release between pH 7.4 and 5 was only minimal, strongly questioning whether this selectivity would be meaningful *in vivo*. For a more in depth investigation regarding the pH-sensitivity and cellular internalization of the PEtOx-PLA micelles please refer to the literature [270]. Cytotoxicity of PTX&HNK/PEtOx-PLA (HNK acts as P-gp inhibitor) was significantly increased (IC_{50}: 1.8–5.8 mg/L) compared to single PTX and HNK formulations ($IC_{50,PTX}$ = 18.1 mg/L; $IC_{50,HNK}$ = 24.5 mg/L) in MDA-MB-231 cells. The combination index (CI) revealed a strong synergistic effect between PTX and HNK at equal drug concentrations. Furthermore, cellular Rh123 uptake of Rh123&HNK/PEtOx-PLA (Rh123/HNK = 1/1 w/w) in MCF-7/ADR cells was 2-fold higher than that of Rh123/PEtOx-PLA. Mechanistic studies revealed, that the decrease in plasma membrane microviscosity and down-regulation of P-gp expression might be mainly responsible for inhibition of P-gp efflux for PTX&HNK/PEtOx-PLA and a positive effect of the formulations in preventing lung metastasis *in vivo* (Fig. 51). The results suggest that the drug enters independently from the nanoparticle, since its uptake should not be affected otherwise.

6. Targeted and theranostic drug delivery systems

6.1. Targeted drug delivery systems

Targeted drug delivery refers to enhanced drug accumulation within a target tissue or compartment independent of the method and route of drug administration [271]. The concepts of targeted drugs or targeted drug delivery dates back to 1906, when Ehrlich first postulated the magic bullet [272]. A plethora of studies can be found regarding active and passive targeting of tumors [273]. Passive targeting facilitates deposition of carriers within the tumor microenvironment or other pathologies, owing to distinctive biochemical and biophysical characteristics inherent to the respective milieu [274], while in active targeting various bio-recognition moieties are employed on the surface of carrier which supposedly make the system more selective and specific. However, even though active targeting has been highly successful *in vitro* and more simple animal models, no real breakthrough in the clinics has been achieved. In a controversial review by Chan and co-workers, this failure of targeted delivery has been discussed recently [275]. Irrespective of this debate, POx polymers have also gained attention for the development of targeted drug delivery system in the past decade.

Very recently, Magarkar et al. [276] studied the aggregation behavior of POx using a molecular dynamics simulation model with an all atom resolution to investigate the cause of failure of a newly proposed targeting ligand (activated endothelium targeting peptide (AETP)) when attached to PEGylated liposomes. According to the calculations, by replacing PEG with POx (PEtOx, PMeOx), the relative exposure of the targeting ligand to the solvent should be increased. Although it was not possible to explain this phenomena on a molecular level, this study corroborates interesting and potentially important physicochemical differences between PMeOx and PEG. It would be interesting to see if the calculations can be confirmed by experimental data.

Folic acid (FA) is extensively used as targeting ligand, because of its small size, low cost, non-immunogenic nature and the over-expression of its receptor on variety of tumors [277]. In 2013, Qiu

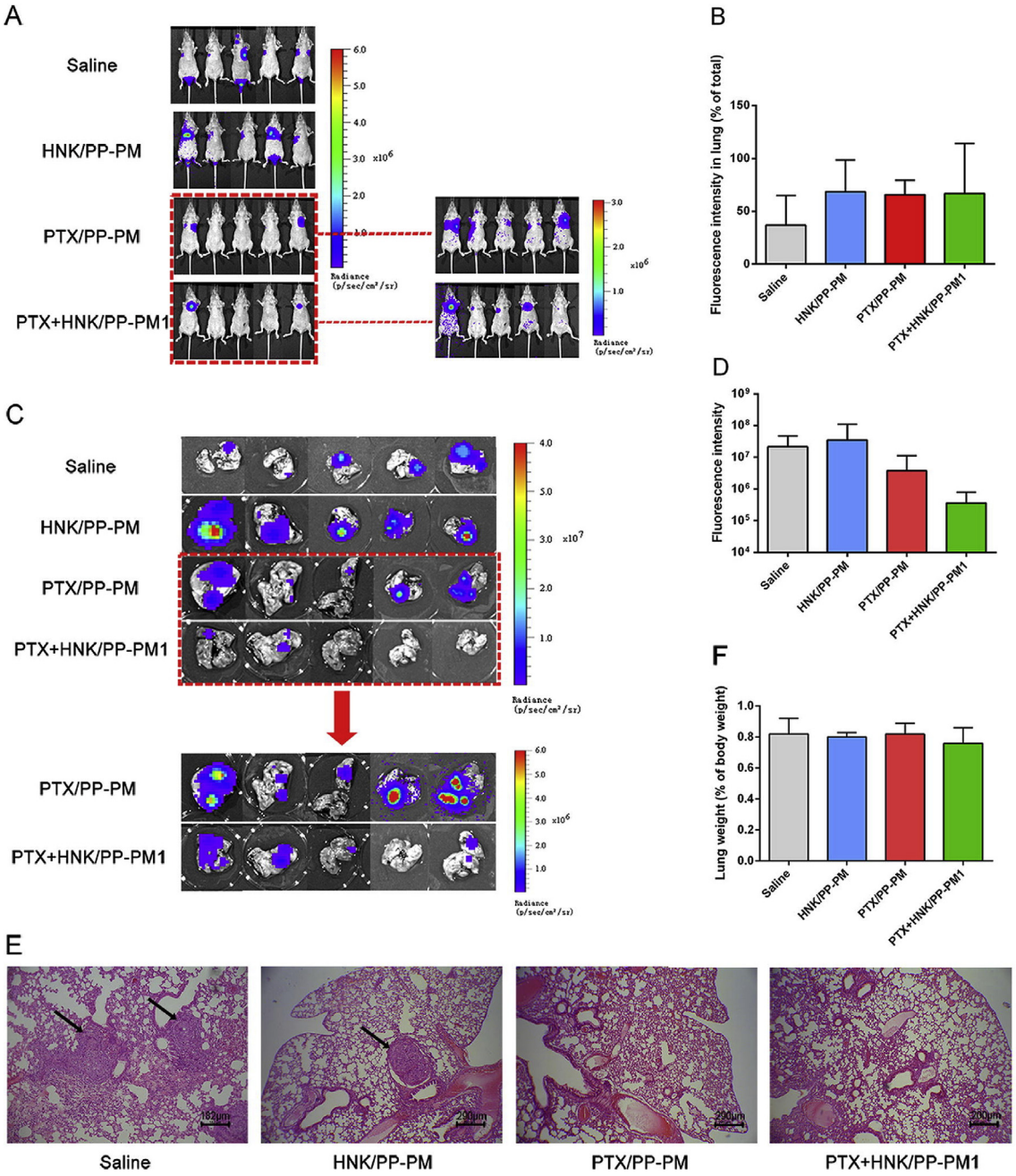

Fig. 51. (A) *In vivo* bioluminescent images of normal male BALB/c nude mice with pulmonary metastasis (MDA-MB-231-luc-FGP) treated with saline, HNK/PEtOx-PLA, PTX/PEtOx-PLA and PTX + HNK/PEtOx-PLA given equivalent doses of PTX at 25 mg/kg and HNK at 25 mg/kg, respectively (n = 5). The images marked with red dotted lines are shown separately for easy comparison under another scale bar. (B) The bioluminescence intensity of *in situ* lungs in mice treated with various formulations. (C) *Ex vivo* bioluminescent images of the excised lungs for mice treated with various formulations. The images marked with red dotted lines are shown separately for easy comparison under another scale bar. (D) The bioluminescence intensity of *ex vivo* lungs in mice treated with various formulations. (E) Representative micrographs of lung sections stained with H&E. (F) The wet weight of lung for mice treated with various formulations. Reprinted with permission from ref. [269]. Copyright 2017 Elsevier.

et al. [278] reported DOX loaded folate modified PEtOx-*b*-PCL aggregates for the targeted delivery of DOX to folate receptor expressing tumors. FA was attached via amide-bond to the PEtOx corona. Increase in FA content from 0 to 48 wt% only slightly reduced drug loading from 12.9 ($D_h = 162$ nm) to 10.2 wt% ($D_h = 187$ nm). IC_{50} values were slightly reduced for FA modified micelles compared to unmodified micelles. Specifically, they decreased from 0.76 to 0.30 mg/L for HeLa cells and from 0.96 to 0.40 mg/L for human nasopharyngeal epidermal carcinoma KB cells by increasing the FA content on the carriers, which is, according to the authors, indicating receptor mediated endocytosis and drug release. However, proper control would be needed to qualify such statement and such little difference in IC_{50} is unlikely to be relevant *in vivo*. *In vitro* drug release experiments showed the least release at pH 7.4 (10%) with unmodified micelles and maximum release at pH 5.5 (60%) with FA modified micelles at 60 h duration. Again, this different release is not necessarily due to carrier properties. The intracellular fluorescence signal (intrinsic fluorescence of DOX) of FA modified carriers was 3-folds higher compared to unmodified DOX-loaded micelles in both, HeLa cells and KB cells. *In vivo* tumor

inhibition ratio at 35 days post treatment for free DOX, unmodified carriers and FA modified carriers was 45%, 38% and 53%, respectively. The low tumor inhibition ratio of unmodified carriers is attributed to the incomplete drug release at physiological pH as shown *in vitro*. An apparent weight decrease was observed after free DOX administration, while this was not observed in micelle groups showing that overall systemic toxicity of DOX was reduced upon encapsulation into micelles.

Kampmann et al. [279] synthesized a bifunctional POx macromonomer with multiple acrylate groups as hydrophobic block and azide end groups which could be converted into amines via Staudinger reaction. Microemulsion polymerization technique was used to obtain core-crosslinked nanoparticles. To this end, the methacrylates present in the hydrophobic core were crosslinked with 1,6-hexanediol dimethacrylate (HDDMA). Particle size varied between 20 and 75 nm depending on the amount of crosslinker used. Nanoparticles containing primary amine moieties were modified with FA, a RGD-peptide derivative and fluorescein isothiocyanate (FITC). Depending on the coupling chemistry (FA, RGD: amidation; FITC: thiourea formation) and steric demand of the compounds, degrees of modification varied from 4 wt% (FITC), 8 wt% (FA) and 20 wt% (RGD). Moderate size increase was found at constant HDDMA wt.% in case of FA ($D_h = 60$ nm) and FITC ($D_h = 59$ nm), while for the RGD peptide ($D_h = 68$ nm), a more pronounced increase was observed. Another approach to use folic acid as active targeting moiety was reported by Chen et al. [280]. However, as the FA-bearing polymer was immobilized on a glass surface, this approach is described in more detail below in the chapter on POx at interfaces.

Figueiredo et al. [281] reported on a polymersome based targeted DDS comprising PDMS-*b*-PMeOx diblock copolymers. The targeting peptide Angiopep 2 (AP2) being a ligand for the low density lipoprotein receptor usually overexpressed in the blood-brain barrier was conjugated to the surface of the polymersomes by EDC and NHS chemistry for the specific targeting of glioblastoma. Conjugation efficiency was found to be 24% estimated by measuring the fluorescence of FITC conjugated to AP2. The loading efficiency for DOX was found to be 4% (film hydration method) and 13% (co-solvent method), respectively. AP2 modified and unmodified polymersomes were incubated in human plasma for 2 h to investigate the effect of plasma proteins on the polymersome structure. Size changed from 236 to 331 nm and 226–282 nm for unmodified and modified polymersomes, respectively. U87MG cell viability studies showed that AP2 modified polymersomes caused no significant cytotoxicity up to 1 g/L. CLSM revealed that AP2 modified polymersomes were taken up more efficiently by U87MG cells than unmodified polymersomes. A sustained drug release pattern was observed for both, DOX incorporated in AP2 modified and unmodified polymersomes. The DOX release from the AP2 modified polymersomes was 50% up to 48 h at pH 5.5 and 7.4. The antiproliferative effect of free DOX and DOX loaded in modified and unmodified polymersomes was similar after 48 h of incubation up to concentrations of 25 μM. At 30 μM DOX, the modified micelles showed minimally higher anti-proliferative activity (25%) than unmodified (33.4%). Most interestingly, according to *in vitro* DOX release studies, 50% of DOX was released after 48 h from the polymersomes, which was equally effective as the administered dose of pristine DOX in case of antiproliferative activity. This suggests that PDMS-PMeOx based sustained release system has rendered the DOX more stable while maintaining its pharmacological effect.

Differences in the pH of normal extracellular compartment (pH 7.4), tumor tissue (pH 6.8) and endosomal/lysosomal compartment within the cell (pH 5–6), can be exploited as triggered drug release. The pH triggered release of drugs can be realized for example by protonation of pH-sensitive moieties within the hydrophobic core solubilizing the drug. Destabilization occurs when the protonatable groups become charged below the pK_a, leading to repulsion between the polymer chains, which results in micelle dissociation. Of course, one also has to consider a possible protonation of the drug, which might also drastically increase its solubility.

Prostate specific membrane antigen (PSMA) is commonly overexpressed about 100 times in prostate cancer and can be targeted with YPSMA-1 mouse monoclonal antibodies. In this context, Gao et al. [282] utilized PEtOx-*b*-PLA based amphiphilic diblock copolymer conjugated with YPSMA-1 (25% conjugation efficiency) for the solubilization and targeted delivery of PTX ($LC = 8.3–8.9$ wt %). Drug release from the micelles was somewhat faster at pH = 5 (100% release after 24 h) compared to pH = 7.4 (70% release after 24 h). The blank micelles were non-cytotoxic up to 10 g/L against the human prostate cancer cell lines PC-3 (PSMA negative) and 22Rv1 (PSMA-positive). Cytotoxicity of PTX loaded into unmodified (PTX/PM) and modified formulation (PTX/PM-Y) was same in PC-3 cells (IC_{50} approx. 60 μg/L) and PSMA-positive 22Rv1 cells (IC_{50} (free PTX) = 66 μg/L, IC_{50} (PTX/PM-Y) = 64 μg/L, IC_{50} (PTX/PM) = 71 μg/L after 72 h). Subsequently, Coumarin 6 was encapsulated within the hydrophobic core to study the intracellular trafficking of the pH sensitive micelles. PTX/PM-Y showed 1.55-fold higher fluorescence intensity than unmodified micelles (PTX/PM) in 22Rv1 cell lines after 4 h incubation. Normally, after cellular internationalization of micelles , they end up by endo/lysosomal pathway. Real time CLSM showed a reduced co-localization of the modified PEtOx-*b*-PLA micelles in endo/lysosomes (after 0.5 h, 1 h and 3 h) as compared to PEG-*b*-PLA based micelles. Results from the 2D-cell cultures were confirmed *in vivo*, as tumor suppression of PTX/PM-Y was more effective only in 22Rv1 xenograft mouse models, albeit minimally, whereas for the PC-3 tumor model, no difference was observed compared to non-modified PTX-loaded micelles and the commercially available PTX-formulation Taxol® (Fig. 52). Unfortunately, no survival data was provided without which the presented data is not very strong.

In a follow up study [283], the YPSMA-1 conjugated micelles were further modified with cyclic RGD (cRGDyK), having a high binding affinity for integrin $\alpha_v\beta_3$. The *LC* for PTX was 8–9 wt% for unmodified, cRGDyK modified, YPSMA-1 modified and dual modified micelles. In the PSMA and integrin $\alpha_v\beta_3$ expressing cell line 22Rv1, a higher cellular uptake of the dual-modified micelles compared to unmodified micelles was visualized by CLSM and by encapsulation of coumarin 6 (Fig. 53). After 72 h of incubation, no difference (considering experimental variability) in cell cytotoxicity against 22Rv1 cells of free PTX ($IC_{50} = 66.3 \pm 3.9$ μg/L), unmodified ($IC_{50} = 70.6 \pm 7.1$ μg/L) and modified PTX-loaded micelles ($IC_{50} = 64.0 \pm 3.3$ μg/L, 56.2 ± 4.7 μg/L and 55.1 ± 3.5 μg/L for YPSMA-1, cRGDyK and dual ligand modified micelles, respectively) was observed. From flow cytometry experiments and confocal microscopy images (Fig. 53) it is argued that integrin $\alpha_v\beta_3$ mediated endocytosis (ligand is cRGDyK) is more pronounced than PSMA (ligand is YPSMA-1) dependent endocytosis. Importantly, the uptake of RGD modified nanoparticles could be blocked by free RGD and that of YPSMA-1 modified nanoparticles by addition of free YPSMA-1. It would have been most interesting to assess the effect of free RGD and YPSMA-1, alone and in combination, on endocytosis of nanoparticles modified with both ligands. Unfortunately, the authors apparently did not consider this control group.

Building on these results, Gao and co-workers [284] further extended the study to *in vivo* level using PC-3 xenograft bearing nude mice and single cRGDyK modified pH sensitive PTX loaded PEtOx-PLA micelles as a potential candidate for the treatment of prostate cancer. The FRET analysis (Dil/DiO) confirmed that the micelles remained intact during circulation until their internalization into the cells. FRET was also observed after 1 h incubation in

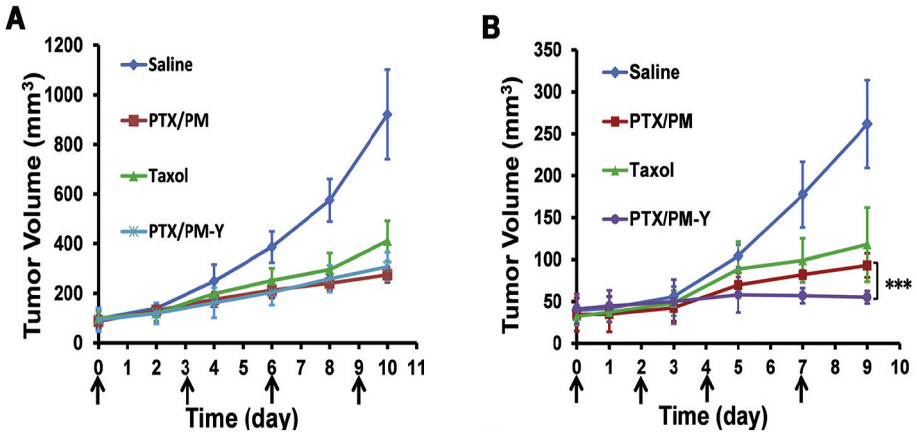

Fig. 52. Tumor suppression at the whole-body level of PC-3 (A) and 22Rv1 (B) model. Changes of tumor volume after intravenous injection of saline, Taxol®, PEtOx-PLA nanoparticles loaded with paclitaxel with (PTX/PM-Y) and without YPSMA-1 (PTX/PM) in PC-3 (A) and 22Rv1 (B) tumor-bearing nude mice (n = 6). The arrows indicated injection time points. ***p < 0.001. Reprinted with permission from Ref. [282]. Copyright 2015 Royal Society of Chemistry.

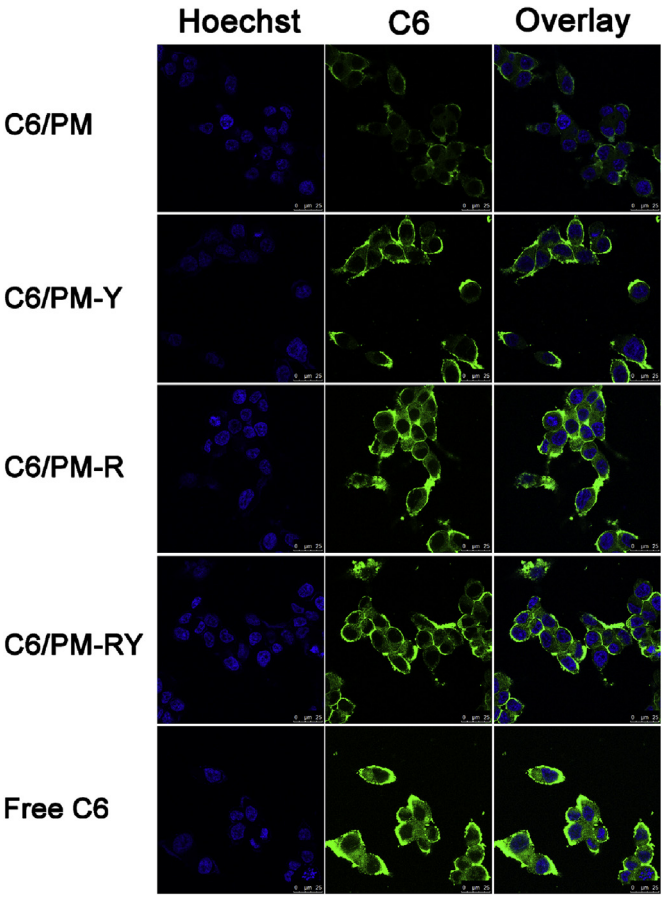

Fig. 53. CLSM images of 22Rv1 cells incubated with various coumarin 6 (C6) formulations at 37 °C for 1.5 h. The final C6 concentration in each formulation was 50 ng/mL. Cell nuclei were stained blue with Hoechst 33258, and green fluorescence is from C6 encapsulated in micelles (PM; polymeric nanoparticles, Y; YPSMA, R; cRGDyK, RY; cRGDyK and YPSMA). Reprinted with permission from Ref. [283]. Copyright 2015 Springer Science + Business Media New York.

PC-3 cells. C6 was used to investigate the endo/lysosomal escape and cellular uptake study. The *in vitro* cytotoxicity studies of PTX loaded cRGDyK micelles were performed on PC-3 cells. Again, no relevant difference in cytotoxicity was observed between unmodified PTX loaded micelles ($IC_{50} = 64.53 \pm 5.15$ μg/L), free PTX ($IC_{50} = 62.95 \pm 5.77$ μg/L) and modified micelles ($IC_{50} = 51.16 \pm 1.09$ μg/L). cRGDyK modified micelles showed 2-fold higher fluorescence intensity than unmodified micelles. The fluorescence intensity of C6 loaded PEtOx-PLA micelles was significantly decreased at 0.5 and 1 h of incubation suggesting the escape of micelles from endo/lysosomes. *In vivo* antitumor studies on PC-3 xenograft bearing nude mice were carried out at a dose of 15 mg/kg body weight. Whole body imaging revealed that ligand modified, 10-dioctadecyl tetramethyl indotricarbocyanine iodide (DiR) loaded micelles exhibited maximum tumor accumulation as compared to unmodified sample, corroborating significant contribution of cRGDyK moiety for targeted drug release. Control experiments with control peptides such as RGD or RGE would further help to clarify the active nature of targeting. *Ex vivo* imaging of various organs of mice, sacrificed after 24 h also confirmed the maximum accumulation in tumor and liver.

Zhao et al. [285] from the same research group used the PEtOx-PLA micelles for the co-delivery of DOX and P-gp inhibitor D-alpha-tocopheryl PEG-1000 succinate (TPGS1000). The co-administration of TPGS1000 increased the intracellular levels of DOX by inhibiting P-gp, which indicates that it is released probably outside the cell. Rather than attaching folate to the PEtOx-PLA polymers directly, the authors used 1,2-distearoyl-3-*sn*-phosphatidylethanolamine-PEG-folic acid (DSPE-PEG-5000-FA), which is a phospholipid PEG derivative that can be used for folate receptor targeting. DOX loaded micelles had a diameter of approx 40 nm. The *LC* ranged between 6.5 and 8.2 wt% for PEtOx-PLA and PEtOx-PLA/DSPE-PEG-5000-FA (10:1) mixed micelles, which were prepared by dialysis method. PEtOx-PLA/DSPE-PEG-5000-FA micelles showed pH dependent drug release. Drug release from the FA modified mixed micelles was 20%, 40%, and 60% at pH 7.4, 6.5 and 5 respectively. The IC_{50} values were found to be 60.40 ± 5.29 μg/L, 19.68 ± 3.36 μg/L and 21.20 ± 2.61 μg/L for free DOX, dual loaded unmodified micelles and dual loaded modified micelles respectively against KBv cell line (MDR cell line which over expresses P-gp). PEtOx-PLA/DSPE-PEG-5000-FA micelles loaded with DiR showed tumor specific distribution in KBv tumor bearing nude mice. However, maximum accumulation was found in the liver and no investigations were performed with pure DSPE-PEG-5000-FA micelles as control to effect their impact on tumor targeting.

Platelet activation is the major thrombotic event inducing the formation of platelet rich thrombus. To prevent this formation, Gunawan et al. [286] prepared antibody decorated, thrombin

cleavable, urokinase plasminogen activator (uPA) loaded brush-like PEtOx capsules bearing alkyne moieties (B-PEtOx$_{Alk}$) by LbL. uPA was loaded into mesoporous silica NP template upon which poly(methacrylic acid) (PMA) and B-PEtOx$_{Alk}$ were deposited by LbL technique. Crosslinking of the layers was performed with thrombin sensitive crosslinkers to facilitate cargo release in the area of thrombosis. After crosslinking, the mesoporous silica NP template as well as the PMA layers were removed to obtain uPA-loaded B-PEtOx$_{Alk}$ capsules. The particle surface was functionalized with single chain variable fragment (scFv) antibodies (9.3×10^{-14} g scFv (1.75×10^{6} scFv molecules) per capsule) to target activated platelets. The release of cargo was investigated in the presence and absence of thrombin. uPA release accelerated with increasing thrombin content (100% release after 4 h at 1 U/mL thrombin). Exposure to even higher thrombin concentrations (5 or 10 U/mL) resulted in almost instantaneous (within 15 min) capsule degradation and cargo release (Fig. 54). Surface-functionalization with scFv antibody resulted in high affinity for abundant GPIIb/IIIa integrins to specifically target activated platelets.

Dendritic cells (DC) are antigen presenting cells of the immune system. They process and present the antigen to T-cells which further trigger the immunological cascade. DEC-205 is a protein expressed primarily by DCs. Bühler et al. [287] synthesized three different azide (N_3) functionalized POx acrylamide macromonomers namely N_3-P*i*PrOx, N_3-PEtOx and N_3-PEtOx-*b*-P*i*PrOx (with the molar masses of 5 kg/mol, 3.7 kg/mol and 5.9 kg/mol respectively) for the further development of anti-DEC205 antibody conjugated cylindrical brushes. The brushes were obtained by polymerization of the azide-functionalized macromonomers leading to core-shell cylindrical brushes with a slightly hydrophobic P*i*PrOx core and a hydrophilic PEtOx shell. DLS showed R_h of 26, 21 and 42 nm for N_3-P*i*PrOx, N_3-PEtOx and N_3-PEtOx-*b*-P*i*PrOx, respectively. AFM images confirmed a worm-like structure. Cytotoxicity (against mouse bone marrow derived DC (BMDC)) by MTT assay revealed that 70% of cells were viable up to concentration of 1 g/L (maximum tested concentration) for N_3-P*i*PrOx and N_3-PEtOx-*b*-P*i*PrOx. Aggregation behavior of these brushes in the human serum showed that N_3-PEtOx and N_3-PEtOx-*b*-PiPrOx formed negligible aggregate (size is not given) while the N_3-P*i*PrOx showed an aggregate size of 360 nm (R_h). Dibenzocyclooctyne-modified anti-DEC205 antibody (DBCO-anti-DEC205) were conjugated to N_3-PEtOx-*b*-P*i*PrOx brushes using copper-free 1,3 dipolar cycloaddition chemistry. UV/Vis analysis revealed that on average 8 to 10 antibodies were attached to one cylindrical brush. The mean fluorescence intensity (MFI) was found three-fold higher in $CD11^+$ $DEC205^+$ BMDC population for anti-DEC205 modified PEtOx-*b*-P*i*PrOx brushes after 4 h incubation in comparison to unmodified brushes. The uptake was blocked in the presence of native anti-DEC205 antibodies. For the further biological application, these brushes were conjugated with SIINFEKL sequence of OVA antigen (a glycoprotein obtained from chicken egg white, mildly immunogenic, used for immunization research) followed by the conjugation of anti-DEC205 antibodies. On average, the final PEtOx-*b*-P*i*PrOx brush contained 17 OVA antigens and 7.5 anti-DEC205 antibodies. Because of anti-DEC205 antibodies and the OVA antigen, these PEtOx-*b*-P*i*PrOx brushes showed the maximum cellular uptake and the expression of OVA antigen on the surface of BMDCs, which ultimately lead to higher T cell proliferation in comparison to freely available antigen and unconjugated brushes (this experiment was done in the co-culture of BMDC and T cells, incubation time was 4 h).

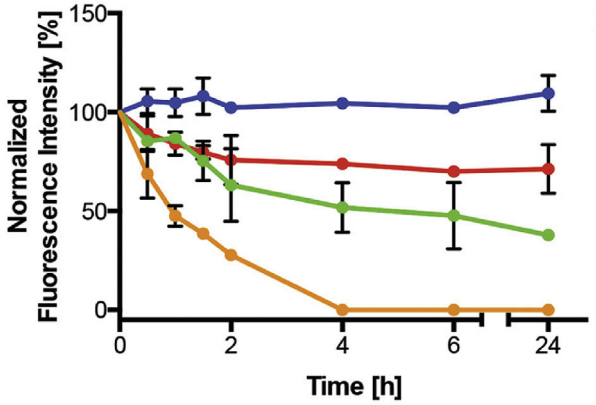

Fig. 54. Enzymatic degradation of AF555-labeled (red) urokinase plasminogen activator (uPA) loaded B-PEtOx$_{Alk}$ polymer capsules. Thrombin sensitive capsules were subjected to 0 U/mL (blue), 0.05 U/mL (red), 0.1 U/mL (green), or 1 U/mL (orange) of thrombin. The reactions were performed in $NaHCO_3$ (50×10^{-3} M, pH 8.0) at 37 °C, with constant shaking (means ± SD, n = 3). Reprinted with permission from Ref. [286]. Copyright 2015 John Wiley & Sons, Inc.

Dieu et al. developed PDMS-b-PMeOx polymersomes for the active targeting of brain capillary endothelial cells [288]. The active targeting was achieved by conjugating anti-human insulin receptor antibody 83-14 (83-14 mAb) to the polymersomes. Two different end functionalized diblock copolymers were synthesized i.e $PDMS_{65}$-b-$PMeOx_{14}$-COOH and $PDMS_{65}$-b-$PMeOx_{32}$-NHS and combined (95% and 5%, respectively) for the development of polymersomes (by thin film hydration method). 83-14 mAb were first labeled with 5(6)-carboxyfluorescein (CF) NHS ester. The fluorophore to protein ratio (F/P) revealed that the 83-14 mAb retained their functionality even after modification with an average of 9.4 dye molecules per mAb molecule. For further analysis mAb with an average of five CF molecules were selected. DLS showed the radius of 115 nm and 117 nm for non-functionalized and functionalized polymersomes, respectively. Fluorescence correlation spectroscopy (FCS) (using Dylight 488 dye labeled 83-14 mAb) revealed in total 13 antibodies were attached to one polymersome. Cellular uptake studies (human BBB *in vitro* model cell line i.e hCMEC/D3 cells, out of which 94% cell express insulin receptor) showed time dependent uptake of polymersomes. The MFI value increased from 5.6 to 10.8 from 1 h to 2 h respectively. Upon competitive inhibition analysis in the presence of free 83-14 mAb the MFI decreased to 3.5 after incubation for 2 h. CLSM studies showed that free mAb were colocalized in early endosomes/lysosomes within 20 min of incubation while the conjugated mAb to polymersomes were randomly localized even after 2 h of incubation. It would be interesting to further explore how the conjugation of mAb to polymersome can alter the intracellular localization of polymersome.

Targeted drug delivery is highly complex including biological, mechanical and chemical processes/barriers *in vivo*. Despite its promising results *in vitro* and simplified *in vivo* models, translation of targeted drug delivery systems into the clinics is hampered mainly due to insufficient reproducibility of the targeting properties in human as well as high cost of the sophisticated drug-carriers themselves. Although being highly beneficial for the production of new publications, those obstacles should always be kept in mind when developing new systems [289]. Nevertheless, targeted drug delivery remains to hold the promise of strongly decreasing side-effects and improve therapeutic outcomes. The versatile and easy-to-modify properties of POx makes this class certainly promising candidates for future developments in this regard.

6.2. Diagnostic and theranostic systems

As shown in the severe supply problems of the blockbuster liposomal drug Doxil [290] well-controlled production processes

that guarantee quality, reproducibility and sterility can be particularly challenging for the production of (polymeric) nanosystems for biomedical purposes. In this context, Liu et al. [291] suggested a single-step in-line nano-coprecipitation of PMeOx-*b*-PDMS-*b*-PMeOx block copolymers with different model compounds to manufacture injection-ready nanosystems for medical imaging and drug delivery. For encapsulation of the hydrophobic drug tamoxifen, polymer and drug were dissolved in EtOH and the organic solution was sheathed by two adjacent aqueous streams in a microfluidic setup (Fig. 55A). Loading capacities up to 11 wt% (ρ(drug) = 0.45 g/L) could be obtained, however loading efficiency (*LE*) decreased from 90% to 47% by increasing the drug feed from 10 to 30 wt%. The release of tamixofen from NPs exhibited linear release profile with a release of 50% over 3 days and 94% over 5 days. Positively charged PMeOx-PDMS-PMeOx copolymers (terminated with piperazine) encapsulating a hydrophobically modified Rhodamine B (H-RhB; $LC = 0.5$ wt%; $D_h < 40$ nm, PDI < 0.1) exhibited strong binding and uptake into HeLa cells, whereas micelles assembled from neutral or negatively charged copolymers showed negligible uptake even after extended incubation time (Fig. 55B). This emphasizes a possible important role even of small functional groups in polymer-cell interactions. A hydrophobically-modified zinc(II) phthalocyanine (H-Zn(II)PC) encapsulated into the polymeric micelles ($D_h < 80$ nm; strongly dependent on the polymer used) for near-infrared (NIR) photodynamic therapy (PDT) exhibited similar cell binding characteristics (@ 1.0 wt%) as H-RhB loaded micelles (Fig. 55C). The positively charged, phthalocyanine-loaded copolymer micelles exhibited dose-dependent cytotoxicity in HeLa cells after light exposure (cell viability = 23% (70%) at c[Zn] = 8.25 μM (0.825 μM)). In contrast, no effect on cell viability was observed after treatment with micelles assembled from neutral, or negatively charged copolymers. Important to note, the piperazine terminated polymer slightly reduced cell viability (approx. 80%) even without illumination independent of the incorporated Zn concentration which is not expected at such low concentration.

Zhang and co-workers reported on POx bottle-brush brushes from cellulose nanocrystals (CNC), which were used to electrostatically complex indocyanine green [292]. In a first step, P*i*POx was grafted from CNC via SIPGP, which can be considered a polymer brush on the CNC. In a secondary reaction, the P*i*POx brushes were used as a multi-initiator for the LCROP of MeOx or *n*PrOx, respectively. The resulting bottle-brush brushes were terminated with piperidine to yield (P*i*POx-*g*-PMeOx)-*g*-CNC and (P*i*POx-*g*-P*n*PrOx)-*g*-CNC. These piperidine units, present in high density along and inside the bottle brush were employed to complex ICG via electrostatic interactions. Cell viability (HeLa) was tested at very low concentrations (≤25 mg/L) in the presence and absence of irradiation at 808 nm (2.0 W cm^{-2}, 10 min). Interestingly, even though cell viability remained above 80%, the presented data suggests a concentration dependent reduction in cell viability even in the absence of irradiation. However, with irradiation, the cytotoxicity was markedly increased and the authors argue that the dye is stabilized within the polymer brushes, which would help with the efficacy of the photothermal therapy.

Polymeric nanoplatforms are currently under investigation as integrated theranostic vehicles, for example in cancer diagnostics and therapy. In this context, Lin et al. [293] investigated unimolecular micelles formed by 21-arm star-like polymers based on β-cyclodextrin-[PLA-*b*-poly(2-(dimethylamino)ethylmethacrylate)-POEtOxMA]$_{21}$ (β-CD-(PLA-*b*-PDMAEMA-*b*-PEtOxMA)$_{21}$ ($R_h < 30$ nm; no aggregation after 1 month storage in aqueous

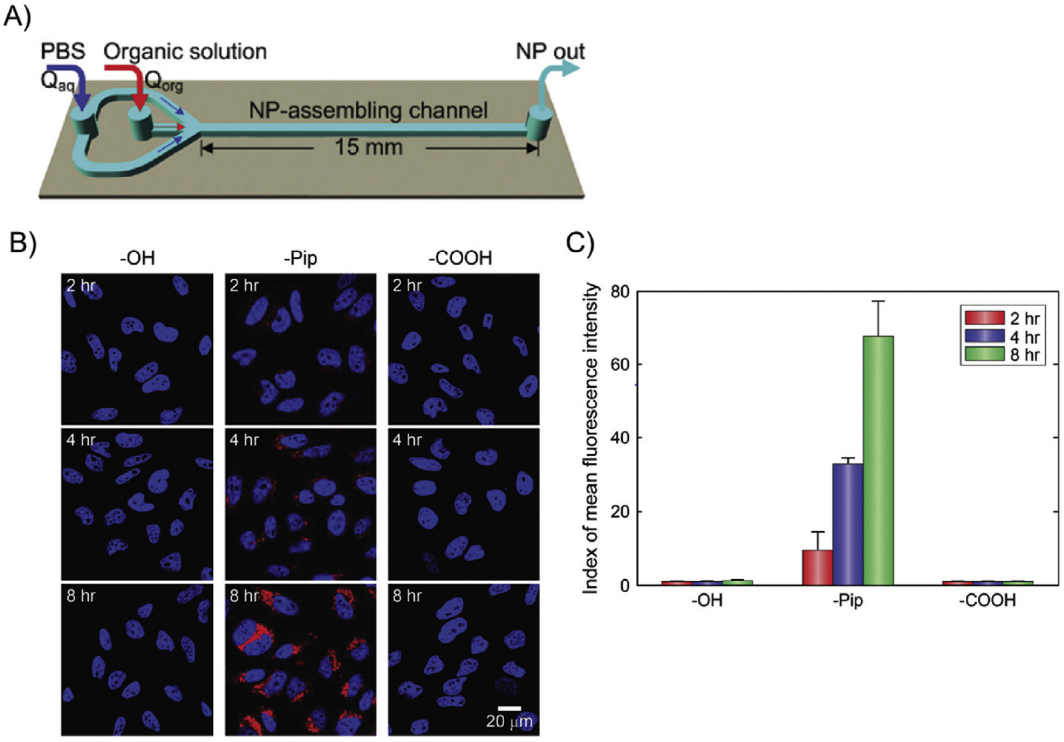

Fig. 55. A) Topology of microchannels and fluidic interfacing utilized for nanoparticle (NP) fabrication. An organic solvent/polymer solution is hydrodynamically focused in the NP-assembling channel by aqueous solution in a sheath flow configuration; B) Laser scanning confocal micrographs of HeLa cells cultured with H-RhB (0.5 wt%) encapsulated in NPs with neutral (-OH), positively (-Pip) and negatively charged (-COOH) end groups after 2, 4, 8 h of incubation; C) FACS measurement of HeLa cells cultured with H-Zn(II)PC (1.0 wt %)-loaded NPs with different termini. The mean fluorescence intensity was normalized to control. Copolymer concentration in organic solution for assembly was 100 g/L in all cases. Reprinted with permission from ref. [291]. Copyright 2015 The Royal Society of Chemistry.

media) for the *in situ* formation of gold nanoparticles (Au-NPs) and the subsequent encapsulation of doxorubicin (DOX; $LC \leq 22$ wt%; $LE = 59\%$; $D_h \approx 40$ nm). According to dissipative particle dynamics (DPD) simulation, DOX was mainly distributed in the PDMAEMA mesosphere at low drug concentrations, whereas at higher concentrations, DOX would integrate into the PLA core. Notably, the PDMAEMA mesosphere served as both, reducing agent (no external reducing agent needed) and stabilizer to ensure the *in situ* reduction of the precursor $AuCl_4^-$. The protonation of the tertiary amine group of PDMAEMA (leading to swelling of the micelles) and DOX (increasing its solubility) along with degradation of the PLA core resulted in rapid DOX release at pH = 5 (88% after 102 h), whereas at pH = 7.4, only 18% were released in the same time frame. HepG2 human liver cancer treated with Au-NPs loaded nanoparticles showed a higher CT contrast enhancement compared to Omnipaque at the same concentrations *in vitro* and *in vivo*. The authors claim that CLSM analysis showed strong DOX fluorescence in the cytoplasm of HepG2 cells *in vitro* after 4 h treatment with formulated DOX, whereas free DOX showed strong fluorescence in the nucleus, however, the provided images do not support such claim. *In vitro*, an IC_{50} value (HepG2 cells) of the DOX loaded nanoparticles after 24 h incubation was determined at 4.34 mg/L, essentially identical to that of free DOX ($IC_{50,\ free\ DOX} = 2.72$ mg/L). After 18 days post injection of β-CD-(PLA-PDMAEMA-PEtOxMA)$_{21}$/Au/DOX (2 doses of 4 mg/kg once every 3 days) or free-DOX in a NOD scid mice model of HepG2, tumor weights were lower than compared to non-DOX treated groups with tumor inhibition rate (TIR) values of 39% (free-DOX: 53%) (Fig. 56). However, a slightly stronger decrease in the tumor volume was achieved with free-DOX compared to formulated one. Unfortunately, no survival data was provided.

Quantum dots (QDs) are highly fluorescent and stable probes for cellular and molecular imaging. However, poor intracellular delivery, stability and toxicity of QDs *in vivo* hamper their use in cellular imaging. To overcome these limitations, Camblin et al.

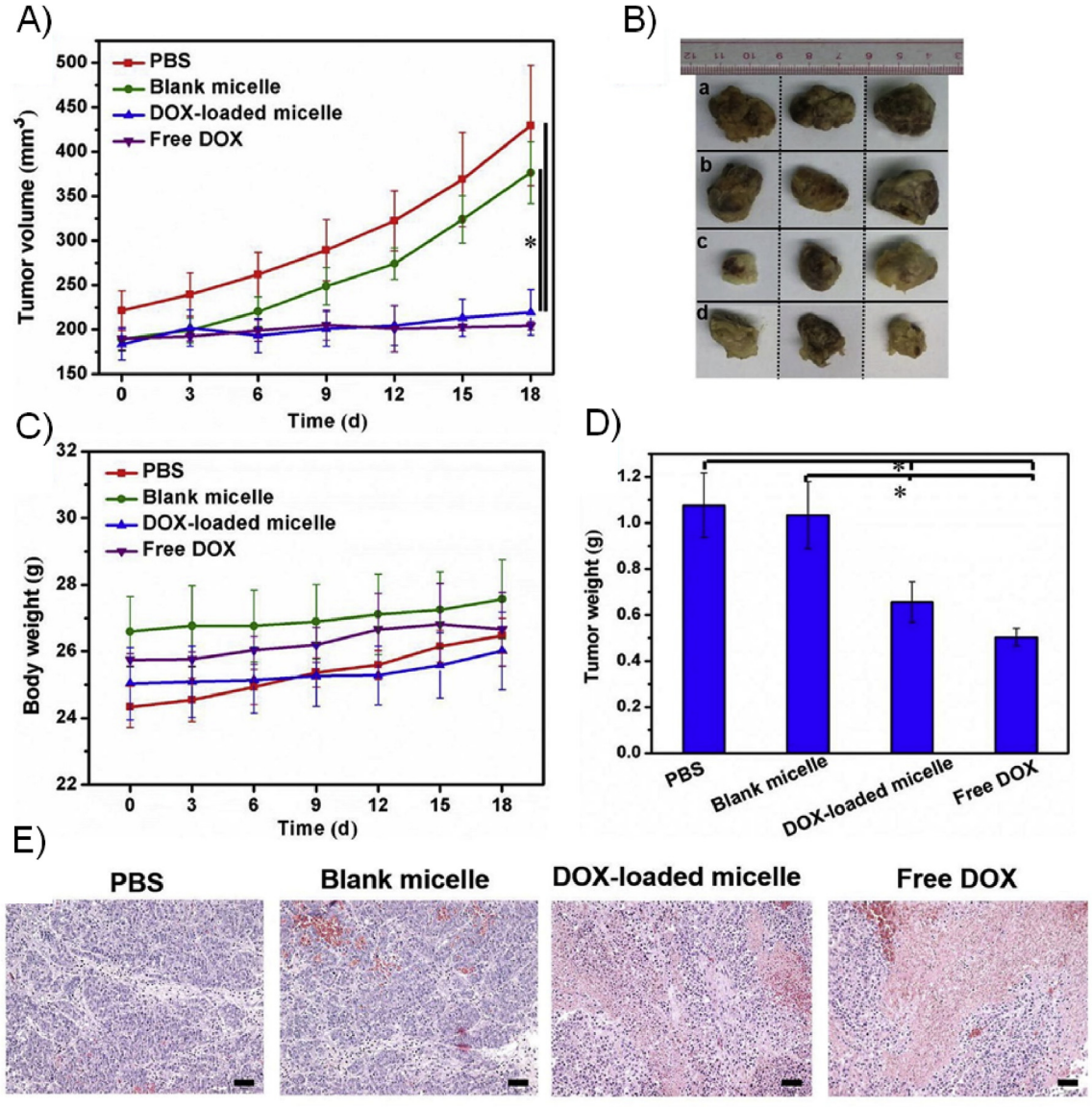

Fig. 56. *In vivo* anticancer activity in HepG2 tumor models generated by subcutaneous injection of HepG2 cells in NOD-scid mouse models. (A) Changes in tumor volumes as a function of time (n = 3). (B) Images of tumors of each group treated with PBS (a), β-CD-(PLA-PDMAEMA-PEtOxMA)$_{21}$ blank micelles (b), β-CD-(PLA-PDMAEMA-PEtOxMA)$_{21}$/Au/DOX (c), and free DOX (d) on day 18 (n = 3). (C) Body weights as a function of time (n = 3). (D) Tumor weights on day 18. (E) Representative histologic images of tumor tissue sections on day 18 (scale bar, 50 μm, n = 3). *p < 0.05. Reprinted with permission from ref. [293]. Copyright 2017 Elsevier.

[294] encapsulated QDs into the aqueous compartment of polymersomes composed of PDMS-*b*-PMeOx diblock copolymers ($D_h = 223$ nm; stable over a period of 6 weeks @ pH = 7.4). The initially low loading capacity (four QDs/polymersomes) could be doubled by introduction of 5% amine groups to generate charges in the copolymer. The low uptake in HepG2 cells between 1 h and 7 h is in line with stealth properties of PMeOx, reducing cellular interactions of polymersomes. However, after prolonged incubation of 24 h, efficient intracellular delivery in human liver carcinoma HepG2 cells was visualized by CLSM (no cellular toxicity after 24 h; ρ(polymersomes) $\leq$ 0.3 g/L).

In 2012, Pánek et al. [295] incorporated P(*i*PrOx-*co*-*n*BuOx) copolymers into micelles of Pluronic F127 (F127) by mixing both polymers below their cloud point temperature (T_{CP}) in aqueous media to prevent phase separation and slowly increasing the temperature above the T_{CP}. Incorporation of small quantities of ButEnOx enabled introduction of phenolic moieties via thiol-ene reaction and subsequent radionuclide labeling with ^{125}I (ca. 70% radiochemical yield; radiochemical stability was 97% and 91% after 3 and 24 h, respectively) as radioimaging tool for solid tumor diagnostics. Interestingly, not only radiolabeling had negligible effects on particle size, but also the size of pure F127 ($D_h = 19$ nm) differed only marginally from that of the POx/F127 system. At polymer concentrations and temperatures where no micelles should be formed, ITC revealed exothermic interactions between F127 and the POx which gave a hint towards specific interactions between both surfactants. It would be interesting to explore this further.

7. Protein and gene complexes

Polyion complexes of nucleic acids and proteins with cationic polymers of various architectures have been studied extensively for the delivery of the nucleic acids and proteins *in vitro* and *in vivo* [296–299]. Such complexes are known as “polyplexes”, a term first applied for the complexes entrapping DNA and then extended to complexes of various other charged biopolymers [300]. In recent studies, as described below, POx polymers have attracted increasing attention as gene delivery carriers for delivery of DNA and siRNA. Most typically, negatively charged biopolymers are to be complexed with cationic polymers, one of the most common being poly(ethylene imine) PEI, which typically comes in two versions, linear and branched, and, of course different molar mass. Linear PEI is unfailingly a POx derivative, as it is synthesized by exhaustive hydrolysis of POx [301]. Branched PEI, in contrast, is obtained *via* cationic ring opening polymerization of aziridine. It has been known for some time that partially hydrolyzed POx exhibits, depending on the degree of hydrolysis, much less cytotoxicity then PEI. This issue has been revisited in several contributions in recent years (*vide supra*). However, one can also find reports on protein complexed in amphiphilic POx, which exhibited increased enzymatic activity in water and also higher enzymatic activity in organic solvents [108,302].

7.1. Partially hydrolyzed POx polymers

As mentioned, PEI is one of the most well-known and successful polycations used in transfection of cells [303]. Due to its high charge density, ability to condense DNA and small interfering RNA at physiological pH, and proton-buffering effect, PEI is one of the most common standards of synthetic gene delivery vectors available to date. A commercial cell transfection reagent used in hundreds of laboratories across the globe is called ExGen 500, which is one representative of linear PEI [304]. The well-known shortcomings of PEI include its relatively high toxicity, which severely hampers applications of PEI *in vivo*. Linear PEI is synthesized by acidic hydrolysis of POx, in particular of PMeOx or PEtOx [305]. The acid hydrolysis cleaves the peptide bond and thus, the side chain from the POx backbone, and in the case of incomplete hydrolysis transforms POx into a more or less random copolymer of non-ionic 2-oxazoline units and cationic ethylene imine units. This opens an opportunity of using incomplete hydrolysis of POx to lower the charge density of PEI to mitigate its toxicity while retaining its high transfection activity. This has been explored for some years by several groups as discussed in the first chapter of this review.

Fernandes et al. [46] synthesized a series of cationic P(EtOx-*co*-EI) copolymers by partial acid hydrolysis (30%, 70%, and 96%) of 10 kg/mol PEtOx. They produced polyplexes by mixing the copolymers with plasmid DNA and siRNA and evaluated the relationships between the copolymer structure and the polyplexes size, zeta-potential, transfection activity or gene knockdown and cytotoxicity in cell culture. The copolymer with the lowest degree of hydrolysis, P(EtOx$_{0.70}$-*co*-EI$_{0.30}$) (i.e. with the excess of non-charged EtOx repeating units) produced negatively charged polyplexes upon mixing with the DNA with the particle sizes strongly depending on the N/P ratios (varied from 1 to 100). Such polyplexes were relatively safe to cells but also displayed low transfection activity. The copolymers with higher degrees of hydrolysis, P(EtOx$_{0.30}$-*co*-EI$_{0.70}$) and P(EtOx$_{0.04}$-*co*-EI$_{0.96}$), condensed the DNA and formed polyplexes with the particles sizes of over 400 nm, which tended to aggregate at most tested N/P ratios. These polyplexes at N/P ratios 50 and 100 displayed high transfection activity in Hela cells, which was comparable with or exceeded that of a commercial cationic lipid transfection agent, Lipofectamine™. The ability of P(EtOx-*co*-EI) copolymers to deliver siRNA and knockdown a Sjögren syndrome antigen (SSB) gene in the Hela cells appeared to increase as the degree of the copolymer hydrolysis increased: P(EtOx$_{0.70}$-*co*-EI$_{0.30}$) < P(EtOx$_{0.30}$-*co*-EI$_{0.70}$) <P(EtOx$_{0.04}$-*co*-EI$_{0.96}$). However, the copolymer with the highest degree of hydrolysis, P(EtOx$_{0.04}$-*co*-EI$_{0.96}$), was also the most cytotoxic. The copolymer with the intermediate charge density, P(EtOx$_{0.30}$-co-EI$_{0.70}$), was relatively less toxic and therefore appeared to be more promising for nucleic acids into cells.

Ivanova et al. [306] reported the synthesis and characterization of polyplexes based on the partially hydrolyzed P*n*PrOx, P(*n*PrOx-*co*-EI) with only about 9% of ethylene imine repeating units. Due to the presence of the propyl moiety, P(nPrOx-co-EI) is more hydrophobic than P(EtOx-co-EI) and exhibits a lower critical solution temperature (LCST) around 30 °C. The polyplexes were prepared by mixing this copolymer with the DNA at N/P ratio of 4, at 65 °C. Under these conditions, stable polyplexes were formed with the average particle hydrodynamic diameter of about 180 nm. However, as the temperature decreased to 30 °C the polyplexes rapidly aggregated. To improve the stability, these polyplexes were coated with a cross-linked polymeric shell formed by seeded radical copolymerization of NIPAAm and *N*,*N*-methylenbisacrylamide as a cross-linker. The thickness of the resulting shell was about 30 nm as estimated based on the differences of the polyplex particle size after and before polymerization of NIPAM. The P(nPrOx-co-EI) copolymer and the polyplexes exhibited lower toxicity when compared to regular PEI, and produced relatively safe polyplexes. The PNIPAAm shell further slightly reduced the toxicity of the polyplexes but also reduced the transfection efficacy in HEK 293 and REH cells. Nevertheless, the transfection activity was about 65% of the activity of the regular PEI-based polyplex suggesting some potential of the proposed approach for successful DNA delivery into cells.

As a follow up to this study, Mees et al. [307] prepared a series of P(nPrOx-co-EI) copolymers with different content of EI units ranging from 3% to 65%. Consistent with the previous study, these copolymers were thermo-sensitive in aqueous media and displayed different cloud point temperatures (T_{CP}), forming well-defined nanoparticles (mesoglobules) with nPrOx enriched core and EI enriched shell. The T_{CP} increased with increasing EI content, from 24 °C observed for non-hydrolyzed PnPrOx to 50 °C for P($nPrOx_{0.35}$-co-$EI_{0.65}$). As recently reported by the same group, the mesoglobules typically range in size from about 200 to 500 nm, depending on the degree of the hydrolysis and the preparation protocol as confirmed by dynamic light scattering (DLS) [308]. Generally, smaller mesoglobules were formed from the polymers with the higher degree of hydrolysis through an abrupt heating regime. The mesoglobules formed at the elevated temperatures were used for DNA complexation to prepare polyplexes [307]. To minimize the toxicity of the resulting polyplexes the study focused on P(nPrOx-co-EI) copolymers with relatively low EI content of about 5–10% and varied the degrees of polymerization from 75 to 200. Again, polyplexes were formed by mixing the copolymers with plasmid DNA at 65 °C at varying N/P ratios from 1 to 10 followed by cooling the solution down to 24 °C. For all tested copolymers the temperature/size correlations were similar - the smallest particles of about 100 nm were formed at 65 °C while upon cooling at 25 °C and 37 °C the particles aggregated to above a micron-size range. The only exception was stoichiometric condition N/P = 1 where the temperature induced aggregation was attenuated. Interestingly at N/P = 1 the polyplexes had a strong negative zeta-potential, presumably due to exposure of the DNA chains at the particle surface with the uncomplexed cationic ethyleneimine moieties being trapped inside and spatially inaccessible to DNA. As the N/P ratio increased the zeta potential became positive suggesting exposure of the excess of EI units at the polyplex surface. Based on this, aggregation at 25 °C and 37 °C may involve swelling of the PnPrOx segments of P(nPrOx-co-EI) followed by inter-particle polyion interchange where the DNA molecules interconnect multiple polyplex species together in aggregates. At N/P = 1 the swelling of the PPrOx segments should also occur but the inter-particle polyion interchange is slowed down by electrostatic repulsion of DNA since there are no excess cationic moieties available to cross-link the DNA. To stabilize the polyplexes at N/P > 1, they were coated with cross-linked PNIPAAm shell as described above. Not surprisingly, the uncoated cationic polyplexes were quite toxic in cell cultures resulting in decrease of cell viability well below 80% in most cases. Although the cytotoxicity of the resulting polyplexes in cells was decreased compared to regular PEI/DNA complexes, the reported values of cell viability suggested that even the coated polyplexes could be used for cell transfection at the lowest concentrations only. Unfortunately, no transfection data was reported in this or subsequent study [308].

It has been well known that the architecture of polymers is critical for many of its properties. Accordingly, many studies have compared linear and branched PEI. In a very interesting work, Grayson recently compared cyclic and linear PEI [309]. Even though these do not contained POx anymore, this contribution shall briefly be discussed. Most interestingly, it is reported that the cyclic PEI show higher transfection efficiencies compared to the linear ones, especially at higher degrees of polymerization (70 and 84). More importantly, the cytotoxicity was found to be equivalent or lower as compared to the linear polymers. Obviously, it would be interesting to compare partially hydrolyzed cyclic and linear POx. Combination of both concepts may well produce polyplexes with good cytocompatibility and good transfection efficiency.

7.2. Random and block copolymers of cationic and non-ionic POx

Apart from hydrolysis, cationic POx can also be obtained by copolymerization if a functional monomer, which is either a protected amine [310] or can be transformed into an amine. Accordingly, Rinkenauer et al. [311] described random copolymers containing cationic and non-ionic 2-oxazoline repeating units as transfection agents. To identify the “best” cationic POx structure, having high transfection activity and low toxicity the authors used 18-member library of POx-based copolymers. Structurally, this library represented random copolymers of MeOx with one of the alkene containing 2-oxazolines, namely DecEnOx or ButEnOx. Subsequent functionalization of the alkene side groups by thiol-ene photo-addition yielded cationic copolymers with either primary or tertiary amine groups and amine content ranging from 10 to 40%, with respect to the total number of repeating units. The study evaluated the influence of 1) the polymer side chain hydrophobicity and 2) the type and content of amino groups on the copolymer ability to form polyplexes with plasmid DNA as well as the stability, toxicity, and transfection efficacy of these polyplexes. The copolymers containing primary amines displayed ability to condense the plasmid DNA and produce stable polyplexes, while the copolymers with the tertiary amines were binding DNA weakly and releasing it prematurely. As the amine content in the copolymers increased, the transfection activity also increased, which, however, came at a cost of increased toxicity. The cutoff point was about 40% of amines, which was needed for successful transfection. While the copolymers with short butenyl side chains having up to 40% of amino groups were relatively safe to cells, the copolymers with long hydrophobic decenyl side chains displayed higher toxicity. Overall, copolymers containing short butenyl side chains and 40% content of primary amines were found superior for formation of polyplexes of DNA with these particular copolymers, were internalized in cells faster than others, and displayed superior transfection and little toxicity when compared to PEI-based polyplex.

Gene delivery can also be combined with chemotherapy. In this regard, the co-administration of minicircle DNA (mcDNA) and various chemotherapeutics has been investigated. PEI is one of the most efficient gene delivery carrier and also known for its endosomal/lysosomal escape property. Gaspar and co-workers [312] reported for the first time the co-delivery of mcDNA and DOX. The carrier was PEtOx-*b*-PLA conjugated to PEI by carbonyldiimidazole mediated coupling of PLA and PEI to yield PEtOx-*b*-PLA-*g*-PEI (PPP). As is the case for other types of DNA, mcDNA is sensitive to serum nucleases and exhibits poor cell penetration due to its negative charge. Therefore, the positively charged graft blockcopolymer was used as carrier for mcDNA and DOX to increase intracellular delivery and to prevent mcDNA degradation. PPP based polyplexes with various N/P ratios (N/P = 12, 14, 16, 30) showed negligible hemolysis (<1%) and the polymers were non-cytotoxic against MCF-7 breast cancer cells and normal human skin fibroblasts up to polymer concentrations of 1 g/L upon 72 h incubation. DOX was loaded into the hydrophobic PLA core (*LC* = 3.6 wt%) followed by complexation of mcDNA (N/P ratio ≥ 12 necessary for complexation). DLS measurements showed an increase in size from D_h = 140 nm (N/P = 30) to D_h = 280 nm (N/P = 12) dependent on the N/P ratio. DOX-mcDNA loaded polyplexes with a N/P value of 30 showed a higher cellular uptake and gene expression (green fluorescent protein, GFP). MFI of DOX was 45 for neat DOX, 190 for DOX micelles and 95 for DOX-mcDNA micelles. Both, single- and co-loaded formulations were less toxic (IC_{50} = 52 μM and 69 μM for single and co-formulations, respectively) than neat DOX (IC_{50} = 7 μM). Further investigations on 3D MCF-7 cell spheroids confirmed mcDNA mediated GFP expression and showed the

deeper penetration and better distribution of polyplexes throughout the spheroids. The homogeneous distribution was confirmed by quantitative analysis of GFP which was found maximal for N/P 30 formulations. *In vivo* assays on orthotopic 4T1 breast cancer tumor models in mice revealed intense GFP expression which was confirmed by *ex vivo* fluorescence imaging. Important to note, negligible fluorescence was observed in liver and lungs.

In a follow up study, Gaspar and co-workers [47] synthesized bioreducible PEI (PEI-SS) by Michael-type addition chemistry between PEI and *N*′,*N*′-cystamine bisacrylamide (CBA). PEI-SS was further conjugated to PEtOx-PLA for the co-delivery of mcDNA and DOX ($LC = 7$ wt%). The addition of disulfide linkers rendered the system bioreducible. Therefore, common overexpression of redox enzymes and/or glutathione in the tumor microenvironment could lead to triggered release of mcDNA and DOX. In this case complexation of mcDNA was also observed at N/P ratios of 8 and 10. The modified polymers with N/P ratios of 20, 22, 24 and 30 showed no cytotoxicity (cell viability > 90%) against HeLa cells and B16F10 cell line upon 48 h incubation. Unfortunately, no concentration for this assay was provided. When exposed to disulfide reducing conditions, the stimuli responsive complexes showed a 7.2 fold higher release of mcDNA. Furthermore, the bioreducible complexes (N/P ratio 20) exhibited a higher GFP expression (2.7 fold in HeLa cells; 1.9 fold in B16F10 melanoma cells) as compared to positive control and non-bioreducible formulations. Dual loaded formulations showed higher DOX fluorescence as compared to free DOX and their non-bioreducible counterparts. Cytotoxic activity on B16F10 cell line showed the IC_{50} values of 129 μM and 258 μM for dual and single loaded DOX formulation respectively. *In vitro* and *in vivo* studies revealed prolonged gene expression up to 8 days. In both studies intratumoral delivery was achieved by local injection. Unfortunately, the formulations were not further evaluated for IV administration with respect to non-specific release of DOX or mcDNA in the circulation or in healthy cells.

The use of cationic block or graft copolymers with a hydrophilic non-ionic block or grafted chains allows producing micelle-like core-shell polyplexes with a polycation/nucleic acid complex core and a non-ionic hydrophilic shell [313]. Most of the earliest studies in this field used PEG as hydrophilic shell-forming block due to its biocompatibility and widespread use in pharmaceutics. As the concerns about stability, toxicity and immune response of PEG emerged [28] replacing PEG with the hydrophilic POx became an area of active research.

As a successful alternative to PEI or other polycations such as PLL, the use of PAsA modified with diethylenetriamine (DET) (PAsA(DET)) in PEG-based cationic copolymers PEG-b-PAsA(DET) has been reported to decrease the cytotoxicity and improve the transfection [314]. Witzigmann et al. [315] extended this approach and exchanged the PEG block to a PMeOx block. The reported block copolymers formed stable DNA polyplexes at N/P ratios above 2. The morphology of the polyplexes was dependent on the N/P ratio. The polyplexes formed at N/P of 20 represented worm-like structures while at higher N/P ratios the particles became spherical. The transfection efficiency of the polyplexes was evaluated in two cell lines, HeLa and HEK293 increased as the N/P increased. Interestingly, even at the highest tested N/P ratio of 300 the zeta-potential of the polyplexes was reported slightly negative which seems quite unusual. Nevertheless, the transfection at this N/P ratio was the highest of all other ratios and comparable to that of DNA/PEI polyplexes. Furthermore, the PMeOx-b-PAsA(DET) based polyplexes were significantly less toxic in both cell lines when compared to DNA/PEI.

He et al. [316] synthesized cationic block copolymer having two POx blocks: 1) a non-ionic PMeOx and 2) POx polycation based on a new 2-oxazoline monomer, 2-(*N*-methyl, *N*-Boc amino)-methyl-2-oxazoline (BocMAMeOx). The living polymerization was initiated using propargyl tosylate in order to incorporate a functional alkyne group at the hydrophilic non-ionic PMeOx block end for consecutive "click" chemistry reactions. After deprotection of the amine groups, the copolymer was evaluated for its ability to form complexes with plasmid DNA, interact with serum and transfect B16 murine melanoma cells. The resulting polyplexes were compared to traditional polyplexes prepared using PEG-*b*-PLL block copolymers. Upon mixing the plasmid DNA and PMeOx-b-PMAMeOx, 80 nm polyplex particles were observed. These polyplexes were stable and exhibited very low protein binding and cytotoxicity, when compared to DNA/PEG-b-PLL polyplexes. Their cell uptake was time dependent with the maximal uptake and transfection observed after 10 h of incubation with DNA/PMeOx-*b*-PMAMeOx. However, the transfection activity was lower even when compared to DNA/PEG-b-PLL known for pretty low transfection activity. However, it is argued in this contribution that low transfection of untargeted cells may be an advantage for vectorized delivery of DNA/PMeOx-*b*-PMAMeOx to target cells while minimizing interaction with and transfection of non-targeted cells. However, this possibility was not evaluated in this report.

Lehner et al. [317] reported on diblock copolymers having PMeOx non-ionic block and a functional poly(2-(4-azidobutyl)-oxazoline) (PABOx) block that was derivatized with primary or tertiary amines yielding PMeOx-*b*-PABOx—PA and PMeOx-*b*-PABOx—TA, respectively. Polyplexes formed by these copolymers with plasmid DNA were examined by TEM and AFM. The PMeOx-*b*-PABOx—PA/DNA polyplexes represented condensed flowerlike structures that revealed a tendency for aggregation. In contrast, PMeOx-*b*-PABOx—TA/DNA mixtures showed little if any condensation when compared to the naked plasmid DNA. The polyplexes were further evaluated in HeLa and HEK293T cells. Both copolymers exhibited low toxicity, which was consistent with the other reports for PMeOx-based cationic copolymers as described in this section. The condensed PMeOx-*b*-PABOx—PA/DNA at N/P ratio of 40 displayed relatively high transfection, albeit vastly inferior to that of the PEI/DNA complexes. The PMeOx-*b*-PABOx—TA/DNA mixtures that did not show DNA condensation, were practically inactive in cell transfection.

7.3. POx-based amphiphilic cationic copolymers

Amphiphilic cationic block copolymers combining cationic blocks, nonionic water-soluble blocks, and non-ionic hydrophobic blocks, such as PEI modified by amphiphilic non-ionic Pluronic triblock copolymers have been previously used to produce efficient cell transfection systems [318]. Such multifunctional block copolymers are capable of reacting with nucleic acids forming polyion complex domains, self-assembling due to segregation of hydrophobic chains and still keeping the polyplexes dispersed due to the effect of nonionic water-soluble chains forming a stabilizing corona. In addition to hydrophobic domain formation the hydrophobic chains in such polyplexes, depending on their chemical structure, can interact with cell membranes and thus, in some cases, facilitate gene delivery into cells. Osawa et al. [319] synthesized triblock copolymers consisting of hydrophilic/amphiphilic PEtOx, thermoresponsive and amphiphilic P*n*PrOx, and cationic PLL (PEtOx-*b*-P*n*PrOx-*b*-PLL) and evaluated their polyplexes with plasmid DNA. The thermo-switchable nature of the hydrophobic PnPrOx block allowed preparing polyplex micelles with uniform sizes and well-defined structures. This was achieved by polyion complexation of the copolymer and DNA below the LCST when the P*n*PrOx chains were soluble and then increasing the temperature

above the LCST inducing collapse and aggregation of these domains. The aggregated P*n*PrOx chains formed the protective layer around the DNA/PLL polyion complex core, further surrounded by PEtOx. The polyplexes had a rod-like shape with the rod length being dependent on the temperature and were stable in the presence of chondroitin sulfate. Upon incorporation into these polyplexes, DNA was shown to be protected against DNase I, and displayed increased ability to internalize into and transfect the human hepatoma (Huh7) cells.

7.4. Nonionic POx copolymers for gene therapy

Non-ionic non-condensing amphiphilic block copolymers such as Pluronics have shown remarkable ability to increase the levels and duration of gene expression of naked DNA administered into muscle [320]. Therefore, evaluating nonionic POx block copolymers in such applications seems promising. Recently, Rasolonjatovo et al. [321] synthesized star shaped block copolymers with a hydrophobic PTHF central block and a PMeOx external block. A series of block copolymers with varying PTHF/PMeOx ratios (25:75, 40:60 and 67:33) and molar masses of 2.7, 2.8 and 3.9 kg/mol were prepared. The copolymers were co-injected with the luciferase encoding plasmid DNA and the gene expression was measured seven days after the injections. Notably, there was a distinct increase in the gene expression when compared to the naked DNA injections, which was the most pronounced for the 2.8 kg/mol copolymer with 40:60 PTHF/PMeOx ratio at relatively low treatment concentrations (0.01% and 0.1% w/w) or the 2.7 kg/mol copolymer with 25:75 PTHF/PMeOx at 0.1% and 1% w/w. The levels of the transgene expression were comparable to those of the positive control, Lutrol 3%, while the administered dose was nearly half. Unfortunately, the authors did not provide any information as to which Lutrol was being used also the effect on gene expression is highly structure sensitive [322]. Judging from an earlier report [323], it stands to reason to assume that PEG_{75}-*b*-poly(propylene glycol)$_{30}$-*b*-PEG_{75} was used. Also, it would have been interesting to also see the effect of Lutrol control at different concentrations, as it is well known that the various and complex effects of Pluronics/Lutrol is highly concentration dependent and often decreases at higher concentration. For example, for Pluronic P85, the maximum effect of boosting gene expression in skeletal muscle was found between 0.1 and 1 wt% while SP1017, a mixture of L61 and F127 has a maximum at only 0.01 wt% [322].

8. POx at interfaces

In the past, POx at interfaces were investigated especially with regard to synthesis of POx on surfaces by *grafting from* [324], *grafting to* [325] or *grafting through* [326]. Applications of the derived surfaces were shown, e.g. in antifouling surfaces, but true advantages of the POx's versatility and functionality with regard to interfacial functionalization, i.e. mostly between solid and liquid phase, were not fully exploited. The progress in surface functionalization was reviewed by Tauhardt et al. [19] and more recently by Morgese and Benetti with respect to grafting techniques [20]. Besides the straightforward functionalization of POx, the similarity of POx to proteins (while still being distinct in some critical properties) is one of the most striking benefits for their application in any bio-related topic.

Weydert et al. used patterned Si surfaces to deposit poly(D-lysine) (PDL) as adhesive layer and poly(acrylamide)-*g*-PMeOx (PAAm-*g*-PMeOx) as non-adhesive layer for directed neuronal cell culture [327]. The authors could show that the fabricated patterns of POx resist outgrowth of the cells (Fig. 57) and outperform similar PEG based polymers. Further, the pattern's protein interactions and performance is not influenced by long term immersion in cell culture media, which enables their use as platform for controllable neuronal network topologies.

A comparable approach was used by Chen et al. in which FA was coupled to COOH functionalized PMeOx using EDC chemistry. Subsequently, FA-PMeOx was grafted to PLL applying EDC coupling [280]. It should be noted that the characterization data are ambiguous, since prior to functionalization of PLL with FA-PMeOx, the degree of functionalization is twice the theoretical value. Since D_2O as NMR solvent may induce micellization of the conjugates due to the low solubility of FA, NMR analysis may be problematic. After surface functionalization and characterization, FA-receptor bearing and deficient cells were demonstrated to exhibit adhesion depending on FA receptor on the modified surfaces. Adhesion experiments were carried out in standard cell culture medium and media with increased FA concentration. The authors could show a significant dependence of FA receptor dependent adhesion of cells, also from cell mixtures.

Several papers apply the variable LCST of the homologue series of POx. An et al. synthesized P*i*PrOx-*b*-poly(3-acrylamidopropyltrimethylammonium) (P*i*PrOx-*b*-PAAmTMA), which consists of a positively charged block for physisorption on Si surfaces, and a temperature responsive P*i*PrOx block [328]. The manufactured layers were analyzed thoroughly by QCM measurements with respect to temperature and pH. In subsequent temperature-dependent AFM measurements, force resistance curves were recorded to analyze the friction forces [329].

The group of Dworak used similar responsive POx (P*i*PrOx and P(EtOx-co-NonOx)), which were grafted to aminopropylsilanes (APS) on glass by direct termination of LCROP by the functionalized surface. The derived polymers were characterized for their T_{CP} and surfaces were characterized for contact angles at different temperatures to derive similar trends in responsiveness to temperature (POx thickness ranged from 5 to 11 nm) [330]. Subsequently, the thermal response of the surfaces could be used to detach whole cell sheets of dermal fibroblasts by exchange of environment from 37 °C to room temperature. No control experiment was conducted. Even though it may seem reasonable to assume non-responsive polymer would not lead to detachment, a control experiment would have been desirable. In a follow up study, previously observed fibrils in PiPrOx were characterized for a deeper understanding of this phenomenon [331]. P*i*PrOx fibrils were observed after *grafting-to* reactions that were carried out for longer reaction times (range within days) in relatively polar solvent (typically acetonitrile) at elevated temperatures. The fibrils could be annealed by heating, ultra-fast cooling cycles and it could be shown that cells (human dermal fibroblasts) adhered less on smoother layers with less fibrils and cell sheet detachment was enhanced as well. Tait et al. used the same approach to graft PMeOx, PEtOx, P*i*PrOx and PBuOx on APS glass slides [332]. The glass slides were characterized by the means of XPS and water contact angles and further used to culture 16HBE14o- and MRC5 cells. Unfortunately, no NMR data for residual POx in solution was provided, which would have helped with a better understanding of the resulting surfaces. Using contact angle, higher hydrophobicity of the surfaces was observed for more hydrophobic polymers (contact angle for PMeOx approx. 25°, for P*n*BuOx approx. 75°) and surfaces could be prepared reproducibly. The authors noted an unusual adhesion and proliferation on PMeOx surfaces (for HBE1614o-cells even higher than on P*n*BuOx surfaces), that have been consistently described antifouling in various publications. Unfortunately, no surface characterization by AFM was provided. The coverslips were left in acetonitrile overnight, which would probably cause the formation of fibrils in case of P*i*PrOx (also used here), as discussed before [331]. The formation of fibrils could be a reason for comparably high cell adhesion on these surfaces.

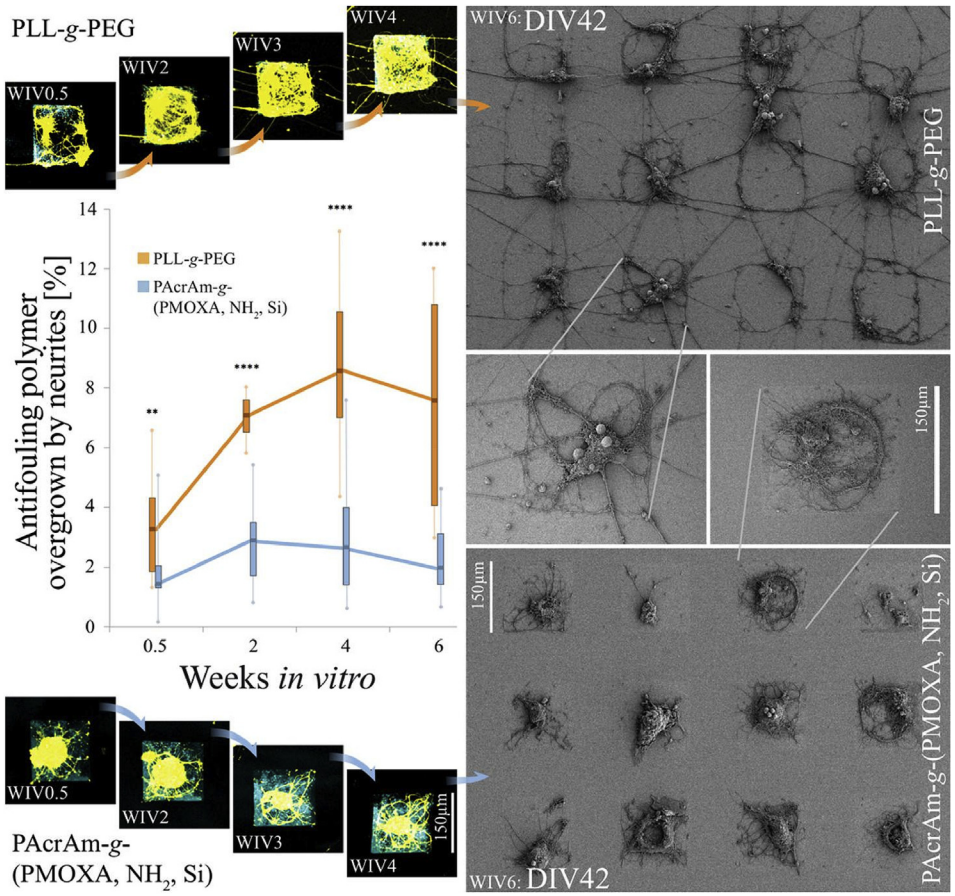

Fig. 57. Comparison of outgrowth of neurites from PDL layers into PLL-g-PEG (top) or PAAm-g-PMeOx (bottom) modified areas by fluorescence microscopy (left, yellow - neurons, cyan - PDL) and SEM (right). Diagram insert on the left shows the amount of overgrown (from one node to a neighboring one) nodes with time ($p < 0.05$ **, $p < 0.005$ ****). Reprinted with permission from Ref. [327]. Copyright (2017) American Chemical Society.

Kroning et al. grafted PMeOx, poly(2-cyclopropyl-2-oxazoline) and a respective copolymer via distal ester functionality to epoxide functionalized glass slides [333]. Infrared spectral ellipsometry was used to characterize the temperature-dependent hydration states, which is the first step towards understanding protein interaction. Such protein interactions were studied by Benetti and co-workers in another contribution. Telechelic PEtOx (α-propargyl, ω-azido) were functionalized with dopamine. The telechelic ends were designed to react intramolecularly via click chemistry to yield a cyclic polymer [334]. Subsequently, cyclic and linear polymers were grafted to TiO_2 surfaces via dopamine and protein adsorption (BSA, FN, IgG as well as from full human serum) was determined via ellipsometry. Force-distance and force-friction characteristics were evaluated by AFM. Most interestingly, cyclic PEtOx exhibited lowest friction coefficients and high repulsion, which was attributed to missing interdigitation of chain ends lacking in cyclic POx. Follow-up studies with linear, cyclic and looping polymer structures revealed a similar trend in adjustable friction coefficients between modified surfaces [335].

A comparable system based on PMeOx (grafted to poly(glutamic acid)) was grafted to cartilage via Schiff base to act as a low friction barrier on degraded cartilage (Fig. 58) [336]. The polymers were synthesized by a procedure that grafted amine-terminated PMeOx and *p*-hydroxybenzaldehyde (HBA) via DCC chemistry to poly(-glutamic acid). A large variety of polymer grafts was synthesized by variation of used PMeOx with respect to DP and PMeOx/HBA ratios. Using these grafts, films were prepared on APS-Si and cartilage via Schiff base formation. The films were characterized by their physical properties (thickness ranged from 0.7 to 1.5 nm in dry state) and subsequent protein (BSA) adsorption. BSA adsorption correlated with PMeOx content and chain length, i.e. higher PMeOx content led to lower protein adsorption. In tribological experiments, polymer grafts on degraded cartilage were compared to native and degraded cartilage using synovial fluid to retain physiological conditions. The coefficient of friction correlated with the amount of adsorbed BSA and was also dependent of the applied load. Most interestingly, coefficients of friction were even lower than those for native cartilage in most cases, which makes this system very interesting as replacement for damaged cartilage. Commercial scaffolds for cartilage regeneration, modified with the polymer grafts, triggered no inflammatory reaction when implanted into mice and no desorption was observed. A follow-up study reproduces protein adsorption experiments and tribological force-friction characterization, and adds data of the same system of AFM force-distance measurements as well as AFM scans to gain insight into the microstructure of the samples [337].

Another example of wide range of possible applications for POx was published by Meier and co-workers. Artificial solid-supported membranes were synthesized from PDMS-b-PMeOx block copolymers by reaction of aldehyde end-group with amino groups from APS-Si, APS-glass or aminoundecanethiol modified gold (NH_2-$(CH_2)_{11}$-S-Au) [338] The formed double layers were characterized thoroughly by AFM, ellipsometry (6.5 nm monolayer, 11.3 nm bilayer), contact angle measurement (80° for the monolayer) and IR

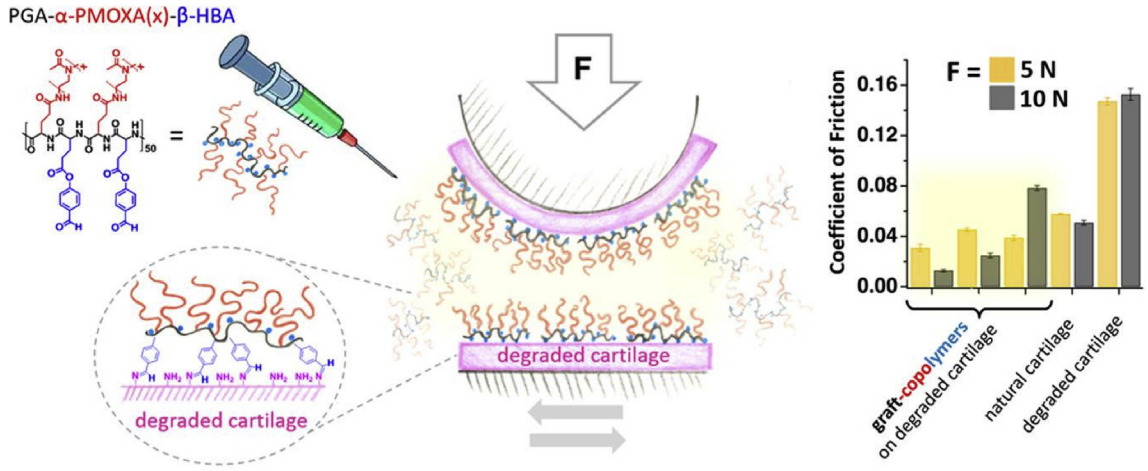

Fig. 58. Schematic representation of poly(glutamic acid)-*g*-PMeOx-*g*-(*p*-hydroxybenzaldehyde) (structure top left) for cartilage regeneration via Schiff base reaction (bottom left) to yield low friction (middle) cartilage replacements. The right side shows coefficients of friction dependent of different grafting densities of PMeOx compared to native and degraded cartilage. Reprinted with permission from Morgese et al. [336]. Copyright (2017) American Chemical Society.

spectroscopy. A bacteria derived membrane protein (potassium channel) could be inserted into the artificial membrane and was shown to maintain its function by conductance measurements. In a follow-up study, the group was able to synthesize free-standing membranes by addition of several lipids and characterize membrane protein insertion [339]. Model protein was once more a bacterial potassium channel, which inserted into the more fluid phase, which was depending on the used lipid.

In order to use the various functionalities of POx on surfaces, Wendler et al. introduced a new way of grafting POx to surfaces, applying maleimide tetrazole photo-ligation [340]. An azide functionalized PEtOx was synthesized and subsequently modified using azide-alkyne click chemistry to add a protected maleimide that could be deprotected by retro-Diels-Alder reaction at elevated temperatures. Subsequently, a tetrazole functionalized Si wafer was immersed in the polymer solution and illuminated to render it reactive towards the functionalized surface. While successful modification was proven by XPS, preceding polymer analogue reactions were found to have only low to good yields (22–73%) depending on DP of PEtOx.

Pan et al. were able to switch protein interactions of mixed PMeOx and PAA surfaces [341]. PMeOx and PAA were sequentially grafted to PDA coated Au substrates and characterized by various physical methods like ellipsometry or XPS. The wettability of the substrates changes with pH from slightly (50°–60° water contact angle) at pH = 5 to highly (below 20°) hydrophilic at pH = 9. This can be attributed to protonation of PAA in acidic conditions and subsequent collapse of PAA. Hence, adsorption of BSA could be controlled by adjustment of composition of the mixed modifications and pH of the surrounding solution.

Another highly application-focussed contribution was reported by the Schubert group. Similar to the hydrogel work by the same group, POx coatings of PP and glass were investigated for DNA isolation [342]. Based on an amine bearing (protected for LCROP) monomer, the authors prepared a functionalized surface by attaching 3-glycidyloxypropyl trimethoxysilane to glass or plasma activated PP. Subsequently, layer by layer (LbL) deposition of amine-bearing POx and epichlorohydrine was used to produce thick (>100 nm) functional POx layers. The robust system allows lysis of cells, cleaning (by washing off non-adhered fragments) and even qPCR amplification of surface bound DNA in one and the same laboratory PP microcentrifuge tube (Fig. 59).

8.1. Plasma polymerized 2-oxazolines

A polymerization method using 2-oxazolines that was recently introduced is plasma polymerization (PP). It is important to note and understand that PP differs very significantly from other polymerization technique for 2-oxazolines. An electromagnetic field (capacitive or inductive) is used to activate 2-oxazoline monomers that are transported into a vacuum chamber by a carrier gas flow. The resulting polymers are not chemically well defined and probably only vaguely resemble POx obtained by LCROP. Moreover, the parameters (plasma power, pressure, carrier gas flow, precursor feed and others) of this process greatly influence the properties of the resulting layers. The method emerged in early 2015 to yield plasma polymerized 2-oxazolines (ppOx) and was published almost simultaneously by the groups of Arefi-Khonsari [343] and Vasilev [344]. Bhatt et al. used an inductively excited pulsed PP of EtOx to generate ppEtOx layers with thickness between 20 and 140 nm in 20 min, dependent upon plasma power. Also depending on the duty-cycle of the plasma reactor, different amide I/amide II band ratios in IR spectra were observed. Differences depending on the duty-cycle were also found in XPS spectra and water contact angles (ranged between 25° and 50° after washing). The most striking difference was cell adhesion and proliferation of NIH:OVCAR-3 cells that was observed for low and high plasma powers (0.25 W and ≥5 W, respectively) but not intermediate plasma powers, independent of used carrier gas flow (Fig. 60).

Ramiasa et al. showed first PP of MeOx using a capacitively coupled plasma [345]. Used plasma powers were higher than before and the authors observed ppMeOx layers of around 80 nm after 5 min of deposition. The obtained films were characterized by XPS, IR, water contact angles (ranged between <20° and 60° depending on plasma power) as well as by QCM to show permanent protein binding. While fibroblasts and macrophages adhered well (same viability but lower IL-6 and TNF-a expression than on TCPS) on the surfaces, bacterial growth was hindered. Further, the group of Vasilev showed the potential of ppOx by changing the surface properties through easily adjustable plasma parameters, e.g. for surface modification to bind NPs or for good interaction with proteins. After deposition of ppMeOx, using different plasma powers, carboxylic acid functionalized Au-NPs were covalently bound to the surfaces [346]. The authors argue that the binding occurs via a reaction with preserved oxazoline ring structures on the surface. Deposition of the intact 2-oxazoline ring on the surface was also

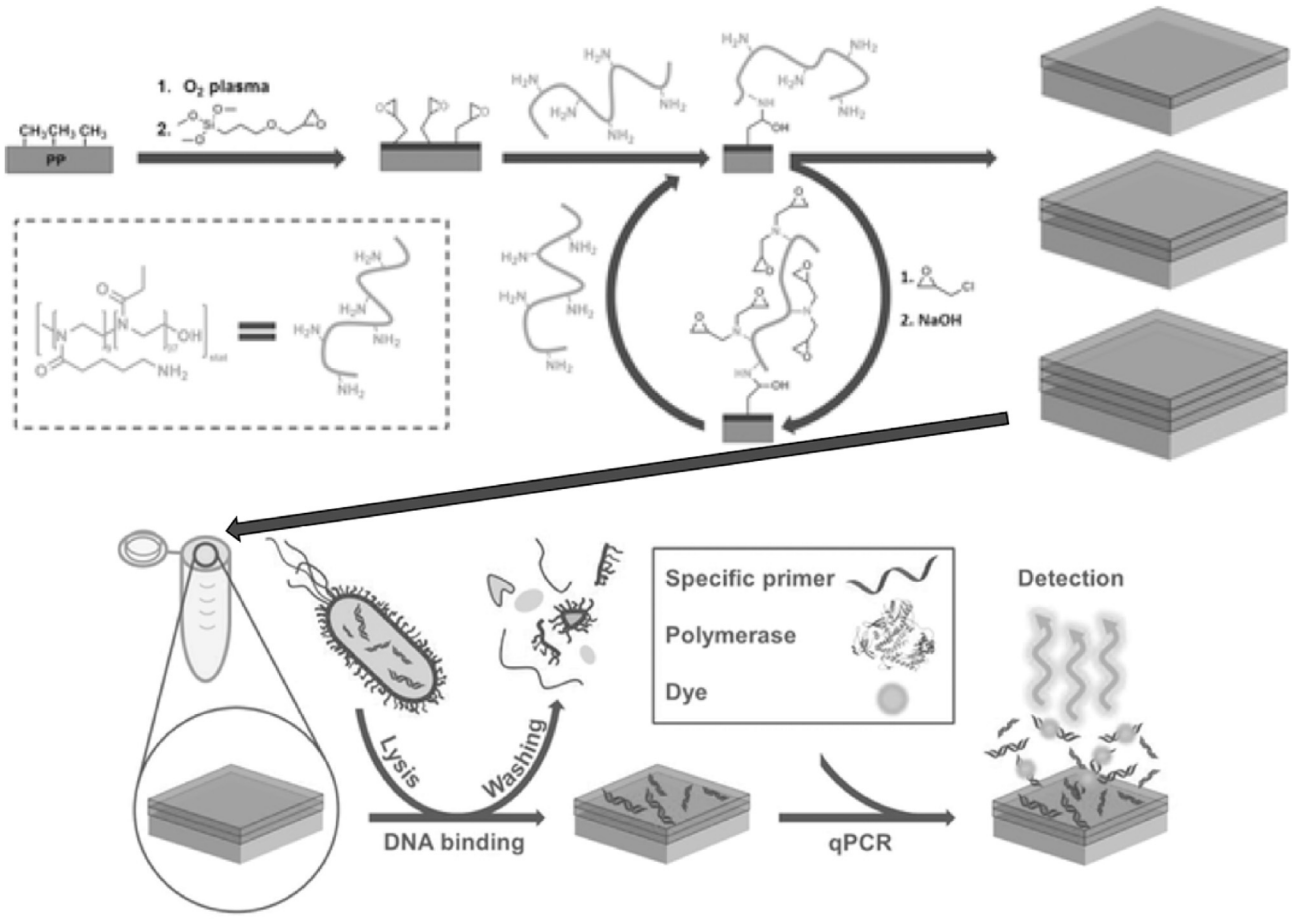

Fig. 59. Activation and functionalization of poly(propylene) by plasma and reaction 3-glycidyloxypropyl trimethoxysilane and subsequent LbL deposition of POx and epichlorohydrin (top). Use of manufactured surfaces for lysis, adhesion of DNA, washing and qPCR of adhered DNA in one tube (bottom). Adapted with permission from Ref. [342]. Copyright (2015) John Wiley & Sons, Inc.

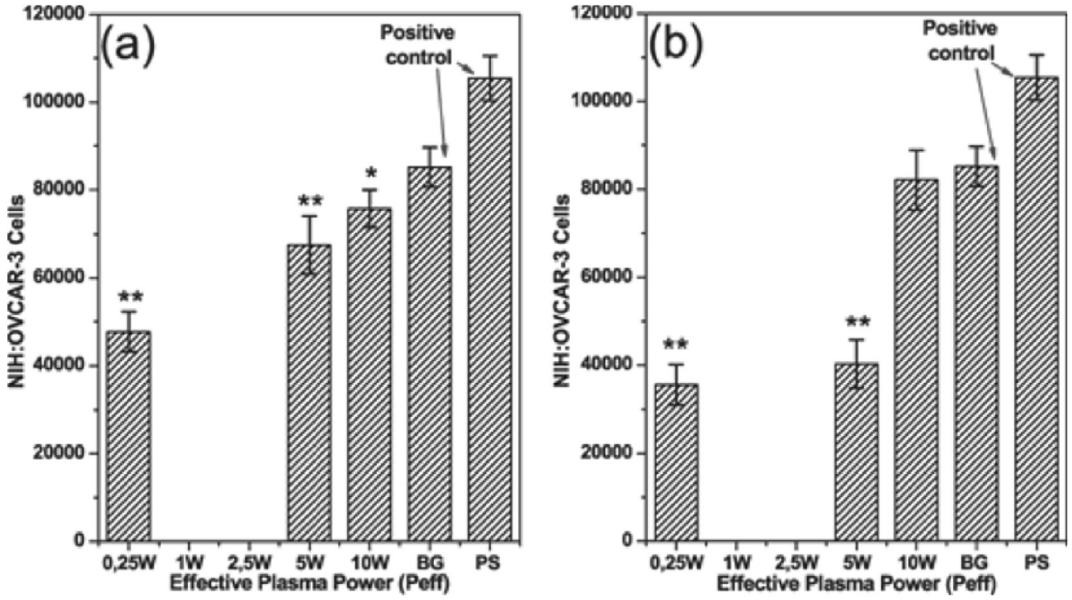

Fig. 60. Cell adhesion and proliferation of NIH:OVCAR-3 on ppEtOx after 96 h (means ± SD, n = 3) deposited under different plasma powers at carrier gas flow rates of a) 5 ml/min and b) 10 ml/min. Positive controls: Bare glass (BG) and tissue culture polystyrene (PS). $^{*}p < 0.05$, $^{**}p < 0.01$ compared to PS. Reprinted with permission ref. [343]. Copyright (2015) John Wiley & Sons, Inc.

postulated in the paper previously discussed and the authors refer in further publications to these discussions. The ring structure is postulated due to IR spectra of ppOx. The authors observe C=N stretching bands (1657 cm^{-1}), C-O stretching bands (1130 cm^{-1}) and a deformation band in the fingerprint area (800 cm^{-1}) and they conclude an indication for oxazoline ring structures with respect to literature [326]. However, the authors dismiss the fact, that the same publication shows two bands (990 and 953 cm^{-1}) in PIPOx that disappear after LCROP and that were originally assigned to the ring skeletal vibration of the oxazoline ring with support of NMR spectra [347]. Further, the authors employ chemical reactions to corroborate the existence of the ring structure. However, the purported reaction with COOH groups on Au-NPs is no conclusive proof that an oxazoline ring is present, since a reaction with isocyanates (band was found in IR spectra) is also highly probable. The same group used the adjustable binding properties to create samples with uniform surface coverage by ppMeOx (1.3×10^{-1} mbar, 50 W, 30 s) after deposition of Au-NPs of different sizes [348]. After experiments regarding the adsorption of BSA, it could be shown that the adsorption was successfully modelled based on the parameters of surface topology and wettability.

ppEtOx (6×10^{-2} mbar, 3.6 ml/min monomer flow, 30 s 100 W power, afterwards 4–80 W for 10–30 min) surfaces were investigated by Zanini et al. towards binding of different functional polymers [349]. Deposition of ppEtOx did not follow a linear trend with increasing power. Indeed, a known trend in plasma polymerization is reflected. Yasuda defined a parameter Y=W/(FM) with plasma power W, flow rate F and molecular mass M [350]. With increasing power, while maintaining monomer flow, the increasing energy per monomer leads from a precursor saturated region to a competition in deposition and ablation of the already deposited layer. However, no clear statement is possible without further data. IR spectra show similar characteristics as published by the Vasilev group, but unfortunately the fingerprint area below 1000 cm^{-1} was not reported. The group claims that PP retains oxazoline rings on the surface as demonstrated by NMR spectra, which are, however, inconclusive. Subsequently, deposition of PAA, PEG-NH_2 and a fluorosurfactant was demonstrated. Interestingly, the ppEtOx films showed an intrinsic fluorescence.

The group also worked on the plasma polymerization of *i*PrEnOx [351]. While IR spectra gave similar results (again, fingerprint area was not recorded) to already discussed ppOx, NMR data clearly corroborate the presence of 2-oxazoline rings (Fig. 61) for lower Y parameters (100 W plasma power, 30% duty cycle). The authors demonstrated the stability of the film to aqueous environment (exception against pH 13) and reactivity against PAA. Future utilization of the retained ring structure appears most interesting for surface modifications.

Cavallaro et al. showed that tuning of the surface properties can be achieved by careful variation of the Yasuda parameter from unstable films to low fouling films to biocompatible films for cell adhesion [352]. The authors also showed that the deposition is substrate-independent. Most recently, Macgregor et al. discussed different mechanisms for deposition supported by mass spectrometry and XPS [353].

A plasma-related deposition was published by Popelka et al. to

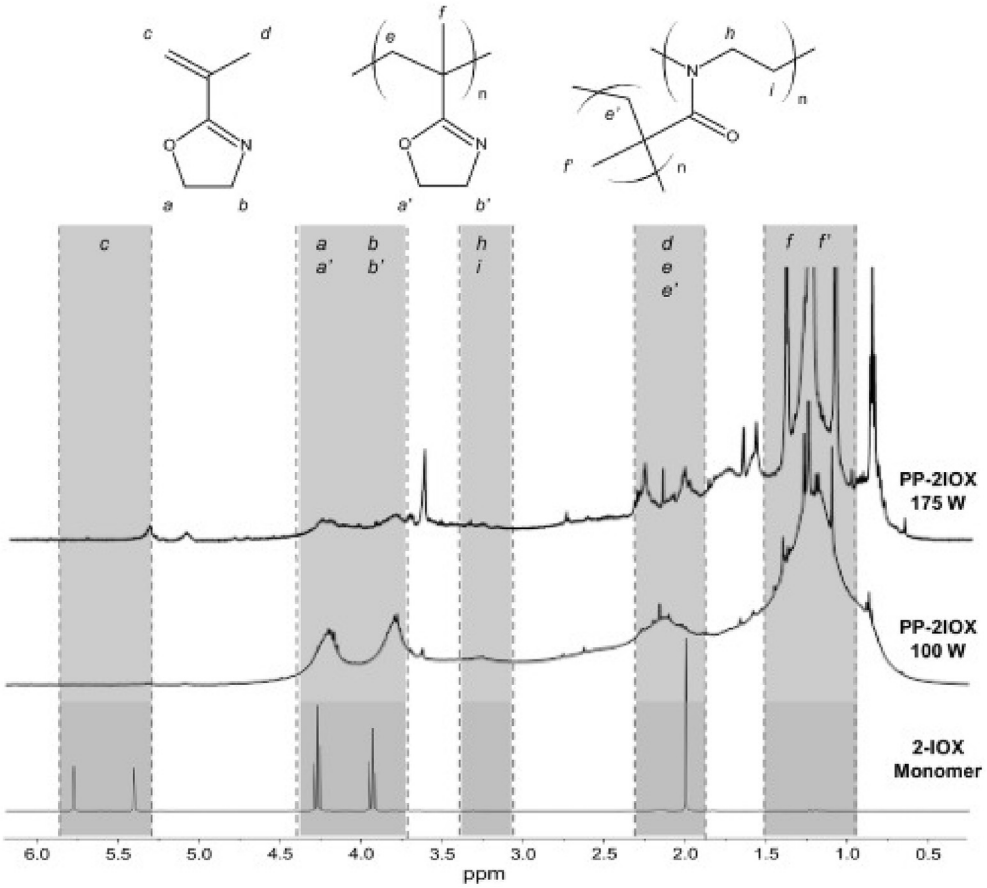

Fig. 61. NMR spectra of different (with respect to deposition power) ppIPOx and comparison to the precursor 2-iso-propenyl-2-oxazoline. Structure on top represent possible structures of monomer and products of LCROP to hint probable groups in the plasma deposited film. Especially the two broad peaks at approximately 4.0 and 4.5 ppm indicate retention of oxazoline ring protons. Reprinted with permission from Ref. [351]. Copyright (2018) Elsevier.

yield high surface energy substrates [354]. LDPE samples were activated by air plasma and subsequently immersed into solutions of PEtOx or PEtOx-acrylate. For both samples, binding of the POx was observed via IR, contact angles and XPS. These high free surface energy samples could be, along with others, used for antifouling applications.

Urothelial cancers are amongst the 10 most common carcinoma, representing a major health problem worldwide. Very recently, Macgregor-Ramiasa et al. [355] investigated a selective cancer cell capture platform for the detection of cancer cells in urine specimen. ppOx films immobilized on microscopy glass slides or the bottom of conventional 96 well plates (film thickness: 54 ± 4 nm; investigated with PMeOx films deposited under same conditions on silicon wafers; no notable change in film thickness after 24 h exposure to PBS or 1 h exposure to urine (or both incubation steps combined)) were used to covalently bind cancer specific anti-epithelial cell adhesion antibodies (anti-EpCAM, surface density of 10^{11} cm^{-2}) via the unique reactivity of pPOx with carboxylic acids. In the absence of antibodies, nonspecific attachment of HTC116 carcinoma cells (exhibiting a high expression of EpCAM) and immortalised human SV40 podocytes (no expression of EpCAM) occurred on PMeOx coated microchannels using native urine from a healthy individual. Binding of both cell types was strongly reduced by blocking the ppMeOx films with skim milk (Fig. 62). In contrast, ppMeOx films functionalized with anti-EpCAM antibodies mainly bound HTC116 cancer cells (Fig. 62 lower panel; 99% specificity HTC116/podocyte cells). No cell depletion did occur during rinsing steps. Thus, irrespective of the initial cell concentration (1000 - 500,000 cells/mL), capture efficiency of the anti-EpCAM functionalized pPMeOx surface for HT116 cells was quantitative within the experimental error.

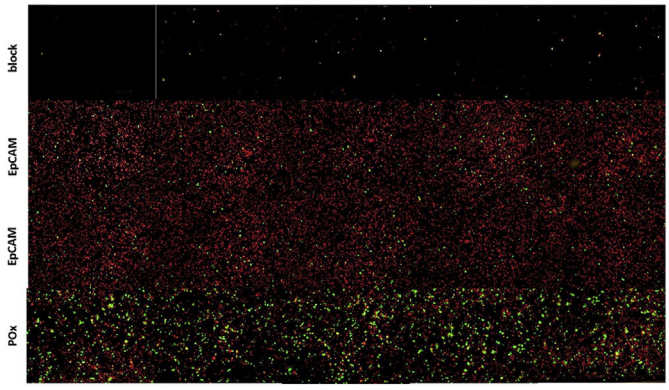

Fig. 62. Micrograph of whole channels showing the cell populations (cancer cells in red and podocytes in green) bound on blocked (top), anti-EpCAM conjugated (middle rows) and pristine (bottom) ppMeOx surfaces. No cells adhered on the blocked substrates, unspecific adsorption is observed on the pristine ppMeOx, and primarily cancer cells are captures on the antibody-functionalized substrates. Reprinted with permission from ref. [355]. Copyright 2017 Elsevier.

8.2. POx-based antifouling surfaces

Previously, POx-based antifouling surfaces were synthesized via *grafting-to* and *grafting-from* methods from various substrates, e.g. by Konradi et al. using a *grafting-to* method via electrostatic interactions to modify negatively charged Nb_2O_5 surfaces with PLL-*g*-PMeOx [356] or by Zhang et al. via *grafting-from* of *i*PrEnOx and subsequent LCROP to form bottle-brush brushes (BBBs) [326] on SiO_2 or glassy carbon. In both examples, protein adsorption was prevented effectively. Since protein adsorption is considered the first step in biofilm formation, it is crucial but not necessarily sufficient to show a low protein adsorption for an antifouling surface. A review by Tauhardt et al. summarizes research on POx based antifouling surfaces before 2013 [19].

Besides the already mentioned ppOx, which exhibit antibacterial, antifouling or biocompatible environments depending on the conditions during the PP, antifouling behavior of conventional POx surfaces was corroborated in recent years by several groups. Wang and co-workers utilized different approaches to modify primarily glass surfaces, but also Au and Si surfaces, with antifouling POx coatings. They will be discussed in order of descending definition of the resulting surface modification. First, functionalization of living OMeOx chain ends with methacrylic acid (OMeOxMA) during LCROP allowed a copolymerization of the resulting macromonomer with glycidyl methacrylate (GMA) to yield P(OMeOxMA-co-GMA) [357]. The polymer was spin-coated on glass wafers and thermocured. The resulting coating thickness and contact angles of the resulting surfaces were depended on the composition of the coated polymer and ranged from 5 to 45 nm and 25–60°, respectively. The samples were found to show low to no protein (BSA) adhesion (Fig. 63), low bacterial adsorption as well as low to no blood platelet adhesion.

Subsequently, the technique was used to coat the inner walls of

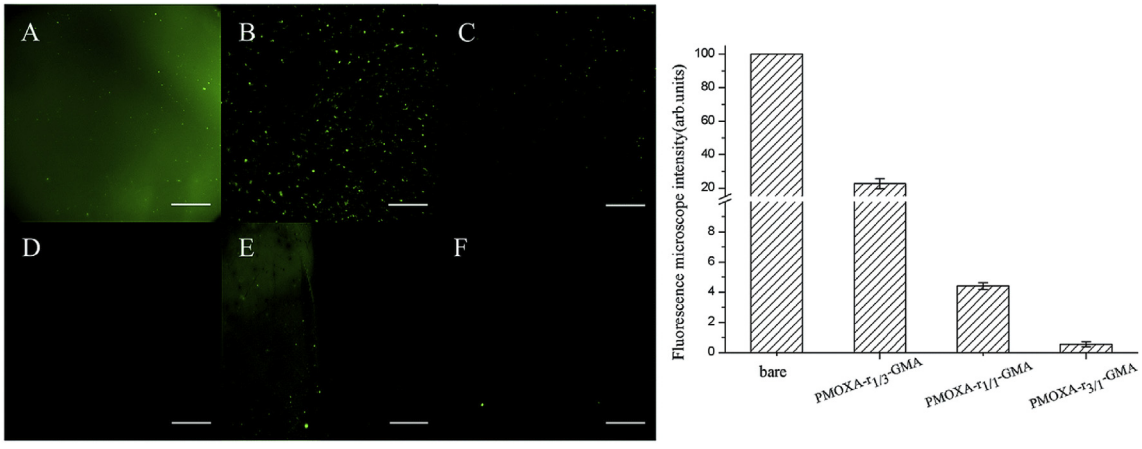

Fig. 63. Left: Epifluorescence images of BSA-FITC incubated P(OMeOxMA-co-GMA) (here: P(MOXA-co-GMA)) surfaces. A) pristine glass, B) P(OMeOxMA-co-GMA) with excess GMA (1/3), C) P(OMeOxMA-co-GMA) with equal amounts of both monomers (1/1), D) P(OMeOxMA-co-GMA) with excess OMEOxMA (3/1), E) left half of waver modified with P(OMeOxMA-co-GMA) (3/1) and F) P(OMeOxMA-co-GMA) (3/1) after 3 week incubation in PBS (prior to protein adsorption experiment). Scale bar = 50 μm. Right: Relative fluorescence intensity means ± SD (n = 3). Reprinted with permission from Ref. [357]. Copyright (2014) Royal Society of Chemistry.

fused-silica capillaries. The modification enhanced separation efficiency of lactoferrin, an important protein in infant formula, in capillary electrophoresis [358]. A similar technique of *grafting-to* was used by Tauhardt et al. for glass modification with amine end-group type PEtOx [359]. Additionally, a phospholipid could be used to mediate surface coating. Biofilm formation experiments revealed a reduction in biofilm formation compared to pristine glass. The coatings were shown to perform well in stress test against fresh and sea water as well as mechanical and thermal stress, but surface coverage was still quite high with respect to antifouling standards.

Further, Wang and co-workers applied electrochemical methods to graft P(MeOx-co-PEI) to poly(dopamine) (PDA) coated steel stents [360]. The stents were characterized towards protein adsorption, cytotoxicity and platelet adhesion. First, stents immersed in the cell culture medium of human umbilical vein endothelial cells (HUVECs) (adhered on culture dishes) did show no effect on proliferation, while bare stents slightly favored proliferation which was attributed to release of Fe-ions. However, the POx coated stents outperformed pristine steel stents in terms of antifouling characteristics against protein (BSA) adsorption and platelet adhesion. Still, adhesion and mobility of HUVECs directly on the modified substrates remains too high to eliminate the risk of restenosis and the authors suggest to cover stents with POx brushes in the future.

Another method of modification applied was UV curing. For this, OMeOxMA macromonomers were copolymerized with 4-vinylpyridine (4VP) via RAFT polymerization, spin-coated on glass substrates and UV cross-linked ($\lambda = 254$ nm) [361]. The resulting layers were only stable after UV curing, 10–30 nm thick, exhibit low zeta potentials between −25 and −70 mV (pH = 7.4) but varied significantly in antifouling performance. While surfaces that comprised of high POMeOxMA content showed almost no BSA adsorption, higher P4VP content lead to very high BSA adsorption. Accordingly, all POMeOxMA containing surfaces showed low cell adhesion from standard cell culture growth medium. Additionally, the surface modification was found to be stable in PBS buffer for at least 28 days as no change in XPS spectra was observed.

Another approach used was surface deposition by electrostatic interaction of PEI with Au and Si, comparable to copolymers with PLL mentioned before. PMeOx was grafted via polymer analogue reactions to hyperbranched PEI. Subsequently, PMeOx and the PEI-*g*-PMeOx grafts were deposited, mediated by dopamine, on substrates [362]. Compared to controls, only the coatings from PEI-*g*-PMeOx were found to resist adsorption of BSA. Interestingly, in further experiments with proteins such as fibrinogen or lysozyme, PEI-*g*-PMeOx coatings that were deposited without dopamine mediation performed worse than those deposited with dopamine. Interestingly, pure PDA coatings greatly enhance protein adsorption. Additionally, the modified surfaces were compared to similar PEI-*g*-PEG deposits regarding cell attachment after immersion in H_2O_2 in PBS solution to simulate alteration by macrophage secretions. The experiments showed, that after one to four weeks of immersion in the given solution PEI-*g*-PEG surfaces are altered in way that allows cell attachment in a larger extent than found for PEI-*g*-PMeOx surface (Fig. 64). The group also used thiol terminated PMAA-*g*-OMeOx for SPR experiments [363]. These revealed no adsorption of fibrinogen and BSA as well as very low adsorption of lysozyme to the surface. Water contact angles of around 20° were found which indicates high hydrophilicity [364].

Several groups also demonstrated superior performance of POx antifouling surfaces compared to PEG films, using electrostatic interactions to graft PLL-*g*-PMeOx to Nb_2O_5 surface. Using comparable compositions, film thicknesses as well as grafting and surface coverage densities, Pidhatika et al. precisely studied differences between PEG and PMeOx coatings using various independent

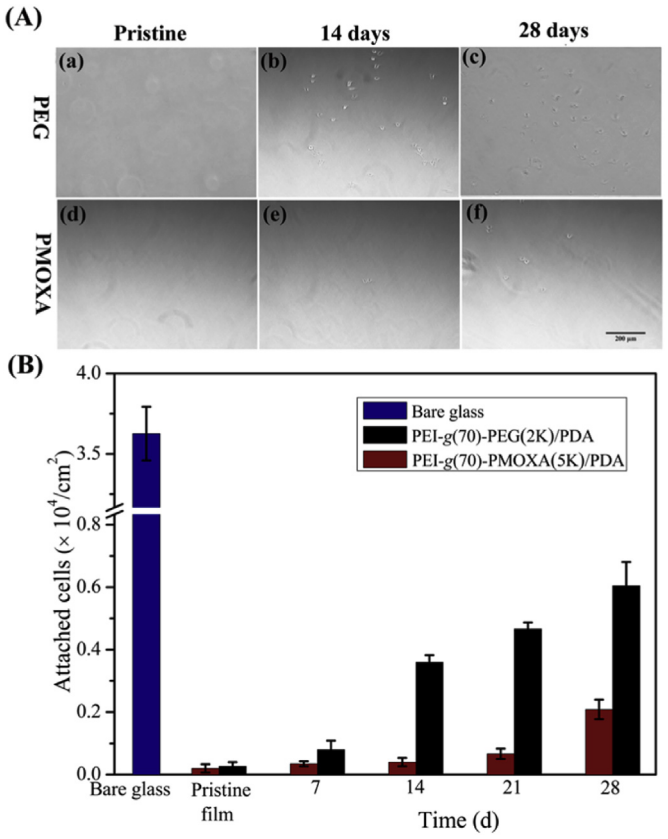

Fig. 64. Microscope images (A) and cell attachment numbers (n = 4) (B) of PEI-*g*-PEG ((A) (a), (b) and (c)) as well as PEI-*g*-PMeOx ((A) (d), (e) and (f)) surface modifications after 0 ((A) (a) and (d)), 2 ((A) (b) and (e)) to 4 weeks ((A) (c) and (f)) of immersion in H_2O_2 in PBS solution. Reprinted with permission from Ref. [362]. Copyright (2015) Royal Society of Chemistry.

surface characterization methods on alteration of the coating by oxidation, salt concentration and synergistic effects [79]. In a follow-up paper by Chen et al. performed *in vitro* cell culture experiments which used patterned areas of the mentioned polymer surfaces to test their stability and outgrowth tendencies of cells [365]. Again, PMeOx coated surfaces outperformed PEG surfaces in long term performance but especially in outgrowth (growth of cells out of adhesion favoring patterns into antifouling modified area) experiments, PEG never reached the remarkable antifouling capacities of POx. In this, various POx grafting density as well as side chain length investigated in this contribution had no influence on the results.

He *at el*. used a *grafting from* approach to UV polymerize PMeOx macromonomers with or without highly hydrophilic METAC from methacrylpropylsilane surfaces [366]. Compared to *grafting-to* approaches, the method yielded thick film of 200–300 nm in 20 min reaction time. In bacterial adhesion experiments, only pure PMeOx grafts showed very high resistance to *E. coli* or *S. aureus*. Further, all surfaces showed high reduction in settlement of cyprids and small reduction in settlement of amphora. However, silicon surfaces were used as control surface and research needs to cover further materials to provide more conclusive evidence for marine antifouling use on relevant surfaces. A method frequently found to deposit POx on surfaces is LbL deposition, which deposits alternatingly POx and PAA or PMA. In another contribution utilizing the simple partial hydrolysis of POx, He et al. could also show that an according LbL deposition of P(EtOx-co-EI) with PAA leads to very low bacterial attachment and controllable cell attachment [367]. The

characteristics of the resulting coatings were greatly dependent on the number of deposited layers. While protein (BSA) and cell adhesion were found to be lowest for 5 bilayers (thickness around 200 nm) of PAA and P(EtOx-co-EI), surface coverage with *E. coli* and *S. aureus* were not affected by bilayer number for n > 1. It should be noted that the antifouling behavior regarding bacterial attachment could also be viewed as antibacterial characteristics due to PEI content, but the missing cell adhesion (although it was not quantified) and protein adsorption allow its classification as antifouling surface. The authors anchored the bilayers to the APS surface and internally by thermal cross-linking. In contrast, Kempe et al. utilized thiol-ene reactions and azide-alkyne cycloaddition, for cross-linking of similar PEtOx copolymers and brushes [368]. LbL assemblies of POx with PMA were formed, cross-linked using low molecular multifunctional thiols and azides, respectively, before PMA was washed out to yield hollow POx capsules. Since the assembly was performed on SiO_2 microparticles, etching yielded hollow capsules with very low protein interaction compared to PVP. PVP as control did not show antifouling properties in this report. However, it should be noted that others have classified PVP as a biocompatible and antifouling polymer [369]. In a follow-up paper, the authors added extensive cell studies as well as protein interaction studies [370]. The capsules were found to be non-toxic and are internalized by cells. Additionally, low protein adsorption, compared to PMA, was found by QCM. Important contributions to the understanding to LbL formation process were given by Su et al. who used PEtOx and PAA films as model system to understand relative influences of pH, polymer concentration, polymer mole fraction and molecular weight [371].

Sethuraman and co-workers investigated electrospun scaffolds comprising PEtOx and poly(lactide-co-caprolactone) (P(LA-co-CL)) [372] for cardiac tissue engineering. The authors report electrospinning of the homopolymers and two mixtures of EtOx and P(LA-co-CL), 70/30 and 50/50 (w/w). The different scaffolds were characterized for their mechanical properties.

Hayashi and Takasu modified stainless steel and bioglass with POx bearing sulfide and sulfone side chains [373]. These coatings allowed cell adherence, as they comprised rather hydrophobic POx but were found non-cytotoxic.

In summary, the LbL methods involving POx seem to give favorable results when PEI is used as cationic counterpart to PAA or PMA. Additional to easier layer formation, PEI containing surfaces can also be considered antibacterial surfaces. To distinguish between the antifouling and antibacterial surfaces, the presence of a functional antibacterial group will be used as distinctive feature.

8.3. Antimicrobial surfaces

In the past, very few publications have dealt with the topic of transferring the very promising antimicrobial properties of functional, antibacterial POx from solution to surfaces. Following their work on *N*,*N*-dimethyldodecylamine (DDA) functionalized telechelic PMeOx polymers, the group of Tiller functionalized double bond bearing glass surfaces with the respective telechelic PMeOx macromonomers by UV copolymerization with methacrylates [374]. The authors could show that macromonomers containing films were stable to leaching and very effectively inhibiting growth of biofilms of *S. aureus* (Fig. 65).

The widely used LbL methods discussed previously were also employed to yield antimicrobial surfaces. Li et al. used LbL deposition of P(EtOx-co-EI) with PAA to produce films, that killed Gram-negative and Gram-positive on contact [375]. For this, layers were deposited by dip coating of alternating P(EtOx-co-EI) and PAA. The layers were thermally cross-linked. Subsequent bacterial adhesions experiments revealed that, after 6 h of incubation time, adhesion of

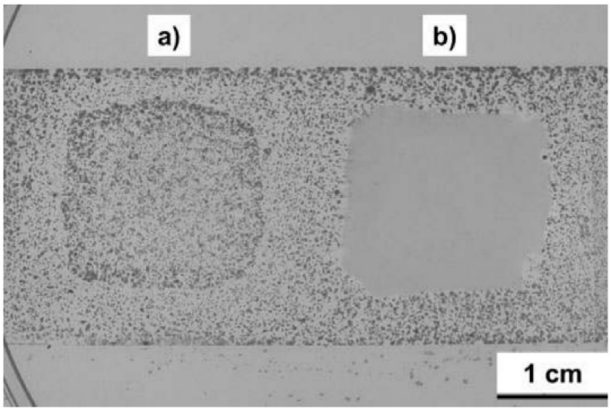

Fig. 65. *S. aureus* growth on glass slide, which was non-coated a) and coated with b) antimicrobial PMeOx macromonomer, respectively. Reprinted with permission from Ref. [374]. Copyright (2008) John Wiley & Sons, Inc.

E. coli and *B. subtilis* was below detection limit. Additionally, the films were shown to be self-healing, i.e. small cuts (25–500 μm) that separated two areas of coating were closed after immersion in water. It should be noted that the antibacterial feature in this coating is provided by PEI and not by any functionalities of POx.

Kelly et al. incorporated partially hydrolyzed PEtOx and PNOx into poly(propylene) matrices by extrusion and injection molding [376]. It could be shown that mixtures derived from hydrolyzed PNOx performed best against *E. coli*, *P. aeruginosa* and *S. aureus* while PEtOx derived mixtures performed better against *C. albicans*. However, none of the mixtures outperformed positive control PEI, which indicates that, not surprisingly, the antibacterial activity is based on PEI and not POx.

Fik et al. copolymerized telechelic POxMA with commercial dental adhesive acrylates [377]. Functionalities were introduced by straightforward use of respective LCROP reactants, e.g. tertiary amine-bearing initiator and methacrylamide-bearing terminating agent. Additional to an antibacterial effect of the coating, it was found that the POx film inhibits metalloproteases, which is favorable for dental applications, since these enzymes hydrolyze dentin and therefore disrupt the mechanical stability of teeth.

Schulz et al. reported on a different approach to created POx grafted surfaces which exhibit stealth effect and biofilm reduction [378]. Here, a copolymer of MeOx and 2-(4-azidophenyl)-2-oxazoline were copolymerized yielding gradient copolymers. The aryl-azide moiety allows modification of a wide variety of standard polymer materials by simple UV irradiation, as shown for PP, PLA and PET. The PP and PLA modified surfaces were tested with respect to their cytotoxicity and cell adherence (L929) as well as bacterial (*S. epidermidis* and *E. coli*) proliferation and biofilm formation. Compared to tissue-culture polystyrene, fibroblast adhesion was reduced in treated and untreated PP and PLA. However, interestingly, POx grafting did not affect much fibroblast proliferation. In contrast, bacterial adhesion and biofilm formation was diminished very significantly. Since a large variety of surfaces, essentially all technical plastics should be amendable to this coating, the authors claim that the described method is particularly attractive and should find industrial use. However, of course, the efficacy will have to be proven in a more application oriented setting.

9. Summary and outlook

The development of POx and related polymers in the context of biomaterials has been a very active and interesting one in the last decade and in particular in the last five years. The synthetic toolbox

available to researchers and appliers has been extended to a degree where most bioconjugation strategies and a wide range of polymer size and architectures are readily accessible. All major fields of biomaterials research have been addressed using POx and quite often, but not always, POx based materials are highly competitive to other materials. It appears many new research groups have joined the community, especially in the last 5 years, which has brought and will continue to bring new ideas and applications. Drug formulations based on POx have been shown to be efficient *in vivo* mainly in the last few years and it appears that *in vivo* work is extended more and more. The notion, that POx are generally rather biocompatible is supported by more and more data. The antibacterial work, mainly driven by the Tiller group has made significant and very interesting progress. Protein-POx conjugates have, so far, seen less attention than one might have assumed a few years back, but there is no obvious reason why this should not change in the near future. Surface modification by different approaches also show great promise, the recent work by Benetti can serve as show-case in this context.

Also, the commercial use of POx has seen changes. Several new monomers and polymers have become commercially available and a significant number of patents have been applied for and some granted. With great interest the community looks forward to see the detailed results of the Phase I clinical trial of SER-214 and the beginning of phase II.

Obviously, compared to PEG, POx based biomaterials are still a niche. However, we strongly believe this gap will remain to close quicker and quicker, in particular if SER-214 remains to produce promising results. There is still a lot of work to be done and lot of potential to be tapped, and the next few years will probably define the future of POx as biomaterials.

Conflicts of interest

MML, TL, RJ, AVK and RL declare potential conflict of interest. MML, TL, RJ, AVK and RL are listed as inventors on various patents and patent applications pertinent to the subject matter of the present contribution. RL, RJ and AVK are founders of DelAqua Pharmaceuticals Inc., intent on commercial development of POx based drug formulations.

Acknowledgement

This work was supported by the Free State of Bavaria. Start-up funding for R.L. by the University Würzburg and SKZ Das Kunststoff-Zentrum is gratefully acknowledged. M.M.L. would like to thank the Evonik Foundation for providing a doctoral fellowship. D.N. gratefully acknowledges financial support by the DFG (#310771104, awarded to R.L.), M.S.H would like to thank the Higher Education Commission, Pakistan (HEC) of Pakistan and Deutscher Akademischer Austauschdienst (DAAD) Germany. S.B. would like to thank the Bavarian Academic Center for Central, Eastern and Southeastern Europe (BAYHOST) for financial support. This work was also supported by the National Cancer Institute (NCI) Alliance for Nanotechnology in Cancer (U54CA198999, Carolina Center of Cancer Nanotechnology Excellence).

Finally, we would like to acknowledge additional support by the DFG SFB Transregio 225 (#397978692).

References

[1] R. Hoogenboom, 50 years of poly(2-oxazoline)s, Eur. Polym. J. 88 (2017) 448–450.
[2] S. Nam, J. Seo, S. Woo, W.H. Kim, H. Kim, D.D. Bradley, Y. Kim, Inverted polymer fullerene solar cells exceeding 10% efficiency with poly(2-ethyl-2-oxazoline) nanodots on electron-collecting buffer layers, Nat. Com. 6 (2015) 1–9.
[3] S. Huber, R. Jordan, Modulation of the lower critical solution temperature of 2-alkyl-2-oxazoline copolymers, Colloid. Polym. Sci. 286 (4) (2008) 395–402.
[4] J.-S. Park, K. Kataoka, Comprehensive and accurate control of thermosensitivity of poly(2-alkyl-2-oxazoline)s via well-defined gradient or random copolymerization, Macromolecules 40 (10) (2007) 3599–3609.
[5] N. Zhang, R. Luxenhofer, R. Jordan, Thermoresponsive poly(2-oxazoline) molecular brushes by living ionic polymerization: modulation of the cloud point by random and block copolymer pendant chains, Macromol. Chem. Phys. 213 (18) (2012) 1963–1969.
[6] N. Zhang, R. Luxenhofer, R. Jordan, Thermoresponsive poly(2-oxazoline) molecular brushes by living ionic polymerization: kinetic investigations of pendant chain grafting and cloud point modulation by backbone and side chain length variation, Macromol. Chem. Phys. 213 (9) (2012) 973–981.
[7] J.-H. Kim, Y. Jung, D. Lee, W.-D. Jang, Thermoresponsive polymer and fluorescent dye hybrids for tunable multicolor emission, Adv. Mater. 28 (18) (2016) 3499–3503.
[8] R. Hoogenboom, H. Schlaad, Thermoresponsive poly(2-oxazoline)s, polypeptoids, and polypeptides, Polym. Chem. 8 (1) (2017) 24–40.
[9] B. Trzebicka, R. Szweda, D. Kosowski, D. Szweda, L. Otulakowski, E. Haladjova, A. Dworak, Thermoresponsive polymer-peptide/protein conjugates, Prog. Polym. Sci. 68 (2017) 35–76.
[10] E. Rossegger, V. Schenk, F. Wiesbrock, Design strategies for functionalized poly(2-oxazoline)s and derived materials, Polymers 5 (3) (2013) 956–1011.
[11] Y. Jung, W.-D. Jang, Recent approaches for clickable poly(2-oxazoline)-based functional stimuli-responsive polymers and related applications, Supramol. Chem. (2017) 1–9.
[12] B. Verbraeken, B.D. Monnery, K. Lava, R. Hoogenboom, The chemistry of poly(2-oxazoline)s, Eur. Polym. J. 88 (2017) 451–469.
[13] M. Glassner, M. Vergaelen, R. Hoogenboom, Poly(2-oxazoline)s: a comprehensive overview of polymer structures and their physical properties, Polym. Int. (2018) 32–45.
[14] M.M. Bloksma, U.S. Schubert, R. Hoogenboom, Poly(cyclic imino ether)s beyond 2-Substituted-2-oxazolines, Macromol. Rapid Commun. 32 (18) (2011) 1419–1441.
[15] R. Luxenhofer, S. Huber, J. Hytry, J. Tong, A.V. Kabanov, R. Jordan, Chiral and water-soluble poly(2-oxazoline)s, J. Polym. Sci., Part A: Polym. Chem. 51 (3) (2013) 732–738.
[16] A.M. Kelly, F. Wiesbrock, Strategies for the synthesis of poly(2-oxazoline)-based hydrogels, Macromol. Rapid Commun. 33 (19) (2012) 1632–1647.
[17] T.R. Dargaville, B.G. Hollier, A. Shokoohmand, R. Hoogenboom, Poly(2-oxazoline) hydrogels as next generation three-dimensional cell supports, Cell Adh. Migr. 8 (2) (2014) 88–93.
[18] M. Hartlieb, K. Kempe, U.S. Schubert, Covalently cross-linked poly(2-oxazoline) materials for biomedical applications – from hydrogels to self-assembled and templated structures, J. Mater. Chem. B 3 (4) (2015) 526–538.
[19] L. Tauhardt, K. Kempe, M. Gottschaldt, U.S. Schubert, Poly(2-oxazoline) functionalized surfaces: from modification to application, Chem. Soc. Rev. 42 (20) (2013) 7998–8011.
[20] G. Morgese, E.M. Benetti, Polyoxazoline biointerfaces by surface grafting, Eur. Polym. J. 88 (2017) 470–485.
[21] https://clinicaltrials.gov/ct2/show/NCT02579473, (accessed 12.02.2018).
[22] R.W. Moreadith, T.X. Viegas, M.D. Bentley, J.M. Harris, Z. Fang, K. Yoon, B. Dizman, R. Weimer, B.P. Rae, X. Li, C. Rader, D. Standaert, W. Olanow, Clinical development of a poly(2-oxazoline) (POZ) polymer therapeutic for the treatment of Parkinson's disease – proof of concept of POZ as a versatile polymer platform for drug development in multiple therapeutic indications, Eur. Polym. J. 88 (2017) 524–552.
[23] M.C. Woodle, C.M. Engbers, S. Zalipsky, New amphipatic polymer-lipid conjugates forming long-circulating reticuloendothelial system-evading liposomes, Bioconjugate Chem. 5 (6) (1994) 493–496.
[24] M. Grube, M.N. Leiske, U.S. Schubert, I. Nischang, POx as an alternative to PEG? A hydrodynamic and light scattering study, Macromolecules 51 (5) (2018) 1905–1916.
[25] A. Gubarev, B.D. Monnery, A.A. Lezov, O. Sedláček, N.V. Tsvetkov, R. Hoogenboom, S.K. Filippov, Conformational properties of biocompatible poly(2-ethyl-2-oxazoline) s in phosphate buffered saline, Polym. Chem. 9 (2018) 2232–2237.
[26] T. Yamaoka, Y. Tabata, Y. Ikada, Distribution and tissue uptake of poly(ethylene glycol) with different molecular weights after intravenous administration to mice, J. Pharm. Sci. 83 (4) (1994) 601–606.
[27] C.W. McGary, Degradation of poly(ethylene oxide), J. Polym. Sci., Part A: Polym. Chem. 46 (147) (1960) 51–57.
[28] M. Barz, R. Luxenhofer, R. Zentel, M.J. Vicent, Overcoming the PEG-addiction: well-defined alternatives to PEG, from structure – property relationships to better defined therapeutics, Polym. Chem. 2 (9) (2011) 1900–1918.
[29] K. Knop, R. Hoogenboom, D. Fischer, U.S. Schubert, Poly(ethylene glycol) in drug delivery: pros and cons as well as potential alternatives, Angew. Chem. Int. Ed. 49 (36) (2010) 6288–6308.
[30] M. Bauer, C. Lautenschlaeger, K. Kempe, L. Tauhardt, U.S. Schubert, D. Fischer, Poly(2-ethyl-2-oxazoline) as alternative for the stealth polymer poly(ethylene glycol): comparison of in vitro cytotoxicity and hemocompatibility, Macromol. Biosci. 12 (7) (2012) 986–998.
[31] M. Bauer, S. Schroeder, L. Tauhardt, K. Kempe, U.S. Schubert, D. Fischer, *In vitro* hemocompatibility and cytotoxicity study of poly(2-methyl-2-

oxazoline) for biomedical applications, J. Polym. Sci. 51 (8) (2013) 1816–1821.
[32] Z. Kroneková, M. Mikulec, N. Petrenčíková, E. Paulovičová, L. Paulovičová, V. Jančinová, R. Nosál, P.S. Reddy, G.D. Shimoga, D. Chorvát, J. Kronek, Ex vivo and in vitro studies on the cytotoxicity and immunomodulative properties of poly(2-isopropenyl-2-oxazoline) as a new type of biomedical polymer, Macromol. Biosci. 16 (8) (2016) 1200–1211.
[33] M.N. Leiske, A.-K. Trützschler, S. Armoneit, P. Sungur, S. Hoeppener, M. Lehmann, A. Traeger, U.S. Schubert, Mission ImPOxable – or the unknown utilization of non-toxic poly(2-oxazoline)s as cryoprotectants and surfactants at the same time, J. Mater. Chem. B 5 (46) (2017) 9102–9113.
[34] M.M. Lübtow, L. Hahn, M.S. Haider, R. Luxenhofer, Drug specificity, synergy and antagonism in ultrahigh capacity poly(2-oxazoline)/poly(2-oxazine) based formulations, J. Am. Chem. Soc. 139 (32) (2017) 10980–10983.
[35] T. Lorson, S. Jaksch, M.M. Lübtow, T. Jüngst, J. Groll, T. Lühmann, R. Luxenhofer, A thermogelling supramolecular hydrogel with sponge-like morphology as a cytocompatible bioink, Biomacromolecules 18 (7) (2017) 2161–2171.
[36] M.M. Lübtow, L.C. Nelke, A. Brown, G. Sahay, G. Dandekar, R. Luxenhofer, Drug Induced Micellization into Ultra-high Capacity and Stable Curcumin Nanoformulations: Comparing in Vitro 2D and 3D-tumor Model of Triple-negative Breast Cancer, ChemRxiv, 2017, https://doi.org/10.26434/chemrxiv.5661736.v1.
[37] Z. Kroneková, T. Lorson, R. Luxenhofer, J. Kronek, Cytotoxicity of 2-oxazines and Poly(2-oxazoline)s in Mouse Fibroblasts, ChemRxiv, 2018, https://doi.org/10.26434/chemrxiv.5793990.v1.
[38] M.M. Bloksma, R.M. Paulus, H.P.C. van Kuringen, F. van der Woerdt, H.M. Lambermont-Thijs, U.S. Schubert, R. Hoogenboom, Thermoresponsive Poly(2-oxazine)s, Macromol. Rapid Commun. 33 (1) (2012) 92–96.
[39] S.C. Lee, C. Kim, I.C. Kwon, H. Chung, S.Y. Jeong, Polymeric micelles of poly(2-ethyl-2-oxazoline)-block-poly(ε-caprolactone) copolymer as a Carrier for paclitaxel, J. Controlled Release 89 (3) (2003) 437–446.
[40] B. Guillerm, V. Darcos, V. Lapinte, S. Monge, J. Coudane, J.-J. Robin, Synthesis and evaluation of triazole-linked poly(ε-caprolactone)-graft-poly(2-methyl-2-oxazoline) copolymers as potential drug carriers, Chem. Commun. 48 (23) (2012) 2879–2881.
[41] W. Wu, S. Cui, Z. Li, J. Liu, H. Wang, X. Wang, Q. Zhang, H. Wu, K. Guo, Mild Brønsted acid initiated controlled polymerizations of 2-oxazoline towards one-pot synthesis of novel double-hydrophilic poly(2-ethyl-2-oxazoline)-block-poly(sarcosine), Polym. Chem. 6 (15) (2015) 2970–2976.
[42] S.C. Lee, Y. Chang, J.-S. Yoon, C. Kim, I.C. Kwon, Y.-H. Kim, S.Y. Jeong, Synthesis and micellar characterization of amphiphilic diblock copolymers based on poly(2-ethyl-2-oxazoline) and aliphatic polyesters, Macromolecules 32 (6) (1999) 1847–1852.
[43] C.H. Wang, G.H. Hsiue, Synthesis and characterization of temperature-and pH-sensitive hydrogels based on poly(2-ethyl-2-oxazoline) and poly(D, L-lactide), J. Polym. Sci., Part A: Polym. Chem. 40 (8) (2002) 1112–1121.
[44] G. Le Fer, C. Le Cœur, J.-M. Guigner, C. Amiel, G. Volet, Self-assembly of poly(2-alkyl-2-oxazoline-)-g-poly(d, l-lactide) copolymers, Eur. Polym. J. 88 (2017) 656–665.
[45] G.-H. Hsiue, H.-Z. Chiang, C.-H. Wang, T.-M. Juang, Nonviral gene carriers based on diblock copolymers of poly(2-ethyl-2-oxazoline) and linear polyethylenimine, Bioconjugate Chem. 17 (3) (2006) 781–786.
[46] J.C. Fernandes, X. Qiu, F.M. Winnik, M. Benderdour, X. Zhang, K. Dai, Q. Shi, Linear polyethylenimine produced by partial acid hydrolysis of poly(2-ethyl-2-oxazoline) for DNA and siRNA delivery in vitro, Int. J. Nanomed. 8 (1) (2013) 4091–4102.
[47] V.M. Gaspar, P. Baril, E.C. Costa, D. de Melo-Diogo, F. Foucher, J.A. Queiroz, F. Sousa, C. Pichon, I.J. Correia, Bioreducible poly(2-ethyl-2-oxazoline)–PLA–PEI-SS triblock copolymer micelles for co-delivery of DNA minicircles and Doxorubicin, J. Control. Release 213 (2015) 175–191.
[48] R. Luxenhofer, G. Sahay, A. Schulz, D. Alakhova, T.K. Bronich, R. Jordan, A.V. Kabanov, Structure-property relationship in cytotoxicity and cell uptake of poly(2-oxazoline) amphiphiles, J. Control. Release 153 (1) (2011) 73–82.
[49] N. Gangloff, J. Ulbricht, T. Lorson, H. Schlaad, R. Luxenhofer, Peptoids and polypeptoids at the frontier of supra-and macromolecular engineering, Chem. Rev. 116 (4) (2016) 1753–1802.
[50] X. Pan, Y. Liu, Z. Li, S. Cui, H. Gebru, J. Xu, S. Xu, J. Liu, K. Guo, Amphiphilic polyoxazoline-*block*-polypeptoid copolymers by sequential one-pot ring-opening polymerizations, Macromol. Chem. Phys. 218 (6) (2017), 1600483.
[51] L. Tauhardt, D. Pretzel, K. Kempe, M. Gottschaldt, D. Pohlers, U.S. Schubert, Zwitterionic poly(2-oxazoline)s as promising candidates for blood contacting applications, Polym. Chem. 5 (19) (2014) 5751–5764.
[52] I. Yildirim, T. Bus, M. Sahn, T. Yildirim, D. Kalden, S. Hoeppener, A. Traeger, M. Westerhausen, C. Weber, U.S. Schubert, Fluorescent amphiphilic hetero-grafted comb polymers comprising biocompatible PLA and PEtOx side chains, Polym. Chem. 7 (39) (2016) 6064–6074.
[53] S. Ma, Y. Li, Y. Zhao, Y. Zhou, J. Li, Y. Gao, Y. Li, X. Li, Y. Liu, X. Wang, Hemocompatibility and cytocompatibility of diblock copolymer poly(2-ethyl-2-oxazoline)-poly(D,L-lactide) based micelles, J. Chin. Pharm. Sci. (2014) 674–680.
[54] J.H. Jeong, S.H. Song, D.W. Lim, H. Lee, T.G. Park, DNA transfection using linear poly(ethylenimine) prepared by controlled acid hydrolysis of poly(2-ethyl-2-oxazoline), J. Control. Release 73 (2–3) (2001) 391–399.
[55] H.P.C. Van Kuringen, J. Lenoir, E. Adriaens, J. Bender, B.G. De Geest, R. Hoogenboom, Partial hydrolysis of poly(2-ethyl-2-oxazoline) and potential implications for biomedical applications? Macromol. Biosci. 12 (8) (2012) 1114–1123.
[56] R. Shah, Z. Kroneková, A. Zahoranová, L. Roller, N. Saha, P. Sáha, J. Kronek, In vitro study of partially hydrolyzed poly(2-ethyl-2-oxazolines) as materials for biomedical applications, J. Mater. Sci. Mater. Med. 26 (4) (2015) 157.
[57] C.-P. Lin, Y.-C. Sung, G.-H. Hsiue, Non-viral pH-sensitive gene carriers based on poly((2-ethyl-2-oxazoline)-co-ethylenimine)-*block*-poly(2-ethyl-2-oxazoline): a study of gene release behavior, J. Med. Biol. Eng. 32 (2012) 365–372.
[58] R.M. England, J.I. Hare, P.D. Kemmitt, K.E. Treacher, M.J. Waring, S.T. Barry, C. Alexander, M. Ashford, Enhanced cytocompatibility and functional group content of poly(L-lysine) dendrimers by grafting with poly(oxazolines), Polym. Chem. 7 (28) (2016) 4609–4617.
[59] M. Wang, O.J.R. Gustafsson, G. Siddiqui, I. Javed, H.G. Kelly, T. Blin, H. Yin, S.J. Kent, D.J. Creek, K. Kempe, P.C. Ke, T.P. Davis, Human plasma proteome association and cytotoxicity of nano-graphene oxide grafted with stealth polyethylene glycol and poly(2-ethyl-2-oxazoline), Nanoscale (2018), https://doi.org/10.1039/C8NR00835C.
[60] J. Kronek, Z. Kroneková, J. Lustoň, E. Paulovičová, L. Paulovičová, B. Mendrek, In vitro bio-immunological and cytotoxicity studies of poly(2-oxazolines), J. Mater. Sci. Mater. Med. 22 (7) (2011) 1725–1734.
[61] J. Kronek, J. Lustoň, Z. Kronekova, E. Paulovičová, P. Farkaš, N. Petrenčíková, L. Paulovičová, I. Janigová, Synthesis and bioimmunological efficiency of poly (2-oxazolines) containing a free amino group, J. Mater. Sci. Mater. Med. 21 (3) (2010) 879–886.
[62] J. Kronek, E. Paulovičová, L. Paulovičová, Z. Kroneková, J. Lustoň, Immunomodulatory efficiency of poly(2-oxazolines), J. Mater. Sci. Mater. Med. 23 (6) (2012) 1457–1464.
[63] D.L. Kyluik-Price, L. Li, M.D. Scott, Comparative efficacy of blood cell immunocamouflage by membrane grafting of methoxypoly(ethylene glycol) and polyethyloxazoline, Biomaterials 35 (1) (2014) 412–422.
[64] P. Goddard, L.E. Hutchinson, J. Brown, L.J. Brookman, Soluble polymeric carriers for drug delivery. Part 2. Preparation and in vivo behaviour of N-acylethylenimine copolymers, J. Control. Release 10 (1) (1989) 5–16.
[65] F.C. Gaertner, R. Luxenhofer, B. Blechert, R. Jordan, M. Essler, Synthesis, biodistribution and excretion of radiolabeled poly(2-alkyl-2-oxazoline)s, J. Control. Release 119 (3) (2007) 291–300.
[66] L. Wyffels, T. Verbrugghen, B.D. Monnery, M. Glassner, S. Stroobants, R. Hoogenboom, S. Staelens, μPET imaging of the pharmacokinetic behavior ofmedium and high molar mass ^{89}Zr-labeled poly(2-ethyl-2-oxazoline) in comparison to poly(ethylene glycol), J. Control. Release 235 (2016) 63–71.
[67] M. Glassner, L. Palmieri, B.D. Monnery, T. Verbrugghen, S. Deleye, S. Stroobants, S. Staelens, L. Wyffels, R. Hoogenboom, The label matters: μPET imaging of the biodistribution of low molar mass ^{89}Zr and ^{18}F-labeled poly(2-ethyl-2-oxazoline), Biomacromolecules 18 (1) (2016) 96–102.
[68] P.H. Kierstead, H. Okochi, V.J. Venditto, T.C. Chuong, S. Kivimae, J.M. Fréchet, F.C. Szoka, The effect of polymer backbone chemistry on the induction of the accelerated blood clearance in polymer modified liposomes, J. Control. Release 213 (2015) 1–9.
[69] H. Bludau, A.E. Czapar, A.S. Pitek, S. Shukla, R. Jordan, N.F. Steinmetz, POxylation as an alternative stealth coating for biomedical applications, Eur. Polym. J. 88 (2017) 679–688.
[70] S. Berke, A.L. Kampmann, M. Wuest, J.J. Bailey, B. Glowacki, F. Wuest, K. Jurkschat, R. Weberskirch, R. Schirrmacher, ^{18}F-Radiolabeling and *in vivo* analysis of sifa-derivatized polymeric core-shell nanoparticles, Bioconjug Chem 29 (1) (2018) 89–95.
[71] Z. He, X. Wan, A. Schulz, H. Bludau, M.A. Dobrovolskaia, S.T. Stern, S.A. Montgomery, H. Yuan, Z. Li, D. Alakhova, M. Sokolsky, D.B. Darr, C.M. Perou, R. Jordan, R. Luxenhofer, A.V. Kabanov, A high capacity polymeric micelle of paclitaxel: Implication of high dose drug therapy to safety and *in vivo* anti-cancer activity, Biomaterials 101 (2016) 296–309.
[72] L. Hrdlička, P. Šrámková, J. Prousek, J. Kronek, Environmental toxicity study of poly(2-oxazoline)s, Chem. Pap. (2018) 1–5.
[73] O.O.N. Yön, C. Akbulut, Ovarian follicle structure of zebrafish (Danio rerio Hamilton) after poly(2-ethyl-2-oxazoline) exposure, Indian J. Exp. Biol. 54 (2016) 829–834.
[74] Y.-S. Hwang, P.-R. Chiang, W.-H. Hong, C.-C. Chiao, I.-M. Chu, G.-H. Hsiue, C.-R. Shen, Study *in vivo* intraocular biocompatibility of *in situ* gelation hydrogels: poly(2-ethyl oxazoline)-*block*-poly(ecaprolactone)-*block*-poly(2-ethyl oxazoline) copolymer, Matrigel and pluronic F127, PLoS One 8 (7) (2013), e67495.
[75] V. Kumar, D.S. Kalonia, Removal of peroxides in polyethylene glycols by vacuum drying: implications in the stability of biotech and pharmaceutical formulations, AAPS PharmSciTech 7 (3) (2006) 62.
[76] T.X. Viegas, M.D. Bentley, J.M. Harris, Z. Fang, K. Yoon, B. Dizman, R. Weimer, A. Mero, G. Pasut, F.M. Veronese, Polyoxazoline: chemistry, properties, and applications in drug delivery, Bioconjugate Chem. 22 (5) (2011) 976–986.
[77] J. Ulbricht, R. Jordan, R. Luxenhofer, On the biodegradability of polyethylene glycol, polypeptoids and poly(2-oxazoline) s, Biomaterials 35 (17) (2014) 4848–4861.
[78] J. Ulbricht, M. Faust, R. Luxenhofer, Degradation of High Molar Mass Poly(-ethylene Glycol), Poly(2-ethyl-2-oxazoline) and Poly(vinyl Pyrrolidone) by Reactive Oxygen Species, ChemRxiv, 2017, https://doi.org/10.26434/chemrxiv.5358079.v1.

[79] B. Pidhatika, M. Rodenstein, Y. Chen, E. Rakhmatullina, A. Mühlebach, C. Acikgöz, M. Textor, R. Konradi, Comparative stability studies of poly(2-methyl-2-oxazoline) and poly(ethylene glycol) brush coatings, Biointerphases 7 (1–4) (2012) 1–15.

[80] K.P. Luef, C. Petit, B. Ottersböck, G. Oreski, F. Ehrenfeld, B. Grassl, S. Reynaud, F. Wiesbrock, UV-mediated thiol-ene click reactions for the synthesis of drugloadable and degradable gels based on copoly(2-oxazoline)s, Eur. Polym. J. 88 (2017) 701–712.

[81] R. Langer, D.A. Tirrell, Designing materials for biology and medicine, Nature 428 (6982) (2004) 487–492.

[82] J. Groll, T. Boland, T. Blunk, J.A. Burdick, D.-W. Cho, P.D. Dalton, B. Derby, G. Forgacs, Q. Li, V.A. Mironov, Biofabrication: reappraising the definition of an evolving field, Biofabrication 8 (1) (2016), 013001.

[83] J. Kopeček, Hydrogel biomaterials: a smart future? Biomaterials 28 (34) (2007) 5185–5192.

[84] Y. Chujo, Y. Yoshifuji, K. Sada, T. Saegusa, A novel nonionic hydrogel from 2-methyl-2-oxazoline, Macromolecules 22 (3) (1989) 1074–1077.

[85] Y. Chujo, K. Sada, K. Matsumoto, T. Saegusa, Synthesis of nonionic hydrogel, lipogel, and amphigel by copolymerization of 2-oxazolines and a bisoxazoline, Macromolecules 23 (5) (1990) 1234–1237.

[86] Y. Chujo, K. Sada, T. Saegusa, Reversible gelation of polyoxazoline by means of Diels-Alder reaction, Macromolecules 23 (10) (1990) 2636–2641.

[87] Y. Chujo, K. Sada, A. Naka, R. Nomura, T. Saegusa, Synthesis and redox gelation of disulfide-modified polyoxazoline, Macromolecules 26 (5) (1993) 883–887.

[88] Y. Chujo, K. Sada, R. Nomura, A. Naka, T. Saegusa, Photogelation and redox properties of anthracene-disulfide-modified polyoxazolines, Macromolecules 26 (21) (1993) 5611–5614.

[89] Y. Chujo, K. Sada, T. Saegusa, Iron (II) bipyridyl-branched polyoxazoline complex as a thermally reversible hydrogel, Macromolecules 26 (24) (1993) 6315–6319.

[90] Y. Chujo, K. Sada, T. Saegusa, Cobalt (III) bipyridyl-branched polyoxazoline complex as a thermally and redox reversible hydrogel, Macromolecules 26 (24) (1993) 6320–6323.

[91] Y. Imai, H. Itoh, K. Naka, Y. Chujo, Thermally reversible IPN organic-inorganic polymer hybrids utilizing the diels-alder reaction, Macromolecules 33 (12) (2000) 4343–4346.

[92] T.R. Dargaville, J.R. Park, R. Hoogenboom, Poly(2-oxazoline) Hydrogels: State-of-the-Art and Emerging Applications, Macromol. Biosci. (2018), https://doi.org/10.1002/mabi.201800070.

[93] S.R. Peyton, C.B. Raub, V.P. Keschrumrus, A.J. Putnam, The use of poly(-ethylene glycol) hydrogels to investigate the impact of ECM chemistry and mechanics on smooth muscle cells, Biomaterials 27 (28) (2006) 4881–4893.

[94] A. Zahoranová, Z. Kroneková, M. Zahoran, D. Chorvát, I. Janigová, J. Kronek, Poly(2-oxazoline) hydrogels crosslinked with aliphatic bis(2-oxazoline)s: properties, cytotoxicity, and cell cultivation, J. Polym. Sci., Part A: Polym. Chem. 54 (11) (2016) 1548–1559.

[95] P. Šrámková, A. Zahoranová, Z. Kroneková, A. Šišková, J. Kronek, Poly(2-oxazoline) hydrogels by photoinduced thiol-ene "click" reaction using different dithiol crosslinkers, J. Polym. Res. 24 (5) (2017) 82.

[96] T.R. Dargaville, R. Forster, B.L. Farrugia, K. Kempe, L. Voorhaar, U.S. Schubert, R. Hoogenboom, Poly(2-oxazoline) hydrogel monoliths via thiol-ene coupling, Macromol. Rapid Commun. 33 (19) (2012) 1695–1700.

[97] B.L. Farrugia, K. Kempe, U.S. Schubert, R. Hoogenboom, T.R. Dargaville, Poly(2-oxazoline) hydrogels for controlled fibroblast attachment, Biomacromolecules 14 (8) (2013) 2724–2732.

[98] V. Schenk, E. Rossegger, C. Ebner, F. Bangerl, K. Reichmann, B. Hoffmann, M. Höpfner, F. Wiesbrock, RGD-functionalization of poly(2-oxazoline)-based networks for enhanced adhesion to cancer cells, Polymers 6 (2) (2014) 264–279.

[99] P. Anzenbacher, Y.-l. Liu, M.E. Kozelkova, Hydrophilic polymer matrices in optical array sensing, Curr. Opin. Chem. Biol. 14 (6) (2010) 693–704.

[100] D. Guschin, G. Yershov, A. Zaslavsky, A. Gemmell, V. Shick, D. Proudnikov, P. Arenkov, A. Mirzabekov, Manual manufacturing of oligonucleotide, DNA, and protein microchips, Anal. Biochem. 250 (2) (1997) 203–211.

[101] M. Hartlieb, D. Pretzel, K. Kempe, C. Fritzsche, R.M. Paulus, M. Gottschaldt, U.S. Schubert, Cationic poly(2-oxazoline) hydrogels for reversible DNA binding, Soft Matter 9 (18) (2013) 4693–4704.

[102] M. Hartlieb, D. Pretzel, C. Englert, M. Hentschel, K. Kempe, M. Gottschaldt, U.S. Schubert, Matrix supported poly(2-oxazoline)-based hydrogels for DNA catch and release, Biomacromolecules 15 (6) (2014) 1970–1978.

[103] C. Englert, L. Tauhardt, M. Hartlieb, K. Kempe, M. Gottschaldt, U.S. Schubert, Linear poly(ethylene imine)-based hydrogels for effective binding and release of DNA, Biomacromolecules 15 (4) (2014) 1124–1131.

[104] M. Hartlieb, S. Schubert, K. Kempe, N. Windhab, U.S. Schubert, Stabilization of factor VIII by poly(2-oxazoline) hydrogels, J. Polym. Sci., Part A: Polym. Chem. 53 (1) (2015) 10–14.

[105] S. Dech, V. Wruk, C.P. Fik, J.C. Tiller, Amphiphilic polymer conetworks derived from aqueous solutions for biocatalysis in organic solvents, Polymer 53 (3) (2012) 701–707.

[106] I. Schoenfeld, S. Dech, B. Ryabenky, B. Daniel, B. Glowacki, R. Ladisch, J.C. Tiller, Investigations on diffusion limitations of biocatalyzed reactions in amphiphilic polymer conetworks in organic solvents, Biotechnol. Bioeng. 110 (9) (2013) 2333–2342.

[107] I. Sittko, K. Kremser, M. Roth, S. Kuehne, S. Stuhr, J.C. Tiller, Amphiphilic polymer conetworks with defined nanostructure and tailored swelling behavior for exploring the activation of an entrapped lipase in organic solvents, Polymer 64 (2015) 122–129.

[108] K. Naka, T. Nakamura, A. Ohki, S. Maeda, Aggregates of amphiphilic block copolymers derived from poly[(N-acylimino)ethylene]s and their complexes with lipase in water, Polym. J. 27 (11) (1995) 1071–1078.

[109] R. Plothe, I. Sittko, F. Lanfer, M. Fortmann, M. Roth, V. Kolbach, J.C. Tiller, Poly(2-ethyloxazoline) as matrix for highly active electrospun enzymes in organic solvents, Biotechnol. Bioeng. 114 (1) (2017) 39–45.

[110] S. Ross, N. Scoutaris, D. Lamprou, D. Mallinson, D. Douroumis, Inkjet printing of insulin microneedles for transdermal delivery, Drug Deliv. Transl. Res. 5 (4) (2015) 451–461.

[111] A.L. Fisher, J.M. Schollick, D.G. Aarts, M.C. Grossel, Synthesis and gelation properties of poly(2-alkyl-2oxazoline) based thermo-gels, RSC Adv. 6 (71) (2016) 66438–66443.

[112] J.N. Haigh, Y.m. Chuang, B. Farrugia, R. Hoogenboom, P.D. Dalton, T.R. Dargaville, Hierarchically structured porous poly(2-oxazoline) hydrogels, Macromol. Rapid Commun. 37 (1) (2016) 93–99.

[113] G. Hochleitner, T. Jüngst, T.D. Brown, K. Hahn, C. Moseke, F. Jakob, P.D. Dalton, J. Groll, Additive manufacturing of scaffolds with sub-micron filaments via melt electrospinning writing, Biofabrication 7 (3) (2015), 035002.

[114] G. Hochleitner, J.F. Hümmer, R. Luxenhofer, J. Groll, High definition fibrous poly(2-ethyl-2-oxazoline) scaffolds through melt electrospinning writing, Polymer 55 (20) (2014) 5017–5023.

[115] O.I. Kalaoglu-Altan, B. Verbraeken, K. Lava, T.N. Gevrek, R. Sanyal, T. Dargaville, K. De Clerck, R. Hoogenboom, A. Sanyal, Multireactive poly(2-oxazoline) nanofibers through electrospinning with crosslinking on the fly, ACS Macro Lett. 5 (6) (2016) 676–681.

[116] M. Hartlieb, D. Pretzel, M. Wagner, S. Hoeppener, P. Bellstedt, M. Görlach, C. Englert, K. Kempe, U.S. Schubert, Core cross-linked nanogels based on the selfassembly of double hydrophilic poly(2-oxazoline) block copolymers, J. Mater. Chem. B 3 (9) (2015) 1748–1759.

[117] C. Legros, A.-L. Wirotius, M.-C. De Pauw-Gillet, K.C. Tam, D. Taton, S. Lecommandoux, Poly(2-oxazoline)-based nanogels as biocompatible pseudopolypeptide nanoparticles, Biomacromolecules 16 (1) (2014) 183–191.

[118] M. Platen, E. Mathieu, S. Lück, R. Schubel, R. Jordan, S. Pautot, Poly(2-oxazoline)-Based microgel particles for neuronal cell culture, Biomacromolecules 16 (5) (2015) 1516–1524.

[119] M. Hartlieb, T. Bus, J. Kübel, D. Pretzel, S. Hoeppener, M.N. Leiske, K. Kempe, B. Dietzek, U.S. Schubert, Tailoring cellular uptake and fluorescence of poly(2-oxazoline)-based nanogels, Bioconjugate Chem. 28 (4) (2017) 1229–1235.

[120] B. Kostova, K. Ivanova-Mileva, D. Rachev, D. Christova, Study of the potential of amphiphilic conetworks based on poly(2-ethyl-2oxazoline) as new platforms for delivery of drugs with limited solubility, AAPS PharmSciTech 14 (1) (2013) 352–359.

[121] O. Sedlacek, J. Kucka, B.D. Monnery, M. Slouf, M. Vetrik, R. Hoogenboom, M. Hruby, The effect of ionizing radiation on biocompatible polymers: from sterilization to radiolysis and hydrogel formation, Polym. Degrad. Stab. 137 (2017) 1–10.

[122] M.A. Boerman, E. Roozen, M.J. Sánchez-Fernández, A.R. Keereweer, R.P. Félix Lanao, J.C. Bender, R. Hoogenboom, S.C. Leeuwenburgh, J.A. Jansen, H. Van Goor, J.C.M. Van Herst, Next generation hemostatic materials based on NHS-ester functionalized poly(2-oxazoline)s, Biomacromolecules 18 (8) (2017) 2529–2538.

[123] S. Kobayashi, E. Masuda, S. Shoda, Y. Shimano, Synthesis of acryl-and methacryl-type macromonomers and telechelics by utilizing living polymerization of 2-oxazolines, Macromolecules 22 (7) (1989) 2878–2884.

[124] O. Nuyken, G. Maier, A. Groß, H. Fischer, Systematic investigations on the reactivity of oxazolinium salts, Macromol. Chem. Phys. 197 (1) (1996) 83–95.

[125] R. Luxenhofer, R. Jordan, Click chemistry with poly(2-oxazoline)s, Macromolecules 39 (10) (2006) 3509–3516.

[126] A. Gress, A. Völkel, H. Schlaad, Thio-click modification of poly[2-(3-butenyl)-2-oxazoline], Macromolecules 40 (22) (2007) 7928–7933.

[127] G. Orts-Gil, K. Natte, R. Thiermann, M. Girod, S. Rades, H. Kalbe, A.F. Thünemann, M. Maskos, W. Österle, On the role of surface composition and curvature on biointerface formation and colloidal stability of nanoparticles in a protein-rich model system, Colloids Surfaces B Biointerfaces 108 (2013) 110–119.

[128] O. Koshkina, T. Lang, R. Thiermann, D. Docter, R.H. Stauber, C. Secker, H. Schlaad, S. Weidner, B. Mohr, M. Maskos, A. Bertin, Temperature -triggered protein adsorption on polymer-coated nanoparticles in serum, Langmuir 31 (32) (2015) 8873–8881.

[129] M.P. Monopoli, C. Åberg, A. Salvati, K.A. Dawson, Biomolecular coronas provide the biological identity of nanosized materials, Nat. Nanotechnol. 7 (12) (2012) 779.

[130] N. Bertrand, J.-C. Leroux, The journey of a drug-Carrier in the body: an anatomo-physiological perspective, J. Control. Release 161 (2) (2012) 152–163.

[131] P. Wilson, P.C. Ke, T.P. Davis, K. Kempe, Poly(2-oxazoline)-based micro - and nanoparticles: a review, Eur. Polym. J. 88 (2017) 486–515.

[132] M.A. Cole, N.H. Voelcker, H. Thissen, H.J. Griesser, Stimuli-responsive

interfaces and systems for the control of protein – surface and cel l– surface interactions, Biomaterials 30 (9) (2009) 1827–1850.
[133] S. Kurzhals, N. Gal, R. Zirbs, E. Reimhult, Controlled aggregation and cell uptake of thermoresponsive polyoxazoline-grafted superparamagnetic iron oxide nanoparticles, Nanoscale 9 (8) (2017) 2793–2805.
[134] N. Gal, A. Lassenberger, L. Herrero-Nogareda, A. Scheberl, V. Charwat, C. Kasper, E. Reimhult, Interaction of size-tailored PEGylated iron oxide nanoparticles with lipid membranes and cells, ACS Biomater. Sci. Eng. 3 (3) (2017) 249–259.
[135] O. Koshkina, D. Westmeier, T. Lang, C. Bantz, A. Hahlbrock, C. Würth, U. Resch-Genger, U. Braun, R. Thiermann, C. Weise, M. Eravci, B. Mohr, H. Schlaad, R.H. Stauber, D. Docter, A. Bertin, M. Maskos, Tuning the surface of nanoparticles: impact of poly(2-ethyl-2-oxazoline) on protein adsorption in serum and cellular uptake, Macromol. Biosci. 16 (9) (2016) 1287–1300.
[136] E.D.H. Mansfield, V.R. de la Rosa, R.M. Kowalczyk, I. Grillo, R. Hoogenboom, K. Sillence, P. Hole, A.C. Williams, V.V. Khutoryanskiy, Side chain variations radically alter the diffusion of poly(2-alkyl-2-oxazoline) functionalised nanoparticles through a mucosal barrier, Biomater. Sci. 4 (9) (2016) 1318–1327.
[137] E.D.H. Mansfield, K. Sillence, P. Hole, A.C. Williams, V.V. Khutoryanskiy, POZylation: a new approach to enhance nanoparticle diffusion through mucosal barriers, Nanoscale 7 (32) (2015) 13671–13679.
[138] A. Bernkop-Schnürch, V. Schwarz, S. Steininger, Polymers with thiol groups: a new generation of mucoadhesive polymers? Pharm. Res. 16 (6) (1999) 876–881.
[139] R. Luxenhofer, Polymers and nanomedicine: considerations on variability and reproducibility when combining complex systems, Nanomedicine 10 (20) (2015) 3109–3119.
[140] J.C. Leroux, Editorial: drug delivery: too much complexity, not enough reproducibility? Angew. Chem. Int. Ed. 56 (48) (2017) 15170–15171.
[141] G. Bissadi, R. Weberskirch, Efficient synthesis of polyoxazolin-silica hybrid nanoparticles by using the “grafting-onto” approach, Polym. Chem. 7 (6) (2016) 1271–1280.
[142] G. Bissadi, R. Weberskirch, Formation of polyoxazoline-silica nanoparticles via the surface-initiated cationic polymerization of 2-methyl-2-oxazoline, Polym. Chem. 7 (32) (2016) 5157–5168.
[143] G. Morgese, B. Shirmardi Shaghasemi, V. Causin, M. Zenobi-Wong, S.N. Ramakrishna, E. Reimhult, E.M. Benetti, Next-generation polymer shells for inorganic nanoparticles are highly compact, ultra-dense, and long-lasting cyclic brushes, Angew. Chem. Int. Ed. 56 (16) (2017) 4507–4511.
[144] S.H. Lahasky, X. Hu, D. Zhang, Thermoresponsive poly(α-peptoid)s: tuning the cloud point temperatures by composition and architecture, ACS Macro Lett. 1 (5) (2012) 580–584.
[145] Y. Jung, J.-H. Kim, W.-D. Jang, Linear and cyclic poly(2-isopropyl-2-oxazoline) s for fine control of thermoresponsiveness, Eur. Polym. J. 88 (2017) 605–612.
[146] A.S. Silva, M.C. Silva, S.P. Miguel, V.D. Bonifácio, I.J. Correia, A. Aguiar-Ricardo, Nanogold POxylation: towards always-on fluorescent lung cancer targeting, RSC Adv. 6 (40) (2016) 33631–33635.
[147] A.S. Silva, A.M. Sousa, R.P. Cabral, M.C. Silva, C. Costa, S.P. Miguel, V.D. Bonifácio, T. Casimiro, I.J. Correia, A. Aguiar-Ricardo, Aerosolizable gold nano-in-micro dry powder formulations for theragnosis and lung delivery, Int. J. Pharm. 519 (1) (2017) 240–249.
[148] O. Eckardt, C. Pietsch, O. Zumann, M. von der Lühe, D.S. Brauer, F.H. Schacher, Well-defined SiO2 @P(EtOx-*stat*-EI) core – shell hybrid nanoparticles via sol-gel processes, Macromol. Rapid Commun. 37 (4) (2016) 337–342.
[149] D. Soma, R.-H. Jin, Sub-5 μm balls possessing forest-like poly(methyloxazoline)/polyethyleneimine side chains and templated silica microballs with unusual internal structures, RSC Adv. 7 (58) (2017) 36302–36312.
[150] G. Volet, C. Amiel, Polyoxazoline adsorption on silica nanoparticles mediated by host – guest interactions, Colloids Surf. B: Biointerfaces 91 (2012) 269–273.
[151] G. Morgese, V. Causin, M. Maggini, S. Corrà, S. Gross, E.M. Benetti, Ultrastable suspensions of polyoxazoline-functionalized ZnO single nanocrystals, Chem. Mater. 27 (8) (2015) 2957–2964.
[152] J. Safari, S.F. Masouleh, Z. Zarnegar, A.E. Najafabadi, Water-dispersible Fe3O4 nanoparticles stabilized with a biodegradable amphiphilic copolymer, C. R. Chimie 17 (2) (2014) 151–155.
[153] J. Safari, Z. Zarnegar, S.F. Masoule, A.E. Najafabadi, Aqueous dispersions of iron oxide nanoparticles with linear-dendritic copolymers, Ind. Eng. Chem. Res. 20 (4) (2014) 2389–2393.
[154] H.J. Gabius, H.C. Siebert, S. André, J. Jiménez-Barbero, H. Rüdiger, Chemical biology of the sugar code, Chembiochem 5 (6) (2004) 740–764.
[155] C. Weber, J.A. Czaplewska, A. Baumgaertel, E. Altuntas, M. Gottschaldt, R. Hoogenboom, U.S. Schubert, A sugar decorated macromolecular bottle brush by CarbohydrateInitiated cationic ring-opening polymerization, Macromolecules 45 (1) (2011) 46–55.
[156] L. Tauhardt, D. Pretzel, S. Bode, J.A. Czaplewska, K. Kempe, M. Gottschaldt, U.S. Schubert, Synthesis and *in vitro* activity of platinum containing 2-oxazoline-based glycopolymers, J. Polym. Sci. 52 (18) (2014) 2703–2714.
[157] M.A. Mees, C. Effenberg, D. Appelhans, R. Hoogenboom, Sweet polymers: poly(2-ethyl-2-oxazoline) glycopolymers by reductive amination, Biomacromolecules 17 (12) (2016) 4027–4036.
[158] K. Katagiri, A. Takasu, M. Higuchi, Synthesis of glycopolymer containing cell-penetrating peptides as inducers of recombinant protein expression under the control of lactose operator/repressor systems, Biomacromolecules 17 (5) (2016) 1902–1908.
[159] R. Luxenhofer, Novel Functional Poly(2-oxazoline)s as Potential Carriers for Biomedical Applications, PhD thesis, TU Munich, Garching, 2007.
[160] R. Luxenhofer, M. López-García, A. Frank, H. Kessler, R. Jordan, First poly(2-oxazoline)-peptide conjugate for targeted radionuclide cancer therapy, PMSE Prepr 95 (2006) 283–284.
[161] M. Schmitz, M. Kuhlmann, O. Reimann, C.P.R. Hackenberger, J. Groll, Side-chain cysteine-functionalized poly(2-oxazoline)s for multiple peptide conjugation by native chemical ligation, Biomacromolecules 16 (4) (2015) 1088–1094.
[162] R. Luxenhofer, Y. Han, A. Schulz, J. Tong, Z. He, A.V. Kabanov, R. Jordan, Poly(2-oxazoline)s as polymer therapeutics, Macromol. Rapid Commun. 33 (19) (2012) 1613–1631.
[163] S. Konieczny, C.P. Fik, N.J. Averesch, J.C. Tiller, Organosoluble enzyme conjugates with poly(2-oxazoline)s via pyromellitic acid dianhydride, J. Biotechnol. 159 (3) (2012) 195–203.
[164] M. Miyamoto, K. Naka, M. Shiozaki, Y. Chujo, T. Saegusa, Preparation and enzymatic activity of poly[N-acy1imino)ethylenel]-modified catalase, Macromolecules 23 (13) (1990) 3201–3205.
[165] S. Konieczny, C. Krumm, D. Doert, K. Neufeld, J.C. Tiller, Investigations on the activity of poly(2-oxazoline) enzyme conjugates dissolved in organic solvents, J. Biotechnol. 181 (2014) 55–63.
[166] S. Konieczny, M. Leurs, J.C. Tiller, Polymer enzyme conjugates as chiral ligands for sharpless dihydroxylation of alkenes in organic solvents, Chembiochem 16 (1) (2015) 83–90.
[167] X. Yi, M.C. Zimmerman, R. Yang, J. Tong, S. Vinogradov, A.V. Kabanov, Pluronic-modified superoxide dismutase 1 attenuates angiotensin II-induced increase in intracellular superoxide in neurons, Free Radical Biol. Med. 49 (4) (2010) 548–558.
[168] X. Yi, E. Batrakova, W.A. Banks, S. Vinogradov, A.V. Kabanov, Protein conjugation with amphiphilic block copolymers for enhanced cellular delivery, Bioconjugate Chem. 19 (5) (2008) 1071–1077.
[169] J. Tong, X. Yi, R. Luxenhofer, W.A. Banks, R. Jordan, M.C. Zimmerman, A.V. Kabanov, Conjugates of superoxide dismutase 1 with amphiphilic Poly(2oxazoline) block copolymers for enhanced brain delivery: synthesis, characterization and evaluation in vitro and in vivo, Mol. Pharmaceutics 10 (1) (2012) 360–377.
[170] A. Mero, Z. Fang, G. Pasut, F.M. Veronese, T.X. Viegas, Selective conjugation of poly(2-ethyl 2-oxazoline) to granulocyte colony stimulating factor, J. Control. Release 159 (3) (2012) 353–361.
[171] C. Maullu, D. Raimondo, F. Caboi, A. Giorgetti, M. Sergi, M. Valentini, G. Tonon, A. Tramontano, Site-directed enzymatic PEGylation of the human granulocyte colony-stimulating factor, FEBS J. 276 (22) (2009) 6741–6750.
[172] J.F. Nawroth, J.R. McDaniel, A. Chilkoti, R. Jordan, R. Luxenhofer, Maleimide-functionalized poly(2-oxazoline)s and their conjugation to elastin-like polypeptides, Macromol. Biosci. 16 (3) (2016) 322–333.
[173] G.G. Alvaradejo, M. Glassner, R. Hoogenboom, G. Delaittre, Maleimide end-functionalized poly(2-oxazoline)s by the functional initiator route: synthesis and (bio) conjugation, RSC Adv. 8 (17) (2018) 9471–9479.
[174] T. Lühmann, M. Schmidt, M.N. Leiske, V. Spieler, T.C. Majdanski, M. Grube, M. Hartlieb, I. Nischang, S. Schubert, U.S. Schubert, L. Meinel, Site-specific POxylation of Interleukin4, ACS Biomater. Sci. Eng. 3 (3) (2017) 304–312.
[175] M. Hijazi, C. Krumm, S. Cinar, L. Arns, W. Alachraf, W. Hiller, W. Schrader, R. Winter, J.C. Tiller, Entropically driven polymeric enzyme inhibitors by end-group directed conjugation, Chem. Eur. J. 24 (18) (2018) 4523–4527.
[176] C.A. Naumann, O. Prucker, T. Lehmann, J. Rühe, W. Knoll, C.W. Frank, The polymer-supported phospholipid bilayer: tethering as a new approach to substrate – membrane stabilization, Biomacromolecules 3 (1) (2002) 27–35.
[177] R. Jordan, K. Graf, H. Riegler, K.K. Unger, Polymer-supported alkyl monolayers on silica: synthesis and self-assembly of terminal functionalized poly(N-propionylethy1enimine)s, Chem. Commun. (9) (1996) 1025–1026.
[178] M. Foreman, J. Coffman, M. Murcia, S. Cesana, R. Jordan, G. Smith, C. Naumann, Gelation of amphiphilic lipopolymers at the air - water interface: 2D analogue to 3D gelation of colloidal systems with grafted polymer chains? Langmuir 19 (2) (2003) 326–332.
[179] R. Hoogenboom, Poly(2-oxazoline)s: a polymer class with numerous potential applications, Angew. Chem. Int. Ed. 48 (43) (2009) 7978–7994.
[180] R. Hoogenboom, H. Schlaad, Bioinspired poly(2-oxazoline)s, Polymers 3 (1) (2011) 467–488.
[181] V.R. de la Rosa, Poly(2-oxazoline)s as materials for biomedical applications, J. Mater. Sci. Mater. Med. 25 (5) (2014) 1211–1225.
[182] H. Xu, M. Hu, X. Yu, Y. Li, Y. Fu, X. Zhou, D. Zhang, J. Li, Design and evaluation of pH-sensitive liposomes constructed by poly(2-ethyl-2-oxazoline)-cholesterol hemisuccinate for doxorubicin delivery, Eur. J. Pharm. Biopharm. 91 (2015) 66–74.
[183] H. Xu, W. Zhang, Y. Li, F.F. Ye, P.P. Yin, X. Yu, M.N. Hu, Y.S. Fu, C. Wang, D.J. Shang, The bifunctional liposomes constructed byPoly(2-ethyl-oxazoline)-cholesteryl methyl carbonate: an Effectual approach to enhance liposomal circulation time, pH-sensitivity and endosomal escape, Pharm. Res. (N. Y.) 31 (11) (2014) 3038–3050.
[184] N. Pippa, E. Kaditi, S. Pispas, C. Demetzos, DPPC/poly(2-methyl-2-oxazoline)-grad-poly(2-phenyl-2-oxazoline) chimeric nanostructures as potential drug nanocarriers, J. Nanopart. Res. 15 (6) (2013) 1685.
[185] N. Pippa, M. Merkouraki, S. Pispas, C. Demetzos, DPPC:MPOx chimeric advanced Drug Delivery nano Systems (chi-aDDnSs): physicochemical and

structural characterization, stability and drug release studies, Int. J. Pharm. 450 (1–2) (2013) 1–10.
[186] N. Pippa, A. Dokoumetzidis, S. Pispas, C. Demetzos, The interplay between the rate of release from polymer grafted liposomes and their fractal morphology, Int. J. Pharm. 465 (1–2) (2014) 63–69.
[187] N. Pippa, S. Pispas, C. Demetzos, The metastable phases as modulators of biophysical behavior of liposomal membranes, J. Therm. Anal. Calorim. 120 (1) (2015) 937–945.
[188] G. Xia, Z. An, Y. Wang, C. Zhao, M. Li, Z. Li, J. Ma, Synthesis of a novel polymeric material folate-poly(2-ethyl-2-oxazoline)-distearoyl phosphatidyl Ethanolamine tri-block polymer for dual receptor and pH-sensitive targeting liposome, Chem. Pharm. Bull. 61 (4) (2013) 390–398.
[189] L. Hespel, A. El Asmar, G. Morandi, L. Lecamp, L. Picton, F. Burel, Synthesis of dual-sensitive core cross-linked mixed micelles through thiol–ene addition and subsequent drug release behavior, Macromol. Chem. Phys. 218 (15) (2017).
[190] E. Sackmann, Supported membranes: scientific and practical applications, Science 271 (1996) 43–48.
[191] M. Tanaka, E. Sackmann, Polymer-supported membranes as models of the cell surface, Nature 437 (2005) 656–663.
[192] O. Purrucker, A. Förtig, R. Jordan, M. Tanaka, Supported membranes with well-defined polymer tethers – incorporation of cell receptors, ChemPhysChem 5 (3) (2004) 327–335.
[193] A. Förtig, R. Jordan, K. Graf, G. Schiavon, O. Purrucker, M. Tanaka, Solid-supported Biomimetic Membranes with Tailored Lipopolymer Tethers, Macromolecular Symposia, Wiley Online Library, 2004, pp. 329–338.
[194] O. Purrucker, A. Förtig, K. Lüdtke, R. Jordan, M. Tanaka, Confinement of transmembrane cell receptors in tunable stripe micropatterns, J. Am. Chem. Soc. 127 (4) (2005) 1258–1264.
[195] K. Lüdtke, R. Jordan, P. Hommes, O. Nuyken, C.A. Naumann, Lipopolymers from new 2-substituted-2-oxazolines for artificial cell membrane constructs, Macromol. Biosci. 5 (5) (2005) 384–393.
[196] O. Purrucker, A. Förtig, R. Jordan, E. Sackmann, M. Tanaka, Control of frictional coupling of transmembrane cell receptors in model cell membranes with linear polymer spacers, Phys. Rev. Lett. 98 (7) (2007), 078102.
[197] O. Purrucker, S. Gönnenwein, A. Förtig, R. Jordan, M. Rusp, M. Bärmann, L. Moroder, E. Sackmann, M. Tanaka, Polymer-tethered membranes as quantitative models for the study of integrin-mediated cell adhesion, Soft Matter 3 (3) (2007) 333–336.
[198] S. Garg, J. Rühe, K. Lüdtke, R. Jordan, C.A. Naumann, Domain registration in raft-mimicking lipid mixtures studied using polymer-tethered lipid bilayers, Biophys. J. 92 (4) (2007) 1263–1270.
[199] K. Lüdtke, R. Jordan, N. Furr, S. Garg, K. Forsythe, C.A. Naumann, Two-dimensional center-of-mass diffusion of lipid-tethered poly(2-methyl-2-oxazoline) at the air – water interface studied at the single molecule level, Langmuir 24 (10) (2008) 5580–5584.
[200] M.A. Deverall, S. Garg, K. Lüdtke, R. Jordan, J. Rühe, C.A. Naumann, Transbilayer coupling of obstructed lipid diffusion in polymer-tethered phospholipid bilayers, Soft Matter 4 (9) (2008) 1899–1908.
[201] A.P. Siegel, M.J. Murcia, M. Johnson, M. Reif, R. Jordan, J. Rühe, C.A. Naumann, Compartmentalizing a lipid bilayer by tuning lateral stress in a physisorbed polymer-tethered membrane, Soft Matter 6 (12) (2010) 2723–2732.
[202] A.P. Siegel, A. Kimble-Hill, S. Garg, R. Jordan, C.A. Naumann, Native ligands change integrin sequestering but not oligomerization in raft-mimicking lipid mixtures, Biophys. J. 101 (7) (2011) 1642–1650.
[203] N.F. Hussain, A.P. Siegel, Y. Ge, R. Jordan, C.A. Naumann, Bilayer asymmetry influences integrin sequestering in raft-mimicking lipid mixtures, Biophys. J. 104 (10) (2013) 2212–2221.
[204] Y. Ge, A.P. Siegel, R. Jordan, C.A. Naumann, Ligand binding alters dimerization and sequestering of urokinase receptors in raft-mimicking lipid mixtures, Biophys. J. 107 (9) (2014) 2101–2111.
[205] Y. Ge, J. Gao, R. Jordan, C.A. Naumann, Changes in cholesterol level alter integrin sequestration in raft-mimicking lipid mixtures, Biophys. J. 114 (1) (2018) 158–167.
[206] H. Jatzkewitz, Über den Einbau physiologisch wirksamer Substanzen in ein kollodiales Blutplasma-Ersatzmittel, Hoppe-Seyleŕ s Zeitschrift für physiologische Chemie 297 (1) (1954) 149–156.
[207] H. Jatzkewitz, An ein kolloidales Blutplasma-Ersatzmittel (Polyvinylpyrrolidon) gebundenes Peptamin (Glycyl-L-leucyl-mezcalin) als neuartige Depotform für biologisch aktive primäre Amine (Mezcalin), Z. Naturforsch. B Chem. Sci. 10 (1) (1955) 27–31.
[208] J. Kopeček, Polymer–drug conjugates: origins, progress to date and future directions, Adv. Drug Deliv. Rev. 65 (1) (2013) 49–59.
[209] D.R. Vogus, V. Krishnan, S. Mitragotri, A review on engineering polymer drug conjugates to improve combination chemotherapy, Curr. Opin. Colloid Interface Sci. 31 (2017) 75–85.
[210] X. Pang, Y. Jiang, Q. Xiao, A.W. Leung, H. Hua, C. Xu, pH-responsive polymer–drug conjugates: design and progress, J. Control. Release 222 (2016) 116–129.
[211] X. Pang, H.-L. Du, H.-Q. Zhang, Y.-J. Zhai, G.-X. Zhai, Polymer–drug conjugates: present state of play and future perspectives, Drug Discov. Today 18 (23) (2013) 1316–1322.
[212] A.A. Natfji, H.M. Osborn, F. Greco, Feasibility of polymer-drug conjugates for non-cancer applications, Curr. Opin. Colloid Interface Sci. 31 (2017) 51–66.
[213] Q. Feng, R. Tong, Anticancer Nanoparticulate Polymer-drug Conjugate, Bioeng. Transl. Med. 1 (3) (2016) 277–296.
[214] K.L. Eskow Jaunarajs, D.G. Standaert, T.X. Viegas, M.D. Bentley, Z. Fang, B. Dizman, K. Yoon, R. Weimer, P. Ravenscroft, T.H. Johnston, M.P. Hill, J.M. Brotchie, R.W. Moreadith, Rotigotine polyoxazoline conjugate SER-214 provides robust and sustained antiparkinsonian benefit, Mov. Disord. 28 (12) (2013) 1675–1682.
[215] R.M. England, J.I. Hare, J. Barnes, J. Wilson, A. Smith, N. Strittmatter, P.D. Kemmitt, M.J. Waring, S.T. Barry, C. Alexander, M.B. Ashford, Tumour regression and improved gastrointestinal tolerability from controlled release of SN-38 from novel polyoxazoline-modified dendrimers, J. Control. Release 247 (2017) 73–85.
[216] M. Schmidt, S. Harmuth, E.R. Barth, E. Wurm, R. Fobbe, A. Sickmann, C. Krumm, J.C. Tiller, Conjugation of ciprofloxacin with poly (2-oxazoline) s and polyethylene glycol via end groups, Bioconjugate Chem. 26 (9) (2015) 1950–1962.
[217] M. Schmidt, L.K. Bast, F. Lanfer, L. Richter, E. Hennes, R. Seymen, C. Krumm, J.C. Tiller, Poly(2-oxazoline) – antibiotic conjugates with penicillins, Bioconjugate Chem. 28 (9) (2017) 2440–2451.
[218] O. Sedlacek, B.D. Monnery, J. Mattova, J. Kucka, J. Panek, O. Janouskova, A. Hocherl, B. Verbraeken, M. Vergaelen, M. Zadinova, R. Hoogenboom, M. Hruby, Poly(2-ethyl-2-oxazoline) conjugates with doxorubicin for cancer therapy: *In vitro* and *in vivo* evaluation and direct comparison to poly[N-(2-hydroxypropyl)methacrylamide] analogues, Biomaterials 146 (2017) 1–12.
[219] K. Kanazaki, K. Sano, A. Makino, T. Homma, M. Ono, H. Saji, Polyoxazoline multivalently conjugated with indocyanine green for sensitive *in vivo* photoacoustic imaging of tumors, Sci. Rep. 6 (2016), 33798.
[220] K. Sano, Y. Kanada, K. Kanazaki, N. Ding, M. Ono, H. Saji, Brachytherapy with intratumoral injections of RadiometalLabeled polymers that thermoresponsively self-aggregate in tumor tissues, J. Nucl. Med. 58 (9) (2017) 1380–1385.
[221] L. Loukotová, J. Kučka, M. Rabyk, A. Höcherl, K. Venclíková, O. Janoušková, P. Páral, V. Kolářová, T. Heizer, L. Šefc, P. Štěpánek, M. Hrubý, Thermoresponsive β-glucan-based polymers for bimodal immunoradiotherapy – are they able to promote the immune system? J. Control. Release 268 (2017) 78–91.
[222] C.J. Waschinski, J.C. Tiller, Poly(oxazoline)s with telechelic antimicrobial functions, Biomacromolecules 6 (1) (2005) 235–243.
[223] C.J. Waschinski, V. Herdes, F. Schueler, J.C. Tiller, Influence of satellite groups on telechelic antimicrobial functions of polyoxazolines, Macromol. Biosci. 5 (2) (2005) 149–156.
[224] C.J. Waschinski, S. Barnert, A. Theobald, R. Schubert, F. Kleinschmidt, A. Hoffmann, K. Saalwächter, J.C. Tiller, Insights in the antibacterial action of poly(methyloxazoline)s with a biocidal end group and varying satellite groups, Biomacromolecules 9 (7) (2008) 1764–1771.
[225] C.P. Fik, C. Krumm, C. Muennig, T.I. Baur, U. Salz, T. Bock, J.C. Tiller, Impact of functional satellite groups on the antimicrobial activity and hemocompatibility of telechelic poly(2-methyloxazoline)s, Biomacromolecules 13 (1) (2011) 165–172.
[226] C. Krumm, S. Harmuth, M. Hijazi, B. Neugebauer, A.L. Kampmann, H. Geltenpoth, A. Sickmann, J.C. Tiller, Antimicrobial poly(2-methyloxazoline)s with bioswitchable activity through satellite group modification, Angew. Chem. Int. Ed. 53 (15) (2014) 3830–3834.
[227] C. Krumm, M. Hijazi, S. Trump, S. Saal, L. Richter, G.G.F.K. Noschmann, T.-D. Nguyen, K. Preslikoska, T. Moll, J.C. Tiller, Highly active and selective telechelic antimicrobial poly(2-oxazoline) copolymers, Polymer 118 (2017) 107–115.
[228] C. Martins, V.G. Correia, A. Aguiar-Ricardo, Â. Cunha, M.G.M. Moutinho, Antimicrobial activity of new green-functionalized oxazoline-based oligomers against clinical isolates, SpringerPlus 4 (1) (2015) 382.
[229] L. Richter, M. Hijazi, F. Arfeen, C. Krumm, J.C. Tiller, Telechelic, Antimicrobial Hydrophilic Polycations with Two Modes of Action, Macromol. Biosci. 18 (4) (2018), 1700389.
[230] E. Vlassi, A. Papagiannopoulos, S. Pispas, Amphiphilic poly(2-oxazoline) copolymers as self-assembled carriers for drug delivery applications, Eur. Polym. J. 88 (2017) 516–523.
[231] O. Policianova, J. Brus, M. Hruby, M. Urbanova, *In vitro* dissolution study of acetylsalicylic acid solid dispersions. Tunable drug release allowed by the choice of polymer matrix, Pharmaceut. Dev. Technol. 20 (8) (2015) 935–940.
[232] O. Policianova, J. Brus, M. Hruby, M. Urbanova, A. Zhigunov, J. Kredatusova, L. Kobera, Structural diversity of solid dispersions of acetylsalicylic acid as seen by solid-state NMR, Mol. Pharm. 11 (2) (2014) 516–530.
[233] B. Claeys, A. Vervaeck, C. Vervaet, J.P. Remon, R. Hoogenboom, B.G. De Geest, Poly(2-ethyl-2-oxazoline) as matrix excipient for drug formulation by hot melt extrusion and injection molding, Macromol. Rapid Commun. 33 (19) (2012) 1701–1707.
[234] R. Luxenhofer, A. Schulz, C. Roques, S. Li, T.K. Bronich, E.V. Batrakova, R. Jordan, A.V. Kabanov, Doubly amphiphilic poly(2-oxazoline)s as high-capacity delivery systems for hydrophobic drugs, Biomaterials 31 (18) (2010) 4972–4979.
[235] A. Schulz, S. Jaksch, R. Schubel, E. Wegener, Z. Di, Y. Han, A. Meister, J.r. Kressler, A.V. Kabanov, R. Luxenhofer, C.M. Papadakis, R. Jordan, Drug-induced morphology switch in drug delivery systems based on poly(2-oxazoline)s, ACS Nano 8 (3) (2014) 2686–2696.
[236] S. Jaksch, A. Schulz, Z. Di, R. Luxenhofer, R. Jordan, C.M. Papadakis, Amphiphilic triblock copolymers from poly(2-oxazoline) with different

hydrophobic blocks: changes of the micellar structures upon addition of a strongly hydrophobic cancer drug, Macromol. Chem. Phys. 217 (13) (2016) 1448–1456.
[237] Y. Shi, M.J. van Steenbergen, E.A. Teunissen, L. Novo, S. Gradmann, M. Baldus, C.F. van Nostrum, W.E. Hennink, Π–Π stacking increases the stability and loading capacity of thermosensitive polymeric micelles for chemotherapeutic drugs, Biomacromolecules 14 (6) (2013) 1826–1837.
[238] Z. He, A. Schulz, X. Wan, J. Seitz, H. Bludau, D.Y. Alakhova, D.B. Darr, C.M. Perou, R. Jordan, I. Ojima, A.V. Kabanov, R. Luxenhofer, Poly(2-oxazoline) based micelles with high capacity for 3rd generation taxoids: preparation, in vitro and in vivo evaluation, J. Control. Release 208 (2015) 67–75.
[239] Y. Seo, A. Schulz, Y. Han, Z. He, H. Bludau, X. Wan, J. Tong, T.K. Bronich, M. Sokolsky, R. Luxenhofer, R. Jordan, A.V. Kabanov, Poly(2-oxazoline) block copolymer based formulations of taxanes: effect of copolymer and drug structure, concentration, and environmental factors, Polym. Adv. Technol. 26 (7) (2015) 837–850.
[240] N. Engelhardt, A. Ernst, A.L. Kampmann, R. Weberskirch, Synthesis and characterization of surface functional polymer nanoparticles by a bottom-up approach from tailor-made amphiphilic block copolymers, Macromol. Chem. Phys. 214 (24) (2013) 2783–2791.
[241] A. Schulz, Investigation of Structure-property Relationships of Poly(2-oxazoline) Based Drug Delivery Systems, PhD Thesis, TU Dresden, Dresden, 2014.
[242] H.-C. Shin, A.W.G. Alani, D.A. Rao, N.C. Rockich, G.S. Kwon, Multi - drug loaded polymeric micelles for simultaneous delivery of poorly soluble anticancer drugs, J. Control. Release 140 (3) (2009) 294–300.
[243] H.-C. Shin, A.W.G. Alani, H. Cho, Y. Bae, J.M. Kolesar, G.S. Kwon, A 3-in-1 polymeric micelle nanocontainer for poorly water-soluble drugs, Mol. Pharm. 8 (4) (2011) 1257–1265.
[244] Y. Han, Z. He, A. Schulz, T.K. Bronich, R. Jordan, R. Luxenhofer, A.V. Kabanov, Synergistic combinations of multiple chemotherapeutic agents in high capacity poly(2-oxazoline) micelles, Mol. Pharm. 9 (8) (2012) 2302–2313.
[245] X. Wan, Y. Min, H. Bludau, A. Keith, S.S. Sheiko, R. Jordan, A.Z. Wang, M. Sokolsky-Papkov, A.V. Kabanov, Drug combination synergy in worm-like polymeric micelles improves treatment outcome for small cell and non-small cell lung cancer, ACS Nano 12 (3) (2018) 2426–2439.
[246] X. Qu, Y. Zou, Y. Jin, Y. Zhou, Z. Wang, C. He, Y. Deng, X. Li, Y. Zhou, Y. Liu, Preparation and *in vitro* characterization of paclitaxel-loaded pH-responsive polymeric micelles based on poly(2-ethyl-2-oxazoline)-vitamin E succinate, J. Chin. Pharm. Sci. 26 (8) (2017) 582–588.
[247] M. Pfister, A. Ringhand, C. Fetsch, R. Luxenhofer, Poly(2-ethyl-2-oxazoline-co-N-propylethylene Imine)s by Controlled Partial Reduction of Poly(2-ethyl-2-oxazoline), ChemRxiv, 2018, https://doi.org/10.26434/chemrxiv.5786853.v1.
[248] P. Zhang, X. Qian, Z. Zhang, C. Li, C. Xie, W. Wu, X. Jiang, Supramolecular amphiphilic polymer-based micelles with seven-armed polyoxazoline coating for drug delivery, ACS Appl. Mater. Interfaces 9 (7) (2017) 5768–5777.
[249] J.B. Baell, Feeling Nature's PAINS: natural products, natural product drugs, and Pan assay interference compounds (PAINS), J. Nat. Prod. 79 (3) (2016) 616–628.
[250] M.A.W. Jonathan Baell, Chemical con artists foil drug discovery, Nature 513 (2014) 481–483.
[251] B. Rasolonjatovo, J.-P. Gomez, W. Même, C. Goncalves, C.c. Huin, V. Bennevault-Celton, T. Le Gall, T. Montier, P. Lehn, H. Cheradame, P. Midoux, P. Guégan, Poly(2-methyl-2-oxazoline)-b-poly(tetrahydrofuran)-b-poly(2-methyl-2-oxazoline) Amphiphilic Triblock Copolymers: Synthesis, Physicochemical characterizations, and hydrosolubilizing properties, Biomacromolecules 16 (3) (2015) 748–756.
[252] C. Gonçalves, J.-P. Gomez, W. Même, B. Rasolonjatovo, D. Gosset, S. Nedellec, P. Hulin, C. Huin, T. Le Gall, T. Montier, P. Lehn, C. Pichon, P. Guégan, H. Cheradame, P. Midoux, Curcumin/poly(2-methyl-2-oxazoline-b-tetrahydrofuran-b-2-methyl-2-oxazoline) formulation: an improved penetration and biological effect of curcumin in F508del-CFTR cell lines, Eur. J. Pharm. Biopharm. 117 (2017) 168–181.
[253] R. Raveendran, K.M. Mullen, R.M. Wellard, C.P. Sharma, R. Hoogenboom, T.R. Dargaville, Poly(2-oxazoline) block copolymer nanoparticles for curcumin loading and delivery to cancer cells, Eur. Polym. J. 96 (2017) 682–694.
[254] L. Hahn, M.M. Lübtow, T. Lorson, R. Schobert, R. Luxenhofer, Investigating the Influence of Aromatic Moieties on the Formulation of Hydrophobic Natural Products and Drugs in Poly(2-oxazoline) Based Amphiphiles, Biomacromolecules (2018), https://doi.org/10.1021/acs.biomac.8b00708 in print.
[255] K. Knop, D. Pretzel, A. Urbanek, T. Rudolph, D.H. Scharf, A. Schallon, M. Wagner, S. Schubert, M. Kiehntopf, A.A. Brakhage, F.H. Schacher, U.S. Schubert, Star-shaped drug carriers for doxorubicin with POEGMA and POEtOxMA brush-like shells: a structural, physical, and biological comparison, Biomacromolecules 14 (8) (2013) 2536–2548.
[256] K.Y. Peng, S.W. Wang, R.S. Lee, Amphiphilic Diblock Copolymers Based on Poly(2-ethyl-2-oxazoline) and Poly(4-substituted-e-caprolactone): synthesis, Characterization, and Cellular Uptake, J. Polym. Sci. 51 (13) (2013) 2769–2781.
[257] M. Haktaniyan, S. Atilla, E. Cagli, I. Erel-Goktepe, pH- and temperature-induced release of doxorubicin from multilayers of poly(2-isopropyl-2-oxazoline) and tannic acid, Polym. Int. 66 (12) (2017) 1851–1863.
[258] M. Romio, G. Morgese, L. Trachsel, S. Babity, C. Paradisi, D. Brambilla, E.M. Benetti, Poly(2-oxazoline)-Pterostilbene block-copolymer nanoparticles for dual-anticancer drug delivery, Biomacromolecules 19 (1) (2017) 103–111.
[259] C. von der Ehe, K. Kempe, M. Bauer, A. Baumgaertel, M.D. Hager, D. Fischer, U.S. Schubert, Star-shaped block copolymers by copper-catalyzed azide-alkyne cycloaddition for potential drug delivery applications, Macromol. Chem. Phys. 213 (20) (2012) 2146–2156.
[260] M. Hartlieb, T. Floyd, A.B. Cook, C. Sanchez-Cano, S. Catrouillet, J.A. Burns, S. Perrier, Well-defined hyperstar copolymers based on a thiol–yne hyperbranched core and a poly(2-oxazoline) shell for biomedical applications, Polym. Chem. 8 (13) (2017) 2041–2054.
[261] S. Jana, A. Saha, T.K. Paira, T.K. Mandal, Synthesis and self-aggregation of poly(2-ethyl-2-oxazoline)-based photocleavable block copolymer: micelle, compound micelle, reverse micelle, and dye encapsulation/release, J. Phys. Chem. B 120 (4) (2016) 813–824.
[262] R.B. Restani, A.S. Silva, R.F. Pires, R. Cabral, I.J. Correia, T. Casimiro, V.D. Bonifácio, A. Aguiar-Ricardo, Nano-in-Micro POxylated polyurea dendrimers and chitosan dry powder formulations for pulmonary delivery, Part. Part. Syst. Char. 33 (11) (2016) 851–858.
[263] P. Zhang, K. Yuan, C. Li, X. Zhang, W. Wu, X. Jiang, Cisplatin-rich poly-oxazoline – poly(aspartic acid) supramolecular nanoparticles, Macromol. Biosci. 17 (12) (2017), 1700206.
[264] B. Kostova, S. Ivanova, K. Balashev, D. Rachev, D. Christova, Evaluation of poly(2-ethyl-2-oxazoline) containing copolymer networks of varied composition as sustained metoprolol tartrate delivery systems, AAPS PharmSciTech 15 (4) (2014) 939–946.
[265] L.-C.S. Huang, W.-Y. Hsieh, J.-Y. Chen, S.-C. Huang, J.-K. Chen, M.-H. Hsu, Drug delivery system design and development for boron neutron capture therapy on cancer treatment, Appl. Radiat. Isot. 88 (2014) 89–93.
[266] P. Baumann, M. Spulber, I.A. Dinu, C.G. Palivan, Cellular trojan horse based polymer nanoreactors with light sensitive activity, J. Phys. Chem. B 118 (31) (2014) 9361–9370.
[267] D. Mahata, M. Jana, A. Jana, A. Mukherjee, N. Mondal, T. Saha, S. Sen, G.B. Nando, C.K. Mukhopadhyay, R. Chakraborty, S.M. Mandal, Lignin-*graft*-Polyoxazoline conjugated triazole a novel anti-Infective ointment to control persistent inflammation, Sci. Rep. 7 (2017) 46412.
[268] M.M. Lübtow, L. Keßler, T. Lorson, N. Gangloff, M. Kirsch, S. Dahms, R. Luxenhofer, More Is Less: Curcumin and Paclitaxel Formulations Using Poly(2-Oxazoline) and Poly(2-Oxazine) Based Amphiphiles Bearing Linear and Branched C9 Side Chains, ChemRxiv (2018), https://doi.org/10.26434/chemrxiv.5883109.v1.
[269] Z. Wang, X. Li, D. Wang, Y. Zou, X. Qu, C. He, Y. Deng, Y. Jin, Y. Zhou, Y. Zhou, Y. Liu, Concurrently suppressing multidrug resistance and metastasis of breast cancer by co-delivery of paclitaxel and honokiol with pH-sensitive polymeric micelles, Acta Biomater. 62 (2017) 144–156.
[270] D. Wang, Y. Zhou, X. Li, X. Qu, Y. Deng, Z. Wang, C. He, Y. Zou, Y. Jin, Y. Liu, Mechanisms of pH-sensitivity and cellular internalization of PEOz-b-PLA micelles with varied hydrophilic/hydrophobic ratios and intracellular trafficking routes and fate of the copolymer, ACS Appl. Mater. Interfaces 9 (8) (2017) 6916–6930.
[271] Y.H. Bae, K. Park, Targeted drug delivery to tumors: myths, reality and possibility, J. Contr. Release 153 (3) (2011) 198–205.
[272] K. Strebhardt, A. Ullrich, Paul Ehrlich's magic bullet concept: 100 years of progress, Nat. Rev. Canc. 8 (6) (2008) 473–480.
[273] C.S. Kue, A. Kamkaew, K. Burgess, L.V. Kiew, L.Y. Chung, H.B. Lee, Small molecules for active targeting in cancer, Med. Res. Rev. 36 (3) (2016) 494–575.
[274] R. Bazak, M. Houri, S. El Achy, W. Hussein, T. Refaat, Passive targeting of nanoparticles to cancer: a comprehensive review of the literature, Mol. Clin. Oncol. 2 (6) (2014) 904–908.
[275] S. Wilhelm, A.J. Tavares, Q. Dai, S. Ohta, J. Audet, H.F. Dvorak, W.C.W. Chan, Analysis of nanoparticle delivery to tumours, Nat. Rev. Mater. 1 (2016) 16014.
[276] A. Magarkar, T. Róg, A. Bunker, A computational study suggests that replacing PEG with PMOZ may increase exposure of hydrophobic targeting moiety, Eur. J. Pharmaceut. Sci. 103 (2017) 128–135.
[277] G.L. Zwicke, G. Ali Mansoori, C.J. Jeffery, Utilizing the folate receptor for active targeting of cancer nanotherapeutics, Nano Rev. 3 (1) (2012) 18496.
[278] L.-Y. Qiu, L. Yan, L. Zhang, Y.-M. Jin, Q.-H. Zhao, Folate-modified poly(2-ethyl-2-oxazoline) as hydrophilic corona in polymeric micelles for enhanced intracellular doxorubicin delivery, Int. J. Pharm. 456 (2) (2013) 315–324.
[279] A.-L. Kampmann, T. Grabe, C. Jaworski, R. Weberskirch, Synthesis of well-defined core–shell nanoparticles based on bifunctional poly(2-oxazoline) macromonomer surfactants and a microemulsion polymerization process, RSC Adv. 6 (102) (2016) 99752–99763.
[280] Y. Chen, W. Cao, J. Zhou, B. Pidhatika, B. Xiong, L. Huang, Q. Tian, Y. Shu, W. Wen, I.-M. Hsing, H. Wu, Poly(l-lysine)-graft-folic acid-coupled poly(2-methyl-2-oxazoline)(PLL-g-PMOXA-c-FA): a bioactive copolymer for specific targeting to folate receptor-positive cancer cells, ACS Appl. Mater. Interfaces 7 (4) (2015) 2919–2930.
[281] P. Figueiredo, V. Balasubramanian, M.-A. Shahbazi, A. Correia, D. Wu, C.G. Palivan, J.T. Hirvonen, H.A. Santos, Angiopep2-functionalized polymersomes for targeted doxorubicin delivery to glioblastoma cells, Int. J. Pharm.

511 (2) (2016) 794–803.
[282] Y. Gao, Y. Li, Y. Li, L. Yuan, Y. Zhou, J. Li, L. Zhao, C. Zhang, X. Li, Y. Liu, PSMA-mediated endosome escape-accelerating polymeric micelles for targeted therapy of prostate cancer and the real time tracing of their intracellular trafficking, Nanoscale 7 (2) (2015) 597–612.
[283] Y. Gao, C. Zhang, Y. Zhou, J. Li, L. Zhao, Y. Li, Y. Liu, X. Li, Endosomal pH-responsive polymer-based dual-ligand-modified micellar nanoparticles for tumor targeted delivery and facilitated intracellular release of paclitaxel, Pharm. Res. (N. Y.) 32 (8) (2015) 2649–2662.
[284] Y. Gao, Y. Zhou, L. Zhao, C. Zhang, Y. Li, J. Li, X. Li, Y. Liu, Enhanced antitumor efficacy by cyclic RGDyK-conjugated and paclitaxel-loaded pH-responsive polymeric micelles, Acta Biomater. 23 (2015) 127–135.
[285] Y. Zhao, Y. Zhou, D. Wang, Y. Gao, J. Li, S. Ma, L. Zhao, C. Zhang, Y. Liu, X. Li, pH-responsive polymeric micelles based on poly(2-ethyl-2-oxazoline)poly(D,L-lactide) for tumor-targeting and controlled delivery of doxorubicin and P-glycoprotein inhibitor, Acta Biomater. 17 (2015) 182–192.
[286] S.T. Gunawan, K. Kempe, T. Bonnard, J. Cui, K. Alt, L.S. Law, X. Wang, E. Westein, G.K. Such, K. Peter, C.E. Hagemeyer, F. Caruso, Multifunctional thrombin-activatable polymer capsules for specifi c targeting to activated platelets, Adv. Mater. 27 (35) (2015) 5153–5157.
[287] J. Bühler, S. Gietzen, A. Reuter, C. Kappel, K. Fischer, S. Decker, D. Schäffel, K. Koynov, M. Bros, I. Tubbe, S. Grabbe, M. Schmidt, Selective uptake of cylindrical poly(2-oxazoline) brush-AntiDEC205 antibody-OVA antigen conjugates into dec-positive dendritic cells and subsequent t-cell activation, Chem. Eur J. 20 (39) (2014) 12405–12410.
[288] L.-H. Dieu, D. Wu, C.G. Palivan, V. Balasubramanian, J. Huwyler, Polymersomes conjugated to 83-14 monoclonal antibodies: *In vitro* targeting of brain capillary endothelial cells, Eur. J. Pharm. Biopharm. 88 (2) (2014) 316–324.
[289] J.-C. Leroux, The novelty bubble, J. Controlled Release 278 (2018) 140–141.
[290] S. Barlas, FDA strategies to prevent and respond to drug shortages: Finding a better way to predict and prevent company closures, Pharmacol. Therapeut. 38 (5) (2013) 261–263.
[291] K. Liu, Z. Zhu, X. Wang, D. Gonçalves, B. Zhang, A. Hierlemann, P. Hunziker, Microfluidics-based single-step preparation of injection-ready polymeric nanosystems for medical imaging and drug delivery, Nanoscale 7 (40) (2015) 16983–16993.
[292] L. Hou, J. Fang, W. Wang, Z. Xie, D. Dong, N. Zhang, Indocyanine green-functionalized bottle brushes of poly(2-oxazoline) on cellulose nanocrystals for photothermal cancer therapy, J. Mater. Chem. B 5 (18) (2017) 3348–3354.
[293] W. Lin, N. Yao, L. Qian, X. Zhang, Q. Chen, J. Wang, L. Zhang, pH-responsive unimolecular micelle-gold nanoparticles-drug nanohybrid system for cancer theranostics, Acta Biomater. 58 (2017) 455–465.
[294] M. Camblin, P. Detampel, H. Kettiger, D. Wu, V. Balasubramanian, J. Huwyler, Polymersomes containing quantum dots for cellular imaging, Int. J. Nanomed. 9 (2014) 2287–2298.
[295] J. Pánek, S.K. Filippov, M. Hrubý, M. Rabyk, A. Bogomolova, J. Kučka, P. Štěpánek, Thermoresponsive nanoparticles based on poly(2-alkyl-2-oxazolines) and pluronic F127, Macromol. Rapid Commun. 33 (19) (2012) 1683–1689.
[296] A.V. Kabanov, V.A. Kabanov, DNA complexes with polycations for the delivery of genetic material into cells, Bioconjugate Chem. 6 (1) (1995) 7–20.
[297] Y. Kakizawa, K. Kataoka, Block copolymer micelles for delivery of gene and related compounds, Adv. Drug Deliv. Rev. 54 (2) (2002) 203–222.
[298] E. Wagner, Chapter Eight - polymers for nucleic acid transfer — an overview, Adv. Genet. 88 (2014) 231–261.
[299] M. Sun, K. Wang, D. Oupický, Advances in stimulus-responsive polymeric materials for systemic delivery of nucleic acids, Adv. Healthcare Mater. (2017), 1701070.
[300] P.L. Felgner, Y. Barenholz, J.P. Behr, S.H. Cheng, P. Cullis, L. Huang, J.A. Jessee, L. Seymour, F. Szoka, A.R. Thierry, E. Wagner, G. Wu, Nomenclature for Synthetic Gene Delivery Systems, Hum. Gene Ther. 8 (5) (2008) 511–512.
[301] V.R. de la Rosa, E. Bauwens, B.D. Monnery, B.G. De Geest, R. Hoogenboom, Fast and accurate partial hydrolysis of poly(2-ethyl2-oxazoline) into tailored linear polyethylenimine copolymers, Polym. Chem. 5 (17) (2014) 4957–4964.
[302] K. Naka, Y. Kubo, A. Ohki, S. Maeda, Aggregate of amphiphilic block copolymer derived from poly[(N-acylimino)ethylene]s and guest-binding properties for 8-Anilino-1-naphthalenesulfonic acid, pyrene, and enzymes, Polym. J. 26 (3) (1994) 243–249.
[303] O. Boussif, F. Lezoualc'h, M.A. Zanta, M.D. Mergny, D. Scherman, B. Demeneix, J.P. Behr, A versatile vector for gene and oligonucleotide transfer into cells in culture and *in vivo*: polyethylenimine, Proc. Natl. Acad. Sci. U.S.A. 92 (16) (1995) 7297–7301.
[304] S. Ferrari, E. Moro, A. Pettenazzo, J.P. Behr, F. Zacchello, M. Scarpa, ExGen 500 is an efficient vector for gene delivery to lung epithelial cells in vitro and in vivo, Gene Ther. 4 (10) (1997) 1100–1106.
[305] M. Thomas, J.J. Lu, Q. Ge, C. Zhang, J. Chen, A.M. Klibanov, Full deacylation of polyethylenimine dramatically boosts its gene delivery efficiency and specificity to mouse lung, Proc. Natl. Acad. Sci. Unit. States Am. 102 (16) (2005) 5679–5684.
[306] T. Ivanova, E. Haladjova, M. Mees, D. Momekova, S. Rangelov, G. Momekov, R. Hoogenboom, Characterization of polymer vector systems based on partially hydrolyzed polyoxazoline for gene transfection, Pharmacia 63 (2) (2016) 3–8.
[307] M. Mees, E. Haladjova, D. Momekova, G. Momekov, P.S. Shestakova, C.B. Tsvetanov, R. Hoogenboom, S. Rangelov, Partially hydrolyzed poly(n-propyl-2-oxazoline): synthesis, aqueous solution properties, and preparation of gene delivery systems, Biomacromolecules 17 (11) (2016) 3580–3590.
[308] N. Toncheva-Moncheva, E. Veleva-Kostadinova, C. Tsvetanov, D. Momekova, S. Rangelov, Preparation and properties of positively charged mesoglobules based on poly(2-isopropyl-2-oxazoline) and evaluation of their potential as carriers of polynucleotides, Polymer 111 (2017) 156–167.
[309] M.A. Cortez, W.T. Godbey, Y. Fang, M.E. Payne, B.J. Cafferty, K.A. Kosakowska, S.M. Grayson, The synthesis of cyclic poly(ethylene imine) and exact linear analogues: an evaluation of gene delivery comparing polymer architectures, J. Am. Chem. Soc. 137 (20) (2015) 6541–6549.
[310] S. Cesana, J. Auernheimer, R. Jordan, H. Kessler, O. Nuyken, First poly(2-oxazoline)s with pendant amino groups, Macromol. Chem. Phys. 207 (2006) 183–192.
[311] A.C. Rinkenauer, L. Tauhardt, F. Wendler, K. Kempe, M. Gottschaldt, A. Traeger, U.S. Schubert, A cationic poly(2-oxazoline) with high in vitro transfection efficiency identified by a library approach, Macromol. Biosci. 15 (3) (2015) 414–425.
[312] V.M. Gaspar, C. Gonçalves, D. de Melo-Diogo, E.C. Costa, J.A. Queiroz, C. Pichon, F. Sousa, I.J. Correia, Poly(2-ethyl-2-oxazoline)–PLA-g–PEI amphiphilic triblock micelles for co-delivery of minicircle DNA and chemotherapeutics, J. Control. Release 189 (2014) 90–104.
[313] A.V. Kabanov, S.V. Vinogradov, Y.G. Suzdaltseva, V.Y. Alakhov, Water-soluble block polycations as carriers for oligonucleotide delivery, Bioconjugate Chem. 6 (6) (1995) 639–643.
[314] N. Kanayama, S. Fukushima, N. Nishiyama, K. Itaka, W.D. Jang, K. Miyata, Y. Yamasaki, U.-i. Chung, K. Kataoka, A PEG-based biocompatible block catiomer with high buffering capacity for the construction of polyplex micelles showing efficient gene transfer toward primary cells, ChemMedChem 1 (4) (2006) 439–444.
[315] D. Witzigmann, D. Wu, S.H. Schenk, V. Balasubramanian, W. Meier, J.r. Huwyler, Biocompatible polymer – peptide hybrid-based DNA nanoparticles for gene delivery, ACS Appl. Mater. Interfaces 7 (19) (2015) 10446–10456.
[316] Z. He, L. Miao, R. Jordan, D. S-Manickam, R. Luxenhofer, A.V. Kabanov, A low protein binding cationic poly(2-oxazoline) as non-viral vector, Macromol. Biosci. 15 (7) (2015) 1004–1020.
[317] R. Lehner, K. Liu, X. Wang, M. Wolf, P. Hunziker, A comparison of plasmid DNA delivery efficiency and cytotoxicity of two cationic diblock poly-oxazoline copolymers, Nanotechnology 28 (17) (2017), 175602.
[318] H.K. Nguyen, P. Lemieux, S.V. Vinogradov, C.L. Gebhart, N. Guerin, G. Paradis, T.K. Bronich, V.Y. Alakhov, A.V. Kabanov, Evaluation of polyether-polyethyleneimine graft copolymers as gene transfer agents, Gene Ther. 7 (2) (2000) 126–138.
[319] S. Osawa, K. Osada, S. Hiki, A. Dirisala, T. Ishii, K. Kataoka, Polyplex micelles with double-protective compartments of hydrophilic shell and thermoswitchable palisade of poly(oxazoline)-based block copolymers for promoted gene transfection, Biomacromolecules 17 (1) (2015) 354–361.
[320] P. Lemieux, N. Guerin, G. Paradis, R. Proulx, L. Chistyakova, A. Kabanov, V. Alakhov, A combination of poloxamers increases gene expression of plasmid DNA in skeletal muscle, Gene Ther. 7 (11) (2000) 986–991.
[321] B. Rasolonjatovo, B. Pitard, T. Haudebourg, V. Bennevault, P. Guégan, Synthesis of tetraarm star block copolymer based on polytetrahydrofuran and poly(2-methyl-2-oxazoline) for gene delivery applications, Eur. Polym. J. 88 (2017) 689–700.
[322] Z.Z. Gaymalov, Z. Yang, V.M. Pisarev, V.Y. Alakhov, A.V. Kabanov, The effect of the nonionic block copolymer pluronic P85 on gene expression in mouse muscle and antigen-presenting cells, Biomaterials 30 (6) (2009) 1232–1245.
[323] M. Bello-Roufaï, O. Lambert, B. Pitard, Relationships between the physico-chemical properties of an amphiphilic triblock copolymers/DNA complexes and their intramuscular transfection efficiency, Nucleic Acids Res. 35 (3) (2006) 728–739.
[324] R. Jordan, A. Ulman, Surface initiated living cationic polymerization of 2-oxazolines, J. Am. Chem. Soc. 120 (2) (1998) 243–247.
[325] C. Haensch, T. Erdmenger, M.W.M. Fijten, S. Hoeppener, U.S. Schubert, Fast surface modification by microwave assisted click reactions on silicon substrates, Langmuir 25 (14) (2009) 8019–8024.
[326] N. Zhang, T. Pompe, I. Amin, R. Luxenhofer, C. Werner, R. Jordan, Tailored poly(2-oxazoline) polymer brushes to control protein adsorption and cell adhesion, Macromol. Biosci. 12 (7) (2012) 926–936.
[327] S. Weydert, S. Zürcher, S. Tanner, N. Zhang, R. Ritter, T. Peter, M.J. Aebersold, G. Thompson-Steckel, C. Forró, M. Rottmar, F. Stauffer, I.A. Valassina, G. Morgese, E.M. Benetti, S. Tosatti, J. Vörös, Easy to apply polyoxazoline-based coating for precise and long-term control of neural patterns, Langmuir 33 (35) (2017) 8594–8605.
[328] J. An, A. Dedinaitė, F.M. Winnik, X.-P. Qiu, P.M. Claesson, Temperature-dependent adsorption and adsorption hysteresis of a thermoresponsive diblock copolymer, Langmuir 30 (15) (2014) 4333–4341.
[329] J. An, X. Liu, A. Dedinaite, E. Korchagina, F.M. Winnik, P.M. Claesson, Effect of solvent quality and chain density on normal and frictional forces between electrostatically anchored thermoresponsive diblock copolymer layers, J. Colloid Interface Sci. 487 (2017) 88–96.
[330] A. Dworak, A. Utrata-Wesołek, N. Oleszko, W. Wałach, B. Trzebicka, J. Anioł, A.L. Sieroń, A. Klama-Baryła, M. Kawecki, Poly(2-substituted-2-oxazoline)

surfaces for dermal fibroblasts adhesion and detachment, J. Mater. Sci. Mater. Med. 25 (4) (2014) 1149–1163.
[331] N. Oleszko, W. Wałach, A. Utrata-Wesołek, A. Kowalczuk, B. Trzebicka, A. Klama-Baryła, D. Hoff-Lenczewska, M. Kawecki, M. Lesiak, A.L. Sieron, A. Dworak, Controlling the crystallinity of thermoresponsive poly(2-oxazoline)based nanolayers to cell adhesion and detachment, Biomacromolecules 16 (9) (2015) 2805–2813.
[332] A. Tait, A.L. Fisher, T. Hartland, D. Smart, P. Glynne-Jones, M. Hill, E.J. Swindle, M. Grossel, D.E. Davies, Biocompatibility of poly(2-alkyl-2-oxazoline) brush surfaces for adherent lung cell lines, Biomaterials 61 (2015) 26–32.
[333] A. Kroning, A. Furchner, S. Adam, P. Uhlmann, K. Hinrichs, Probing carbonyl–water hydrogen-bond interactions in thin polyoxazoline brushes, Biointerphases 11 (1) (2016), 019005.
[334] G. Morgese, L. Trachsel, M. Romio, M. Divandari, S.N. Ramakrishna, E.M. Benetti, Topological polymer chemistry enters surface science: linear versus cyclic polymer brushes, Angew. Chem. Int. Ed. 55 (50) (2016) 15583–15588.
[335] M. Divandari, G. Morgese, L. Trachsel, M. Romio, E.S. Dehghani, J.-G. Rosenboom, C. Paradisi, M. Zenobi-Wong, S.N. Ramakrishna, E.M. Benetti, Topology effects on the structural and physicochemical properties of polymer brushes, Macromolecules 50 (19) (2017) 7760–7769.
[336] G. Morgese, E. Cavalli, M. Müller, M. Zenobi-Wong, E.M. Benetti, Nanoassemblies of tissue-reactive, polyoxazoline graft-copolymers restore the lubrication properties of degraded cartilage, ACS Nano 11 (3) (2017) 2794–2804.
[337] G. Morgese, S.N. Ramakrishna, R. Simic, M. Zenobi-Wong, E.M. Benetti, Hairy and slippery polyoxazoline-based copolymers on model and cartilage surfaces, Biomacromolecules 19 (2) (2018) 680–690.
[338] J.Ł. Kowal, J.K. Kowal, D. Wu, H. Stahlberg, C.G. Palivan, W.P. Meier, Functional surface engineering by nucleotide-modulated potassium channel insertion into polymer membranes attached to solid supports, Biomaterials 35 (26) (2014) 7286–7294.
[339] J. Kowal, D. Wu, V. Mikhalevich, C.G. Palivan, W. Meier, Hybrid Polymer–Lipid films as platforms for directed membrane protein insertion, Langmuir 31 (17) (2015) 4868–4877.
[340] F. Wendler, T. Rudolph, H. Görls, N. Jasinski, V. Trouillet, C. Barner-Kowollik, F.H. Schacher, Maleimide-functionalized poly(2-ethyl-2oxazoline): synthesis and reactivity, Polym. Chem. 7 (13) (2016) 2419–2426.
[341] C. Pan, X. Liu, K. Gong, F. Mumtaz, Y. Wang, Dopamine assisted PMOXA/PAA brushes for their switchable protein adsorption/desorption, J. Mater. Chem. B 6 (2018) 556–567.
[342] M.N. Leiske, M. Hartlieb, C. Paulenz, D. Pretzel, M. Hentschel, C. Englert, M. Gottschaldt, U.S. Schubert, Lab in a tube: purifi cation, amplifi cation, and detection of DNA using poly(2-oxazoline) multilayers, Adv. Funct. Mater. 25 (16) (2015) 2458–2466.
[343] S. Bhatt, J. Pulpytel, M. Mirshahi, F. Arefi-Khonsari, Cell resistant peptidomimetic poly(2-ethyl-2-oxazoline) coatings developed by low pressure inductively excited pulsed plasma polymerization for biomedical purpose, Plasma Process. Polym. 12 (6) (2015) 519–532.
[344] M.N. Macgregor, A. Michelmore, H. Safizadeh Shirazi, J. Whittle, K. Vasilev, Secrets of plasma-deposited polyoxazoline functionality lie in the plasma phase, Chem. Mater. 29 (19) (2017) 8047–8051.
[345] M.N. Ramiasa, A.A. Cavallaro, A. Mierczynska, S.N. Christo, J.M. Gleadle, J.D. Hayball, K. Vasilev, Plasma polymerised polyoxazoline thin films for biomedical applications, Chem. Commun. 51 (20) (2015) 4279–4282.
[346] M.N. Macgregor-Ramiasa, A.A. Cavallaro, K. Vasilev, Properties and reactivity of polyoxazoline plasma polymer films, J. Mater. Chem. B 3 (30) (2015) 6327–6337.
[347] N. Zhang, S. Huber, A. Schulz, R. Luxenhofer, R. Jordan, Cylindrical molecular brushes of poly(2-oxazoline)s from 2-Isopropenyl-2-oxazoline, Macromolecules 42 (6) (2009) 2215–2221.
[348] L.E. Gonzalez Garcia, M. MacGregor-Ramiasa, R.M. Visalakshan, K. Vasilev, Protein interactions with nanoengineered polyoxazoline surfaces generated via plasma deposition, Langmuir 33 (29) (2017) 7322–7331.
[349] S. Zanini, L. Zoia, E.C. Dell'Orto, A. Natalello, A.M. Villa, D.R. Pergola, C. Riccardi, Plasma polymerized 2-ethyl-2-oxazoline: chemical characterization and study of the reactivity towards different chemical groups, Mater. Des. 108 (2016) 791–800.
[350] H. Yasuda, T. Hirotsu, Critical evaluation of conditions of plasma polymerization, J. Polym. Sci. 16 (4) (1978) 743–759.
[351] S. Zanini, L. Zoia, D.R. Pergola, C. Riccardi, Pulsed plasma-polymerized 2-isopropenyl-2-oxazoline coatings: chemical characterization and reactivity studies, Surf. Coating. Technol. 334 (2018) 173–181.
[352] A.A. Cavallaro, M.N. Macgregor-Ramiasa, K. Vasilev, Antibiofouling properties of plasma-deposited oxazoline-based thin films, ACS Appl. Mater. Interfaces 8 (10) (2016) 6354–6362.
[353] M.N. Macgregor, A. Michelmore, S.H. Shirazi, J. Whittle, K. Vasilev, Secrets of plasma-deposited polyoxazoline functionality lie in the plasma phase, Chem. Mater. 29 (19) (2017) 8047–8051.
[354] A. Popelka, J. Kronek, I. Novák, A. Kleinová, M. Mičušík, M. Špírková, M. Omastová, Surface modification of low-density polyethylene with poly(2-ethyl-2-oxazoline) using a low-pressure plasma treatment, Vacuum 100 (2014) 53–56.
[355] M. Macgregor-Ramiasa, K. McNicholas, K. Ostrikov, J. Li, M. Michael, J.M. Gleadle, K. Vasilev, A platform for selective immuno-capture of cancer cells from urine, Biosens. Bioelectron. 96 (2017) 373–380.
[356] R. Konradi, B. Pidhatika, A. Mühlebach, M. Textor, Poly-2-methyl-2-oxazoline: a peptide-like polymer for protein-repellent surfaces, Langmuir 24 (3) (2008) 613–616.
[357] L. Bai, L. Tan, L. Chen, S. Liu, Y. Wang, Preparation and characterizations of poly(2-methyl-2-oxazoline) based antifouling coating by thermally induced immobilization, J. Math. Chem. B 2 (44) (2014) 7785–7794.
[358] K. Mao, H. Du, L. Bai, Y. Zhang, H. Zhu, Y. Wang, Poly(2-methyl-2-oxazoline) coating by thermally induced immobilization for determination of bovine lactoferrin in infant formula with capillary electrophoresis, Talanta 168 (2017) 230–239.
[359] L. Tauhardt, M. Frant, D. Pretzel, M. Hartlieb, C. Bücher, G. Hildebrand, B. Schröter, C. Weber, K. Kempe, M. Gottschaldt, K. Liefeith, U.S. Schubert, Amine end-functionalized poly(2-ethyl-2-oxazoline) as promising coating material for antifouling applications, J. Mater. Chem. B 2 (30) (2014) 4883–4893.
[360] S. Liu, C. Chen, L. Chen, H. Zhu, C. Zhang, Y. Wang, Pseudopeptide polymer coating for improving biocompatibility and corrosion resistance of 316L stainless steel, RSC Adv. 5 (119) (2015) 98456–98466.
[361] H. Zhu, F. Mumtaz, C. Zhang, L. Tan, S. Liu, Y. Zhang, C. Pan, Y. Wang, A rapid approach to prepare poly(2-methyl-2-oxazoline)-based antifouling coating by UV irradiation, Appl. Surf. Sci. 426 (2017) 817–826.
[362] C. Zhang, S. Liu, L. Tan, H. Zhu, Y. Wang, Star-shaped poly(2-methyl-2-oxazoline)-based films: rapid preparation and effects of polymer architecture on antifouling properties, J. Mater. Chem. B 3 (27) (2015) 5615–5628.
[363] X. Zheng, C. Zhang, L. Bai, S. Liu, L. Tan, Y. Wang, Antifouling property of monothiol-terminated bottle-brush poly(methylacrylic acid)-*graft*-poly(2-methyl-2-oxazoline) copolymer on gold surfaces, J. Mater. Chem. B 3 (9) (2015) 1921–1930.
[364] M. Schneider, Z. Tang, M. Richter, C. Marschelke, P. Förster, E. Wegener, I. Amin, H. Zimmermann, D. Scharnweber, H.-G. Braun, R. Luxenhofer, R. Jordan, Patterned polypeptoid brushes, Macromol. Biosci. 16 (1) (2016) 75–81.
[365] Y. Chen, B. Pidhatika, T. von Erlach, R. Konradi, M. Textor, H. Hall, T. Lühmann, Comparative assessment of the stability of nonfouling poly(2-methyl-2-oxazoline) and poly(ethylene glycol) surface films: an *in vitro* cell culture study, Biointerphases 9 (3) (2014), 031003.
[366] T. He, D. Jańczewski, S. Jana, A. Parthiban, S. Guo, X. Zhu, S.S.C. Lee, F.J. Parra-Velandia, S.L.M. Teo, G.J. Vancso, Efficient and robust coatings using poly(2-methyl-2-oxazoline) and its copolymers for marine and bacterial fouling prevention, J. Polym. Sci. 54 (2) (2016) 275–283.
[367] T. He, D. Jańczewski, S. Guo, S.M. Man, S. Jiang, W.S. Tan, Stable pH responsive layer-by-layer assemblies of partially hydrolysed poly(2-ethyl-2-oxazoline) and poly(acrylic acid) for effective prevention of protein, cell and bacteria surface attachment, Colloids Surf. B: Biointerfaces 161 (2018) 269–278.
[368] K. Kempe, S.L. Ng, K.F. Noi, M. Müllner, S.T. Gunawan, F. Caruso, Clickable poly(2-oxazoline) architectures for the fabrication of LowFouling polymer capsules, ACS Macro Lett. 2 (12) (2013) 1069–1072.
[369] H. Zhang, M. Chiao, Anti-fouling coatings of poly(dimethylsiloxane) devices for biological and biomedical applications, J. Med. Biol. Eng. 35 (2) (2015) 143–155.
[370] K. Kempe, S.L. Ng, S.T. Gunawan, K.F. Noi, F. Caruso, Intracellularly degradable hydrogen-bonded polymer capsules, Adv. Funct. Mater. 24 (39) (2014) 6187–6194.
[371] C. Su, J. Sun, X. Zhang, D. Shen, S. Yang, Hydrogen-bonded polymer complex thin film of poly(2-oxazoline) and poly(acrylic acid), Polymers 9 (8) (2017) 363.
[372] R. Lakshmanan, U.M. Krishnan, S. Sethuraman, Multidimensional nanofibrous scaffolds of poly(lactide-co-caprolactone) and poly(ethyl oxazoline) with improved features for cardiac tissue engineering, Nanomedicine 10 (23) (2015) 3451–3467.
[373] T. Hayashi, A. Takasu, Design of Electrophoretic and biocompatible poly(2-oxazoline)s initiated by perfluoroalkanesulfoneimides and Electrophoretic deposition with bioactive glass, Biomacromolecules 16 (4) (2015) 1259–1266.
[374] C.J. Waschinski, J. Zimmermann, U. Salz, R. Hutzler, G. Sadowski, J.C. Tiller, Design of contact-active antimicrobial acrylate-based materials using biocidal macromers, Adv. Mater. 20 (1) (2008) 104–108.
[375] Y. Li, T. Pan, B. Ma, J. Liu, J. Sun, Healable antifouling films composed of partially hydrolyzed poly(2ethyl-2-oxazoline) and poly(acrylic acid), ACS Appl. Mater. Interfaces 9 (16) (2017) 14429–14436.
[376] A.M. Kelly, V. Kaltenhauser, I. Mühlbacher, K. Rametsteiner, H. Kren, C. Slugovc, F. Stelzer, F. Wiesbrock, Poly(2-oxazoline)-derived contact biocides: contributions to the understanding of antimicrobial activity, Macromol. Biosci. 13 (1) (2013) 116–125.
[377] C.P. Fik, S. Konieczny, D.H. Pashley, C.J. Waschinski, R.S. Ladisch, U. Salz, T. Bock, J.C. Tiller, Telechelic poly(2-oxazoline)s with a biocidal and a polymerizable terminal as collagenase inhibiting additive for long-term active antimicrobial dental materials, Macromol. Biosci. 14 (11) (2014) 1569–1579.
[378] A. Schulz, A. Stocco, A. Bethry, J.-P. Lavigne, J. Coudane, B. Nottelet, Direct photomodification of polymer surfaces: unleashing the potential of aryl-azide copolymers, Adv. Funct. Mater. (2018), 1800976.